

**ATMOSPHERIC RIVERS IN BRITISH COLUMBIA'S NECHAKO RIVER BASIN:
VARIABILITY, TRENDS AND HYDROLOGICAL IMPACTS**

by

Bruno Serafini Sobral

B.Sc., Federal Fluminense University, 2010

M.Sc., Federal Fluminense University, 2017

DISSERTATION SUBMITTED IN PARTIAL FULFILMENT OF
THE REQUIREMENTS FOR THE DEGREE OF
DOCTOR OF PHILOSOPHY
IN
NATURAL RESOURCES AND ENVIRONMENTAL STUDIES

UNIVERSITY OF NORTHERN BRITISH COLUMBIA

January 2025

© Bruno Serafini Sobral, 2025

ABSTRACT

This dissertation provides a comprehensive analysis of atmospheric rivers (ARs) and their impacts on the Nechako River Basin (NRB) in British Columbia (BC), Canada. The study is divided into three main components: (1) the spatio-temporal distribution and trend analyses of AR types impacting the NRB, (2) AR contributions to the NRB's water budget input and their trends, and (3) the synoptic setting and hydrological responses in the NRB to three exceptional AR events.

Initially, the spatio-temporal distribution and trends of ARs of various categories were examined. The study found a notable shift from mid- to low-intensity AR types in several sub-basins of the NRB. This shift suggests a potential impact on the regional water budget, as lower-intensity ARs are mostly beneficial and less likely to cause hazardous impacts but may also bring less water vapour to precipitate over the NRB. Spatial analysis revealed that the western and northern parts of the NRB are most affected by ARs, mainly in the fall and winter, with November experiencing the highest average AR intensity for the region.

Moreover, the contributions of ARs to the NRB's water budget and their trends were assessed. AR days impacting the NRB are estimated at ~35 AR days yearly, on average, accounting for approximately one-fifth of the total annual precipitation, bringing predominantly rain in the fall and a mix of rain and snow in winter. Additional analyses indicated increasing trends in total precipitation linked to low-intensity ARs in the northern and western sectors of the NRB. The study highlights significant spatial variations in AR contributions to the NRB's hydrological cycle, impacting total precipitation, snowpack formation, runoff, and the overall regional water budget.

The synoptic setting and hydrological responses in the NRB to three exceptional AR events that occurred in 1952, 1978, and 2009 were also explored. These exceptional AR events depict the dual role of ARs in contributing to water replenishment while causing natural

hazards. The exceptional ARs significantly contributed to snowpack formation and water replenishment to the Nechako Reservoir, averaging total precipitation accumulations of 81 mm (1.14 km³) in the Upper Nechako, highlighting their importance for regional water storage.

However, these events also underscored the potential for flash floods and landslides, particularly during rain-on-snow conditions or when ARs make landfall on saturated soils and steep terrain. The findings of this dissertation emphasize the critical role of ARs in shaping the water budget of the NRB. The increasing frequency of some AR types, while others are diminishing, shows the changing nature of ARs, which may require adaptive water management strategies to balance the beneficial and detrimental impacts of these river-shaped storms. Enhanced understanding of AR dynamics and their impacts can inform the development of more effective flood prevention, water storage, and resource management practices, ensuring sustainable water supply for various stakeholders. The insights gained are particularly valuable for managing the Nechako Reservoir, where accurate water management is crucial for balancing agricultural, industrial, residential, and ecological needs in central BC.

TABLE OF CONTENTS

ABSTRACT.....	ii
TABLE OF CONTENTS	iv
LIST OF TABLES.....	ix
LIST OF FIGURES.....	x
LIST OF ACRONYMS	xvi
ACKNOWLEDGEMENTS	xvii
CHAPTER 1: INTRODUCTION.....	1
1.1 INTRODUCTION	1
1.1.1 Escalating Average Air Temperatures in Western Canada.....	6
1.1.2 The Kemano Project.....	6
1.2 OBJECTIVES	7
CHAPTER 2: SPATIO-TEMPORAL DISTRIBUTION AND TREND ANALYSES OF ATMOSPHERIC RIVERS AFFECTING BRITISH COLUMBIA'S NECHAKO WATERSHED.....	10
2.1 INTRODUCTION	12
2.2 STUDY AREA	14
2.3 DATA AND METHODS	16
2.3.1 Datasets.....	16
2.3.1.1 AR Catalogue	16

2.3.1.2 Hydroclimatic data	18
2.3.2 Methods	18
2.3.2.1 Data analysis and figure preparation.....	18
2.3.2.2 AR-related hydroclimatic datasets.....	18
2.3.2.3 Mann-Kendall trend test	20
2.4 RESULTS AND DISCUSSION	20
2.4.1 Multi-scale analysis.....	20
2.4.1.1 Annual.....	20
2.4.1.2 Seasonal	23
2.4.2.1 AR frequency, intensity and duration near the NRB.....	26
2.4.2.2 AR-related hydro-variability in the sub-basins of the NRB.....	27
2.5 CONCLUSIONS	29
CHAPTER 3: WATER BUDGET INPUT LINKED TO ATMOSPHERIC RIVERS IN BRITISH COLUMBIA’S NECHAKO RIVER BASIN	31
3.1 INTRODUCTION	33
3.2 STUDY AREA	35
3.3 DATA AND METHODS	37
3.3.1 Datasets.....	37
3.3.1.1 AR Catalogue	37
3.3.1.2 Water budget input data	38

3.3.1.3 Oceanic Niño Index (ONI)	39
3.3.2 Methods	39
3.3.2.1 Data analysis and visualization.....	39
3.3.2.2 AR-related water budget datasets	39
3.3.2.3 Mann-Kendall trend test	41
3.4 RESULTS	41
3.4.1 Annual Analysis	41
3.4.2 Seasonal Analysis	46
3.4.3 Daily Analysis.....	54
3.5 DISCUSSION.....	60
3.6 CONCLUSIONS	65
CHAPTER 4: METEOROLOGICAL DRIVERS AND HYDROLOGICAL RESPONSES TO EXCEPTIONAL ATMOSPHERIC RIVERS IN BRITISH COLUMBIA’S NECHAKO RIVER BASIN	67
4.1 INTRODUCTION	69
4.2 STUDY AREA	70
4.3 DATA AND METHODS	72
4.3.1 Datasets.....	73
4.3.1.1 AR Catalogue	73
4.3.1.2 Hydroclimatic data	74
4.3.1.3 Discharge and Water Level Data	75

4.3.2 Methods	78
4.3.2.1 Selection of exceptional AR events affecting the NRB.....	78
4.3.2.2 Data analysis.....	80
4.4 RESULTS	82
4.4.1 Climatology of exceptional AR events impacting the NRB.....	82
4.4.1.1 12-14 December 1952.....	82
4.4.1.2 28 October – 1 November 1978.....	87
4.4.1.3 27-31 October 2009	91
4.4.2 Impacts of ARs to the NRB.....	95
4.5 DISCUSSION.....	101
4.6 CONCLUSIONS.....	107
CHAPTER 5: KEY FINDINGS, IMPLICATIONS, CONCLUSIONS AND FUTURE STUDIES	109
5.1 SUMMARY	109
5.1.1 AR Impacts on the NRB’s Ecosystem	111
5.1.2 Implications for Rio Tinto’s Operations of the Nechako Reservoir.....	112
5.1.3 Recommendations for Future-Related Research.....	113
REFERENCES	115
APPENDIX A.....	136
APPENDIX B.....	154

APPENDIX C..... 155

APPENDIX D..... 158

APPENDIX E..... 161

APPENDIX F..... 167

APPENDIX G..... 173

APPENDIX H..... 174

LIST OF TABLES

Table 2.1– Percentage of ARD frequency at AR-monitored regions South and North (1950-2021).	21
Table 3.1 – Annual average of the AR-related water budget input variables of the ERA5-Land (1950-2021) for the sub-basins of the NRB. Fractional results are for total annual values.	42
Table 3.2 –Results of the Mann-Kendall test applied to the time series of AR-related water budget input variables on the annual scale.	45
Table 3.3 – Seasonal average of the AR-related variables of the ERA5-Land (1950-2021) for the sub-basins of the NRB. Fractional results are for total seasonal values.	49
Table 3.4 –Results of the Mann-Kendall test applied to the time series of AR-related water budget input variables in the seasonal scale.	53
Table 3.5 – The frequency of AR and non-AR-related daily precipitation in the Upper Nechako from 1950 to 2021 divided into 5 mm bins. * The single event causing the maximum daily total represented by the 80-85 mm bin is influenced or caused by an AR despite not being classified as an AR-day by the applied methodology.	55
Table 4.1 – Discharge and water level data stations used to assess the hydrological response in the NRB.	77
Table 4.2 – Short list of AR events on the AR Catalogue impacting the NRB after applying the selection criteria based on the percentiles and the scoring mechanism	80
 Appendix A		
Table A.1 - Summarized results for the 364 climate datasets showing basic descriptive statistics and Mann-Kendall's tau and p-values ($\alpha=5\%$, 95% confidence).	133

LIST OF FIGURES

Figure 1.1 – Plan view (a) and vertical cross-section (b) of an atmospheric river according to the Glossary of Meteorology of the American Meteorological Society. Adapted from Cordeira <i>et al.</i> (2013) and Ralph <i>et al.</i> (2004) where IVT stands for integrated water vapour transport ($\text{kg m}^{-1} \text{s}^{-1}$).	2
Figure 1.2 – Atmospheric pathways of ARs (a) worldwide and in (b) North America from 1940-2023 (shaded areas in blue), according to Guan and Waliser (2024).	2
Figure 1.3 – Figure 4 of Ralph <i>et al.</i> (2019) with the proposed AR scale categorizing ARs based on maximum IVT ($\text{kg m}^{-1} \text{s}^{-1}$) and duration of AR events.	4
Figure 1.4 – Map of the NRB including sub-basins, hydrological network (black lines), surrounding lakes (in cyan), the Nechako Reservoir (in dark blue), the Kenney Dam (red rectangle), the Skins Lake Spillway (red triangle), and elevation (m).	5
Figure 2.1 – Map of the NRB with sub-basins and elevation. Inset map with the location of the NRB in BC and the nearest AR-monitored regions of the SIO-R1 catalogue to the NRB.	15
Figure 2.2 – Box and whisker plot for the annual ARD frequency at AR-monitored regions South (52.5° N , 127.5° W) and North (55° N , 130° W). Five-number summary for the non-outlier minimum (Q_0), first quartile (Q_1), median (Q_2), third quartile (Q_3), and non-outlier maximum (Q_4) in addition to outliers (+). Values within the whiskers (Q_0 and Q_4) depict the range excluding outliers.	21
Figure 2.3 – Annual ARD frequency at AR-monitored regions a) South (52.5° N , 127.5° W) and b) North (55° N , 130° W) according to the adapted scale of Ralph <i>et al.</i> (2019).	22
Figure 2.4 – Seasonal ARD frequency at the AR-monitored regions a) South (52.5° N , 127.5° W) and b) North (55° N , 130° W).	24
Figure 2.5 – Seasonal ARD frequency at the AR-monitored region South (52.5° N , 127.5° W) according to the adapted scale of Ralph <i>et al.</i> (2019).	25
Figure 2.6 – Seasonal ARD frequency at the AR-monitored region North (55° N , 130° W) according to the adapted scale of Ralph <i>et al.</i> (2019).	25
Figure 2.7 – Seasonal ARD average intensity (IVT) at the AR-monitored regions a) South (52.5° N , 127.5° W) and b) North (55° N , 130° W).	26
Figure 2.8 – Diagram depicting significant trends from the MK test for ARD frequency (1950-2021). Triangles facing up (down) show significant increasing (decreasing) trends. Black is for the annual scale, orange is for fall, and blue is for winter. P-values of the MK tests are presented below each symbol.	27
Figure 2.9 – Diagram depicting significant results of the MK test for ARD intensity (1950-2021). Triangles facing up (down) show significant increasing (decreasing) trends. Orange is for fall, and blue is for winter. P-values of the MK tests are presented below each symbol.	27
Figure 2.10– Diagram depicting significant trends of the MK test for the AR-related variables of the ERA5-Land product (1950-2021). Triangles facing up (down) show significant increasing (decreasing) trends. Blue is for AR-related rain, purple is for AR-related total precipitation, and yellow is for AR-related SWE. P-values of the MK tests are presented below each symbol.	29

Figure 3.1 - Map of the NRB with sub-basins, Nechako Reservoir, Kenney Dam, Skins Lake Spillway, the city of Prince George, elevation distribution and nearest AR monitored region (inset map) of the SIO-R1-AR catalogue.	37
Figure 3.2 - Box and whisker plot for the annual AR-related contribution to a) total precipitation, b) rain, c) snow and d) SWE in the sub-basins of the NRB according to ERA5-Land (1950-2021) and AR Catalogue (1950-2021) data associated on the daily scale. Five-number summary for the minimum (Q_0), first quartile (Q_1), median (Q_2), third quartile (Q_3), and maximum (Q_4) frequency in addition to outliers (+). Outliers are defined as measurements that exceed three standard deviations from the mean.	42
Figure 3.3 - Annual AR-related fractional contribution to a) total precipitation, b) rain, c) snow and d) SWE in the sub-basins of the NRB according to ERA5-Land (1950-2021) and AR Catalogue (1950-2021) data associated with the daily scale. The fractional values are associated with 9% of AR-days annually.	44
Figure 3.4 – Seasonal AR-related fractional contribution to total precipitation in the sub-basins of the NRB according to the daily association of the ERA5-Land (1950-2021) and AR Catalogue (1950-2021) data. The fractional values are associated with 4% of AR-days during spring, 9% in summer, 17% in fall and 6% in winter.	46
Figure 3.5 – Seasonal AR-related fractional contribution to rain in the sub-basins of the NRB according to the daily association of ERA5-Land (1950-2021) and AR Catalogue (1950-2021) data. The fractional values are associated with 4% of AR-days during spring, 9% in summer, 17% in fall and 6% in winter.	47
Figure 3.6 – Seasonal AR-related fractional contribution to snow in the sub-basins of the NRB according to the daily association of ERA5-Land (1950-2021) and AR Catalogue (1950-2021) data. The fractional values are associated with 4% of AR-days during spring, 9% in summer, 17% in fall and 6% in winter.	47
Figure 3.7 – Seasonal AR-related fractional contribution to SWE in the sub-basins of the NRB according to the daily association of ERA5-Land (1950-2021) and AR Catalogue (1950-2021) data. The fractional values are associated with 4% of AR-days during spring, 9% in summer, 17% in fall and 6% in winter.	48
Figure 3.8 – Fractional representation of daily AR-related (blue) total precipitation compared to non-AR-related (gray) in the Upper Nechako divided into 5 mm bins. The maximum daily total represented by the 80-85 mm bin is influenced or caused by an AR despite not being classified as an AR-day by the applied methodology.	55
Figure 3.9 – Polar plot with average daily fractions for AR-related precipitation in the Upper Nechako (red) and the NRB (blue).	60
Figure 4.1 – Map of the NRB with sub-basins, elevation (m), hydrological network, the Nechako Reservoir, Kenney Dam, Skins Lake Spillway, Prince George (BC) and discharge or water level monitoring points within the NRB assessed by this study. Inset map with the location of the NRB in BC and the Nechako Reservoir.	72
Figure 4.2 – Climogram of the AR event from 12-14 December 1952. The panels show (a) the total column of water vapour (mm), (b) integrated water vapour transport (IVT - $\text{kg m}^{-1} \text{s}^{-1}$) at five positions along a latitudinal transect, (c) moisture divergence (negative values mean convergence) (mm), (d) total precipitation in light blue (mm) and cumulative precipitation in dark blue (mm), (e) snowfall in light blue (mm of water equivalent) and cumulative snowfall in dark blue (mm), (f) mean 2-metre air temperature ($^{\circ}\text{C}$), and (g) mean sea-level pressure (hPa) during the AR event occurred on 12-14 October 1952.	85

Figure 4.3 – Maps for (a) mean total column of water vapour (mm), (b) mean integrated water vapour transport (IVT - $\text{kg m}^{-1} \text{s}^{-1}$) and the location of the five positions along the latitudinal transect, (c) moisture divergence (negative values mean convergence) (mm), (d) total precipitation (mm), (e) snowfall (mm), (f) mean 2-metre air temperature ($^{\circ}\text{C}$), (g) mean sea-level pressure (hPa) during the peak of moisture convergence with contour lines and (h) accumulated runoff (mm) during the AR event occurred on 12-14 October 1952.	86
Figure 4.4 – Climogram of the AR event from 28 October to 1 November 1978. The panels show (a) the total column of water vapour (mm), (b) integrated water vapour transport (IVT - $\text{kg m}^{-1} \text{s}^{-1}$) at five positions along a latitudinal transect, (c) moisture divergence (negative values mean convergence) (mm), (d) total precipitation in light blue (mm) and cumulative precipitation in dark blue (mm), (e) snowfall in light blue (mm of water equivalent) and cumulative snowfall in dark blue (mm), (f) mean 2-metre air temperature ($^{\circ}\text{C}$), and (g) mean sea-level pressure (hPa) during the AR event occurred on 28 October to 1 November 1978.	89
Figure 4.5 – Maps for (a) mean total column of water vapour (mm), (b) mean integrated water vapour transport (IVT - $\text{kg m}^{-1} \text{s}^{-1}$) and the location of the five positions along the latitudinal transect, (c) moisture divergence (negative values mean convergence) (mm), (d) total precipitation (mm), (e) snowfall (mm), (f) mean 2-metre air temperature ($^{\circ}\text{C}$), (g) mean sea-level pressure (hPa) during the peak of moisture convergence with contour lines and (h) accumulated runoff (mm) during the AR event occurred on 28 October to 1 November 1978.	90
Figure 4.6 – Climogram of the AR event from 27-31 October 2009. The panels show (a) the total column of water vapour (mm), (b) integrated water vapour transport (IVT - $\text{kg m}^{-1} \text{s}^{-1}$) at five positions along a latitudinal transect, (c) moisture divergence (negative values mean convergence) (mm), (d) total precipitation in light blue (mm) and cumulative precipitation in dark blue (mm), (e) snowfall in light blue (mm of water equivalent) and cumulative snowfall in dark blue (mm), (f) mean 2-metre air temperature ($^{\circ}\text{C}$), and (g) mean sea-level pressure (hPa) during the AR event occurred on 27-31 October 2009.	93
Figure 4.7 – Maps for (a) mean total column of water vapour (mm), (b) mean integrated water vapour transport (IVT - $\text{kg m}^{-1} \text{s}^{-1}$) and the location of the five positions along the latitudinal transect, (c) moisture divergence (negative values mean convergence) (mm), (d) total precipitation (mm), (e) snowfall (mm), (f) mean 2-metre air temperature ($^{\circ}\text{C}$), (g) mean sea-level pressure (hPa) during the peak of moisture convergence with contour lines and (h) accumulated runoff (mm) during the AR event occurred on 27-31 October 2009.	94
Figure 4.8 – Water level (m) data in the Nechako Reservoir for the historical period (1955-2021) (black dashed line) in days of the calendar year (1-365), for the 1978 AR event (red line) and the 2009 AR event (magenta line). The gray vertical lines represent the occurrence period of the exceptional AR events in 1978 and 2009. No data are available for the Nechako Reservoir during the exceptional AR event in 1952.	99
Figure 4.9 – Standardized discharge data across the NRB for the exceptional AR events of 1952 (black line), 1978 (red line) and 2009 (blue line).	100

APPENDIX B

Figure B.1 – Annual anomalies related to Atmospheric Rivers (AR) for (a) total precipitation, (b) rainfall, (c) snowfall, and (d) SWE in the NRB, based on daily data from the ERA5-Land (1950-2021) and the AR Catalogue (1950-2021). Panel (e) shows the maximum and minimum values of the ONI. In panels (a), (b), (c), and (d), light blue and light red bars indicate positive and negative anomalies, respectively, from the mean. In panel (e), red areas represent El Niño phases, blue areas represent La Niña phases, and gray areas represent neutral phases of the ENSO climate pattern.	154
--	-------	-----

APPENDIX C

Figure C.1 – Fraction (%) of daily AR-related (blue) total precipitation compared to non-AR-related (gray) in the Lower Nechako divided into 5 mm bins.	155
Figure C.2 – Fraction (%) of daily AR-related (blue) total precipitation compared to non-AR-related (gray) in the Upper Stuart divided into 5 mm bins.	155
Figure C.3 – Fraction (%) of daily AR-related (blue) total precipitation compared to non-AR-related (gray) in the Lower Stuart divided into 5 mm bins.	156
Figure C.4 – Fraction (%) of daily AR-related (blue) total precipitation compared to non-AR-related (gray) in the Endako divided into 5 mm bins.	156
Figure C.5 – Fraction (%) of daily AR-related (blue) total precipitation compared to non-AR-related (gray) in the Chilako divided into 5 mm bins.	156
Figure C.6 – Fraction (%) of daily AR-related (blue) total precipitation compared to non-AR-related (gray) in the Stellako divided into 5 mm bins.	157

APPENDIX D

Figure D.1: Daily standardized discharge graph at the Tahtsa Lake near Kemano station (08JA030) during the exceptional AR event of 2009. No data are available at this station for the 1952 and 1978 AR events.	158
Figure D.2: Daily standardized discharge graph at the Laventie Creek near the Mouth station (08JA015) during the exceptional AR events of 1978 (red) and 2009 (blue). No data are available at this station for the 1952 AR event.	158
Figure D.3: Daily standardized discharge graph at the Nadina River at the outlet of Nadina Lake station (08JB008) during the exceptional AR events of 1978 (red) and 2009 (blue). No data are available at this station for the 1952 AR event.	158
Figure D.4: Daily standardized discharge graph at Francois Lake station (08JB011) during the exceptional AR event of 1978. No data are available at this station for the 1952 and 2009 AR events.	159
Figure D.5: Daily standardized discharge graph at the Stellako River at Glenannan station (08JB002) during the exceptional AR events of 1952 (black), 1978 (red), and 2009 (blue).	159
Figure D.6: Daily standardized discharge graph at the Nautley River near Fort Fraser station (08JB003) during the exceptional AR events of 1952 (black), 1978 (red), and 2009 (blue).	159
Figure D.7: Daily standardized discharge graph at the Stuart River near Fort St. James station (08JE001) during the exceptional AR events of 1952 (black), 1978 (red), and 2009 (blue).	160
Figure D.8: Daily standardized discharge graph at the Tsilcoh River near the Mouth station (08JE004) during the exceptional AR events of 1978 (red) and 2009 (blue).	160

APPENDIX E

Figure E.1: Time sequence of the geopotential at 500 hPa (a to f - in $\text{m}^2 \text{s}^{-2}$) in the 12-hourly (UTC) scale during the 1952 exceptional AR event.	161
Figure E.2: Time sequence of the mean sea-level pressure (a to f - in hPa) in the 12-hourly (UTC) scale during the 1952 exceptional AR event.	162
Figure E.3: Time sequence of the geopotential at 500 hPa (a to j - in $\text{m}^2 \text{s}^{-2}$) in the 12-hourly (UTC) scale during the 1978 exceptional AR event.	163
Figure E.4: Time sequence of the mean sea-level pressure (a to j - in hPa) in the 12-hourly (UTC) scale during the 1978 exceptional AR event.	164
Figure E.5: Time sequence of the geopotential at 500 hPa (a to j - in $\text{m}^2 \text{s}^{-2}$) in the 12-hourly (UTC) scale during the 2009 exceptional AR event.	165
Figure E.6: Time sequence of the mean sea-level pressure (a to j - in hPa) in the 12-hourly (UTC) scale during the 2009 exceptional AR event.	166

APPENDIX F

Figure F.1: Daily total precipitation (mm) in the NRB in 1952. Red crosses indicate AR Days or days when total precipitation is associated with ARs.	167
Figure F.2: Daily rainfall (mm) in the NRB in 1952. Red crosses indicate AR Days or days when rainfall is associated with ARs.	167
Figure F.3: Daily snowfall (mm) in the NRB in 1952. Red crosses indicate AR Days or days when snowfall is associated with ARs.	168
Figure F.4: Daily SWE (mm) in the NRB in 1952. Red crosses indicate AR Days or days when SWE is associated with ARs.	168
Figure F.5 : Daily total precipitation (mm) in the NRB in 1978. Red crosses indicate AR Days or days when total precipitation is associated with ARs.	169
Figure F.6: Daily rainfall (mm) in the NRB in 1978. Red crosses indicate AR Days or days when rainfall is associated with ARs.	169
Figure F.7: Daily snowfall (mm) in the NRB in 1978. Red crosses indicate AR Days or days when snowfall is associated with ARs.	170
Figure F.8: Daily SWE (mm) in the NRB in 1978. Red crosses indicate AR Days or days when SWE is associated with ARs.	170
Figure F.9: Daily total precipitation (mm) in the NRB in 2009. Red crosses indicate AR Days or days when total precipitation is associated with ARs.	171
Figure F.10: Daily rainfall (mm) in the NRB in 2009. Red crosses indicate AR Days or days when rainfall is associated with ARs.	171
Figure F.11: Daily snowfall (mm) in the NRB in 2009. Red crosses indicate AR Days or days when snowfall is associated with ARs.	172

Figure F.12: Daily SWE (mm) in the NRB in 2009. Red crosses indicate AR Days or days when SWE is associated with ARs. 172

APPENDIX G

Figure G.1: IWV and IVT maps at the time of maximum landfalling IVT for the 1978 (a and c) and 2009 (b and d) exceptional AR events. 173

LIST OF ACRONYMS

ALCAN	Aluminum Company of Canada
AR	Atmospheric River
ARD	AR-Day or AR-related Day
ARTMIP	Atmospheric River Tracking Method Intercomparison Project
BC	British Columbia
BC Hydro	British Columbia Hydro and Power Authority
C3S	Copernicus Climate Change Service
ECCC	Environment and Climate Change Canada
ECMWF	European Centre for Medium-Range Weather Forecasts
ENSO	El Niño-Southern Oscillation
ERA5	Fifth Generation of the European Medium-Range Weather Forecasts Reanalysis
ERA5-Land	Fifth Generation of the European Medium-Range Weather Forecasts Land Reanalysis
GWF	Global Water Futures
IVT	Integrated Water Vapour Transport
MK	Mann-Kendall Trend Test
NCAR	National Center for Atmospheric Research
NCEP	National Centers for Environmental Prediction
NHG	Northern Hydrometeorology Group
NRB	Nechako River Basin
NSERC	Natural Sciences and Engineering Research Council of Canada
ONI	Oceanic Niño Index
PCIC	Pacific Climate Impacts Consortium
PDO	Pacific Decadal Oscillation
PNA	Pacific North American Index
SIO	Scripps Institution of Oceanography
SLS	Skins Lake Spillway
SST	Sea Surface Temperature
SWE	Snow Water Equivalent
UCSD	University of California San Diego
UNBC	University of Northern British Columbia

ACKNOWLEDGEMENTS

Thanks to the following institutions and individuals for their support throughout this study: the University of Northern British Columbia (UNBC), Natural Sciences and Engineering Research Council of Canada (NSERC), Rio Tinto, and Global Water Futures (GWF) for financial support, Andy Lecuyer and Alec Mercier from Rio Tinto for providing data and information on their water management operations, past and present members of the Northern Hydrometeorology Group (NHG), the Scripps Institution of Oceanography at the University of California San Diego (UCSD) and Dr. Fred Martin Ralph (UCSD) for acting as the external examiner for the PhD dissertation defense, the Land and Cartography Institute of Rio de Janeiro (ITERJ), Dr. Peter Jackson, Dr. Joseph Shea, Dr. Phil Owens, Dr. Margot Parkes, Dr. Eduardo Martins, Dr. Ellen Petticrew, Dr. Siraj ul Islam and Senior Lab Instructor Chris Jackson of UNBC, Dr. Ruping Mo of Environment and Climate Change Canada (ECCC), Dr. Francis Zwiers, Dr. Aseem Sharma of the BC Ministry of Forests (BC MoF), Dr. Jingwen Wu of the Pacific Climate Impacts Consortium (PCIC), Dr. Uttam Goswami (Post Doctoral Fellow at UNBC), Dr. Jason Cordeira, Dr. Kristen Guirguis and Dr. Brian Kawzenuk of UCSD.

CHAPTER 1: INTRODUCTION

1.1 INTRODUCTION

Atmospheric rivers (ARs) are significant drivers of hydrological processes in midlatitude regions, such as British Columbia (BC), where they account for more than 90% of atmospheric moisture transport originating in the tropics (Ralph *et al.*, 2004; Ralph *et al.*, 2013). According to Newell *et al.* (1992) and Zhu and Newell (1994, 1998), most of these atmospheric moisture pathways that reach North America originate near the Hawaiian Islands, making ARs also known as "Pineapple Expresses" in western North America. The moisture that builds up in the tropical Pacific Ocean is carried northeast by the prevailing westerlies and interacts with extratropical cyclones in the mid-latitudes before streaming into the continental inland areas. BC's unique geographical location in western Canada makes it particularly susceptible to the impacts of these river-shaped storms originating from the Pacific Ocean.

ARs are also described as narrow corridors of water vapour transport (Figure 1.1) in the lower atmosphere, acting globally (Figure 1.2a) like conveyor belts of moisture that can deliver tremendous amounts of precipitation in short periods. They have been identified as key drivers of heavy precipitation in coastal and inland areas of BC. The floods in November 2021 are a recent example of the potential for ARs to cause hazardous impacts on BC (Gillett *et al.*, 2022). Understanding how ARs lead to natural disaster events is particularly important to manage the risks associated with AR-related floods, landslides, and other detrimental outcomes. Despite the various downside impacts of certain ARs on BC, their contributions to the water balance of the province are often overlooked. The physical and climatological characteristics of BC, particularly its diverse mountainous landscape and corresponding climate variations, generate substantial spatial variability in the amount and type of AR-related precipitation.

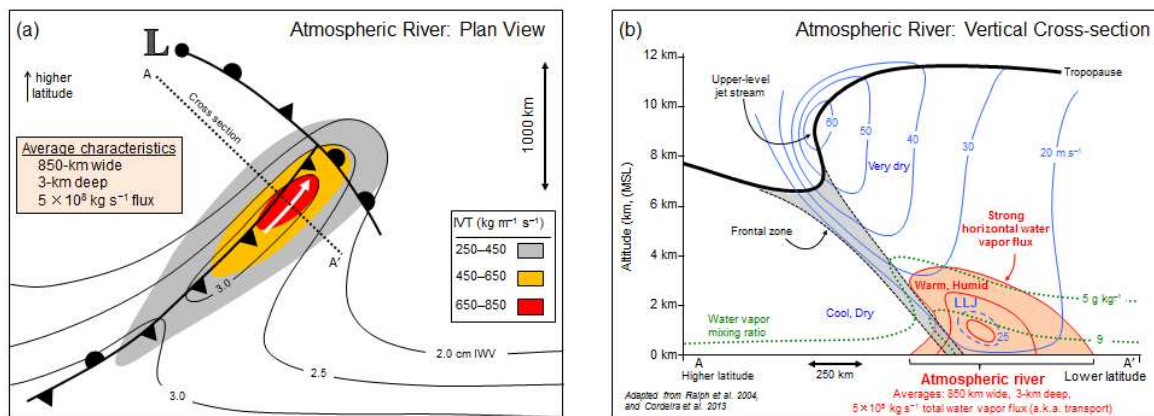


Figure 1.1 – (a) Plan view and (b) vertical cross-section of an atmospheric river according to the Glossary of Meteorology of the American Meteorological Society. Adapted from Cordeira *et al.* (2013) and Ralph *et al.* (2004). IWV denotes integrated water vapour (kg m^{-2}) and IVT represents integrated water vapour transport ($\text{kg m}^{-1} \text{s}^{-1}$).

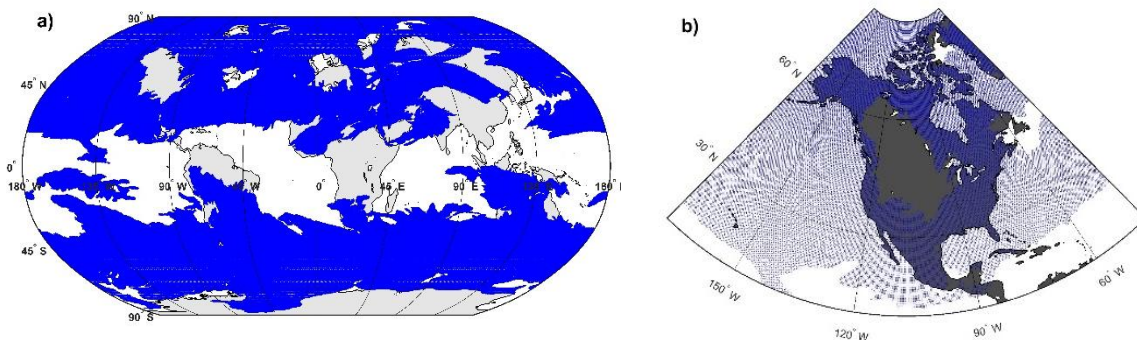


Figure 1.2 – Atmospheric pathways of ARs (a) worldwide (areas shaded in solid blue) and (b) in North America (areas shaded in light blue) for 1940-2023 (Guan and Waliser, 2024).

The Nechako River Basin (NRB) is a nival catchment in BC that ARs frequently impact. It comprises seven major sub-basins and lies on the leeward side of the Coast Mountains, within the Interior Plateau of central BC. The intense precipitation associated with AR events can lead to rapid snowmelt and elevated river flows, increasing the risk of flooding in some areas of the NRB. These floods can cause widespread damage to infrastructure, disrupt communities, and impact local ecosystems. Moreover, the increased sediment load carried by rivers during and after AR events can degrade water quality and affect aquatic habitats in the NRB (Gateuille *et al.*, 2019). The NRB forms part of the headwaters of the Fraser River and plays a vital role in water resource management that supports various uses in one of the largest rivers of western

Canada. Therefore, long-term changes in AR patterns, driven by cyclical climate variations, pose significant concerns to the region. The Nechako Reservoir, located in the western portion of the NRB, benefits considerably from AR activity and is an essential source of water for BC.

Evidence indicates that AR events are becoming more frequent and intense in some regions, a trend linked to rising sea surface temperatures (SSTs), thereby altering global atmospheric circulation patterns (Guan *et al.*, 2023). According to Sharma and Déry (2020a), previous studies report an increase in water vapour transport and landfalling frequency and intensity in North America due to ARs when considering different climate projections (Payne and Magnusdottir, 2014; Warner *et al.*, 2015). This trend could intensify existing challenges and introduce new risks, such as increased magnitude and frequency of landslides and floods, disturbing local populations and ecosystems. Given the NRB's crucial role in regional water management and the potential growing influence of ARs on its water balance, enhancing our understanding of these storms and their terrestrial impacts becomes imperative.

The effects of ARs on the NRB depend on their frequency, duration, and intensity. To enable a more effective evaluation of the impacts associated with different categories of ARs, Ralph *et al.* (2019) introduced a classification scale based on intensity and duration, which has demonstrated promising results worldwide (Guan *et al.*, 2023). One of the key advantages of the AR scale is that it standardizes direct intercomparisons of AR events and impacts globally. Consequently, this study adopts the AR scale (Figure 1.3) proposed by Ralph *et al.* (2019) as the primary reference for classifying AR events affecting the NRB. The AR events are classified into: AR1 - primarily beneficial, AR2 – primarily beneficial, also hazardous, AR3 – balance of hazardous and beneficial, AR4 – mostly hazardous, also beneficial, and AR5 – primarily hazardous. While the terms "beneficial" and "hazardous" are open to interpretation, in the

context of this scale, they refer specifically to the positive and negative impacts of ARs upon landfall at a given location. For the purposes of this study, the AR scale has been extended in Chapter 2 to include AR0 events. AR0s represent short-duration (<24 hours) ARs with IVT $\geq 250 \text{ kg m}^{-1} \text{ s}^{-1}$, highlighting their influence on the NRB's water budget despite their shorter lifespan.

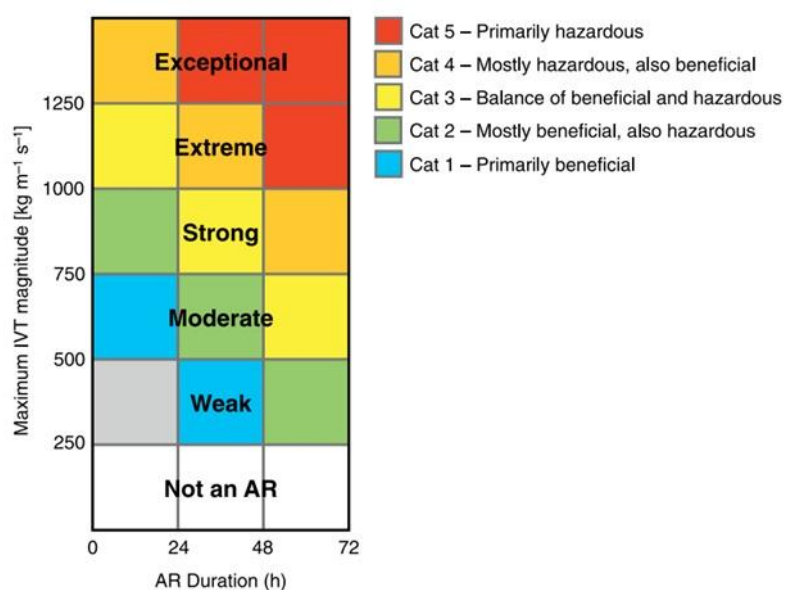


Figure 1.3 – Figure 4 of Ralph *et al.* (2019) with the proposed AR scale categorizing ARs based on maximum IVT ($\text{kg m}^{-1} \text{ s}^{-1}$) and duration of AR events.

In nival watersheds like the NRB (Figure 1.4), elevation, antecedent soil moisture, and snowpack conditions are also major drivers influencing the magnitude of the impacts caused by ARs. ARs making landfall in BC generally have a southwest-to-northeast trajectory influenced by regional midlatitude cyclones. On average, the BC region experiences annually about 35 landfalling AR events, with the impacts of the "AR season" starting earlier at higher latitudes, peaking in the fall, and with lower frequency in March and April (Sharma and Déry, 2020b). ARs contribute about 20% of the total annual precipitation along the Coast Mountains, 11% in the Columbia Mountains, and 6% in the Rocky Mountains (Sharma and Déry, 2020c).

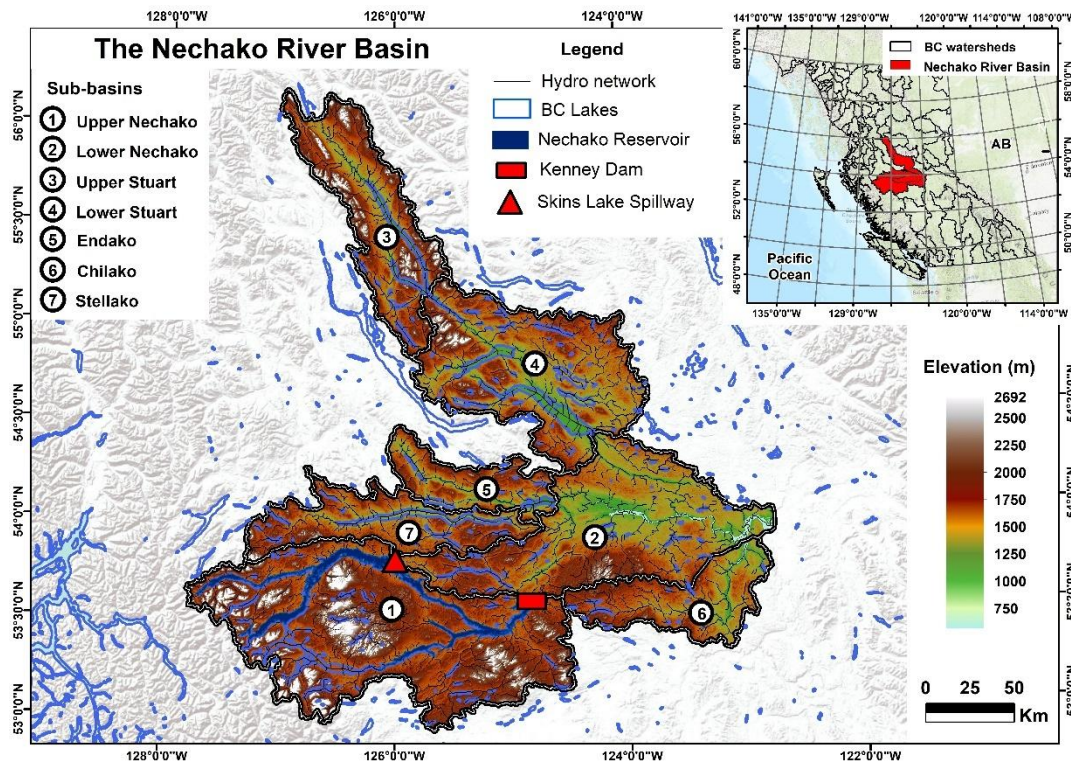


Figure 1.4 – Map of the NRB including sub-basins, hydrological network (black lines), surrounding lakes (in cyan), the Nechako Reservoir (in dark blue), the Kenney Dam (red rectangle), the Skins Lake Spillway (red triangle), and elevation (m).

More recently, high-resolution atmospheric models have been developed for better prediction of AR pathways and effects, and remote sensing technologies have greatly enhanced their detection and analysis. Such technological development has led to the monitoring of AR development and progress in near real-time, making it possible to assess the climatological conditions of such weather events and prepare to mitigate eventual downside impacts. This is particularly important for BC, where accurate forecasting can be used to prepare timely responses to potential flooding and landslides, anticipating water management challenges. Understanding the hydrologic impacts of ARs is essential to developing effective strategies for managing water resources in regions like the NRB.

1.1.1 Escalating Average Air Temperatures in Western Canada

In recent decades, average air temperatures in western Canada have been on the rise and are projected to continue increasing (Bush and Lemmen, 2019). Studies have shown that the average temperature in western Canada has significantly increased over the last century, with even more substantial increases observed in northern areas (Zhang *et al.*, 2019). This warming, particularly during the winter months, has significant impacts on the region's hydrological cycle and natural ecosystems (Vincent *et al.*, 2015). The potentially increasing frequency and intensity of landfalling AR events in BC, related to rising SSTs in the tropical and eastern Pacific (Alexander *et al.*, 2018; Garcia-Soto *et al.*, 2021; Pan *et al.*, 2024), underscore the need for detailed studies on the impacts of ARs in the region. In a warming scenario, the risks of flooding and other AR-induced extremes may be amplified, particularly in areas like BC that are already susceptible to the beneficial and detrimental impacts of ARs. Despite their importance to BC, few studies have focused on the influence of ARs on the hydrological cycle of the NRB. Understanding the relationship between rising sea surface and air temperatures with AR activity is crucial for developing adaptive water management strategies to mitigate AR-related impacts and improve water resiliency in central BC.

1.1.2 The Kemano Project

The Kemano Project is a massive initiative launched by the Aluminum Company of Canada (ALCAN) in the early 1950s to provide power to operate an aluminum smelter in Kitimat, a town in northwestern BC. Among many hydraulic works, the project involved constructing the Kenney Dam (Figure 1.4) to impound the Nechako River and create the Nechako Reservoir (Desreumaux *et al.*, 2014). A consistent supply of hydropower is crucial for industrial operations in Kitimat (Desreumaux *et al.*, 2014), although it relies entirely on inter-basin water

transfers from the NRB to supply the demand. Rio Tinto currently operates the Nechako Reservoir and ensures a steady supply of water for clean electricity generation in northwestern BC (Tannant and Morgenroth, 2020).

The operation of the Nechako Reservoir relies on releasing water from the Skins Lake Spillway (SLS) (Figure 1.4) to maintain adequate flows in the Nechako River. The SLS plays a crucial role in regulating the reservoir's water levels and satisfying multiple demands, including hydropower production, ecological conservation, and water supply for industrial and residential purposes (Hartman, 1996). The system's consistency relies on the volume and timing of water inflows, which in turn are influenced by climatic factors such as AR events, other types of synoptic storms, temperature fluctuations, and snowpack formation, among others.

However, the partial dependence on AR-related precipitation also poses challenges to the NRB. During periods of intense AR activity, the influx of water can overwhelm the reservoir's capacity, leading to increased flows at the SLS and potentially flooding areas downstream of the impoundment. Conversely, reduced AR activity can lead to water shortages, impacting all stakeholders and requiring improved water management to balance socioecological and industrial needs.

1.2 OBJECTIVES

This study contributes to expanding the field of AR science by characterizing the climatology, spatiotemporal distribution, trends, and extremes of AR events impacting the NRB, as well as assessing their respective hydrological responses. It bridges the research gap on ARs impacting the NRB by assessing the overall contributions, trends, and changes in hydroclimatological variables based on climate data from the last seven decades (1950-2021). Ultimately, it also

aims to improve our knowledge of the climatology of ARs during exceptional events affecting the NRB to provide value to water resource management and reduce risks related to extreme weather in this critical watershed of BC. This comprehensive study aims to enhance the understanding of how ARs influence the NRB's hydrology, thereby providing valuable insights for water resource management and climate adaptation strategies in the region.

In summary, the overarching objective of the proposed research is to investigate the association between ARs and the hydrological cycle of the NRB. More specifically, the objectives of the research are as follows:

- 1) to analyze the spatiotemporal variation of various AR types and investigate for trends;
- 2) to quantify the contribution of ARs to the hydrological cycle of the NRB and investigate for trends, and;
- 3) to characterize the synoptic patterns and hydrological impacts of exceptional AR events that have affected the NRB.

To achieve these objectives, this dissertation is organized into five chapters. Chapter 1 serves as the introduction, setting the stage for the research. Chapters 2, 3, and 4 present independent studies on ARs impacting the NRB, each aimed at being published in different scientific outlets based on their specific content. Chapter 2 examines the spatial and temporal patterns and trends of various types of ARs impacting the NRB region. Chapter 3 investigates the impact of ARs on the hydroclimatology of the NRB, focusing on the variability and trends in their contributions to total precipitation, rainfall, snowfall, and snow water equivalent (SWE). Chapter 4 explores the regional synoptic setting and hydrological responses to three exceptional AR events that impacted the NRB in 1952, 1978, and 2009. The dissertation concludes with Chapter 5, which combines the main findings with key conclusions of what is learned from the

individual studies on ARs impacting the NRB. The content—including text, figures, plots, and appendices—within the chapters of this dissertation is authored by Bruno Serafini Sobral and supervised by Dr. Stephen Déry. Consequently, Chapters 2, 3, and 4 are meant to be published as individual studies with Bruno Serafini Sobral as the main author and Dr. Stephen Déry as the co-author.

CHAPTER 2: SPATIO-TEMPORAL DISTRIBUTION AND TREND ANALYSES OF ATMOSPHERIC RIVERS AFFECTING BRITISH COLUMBIA'S NECHAKO WATERSHED

This chapter is published in the International Journal of Climatology.

Publication details:

Sobral, B. S., and Déry, S. J. (2023). Spatiotemporal distribution and trend analyses of atmospheric rivers affecting British Columbia's Nechako Watershed. *International Journal of Climatology*, 43(14), 6720–6732. <https://doi.org/10.1002/joc.8230>

ABSTRACT: Research and shared interest in atmospheric rivers (ARs) have increased significantly in recent years, alongside technological improvements that allow better comprehension of these storms. The Nechako River Basin (NRB) in British Columbia, Canada, is significantly affected by ARs originating in the Pacific Ocean. This work analyses the frequency, intensity, duration and trends of ARs in two regions (South and North) near the NRB. Analyses are based on data provided by an updated AR catalogue. The AR catalogue is matched on a daily scale to an adaptation of the AR scale to compile so-called AR-Days (ARDs). In the South region, ARDs exhibit stronger associations with hydroclimatic variables total precipitation, rain, snow and snow depth water equivalent (SWE). The Mann–Kendall (MK) trend test was applied to 364 time series created by combining the two closest AR-monitored regions to the NRB with the annual and seasonal scales of climate data and the adapted AR scale (ARD0-ARD5). Results show higher AR frequency of mainly beneficial ARDs during fall and a significant reduction of ARD1-ARD3 in both analyzed regions. Rain and total precipitation related to ARD2-ARD3 also present significant decreasing trends for most sub-basins of the NRB. The MK test shows a shift in water contribution from total precipitation and rainfall linked to more potentially dangerous ARDs to short-duration, beneficial ARDs (ARD0). Rain from non-AR-related meteorological systems presents an

increasing trend for the Upper Nechako sub-basin, where the Nechako Reservoir is located. Trends are mainly for AR-related total precipitation and rainfall, and in the northern part of the NRB, results point to the increase of AR-related SWE.

2.1 INTRODUCTION

ARs are filamentary, transient corridors of intense water vapour transport (Zhu and Newell, 1994, 1998), also known in western North America as "Pineapple Expresses." Typically, ARs transport water vapour from warmer areas of the globe, such as humid tropics and subtropics, to mid-latitude regions (Ahrens *et al.*, 2016). As global moisture distribution remains highly heterogeneous, water vapour transport by ARs remains vital for global energy and water budgets (Mo *et al.*, 2021). Indeed, for all mid-latitude regions, including BC, Canada, ARs can account for >90% of atmospheric moisture transport from the tropics (Zhu and Newell, 1998; Ralph *et al.*, 2017; Sharma and Déry, 2020c; Ralph *et al.*, 2020).

Numerous factors can influence the scale of AR impacts at landfall, including the frequency, duration, temperature and concentration of the transported moisture, wind speed and direction, antecedent soil moisture and snowpack conditions (Payne and Magnusdottir, 2014; Fish *et al.*, 2019; Payne *et al.*, 2020). Depending on an AR's orientation, intensity, and duration, the leeward (downslope) sides of a barrier can also receive abundant precipitation due to the hydrometeor drift and spillover effect (Mo *et al.*, 2019). This is the case of BC's Nechako River Basin (NRB), which encompasses east-facing slopes of the Coast Mountains subject to downslope effects of ARs within the predominant mid-latitude westerlies. Consequently, the NRB is likely to be directly impacted by precipitation variation if changes in the frequency, duration and intensity of ARs occur.

ARs are quite common in BC (Sharma and Déry, 2020b), usually presenting a southwest-to-northeast direction influenced by regional wind patterns in the mid-latitudes of the Pacific Ocean. ARs making landfall over BC typically originate with the build-up of atmospheric moisture near the Hawaiian Islands in the tropical Pacific region. The evaporated water then

travels northeast, interacting with other meteorological phenomena, such as extratropical cyclones, shaping into aerial rivers before reaching continental inland areas of North America. In BC and southeastern Alaska, an average of 35 landfalling AR events are registered annually, with maximum (minimum) frequency in September and October (March and April), when a total of ~13 (5) ARs typically occur (Sharma and Déry, 2020b). Landfalling ARs in this region contribute on average to 20%, 11% and 6% of total annual precipitation along the Coast, Columbia and Rocky Mountains, respectively (Sharma and Déry, 2020b). Furthermore, runoff associated with ARs in the Interior Plateau region, where the NRB is located, is estimated at ~11% of annual totals (Sharma and Déry, 2020c).

With global warming temperatures (Garcia-Soto *et al.*, 2021) and higher water vapour concentration in the atmosphere, ARs are increasingly becoming recognized for their contributions to precipitation totals and extremes worldwide (Ralph *et al.*, 2020). The vital role of ARs in transporting water vapour from the tropics and distributing precipitation over BC makes them a key player in the water cycle of the NRB. Hence, it is crucial for the management of the NRB that important precipitation drivers such as ARs are studied in more detail to reveal the AR-related hydrological changes since 1950. Nevertheless, there have not been efforts to quantify the potential impacts and trends of ARs in the NRB, motivating the present study. Thus, the objectives for this study are: (1) to analyze the spatio-temporal variability of landfalling ARs at two locations near the NRB, (2) to investigate trends in the frequency and intensity of ARs, and (3) to investigate trends in AR-related hydroclimatic variables precipitation, rain, snow and snow depth water equivalent (SWE). The overarching objective is to understand how variations in AR frequency, intensity, and duration impact the hydrological cycle in sub-basins of the NRB.

2.2 STUDY AREA

The NRB lies in BC within latitudes 52.93° N to 56.17° N and longitudes 122.72° W to 127.78° W, with elevations ranging from ~650 to ~2700 m (Figure 2.1). The basin experiences an average annual air temperature of 3.7°C and ~600 mm of precipitation per year, with snow representing ~33% of the precipitated water volume (Albers *et al.*, 2016). Draining an area of 47,200 km², the NRB is a sub-basin that makes up an area of ~20% of the culturally, ecologically and economically important Fraser River Basin (Parkes, 2021), with peak flows during the spring freshet caused by melting snow. With headwaters in the Tahtsa and Quanchus Ranges (Helm *et al.*, 1980), the Nechako River flows from two different hydrologic regions: the Interior Plateau (Stuart sub-basin) and the Coast Mountains (Upper Nechako sub-basin) (Moore, 1991), joining the Fraser River as its second-largest tributary in the city of Prince George, BC.

For this study, the NRB is divided into seven sub-basins (Figure 2.1) created by the principal waterways of the watershed, namely the Stuart (upper and lower), Endako, Stellako, Chilako and Nechako (upper and lower) rivers. Several other natural water bodies also encompass the NRB, but the Nechako Reservoir, created in the 1950s by the Kemano Project, is the most prominent, with a volume of ~33 km³ (Déry *et al.*, 2012). The Kemano Project comprises the Nechako Reservoir, two 16-km water tunnels, the 95 m high and 450 m wide earthen Kenney Dam, the Skins Lake Spillway, the ~900 MW hydropower plant and the power transmission lines from the Kemano Powerhouse to the aluminum smelter in Kitimat, BC (Hartman, 1996). These interventions make the NRB the most regulated watershed of the Fraser system and can be considered the most significant source of anthropogenic changes in the NRB. The potential contribution of the Nechako River to the Fraser River Basin is ~5-10% of the annual flows (Déry *et al.*, 2012), of which a significant part is now diverted west for hydroelectricity

generation. The water tunnels of the Kemano Project currently divert ~60% of the flows in the Upper Nechako to the hydropower plant in Kemano, BC, equating to ~3-4 km³ of water annually.

Many socio-economic activities in the NRB, including forestry, manufacturing, agriculture, mining, and tourism, share a substantial dependence on water resources, making climate-related changes to water availability a concern to the region's development (Picketts *et al.*, 2017). Moreover, consistent population growth in the region may adversely impact stakeholders (Hartman, 1996). Potential impacts are diminishing water volumes in the Nechako Reservoir, increasing pollution in local water bodies, land-use change, and alterations in aquatic systems. In sum, the cumulative effects of the high-impact activities undertaken in the NRB can negatively affect many stakeholders if water availability within the Nechako is further reduced.

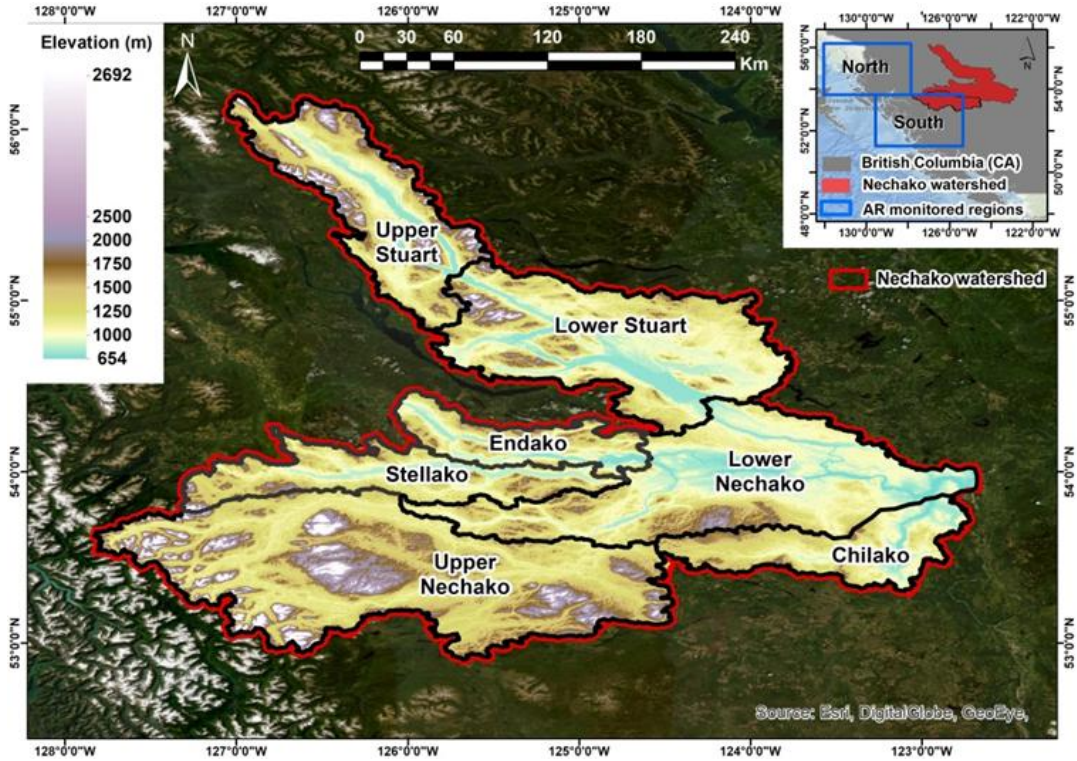


Figure 2.1 – Map of the NRB with sub-basins and elevation. Inset map with the location of the NRB in BC and the nearest AR-monitored regions of the SIO-R1 catalogue to the NRB.

2.3 DATA AND METHODS

2.3.1 Datasets

2.3.1.1 AR Catalogue

While there are various ways to identify and characterize ARs, we use the AR Catalogue described in Gershunov *et al.* (2017) to distinguish AR-related atmospheric features from others influenced by different meteorological phenomena. The AR-Catalogue created by the Scripps Institution of Oceanography (SIO) of the University of California San Diego (UCSD) comprises the period from 1948 to the present. This catalogue (SIO-R1) is based on the NCEP-NCAR Reanalysis 1 product developed by the National Centers for Environmental Prediction (NCEP) and the National Center for Atmospheric Research (NCAR). It provides six-hourly AR information on frequency, duration, intensity (integrated water vapour transport – IVT) and orientation over western North America. Compared to other AR catalogues, such as tARget-V3 from Guan and Waliser (2019) and ARTMIP from Shields *et al.* (2018), the SIO-R1 focuses solely on western North America, allowing a more detailed analysis of the climate-scale variability of ARs in the study region.

The SIO-R1 catalogue has been successfully applied in many studies on the western coast of North America, including our study area (e.g., Gershunov *et al.*, 2017, 2019; Sharma and Déry 2020b; Cao *et al.*, 2020; Guirguis *et al.*, 2021; and Gillett *et al.*, 2022). Therefore, it provides reliable and detailed information for this study on AR frequency, intensity and duration near the NRB, including positions: 52.5° N, 127.5° W – "South" and 55° N, 130° W – "North" (See Figure 2.1 inset map). These positions of the SIO-R1 provide detailed data (converted to daily) for the two closest monitored regions of the AR-Catalogue to the NRB. The AR regions monitored by the AR-Catalogue range between latitudes 22.5° N - 57.5° N and longitudes 105°

W – 135° W with a $2.5^\circ \times 2.5^\circ$ (~250 km) and apply a multi-source approach with observational data, reanalysis datasets, and atmospheric model simulations to provide a more robust regional analysis of AR characteristics.

The frequency and intensity of ARs over the South and North regions are analyzed on the annual and seasonal scales to create two separate and concurrent AR datasets. Each dataset characterizes AR frequency, intensity and duration at a different region, although both regions are often impacted by the same AR events that occur in the $50\text{-}57.5^\circ$ N, $125\text{-}132.5^\circ$ W region. The multi-scale analysis provides detailed knowledge of landfalling ARs near the NRB, and the duration of AR events is used to classify the events according to an adaptation of the scale proposed by Ralph *et al.* (2019).

The scale of Ralph *et al.* (2019) considers the intensity and duration of ARs to classify each AR event into the following five categories: AR1 (Primarily beneficial), AR2 (Mostly beneficial, also hazardous), AR3 (Balance of beneficial and hazardous), AR4 (Mostly hazardous, also beneficial) and AR5 (Primarily hazardous). AR events are classified from AR1 (IVT = 250-500 $\text{kg m}^{-1} \text{s}^{-1}$) to AR5 (IVT >1250 $\text{kg m}^{-1} \text{s}^{-1}$) according to an IVT threshold of 250 $\text{kg m}^{-1} \text{s}^{-1}$ for each classification and are upgraded one position every 24 hours of AR duration, up to 48 hours. The present study adapts the Ralph *et al.* (2019) scale by adding the AR0 category for ARs within the 250-500 $\text{kg m}^{-1} \text{s}^{-1}$ IVT threshold but lasting <24 hours. This allows the inclusion of short-duration ARs (AR0) in the study and comprises most events making landfall near the NRB, which would have been overlooked if no adaptation to the scale had been made.

2.3.1.2 Hydroclimatic data

The land component of the fifth generation of the European Medium-Range Weather Forecasts (ECMWF) Reanalysis product (ERA5-Land) is used in this study. It is a product of the ERA family comprising the period 1940-present and has been successfully used to study the climate of BC (e.g., Hou *et al.*, 2022 and Vore *et al.*, 2020). It provides an improved spatial resolution of $0.1^\circ \times 0.1^\circ$ (~9 km) and an hourly temporal resolution (Muñoz-Sabater *et al.*, 2021). Thus, a dataset with the hydroclimatic variables (precipitation, rain, snow, SWE) of the ERA5-Land product provided hourly (converted to daily) data to investigate trends and how variations in AR frequency, intensity and duration may be impacting these variables in the NRB's sub-basins.

2.3.2 Methods

2.3.2.1 Data analysis and figure preparation

The AR-Catalogue and ERA5-Land data are extracted and handled using a combination of Matlab software version R2021a and Microsoft Excel 2020. All plots and heatmaps are developed using Matlab software version R2021a, and the study area map is created using ArcGIS software version 10.1. The statistical tests were performed using the Forecasting Toolbox of the XLSTAT software (Adinsoft, 2022).

2.3.2.2 AR-related hydroclimatic datasets

Each day of the study period (1950-2021) is analyzed, and whenever one of the four six-hourly daily measurements of IVT surpasses $250 \text{ kg m}^{-1} \text{ s}^{-1}$, the adapted classification of Ralph *et al.* (2019) (AR0-AR5) is assigned to that day based on the highest IVT value and duration of the AR event. This method creates so-called AR-days (ARDs). ARDs are days when values of a climate variable are considered under the influence of ARs, whenever the ERA5-Land data

match AR activity reported by the SIO-R1 catalogue on the daily scale for the two monitored regions in proximity to the NRB. This allows the construction and analysis of hydrological datasets linked to ARs on seasonal and annual scales. The seasonal analysis divided each year into four seasons: spring (March-May), summer (June-August), fall (September-November) and winter (December-February). Notably, the analysis was conducted based on the calendar year, thus resulting in the winter season comprising the months of January, February, and December of the same year. This information holds significance as it informs the interpretation and understanding of the findings within the appropriate temporal context.

The South position is selected to associate AR activity to variations in hydroclimatic variables due to (1) its closer proximity to the watershed and partial coverage of the Upper Nechako sub-basin, (2) higher frequency of ARDs, and (3) higher Pearson correlation coefficients between the values of the ERA5-Land hydroclimatic variables and IVT. ARDs in the South are matched to the AR0-AR5 conditions based on the duration of AR events and the highest daily IVT ($\text{kg m}^{-1} \text{s}^{-1}$) measurement to form the new ARD0-ARD5 classification used in this study. A daily AR-related dataset for each variable is created for variables of the ERA5-Land (precipitation, rain, snow, SWE) and associated with the respective ARD0-ARD5 classification for the South monitored position. Since AR events can persist for several days and assume multiple categories on the scale while making landfall, the creation of ARDs places all AR events on the same temporal scale (daily) to facilitate the comparison of frequencies and intensities among different locations and periods of analysis. Lag times between AR events and the sub-basins of the NRB were not considered and can be addressed in future regional studies on ARs.

2.3.2.3 Mann-Kendall trend test

The Mann-Kendall (MK) (Mann, 1945; Kendall, 1975) non-parametric trend test is broadly used in the field of hydrometeorology (e.g., de Carvalho *et al.*, 2020; Costa *et al.*, 2020; Déry *et al.*, 2021). This study applies the MK test at the 95% confidence level ($p=0.05$) to the frequency and intensity of ARDs on the annual and seasonal temporal scales to identify possible changes in the frequencies and intensities (ARD0-ARD5) affecting the NRB. Moreover, using the same statistical parameters, this study investigates trends in the hydroclimatic variables (precipitation, rain, snow and SWE) associated with AR and non-AR activity in the South position on the same scales. A combination of the two AR-monitored regions with the annual and seasonal scales, the adapted scale of Ralph *et al.* (2019), and the hydroclimatic variables of the ERA5-Land provide 364 time series that are investigated for trends.

2.4 RESULTS AND DISCUSSION

2.4.1 Multi-scale analysis

2.4.1.1 Annual

The frequency of ARs that make landfall in the South and North monitored regions of the AR-Catalogue are analyzed and reveal that, on the annual scale, ARDs in the South are 14% more frequent than in the North. The statistical summary presented in Figure 2.2 shows that ARs are more likely to affect the NRB coming from the South, although AR activity in the North also affects the watershed. The years 1975 (13) and 1977 (11) exhibit the lowest frequencies of ARDs for the North and were considered outliers.

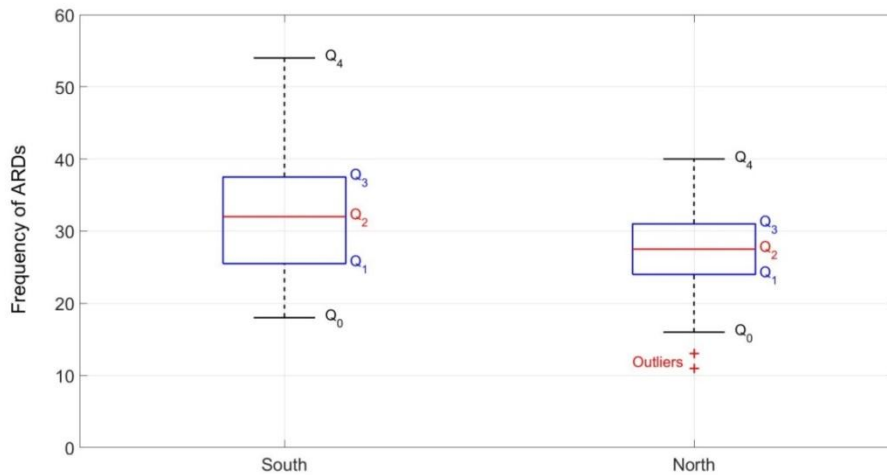


Figure 2.2 – Box and whisker plot for the annual ARD frequency at AR-monitored regions South (52.5° N, 127.5° W) and North (55° N, 130° W). Five-number summary for the non-outlier minimum (Q₀), first quartile (Q₁), median (Q₂), third quartile (Q₃), and non-outlier maximum (Q₄) in addition to outliers (+). Values within the whiskers (Q₀ and Q₄) depict the range excluding outliers.

Applying the adapted AR scale of Ralph *et al.* (2019) to the frequency of landfalling ARs within the study period, the South records ~9% while the North records ~7% of the days as ARDs (Table 2.1). The majority (57%) of ARDs at both positions are of ARD0 that last <24 hours, and ~96% of ARDs are classified within the first three categories (ARD0-ARD2) of the AR scale adopted by this study. Furthermore, it is worth highlighting the mainly beneficial role of the most frequent (ARD0-ARD2) classifications to water replenishment in the NRB.

Table 2.1– Percentage of ARD frequency at AR-monitored regions South and North (1950-2021)

ARDs Classification	South (%)	North (%)
ARD0	5.02	4.19
ARD1	2.30	1.84
ARD2	1.08	0.94
ARD3	0.30	0.30
ARD4	0.05	0.04
ARD5	0.00*	0.00
Total (ARD)	8.75	7.32
* Single event		

Although the annual frequency of ARDs is often higher at lower latitudes (South), it can be higher in the North during some periods, as seen in more than half of the years between 1969 and 1981 (Figure 2.3). During these 13 years, the northeastern Pacific Ocean experienced a shift (1976/1977) in sea surface temperatures, passing from mainly negative to mainly positive anomalies according to the Pacific Decadal Oscillation pattern (PDO) (Hartmann and Wendler, 2005). Negative phases of the PDO index are known to diminish the number of ARs in BC and southeastern Alaska (Sharma and Déry, 2020b), which likely reduced AR frequency in the region during the mid-1970s.

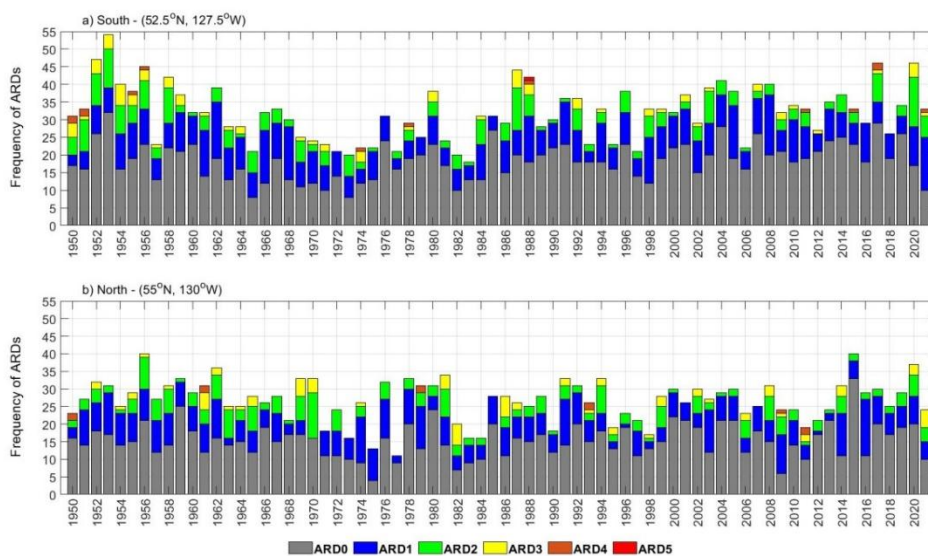


Figure 2.3 – Annual ARD frequency at AR-monitored regions a) South (52.5° N, 127.5° W) and b) North (55° N, 130° W) according to the adapted scale of Ralph *et al.* (2019).

The average annual intensity of ARDs at both positions is similar, with IVT = 421 and 427 $\text{kg m}^{-1} \text{s}^{-1}$ for the South and North, respectively. This implies that the average AR that makes landfall in the positions near the NRB classify as ARD0-ARD3, depending on the duration of the event. This reveals the importance of adapting the AR scale of Ralph *et al.* (2019) also to

consider short-duration (< 24 h) and low-intensity ($250\text{-}500 \text{ kg m}^{-1} \text{ s}^{-1}$) AR events near the NRB, as they are the most common type of ARs making landfall in the region.

2.4.1.2 Seasonal

At a seasonal scale, fall and spring represent the higher and lower frequencies of ARDs at both positions (Figure 2.4). During fall, the North presented a peak of 23 ARDs in 1981, whereas in the South, 1987 had the highest frequency (31) of ARDs. From 1969 to 1982, alongside a cooler (moderate) phase of the equatorial Pacific Ocean according to the Oceanic Niño Index (ONI), the North position recorded more ARDs in the fall on more than half of the period. On average, the seasonal frequency of ARDs in the South (North) for fall is 15 (12), winter is 5 (4), and spring and summer account for 3 and 8 at both positions. This shows that AR frequency is considerably higher (25%) in the South from September (early fall) to February (late winter). More consecutive ARDs of greater magnitude were recorded in the South during the fall in the beginning (1950-1960) of the study period than in the North, a pattern that is inverted (with exceptions) from the late 1950s until the mid-1990s. In 1988, the South recorded the only ARD5 of the 72-year-long series, which escalated from the ARD4 classification due to the event's prolonged duration (>60 hours).

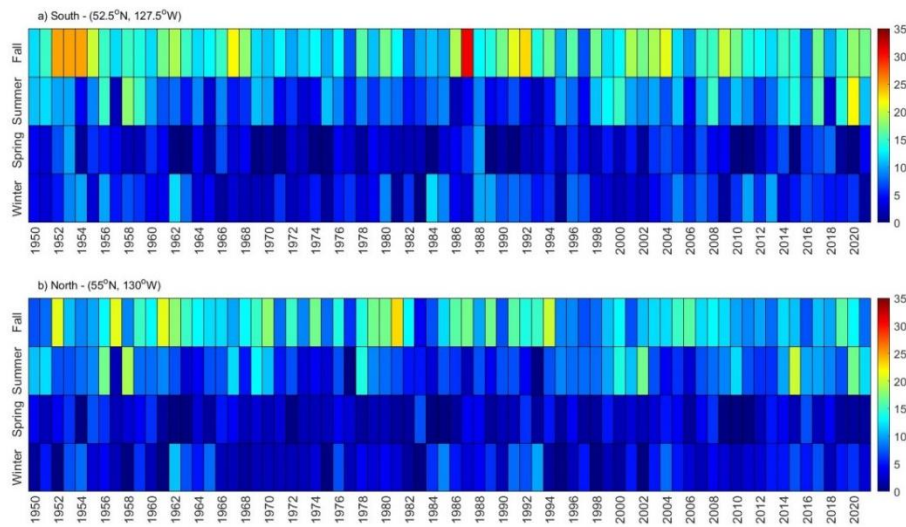


Figure 2.4 – Seasonal ARD frequency at the AR-monitored regions a) South (52.5° N, 127.5° W) and b) North (55° N, 130° W)

During winter, ARDs in the South (Figure 2.5) reached the classification of ARD3 in 1956 and 1980, whereas in the North (Figure 2.6), this was recorded in 1954, 1965 and 1993. An ARD4 was recorded in the North during the winter of 1993, when an AR transporting moisture at a rate of $812 \text{ kg m}^{-1} \text{ s}^{-1}$ approached the region and lasted >54 hours between 29-31 January. The most intense ARD of the spring season occurred in the South and reached the ARD3 classification on 5 May 1953, in the third of a 4-day AR event.

During summer, two ARD4s that lasted over two days made landfall in the South with more than a 70-year interval (June 1951 - August 2021) between events. In the ARD4 event of 15 August 2021, $\text{IVT} = 846 \text{ kg m}^{-1} \text{ s}^{-1}$ was recorded in the South on the last day of an AR event that made landfall at both positions with several intermittent ARs. Favourable atmospheric conditions for landfalling ARs occurred from 3-15 August, when a single AR event brought persistent ARD2-ARD4 conditions to the South and ARD1-ARD3 to the North.

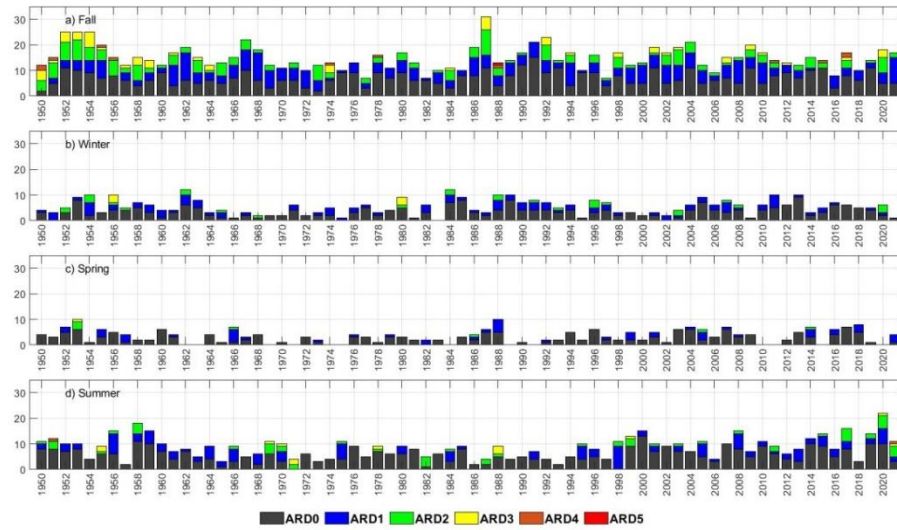


Figure 2.5 – Seasonal ARD frequency at the AR-monitored region South (52.5° N, 127.5° W) according to the adapted scale of Ralph *et al.* (2019)

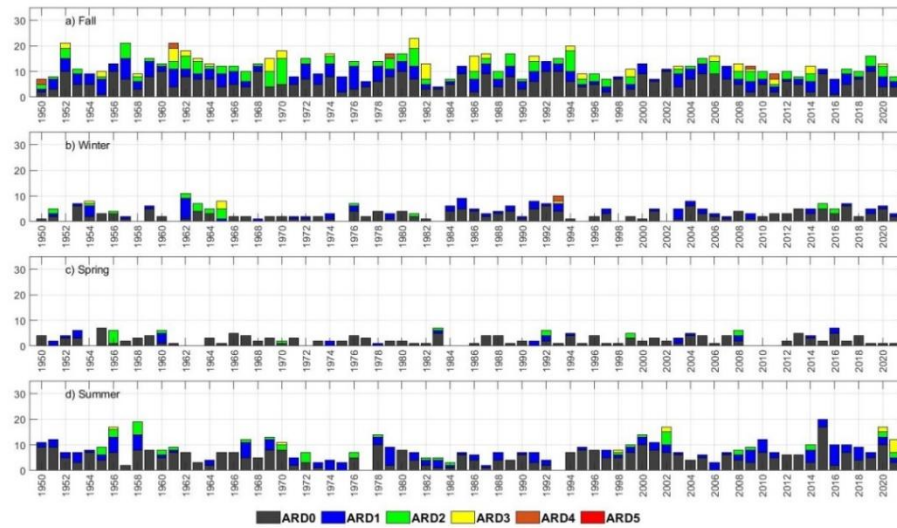


Figure 2.6 – Seasonal ARD frequency at the AR-monitored region North (55° N, 130° W) according to the adapted scale of Ralph *et al.* (2019)

The average intensity of ARDs varies with the seasons and peaks in both monitored regions during fall (Figure 2.7). The South (North) has an average AR intensity of 448 (458) $\text{kg m}^{-1} \text{s}^{-1}$ in fall, 433 $\text{kg m}^{-1} \text{s}^{-1}$ (387 $\text{kg m}^{-1} \text{s}^{-1}$) in winter, 317 $\text{kg m}^{-1} \text{s}^{-1}$ (324 $\text{kg m}^{-1} \text{s}^{-1}$) in spring and 373 $\text{kg m}^{-1} \text{s}^{-1}$ (378 $\text{kg m}^{-1} \text{s}^{-1}$) in summer. While the North registers slightly higher averages for the

fall, summer and spring, the South has a considerably higher average IVT during winter. This points to similar average intensities of ARD at both locations from March to November.

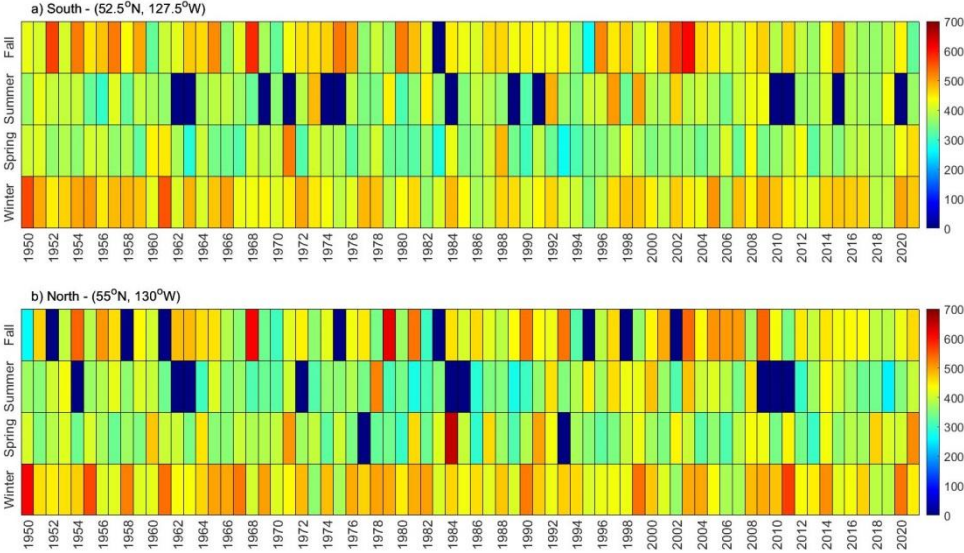


Figure 2.7 – Seasonal ARD average intensity (IVT) at the AR-monitored regions a) South (52.5° N, 127.5° W) and b) North (55° N, 130° W)

2.4.2.1 AR frequency, intensity and duration near the NRB

The complete results of the statistical tests are presented in Table A.1 (Appendix A), whereas the significant results for ARD frequency and intensity are shown in Figures 2.8 and 2.9. The trend analysis for ARD frequency in the South reveals a significant increase in ARD0s and a decrease in ARD3s on the annual scale. On the seasonal scale, ARD1s are decreasing in the North during fall. ARD2s are decreasing in both monitored regions in the fall (South) and winter (North), while the frequency of ARD0s in the North is increasing during the winter.

AR region	ARD	ARD0	ARD1	ARD2	ARD3	ARD4	ARD5
North		 0.030	 0.027	 0.036			
South		 0.026		 0.024	 0.012		

Figure 2.8 – Diagram depicting significant trends from the MK test for ARD frequency (1950-2021). Triangles facing up (down) show significant increasing (decreasing) trends. Black is for the annual scale, orange is for fall, and blue is for winter. P-values of the MK tests are presented below each symbol.

The trend analysis for ARD intensities (Figure 2.9) reveals that only the North region presented significant results for increasing or decreasing trends. ARD2s are decreasing and ARD0s are increasing in intensity during winter in the North, whereas ARD1s are decreasing in the fall. No significant trends were identified for the frequency and intensity of unstratified ARDs.

AR region	ARD	ARD0	ARD1	ARD2	ARD3	ARD4	ARD5
North		 0.011	 0.027	 0.028			
South							

Figure 2.9 – Diagram depicting significant results of the MK test for ARD intensity (1950-2021). Triangles facing up (down) show significant increasing (decreasing) trends. Orange is for fall, and blue is for winter. P-values of the MK tests are presented below each symbol.

2.4.2.2 AR-related hydro-variability in the sub-basins of the NRB

Except for the increasing trend of SWE linked to ARD0 in the Upper Stuart, all other significant trends in the NRB are for total precipitation and rainfall (Figure 2.10). In the Upper Nechako, where the Nechako Reservoir is located, results show decreasing trends of rainfall and total precipitation linked to ARD2 and ARD3. Nevertheless, a non-AR-related increase in rainfall is identified for the Upper Nechako, which may indicate increasing water availability due to the more significant contribution of non-AR-related meteorological systems to the overall water

volume of the sub-basin. In the Lower Nechako, results also show decreasing trends of precipitation and rainfall linked to ARD2 while total precipitation linked to ARD0s increases. Similarly to the Upper Nechako, rainfall and total precipitation related to ARD2s and ARD3s are decreasing in the Stellako.

All significant trends point to the increase of rain (ARD0 and non-AR-related), total precipitation (ARD0) and SWE (ARD0) in the Upper Stuart. Overall (unstratified series – AR + non-AR-related) rain in the Upper Nechako and Upper Stuart show significant increasing trends, which are influenced by the non-AR-related increasing trend for both sub-basins. Notably, these sub-basins have the highest elevations and form the headwaters of the NRB, where increased rainfall can directly impact water storage as snowpack and affect flows. In the Upper Stuart, the increasing trend in ARD0 likely influences the upward trend of annual rain totals. For the Lower Stuart, results reveal a decreasing trend of rainfall linked to ARD2 and an increase in total precipitation related to ARD0. Rainfall and total precipitation for ARD2 are decreasing in the Endako and Chilako, whereas total precipitation linked to ARD0 is increasing at both sub-basins.

Sub-basin	AR + Non-AR-related	ARD	ARD 0	ARD 1	ARD 2	ARD 3	ARD 4	ARD 5	Non-AR-related
Upper Nechako	▲ 0.020		▲ 0.025		▼▼ 0.021 0.025	▼▼ 0.043 0.029			▲ 0.002
Lower Nechako					▼▼ 0.012 0.030				
Upper Stuart	▲ 0.006		▲▲▲ 0.048 0.005 0.038						▲ 0.018
Lower Stuart			▲ 0.015		▼ 0.032				
Endako			▲ 0.049		▼▼ 0.012 0.049				
Chilako			▲ 0.024		▼▼ 0.020 0.048				
Stellako					▼▼ 0.009 0.028	▼▼ 0.037 0.041			

Figure 2.10– Diagram depicting significant trends of the MK test for the AR-related variables of the ERA5-Land product (1950-2021). Triangles facing up (down) show significant increasing (decreasing) trends. Blue is for AR-related rain, purple is for AR-related total precipitation, and yellow is for AR-related SWE. P-values of the MK tests are presented below each symbol.

2.5 CONCLUSIONS

ARDs play a crucial role in replenishing water resources in the NRB, particularly in the fall, and are primarily beneficial, although potentially dangerous if making landfall on saturated soils, mountainous terrain or during rain-on-snow AR events. Results show an overall reduction of ARD1-ARD3 events in both monitored regions, and the average intensity of ARDs at both locations is similar from spring to late fall, which can partly be explained by both regions often being affected by the same AR events due to their proximity. September and October exhibit higher AR activity, and November presents the highest average AR intensity near the NRB. Only ~4% of ARDs reached the ARD3-ARD4 classification, whereas an ARD5 occurred only once in the South.

The MK trend test suggests a total precipitation and rainfall contribution shift from ARD2-ARD3 to ARD0 in the Chilako, Endako, Lower Nechako and Lower Stuart. Results also

revealed increasing trends in total precipitation linked to ARD0s for the north and west sectors of the watershed. The same occurs for rainfall linked to ARD0s in the Upper Stuart and non-AR-related systems in the Upper Stuart and the Upper Nechako, indicating an increase in rainfall contribution in the snow/rainfall ratio for these nival sub-basins, which can affect water storage in the form of the seasonal snowpack.

While the results do not point to an increase in the contribution of the most frequent ARD category (ARD0) to replenish the Nechako Reservoir (Upper Nechako), rainfall from non-AR-related meteorological systems, which make the bulk of the inflows, presents an increasing trend in the Upper Nechako. This increase in rainfall may be linked to an overall warming trend of the Pacific Ocean (Alexander *et al.*, 2018) and worldwide temperatures (Garcia-Soto *et al.*, 2021), favouring evaporation and the build-up of water vapour in the atmosphere west and southwest of the NRB. More water vapour in the atmosphere of the Pacific Ocean increases the chance of moisture being transported to inland areas, such as the NRB, and highlights the importance of further studying the influence of ARs over western Canada.

CHAPTER 3: WATER BUDGET INPUT LINKED TO ATMOSPHERIC RIVERS IN BRITISH COLUMBIA'S NECHAKO RIVER BASIN

This chapter is published in *Hydrological Processes*, in the journal's special issue for the 2023 Canadian Geophysical Union (CGU) Meeting that was held in Banff, Alberta.

Publication details:

Sobral, B. S., and Déry, S. J. (2024). Water budget input Linked to Atmospheric Rivers in British Columbia's Nechako River Basin. *Hydrological Processes*, 38(10), e15301. <https://doi.org/10.1002/hyp.15301>.

ABSTRACT: This study explores the contribution of atmospheric rivers (ARs) to the water budget input of the Nechako River Basin (NRB) in British Columbia (BC), western Canada. The study quantifies the fraction of precipitation, rainfall, snowfall, and snow water equivalent (SWE) associated with ARs at multiple scales and tests for trends using the Mann-Kendall (MK) test. AR-related totals for 1950-2021 were created by linking AR events to the water budget input variables of the ERA5-Land reanalysis product on a daily scale. Associations with different phases of the El Niño-Southern Oscillation (ENSO) climate pattern and AR-related contributions to the NRB are also investigated. Results indicate an increasing fractional contribution of rain in ARs landfalling in the NRB in the last two decades (2000-2020). Moreover, 21% of the total annual precipitation in the NRB is associated with ARs, with decreasing contributions from west to east. October has higher AR-related total precipitation than other months, while March, May, and June are the least affected. ARs contribute disproportionately more to mid- and high-intensity daily precipitation totals and provide up to 45% and 24% of the seasonal rainfall and snowfall, respectively. AR-related SWE is relatively higher in fall due to the increased frequency and intensity of ARs, resulting in a greater fractional contribution of ARs to the snowpack compared to winter. ARs influence snowpack accumulation during fall (18%) and winter (13%) but also increase the risk of natural hazards.

The MK test for AR-related water budget input variables on the annual scale identified no significant trends. However, AR-related snowfall shows decreasing trends in the NRB, more specifically in the Upper Nechako, Lower Nechako and Stellako sub-basins during the summer. Over the study period, ARs consistently contribute up to one-fifth of the annual input to the NRB's water budget. This study provides the first quantitative assessment and trend analyses of AR contributions to the water budget input of a reservoir-regulated watershed in north-central BC, yielding valuable information for hydropower production, ecological flows, irrigation, and domestic and industrial water use.

3.1 INTRODUCTION

Atmospheric Rivers (ARs) are meteorological phenomena characterized by narrow, concentrated, river-shaped bands of water vapour transport in the lower atmosphere (Zhu and Newell, 1994, 1998; Ralph *et al.*, 2020). Many studies have investigated their variability and impacts on water resources and natural disasters worldwide, particularly in coastal regions, where impacts are more pronounced (Dettinger *et al.*, 2011; Payne and Magnusdottir, 2014; Lavers and Villarini, 2015; Barth *et al.*, 2017; Gershunov *et al.*, 2019; Sharma and Déry, 2020a; Eiras-Barca *et al.*, 2021; Prince *et al.*, 2021; Baek *et al.*, 2023). ARs may provide ~90% of the total transported tropical moisture in extratropical (temperate) regions, highlighting the essential role ARs play in the hydrological cycle of western Canadian watersheds (Ralph *et al.*, 2017; Nash *et al.*, 2018; McClenny *et al.*, 2020). The hydrological cycle in western Canada is substantially influenced by ARs formed in the tropical Pacific Ocean, impacting the region's precipitation patterns (Curry *et al.*, 2019; Sharma and Déry, 2020b).

ARs have emerged as a crucial factor in extreme precipitation events in coastal and inland areas of British Columbia (BC), as evidenced by the devastating floods of November 2021 (Gillett *et al.*, 2022; Richards-Thomas *et al.*, 2024). They can deliver copious amounts of precipitation in short periods, which often maximizes their hazardous effects. Moreover, the global escalation of sea surface temperatures (SSTs) (Alexander *et al.*, 2018; Garcia-Soto *et al.*, 2021) may increase the frequency and intensity of ARs. Water vapour fluxes from the ocean to the atmosphere through evaporation may increase due to higher global SSTs, enhancing moisture availability in the lower troposphere and favouring the occurrence of more frequent and intense AR events worldwide (Corringham *et al.*, 2022).

Fluctuations in the El Niño-Southern Oscillation (ENSO) climate pattern are frequently investigated for impacting temperature and precipitation regimes worldwide (Benassi *et al.*, 2022; Campos and Rondanelli, 2023; Arias *et al.*, 2024; Goudard *et al.*, 2024, Espinoza *et al.*, 2024). On the west coast of BC, the cool phase of ENSO (La Niña) is typically associated with wetter hydrological years, whereas the warm phase (El Niño) is linked to reduced precipitation over the region (Shabbar *et al.*, 1997; Williams *et al.*, 2024). However, a more thorough assessment of the fractional contribution and trends of ARs to the water budget input in remote areas of North America is needed to establish their responses to alternating ENSO phases.

The Nechako River Basin (NRB) is a remote and complex catchment in western Canada, forming part of the headwaters of the Fraser River. The susceptibility of the NRB to precipitation accompanying ARs is well-established and known to cause recurrent hazards, mainly in fall (Geertsema *et al.*, 2009; Curry *et al.*, 2019; Sharma and Déry, 2020b; Gillett *et al.*, 2022). Aside from causing potential hazards, ARs play a major role in replenishing water resources in the NRB, including the Nechako Reservoir, lakes, wetlands and waterways. The Nechako Reservoir, located on the leeward side of the Tahtsa Ranges, forms a primary water resource for the region (Albers *et al.*, 2016; Picketts *et al.*, 2017) and benefits significantly from AR activity. Precipitation and warm air advection associated with ARs also directly impact flows (Sharma and Déry, 2020c) and water temperatures (Déry *et al.*, 2024) in other water bodies of the NRB, such as rivers, creeks and lakes. Estimating AR contributions and trends to regional water resources will benefit water security efforts while potentially reducing the negative impacts of AR-associated risks such as floods, landslides, and high winds.

Despite recent advances in assessing AR impacts on the hydrological cycle and processes of western Canadian watersheds, there remains a research gap in addressing AR contributions to

the input of the NRB's water budget. Specifically, the present research aims to address the following research questions: (1) What are the contributions of ARs to the water budget input of the NRB and its sub-basins?; (2) Are there trends in the AR-related water budget input variables in the NRB and its sub-basins?; and (3) Are there links between phases of the ENSO and AR-related contributions to the water budget input of the NRB and its sub-basins? Thus, the novel objective of this paper is to partition total precipitation, rainfall, snowfall, and snow water equivalent (SWE) in the NRB sourced from ARs on annual, seasonal and daily scales, including binned distributions of precipitation accumulations. Additionally, trends for each AR-related water budget input variable are tested on the annual and seasonal scales to provide valuable insights into the changing contribution of ARs to the hydrological cycle of the NRB. Finally, associations between ENSO phases and AR-related contributions to water budget variables are explored from the perspective of water management in a highly regulated system.

3.2 STUDY AREA

The NRB lies in the Interior Plateau region of BC, Canada, bounded by latitudes 52.93° N to 56.17° N and longitudes 127.78° W to 122.72° W (Figure 3.1). It spans an area of 47,200 km² (Parkes, 2021), with the Nechako River as its main waterway, flowing eastward to its confluence with the Fraser River in Prince George, BC (Parkes *et al.*, 2024). Water sourced from the NRB serves many purposes, including crop irrigation, residential consumption, hydroelectricity generation, recreational activities, fish habitat, and industrial activities (Hartman, 1996).

This study divided the NRB into seven sub-basins named after the main rivers of the region: the Nechako and Stuart with upper and lower catchments, Endako, Stellako, and Chilako (Figure 3.1). The Upper Nechako sub-basin greatly influences the region's socio-economic

development, extending well beyond its boundaries. Notably, a significant portion (~60%) of the water volume flowing into the sub-basin, and stored in the Nechako Reservoir, is diverted westward through a pair of 16 km long water tunnels to generate hydroelectricity in Kemano, BC (Tannant and Morgenroth, 2008; Shrestha *et al.*, 2012; Desreumaux *et al.*, 2014). The generating station supplies electricity to the aluminum smelter operated by Rio Tinto in Kitimat, BC, making the ~33 km³ Nechako Reservoir a vital component of the region's industrial activity (Déry *et al.*, 2012).

The NRB experiences the influence of landfalling AR storms for about 30 days each year, with higher frequency during fall and winter (Sobral and Déry, 2023). These storms, occurring mainly from August to January, bring a significant amount of precipitation to the NRB, thereby replenishing lakes, reservoirs, wetlands and waterways (Sharma and Déry, 2020b). This includes the Nechako Reservoir, which serves as an effective "water tower" by regulating downstream water flows of the NRB. This regulation directly impacts the Lower Nechako, where streamflow in the Nechako River relies heavily on water released from the Nechako Reservoir through the Skins Lake Spillway ~80 km west of Kenney Dam (Figure 3.1). Furthermore, the Lower Nechako region is where the largest population centres of the NRB are concentrated, increasing the demand for water resources in the sub-basin. Thus, water management strategies implemented in the Upper Nechako greatly impact stakeholders downstream of the impoundment created by the construction of the Kenney Dam in the 1950s.

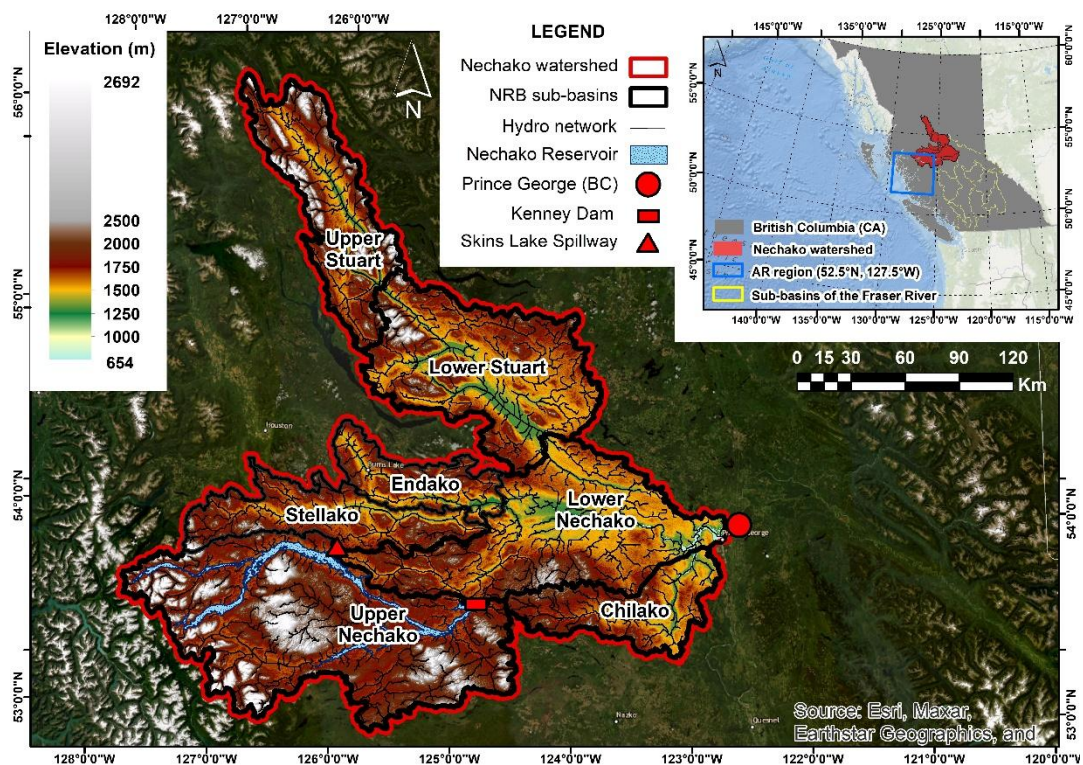


Figure 3.1 - Map of the NRB with sub-basins, Nechako Reservoir, Kenney Dam, Skins Lake Spillway, the city of Prince George, elevation distribution and nearest AR monitored region (inset map) of the SIO-R1-AR catalogue.

3.3 DATA AND METHODS

3.3.1 Datasets

3.3.1.1 AR Catalogue

Gershunov *et al.* (2017) analyzed ARs in western North America using reanalysis datasets and a tracking algorithm. Their efforts yielded a detailed six-hourly AR Catalogue from 1948 to 2017 (SIO-R1-AR catalogue), used in this study with the addition of the 2018-2021 period. The AR Catalogue has since been used to access up-to-date information regarding AR intensity and duration for various monitored regions (AR regions) along the western coast of North America (Guirguis *et al.*, 2019; Sharma and Déry, 2020a). It has enhanced information on the geographic distribution of ARs in these monitored regions of $2.5^\circ \times 2.5^\circ$ resolution. The AR region represented by the central coordinates (52.5°N , 127.5°W) (Figure 3.1 – inset map) is the closest to the NRB, encompassing most of the Upper Nechako. Therefore, AR activity near the NRB

is analyzed based on data from this AR region. In other words, whenever the tracking algorithm of Gershunov *et al.* (2017) identified AR activity in the AR region, the water budget input variables (Section 3.3.1.2) were considered under the influence of an AR and therefore classified as AR-related on a daily scale.

3.3.1.2 Water budget input data

The water budget input variables of the ERA5-Land reanalysis product (Muñoz-Sabater *et al.*, 2021) provide valuable climate data for analyzing hydrometeorological processes. The ERA5-Land data have been widely used for drought monitoring (Huang *et al.*, 2021; Xu *et al.*, 2022), flood forecasting (Rostami *et al.*, 2022), and water resources management (Towner *et al.*, 2019; Mihalevich *et al.*, 2022). This hourly dataset is provided by the Copernicus Climate Change Service (C3S) of the ECMWF with a high resolution of ~9 km encompassing 50 climate variables. The water budget input variables of the ERA5-Land used in this study are total precipitation (tp - mm), snowfall (sf - cm) and SWE (swe - m), whereas the difference between total precipitation and snowfall estimates rainfall (mm). The present study uses the ERA5-Land product due to its reliability for the region and its gap-free temporal coverage from 1950 to the present. The product's ability to cover a large area of the globe at an hourly scale makes it an optimal choice for conducting water budget studies in remote areas. Furthermore, the ERA5-Land dataset provides a reliable alternative to observations in data-sparse regions of North America like the Canadian Prairies (Fatolahzadeh Gheysari *et al.*, 2024) and the NRB (Goswami *et al.*, 2024).

3.3.1.3 Oceanic Niño Index (ONI)

The ONI is calculated as the 3-month running mean of sea-surface temperature (SST) anomalies in region 3.4 of the Pacific Ocean, recording the warm, neutral, and cool phases of the ENSO climate variability pattern (Glantz and Ramirez, 2020). Oscillations in ONI occur as the SST anomalies vary, influencing evaporation rates in the tropical Pacific Ocean, which, in turn, may affect precipitation patterns on the west coast of North America. El Niño and La Niña conditions are defined by SST anomalies exceeding $+0.5^{\circ}\text{C}$ or -0.5°C respectively, from the average SST calculated using the last 30 years of data (Silva *et al.*, 2020). We use the monthly values of the ONI (1950-2021) for each year to create an annual time series of prevailing years of El Niño, La Niña and neutral phase.

3.3.2 Methods

3.3.2.1 Data analysis and visualization

Data extraction, analysis, and visualization are performed using Matlab version R2021a and ArcGIS version 10.1. Matlab is used to extract ERA5-Land data and to create figures and plots for data analysis. ArcGIS software is used to create an enhanced representation of the NRB's location (Figure 3.1).

3.3.2.2 AR-related water budget datasets

A combination of the AR Catalogue (section 3.3.1.1) and ERA5-Land (section 3.3.1.2) dataset is used to create new AR-related daily time series. The datasets are integrated on a daily scale, with the exclusion of the initial eight hourly measurements from the ERA5-Land dataset provided in UTC. Simultaneously, the first eight hours of the subsequent calendar day are incorporated as the last eight hours of each day to align on the daily scale with the AR Catalogue

provided in Pacific Standard Time (PST). Subsequently, we identify days in which ARs occurred (AR days) as per the AR Catalogue (section 3.3.1.1) to create new daily time series of AR-related total precipitation, rainfall, snowfall, and SWE. The new datasets are then used to assess the influence of ARs on the water budget input of each sub-basin of the NRB. The resulting daily time series represent the spatially averaged values for each sub-basin, accounting for spatial heterogeneity. We assign the corresponding daily sums for the water budget input variables on such AR days. The contribution of AR-related SWE is defined by the positive daily variations in SWE during AR events. Using this methodology, we isolate the contribution of ARs to the water budget input variables of the ERA5-Land product (Section 3.3.1.2), providing estimates and valuable insights into the role played by ARs in the water cycle of the NRB.

This methodology also allows the analysis of AR-related and non-AR-related daily maximum contributions to the water budget input variables in the sub-basins of the NRB. To investigate the potential impact of ARs in generating or enhancing precipitation, we also compare AR- and non-AR-related daily totals for the water budget input variables in each sub-basin of the NRB. The method separates AR-related and non-AR-related variables into 5 mm bins and compares AR and non-AR days frequency distributions. The discussion for this part (Section 3.4.3) primarily focuses on the Upper Nechako, as it holds significant relevance to the region due to its high water volume storage in the Nechako Reservoir.

The annual analysis uses calendar years, and the seasons are defined as the three-month periods of March-May (spring), June-August (summer), September-November (fall) and December-February (winter). Note that the seasonal datasets for the winter period are based on a consecutive winter season from December to February, therefore discarding the initial year of the time series when analyzing winter AR-related data.

3.3.2.3 Mann-Kendall trend test

Developed by Mann (1945) and refined by Kendall (1975), the Mann–Kendall (MK) test is extensively utilized in hydrometeorological studies to detect trends (Zhang *et al.*, 2016; Gurbuz and Jin, 2017; Aditya *et al.*, 2021; Chagas *et al.*, 2022; Jiqin *et al.*, 2023). The MK is a non-parametric statistical test, and thus, it can be applied to normal and non-normal datasets to identify statistically significant trends (Hu *et al.*, 2020). Here, the MK test is applied with a significance level of $\alpha = 0.05$ (95% confidence level) to the AR-related time series of total precipitation, rainfall, snowfall and SWE to investigate trends on the annual and seasonal scales.

3.4 RESULTS

This section presents the study's principal findings regarding the influence of ARs on the water budget input variables of the NRB on the annual (Section 3.4.1), seasonal (Section 3.4.2) and daily (Section 3.4.3) scales. Additionally, results of the MK test are presented to reveal trends in the time series of AR-related water budget input variables. The daily analyses focus mainly on the Upper Nechako and offer a more comprehensive understanding of the potential hazard posed by ARs to the sub-basins of the NRB, given the copious amounts of precipitation often associated with these events.

3.4.1 Annual Analysis

Figure 3.2 and Table 3.1 provide information regarding the annual analysis of AR-related variables across the sub-basins of the NRB. The annual deviations from the mean of AR-related total precipitation, rainfall, snowfall, and SWE for 1950-2021 are presented in more detail in Figure B.1 of Appendix B. The influence of ARs is more prominent across all variables in the western and northern regions of the NRB (Figure 3.2), composed of the Upper Nechako,

Stellako and Upper Stuart. Conversely, the Lower Nechako and Chilako, the easternmost sub-basins, are less influenced by ARs.

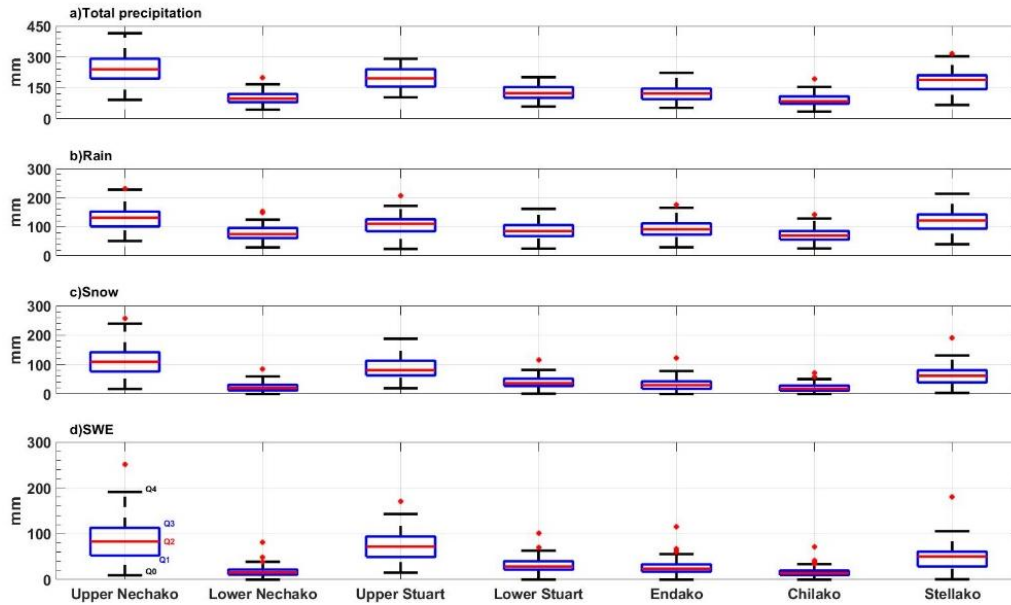


Figure 3.2 - Box and whisker plot for the annual AR-related contribution to a) total precipitation, b) rainfall, c) snowfall and d) SWE in the sub-basins of the NRB according to ERA5-Land (1950-2021) and AR Catalogue (1950-2021) data associated on the daily scale. Five-number summary for the minimum (Q₀), first quartile (Q₁), median (Q₂), third quartile (Q₃), and maximum (Q₄) frequency in addition to outliers (+). Outliers are defined as measurements that exceed three standard deviations from the mean.

Table 3.1 – Annual average of the AR-related water budget input variables of the ERA5-Land (1950-2021) for the sub-basins of the NRB. Fractional results are for total annual values.

Sub-basin	Total Precipitation mm (%)	Rainfall mm (%)	Snowfall mm (%)	SWE mm (%)
Chilako	91 (16%)	70 (19%)	21 (10%)	16 (9%)
Endako	124 (21%)	92 (26%)	32 (13%)	27 (12%)
Lower Nechako	101 (18%)	78 (22%)	23 (11%)	18 (10%)
Lower Stuart	126 (20%)	85 (24%)	41 (15%)	32 (13%)
Stellako	183 (25%)	120 (32%)	63 (17%)	50 (15%)
Upper Nechako	243 (24%)	130 (32%)	113 (19%)	86 (15%)
Upper Stuart	195 (23%)	106 (27%)	90 (20%)	72 (17%)
NRB	152 (21%)	97 (26%)	55 (15%)	43 (13%)

The spatial analysis depicted in Figure 3.3 shows the annual AR-related fractional contribution and further explains how much ARs influence the water budget input variables in each sub-

basin of the NRB. Results show that the Upper Nechako exhibits the highest AR-related totals for all variables, whereas the Chilako exhibits the lowest. The Upper Nechako averages 24% (243 mm) of AR-related total annual precipitation, considerably higher amounts than received in the Lower Nechako at 18% (101 mm) and the Chilako at 16% (91 mm), the most easterly sub-basins. Similarly, the Upper Stuart experiences more AR-related total precipitation than the Lower Stuart, with 23% (195 mm) and 20% (126 mm), respectively. These differences are mainly due to variations in topography, where ARs are more impactful in regions of mountainous terrain due to orographic forcing. On average, the NRB receives 21% of its total annual precipitation from ARs, in agreement with estimates of Ralph *et al.* (2020) for western Canada.

The average fraction of AR-related rainfall varied significantly among the sub-basins, ranging from 19% in the Chilako to nearly one-third in the Upper Nechako and Stellako. Nearly one-fifth of the annual snowfall in the Upper Nechako (19%) and Upper Stuart (20%) is linked to ARs, with the fractional contribution of AR-related SWE being higher in the Upper Stuart (17%) (Figure 3.3). The relative contribution of snowfall in the snowfall/rainfall ratio of precipitation in the NRB rose steadily between the 1960s (29%) and 1990s (43%) and has been declining at a similar rate since the 2000s. No significant results were revealed by the MK test for any water budget input variable on the annual scale for the NRB and also for the sub-basins analyzed independently (Table 3.2).

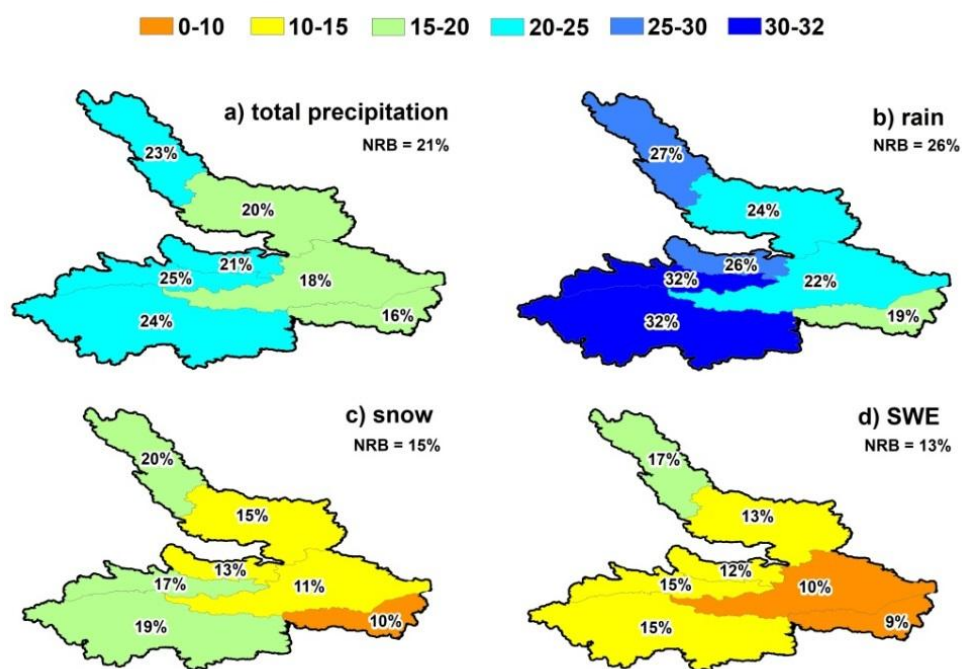


Figure 3.3 - Annual AR-related fractional contribution to a) total precipitation, b) rainfall, c) snowfall and d) SWE in the sub-basins of the NRB according to ERA5-Land (1950-2021) and AR Catalogue (1950-2021) data associated with the daily scale. The fractional values are associated with 9% of AR-days annually.

Table 3.2 –Results of the Mann-Kendall test applied to the time series of AR-related water budget input variables on the annual scale.

AR-related Water Budget Input Variable	Sub-basin	Annual	
		Kendall's tau	p- value
Rainfall	Upper Nechako	-0.049	0.543
Rainfall	Lower Nechako	0.059	0.463
Rainfall	Upper Stuart	0.052	0.524
Rainfall	Lower Stuart	0.088	0.278
Rainfall	Endako	0.048	0.556
Rainfall	Chilako	0.076	0.348
Rainfall	Stellako	-0.040	0.623
Rainfall	NRB	0.024	0.767
Snowfall	Upper Nechako	-0.067	0.406
Snowfall	Lower Nechako	-0.001	0.996
Snowfall	Upper Stuart	0.028	0.730
Snowfall	Lower Stuart	-0.016	0.842
Snowfall	Endako	-0.043	0.596
Snowfall	Chilako	0.013	0.880
Snowfall	Stellako	-0.096	0.234
Snowfall	NRB	-0.040	0.623
Total precipitation	Upper Nechako	-0.026	0.752
Total precipitation	Lower Nechako	0.102	0.208
Total precipitation	Upper Stuart	0.018	0.827
Total precipitation	Lower Stuart	0.129	0.110
Total precipitation	Endako	0.116	0.152
Total precipitation	Chilako	0.099	0.222
Total precipitation	Stellako	0.048	0.556
Total precipitation	NRB	0.052	0.518
SWE	Upper Nechako	0.000	1.000
SWE	Lower Nechako	0.085	0.296
SWE	Upper Stuart	-0.004	0.965
SWE	Lower Stuart	0.127	0.116
SWE	Endako	0.117	0.149
SWE	Chilako	0.073	0.368
SWE	Stellako	0.045	0.583
SWE	NRB	0.054	0.505

3.4.2 Seasonal Analysis

Table 3.3 summarizes the seasonal quantitative analysis, and Table 3.4 the MK test results for the NRB sub-basins. Overall, the contribution of ARs to precipitation in the NRB varies by season and sub-basin (Figures 3.4, 3.5, 3.6 and 3.7), and it is important to understand these patterns to manage water resources more effectively.

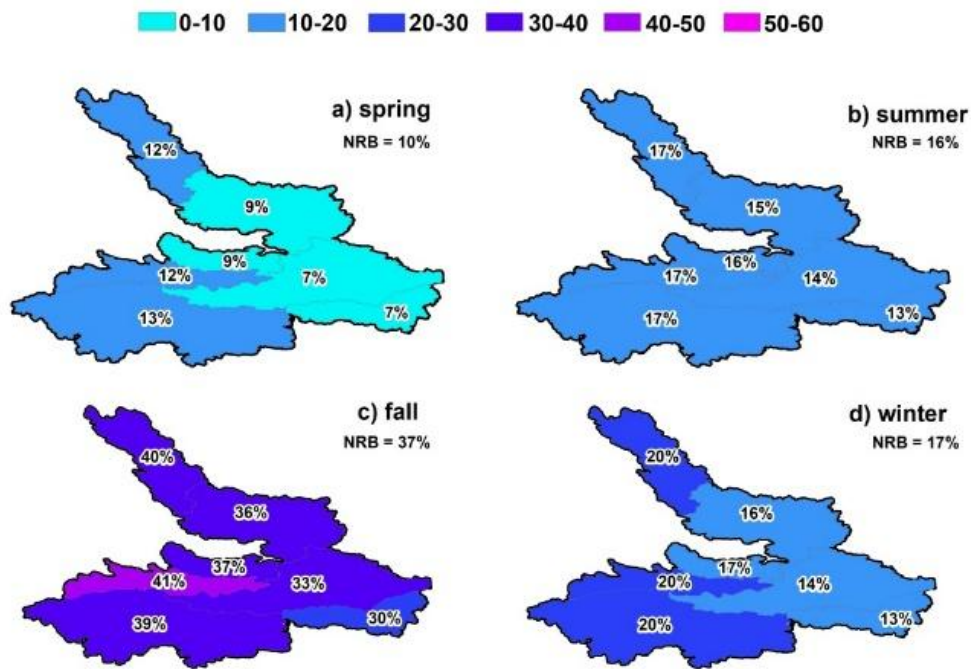


Figure 3.4 – Seasonal AR-related fractional contribution to total precipitation in the sub-basins of the NRB according to the daily association of the ERA5-Land (1950-2021) and AR Catalogue (1950-2021) data. The fractional values are associated with 4% of AR-days during spring, 9% in summer, 17% in fall and 6% in winter.

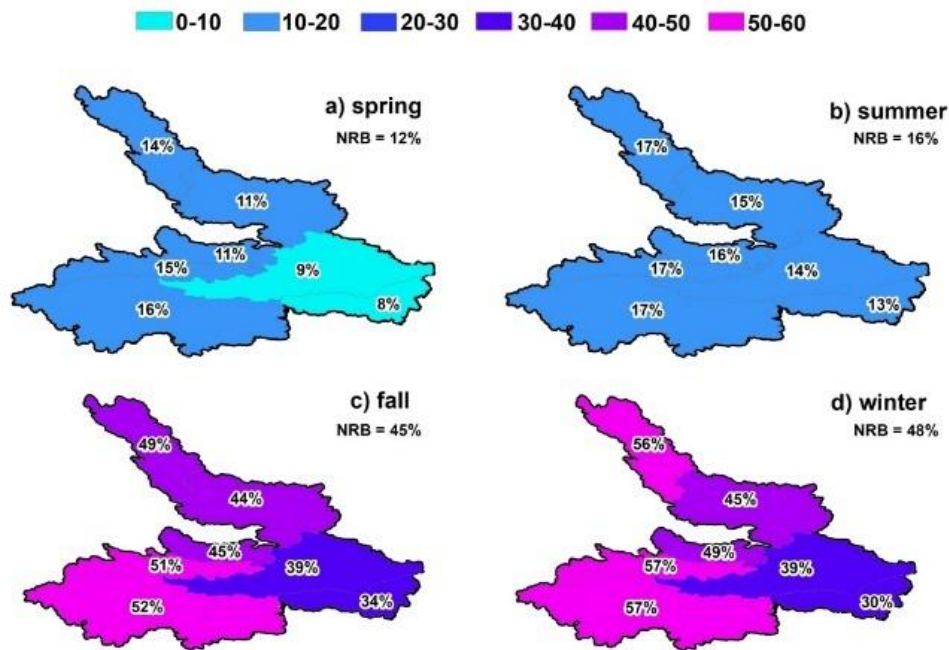


Figure 3.5 – Seasonal AR-related fractional contribution to rainfall in the sub-basins of the NRB according to the daily association of ERA5-Land (1950-2021) and AR Catalogue (1950-2021) data. The fractional values are associated with 4% of AR-days during spring, 9% in summer, 17% in fall and 6% in winter.

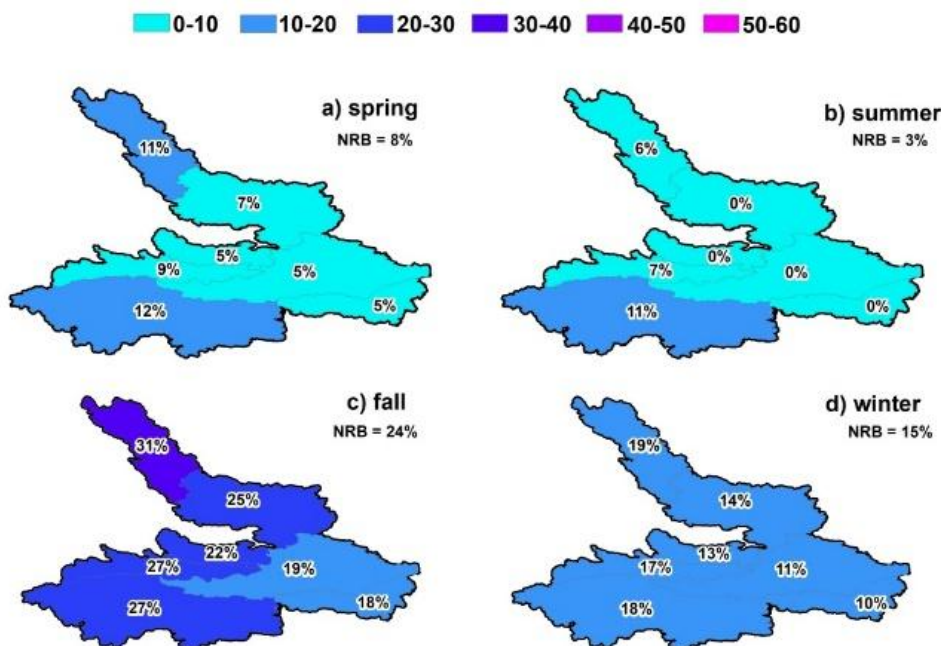


Figure 3.6 – Seasonal AR-related fractional contribution to snowfall in the sub-basins of the NRB according to the daily association of ERA5-Land (1950-2021) and AR Catalogue (1950-2021) data. The fractional values are associated with 4% of AR-days during spring, 9% in summer, 17% in fall and 6% in winter.

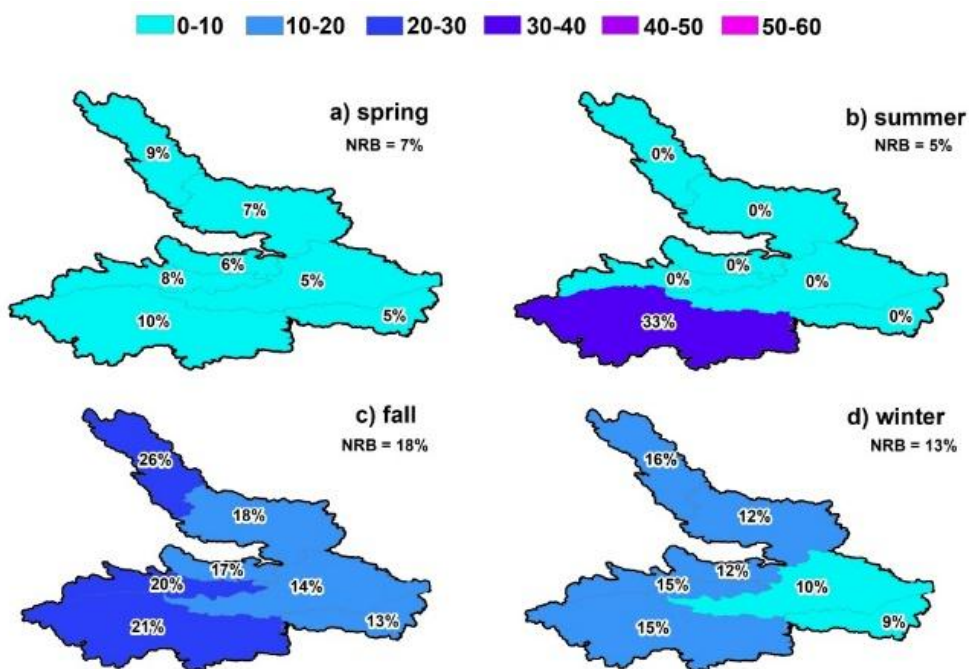


Figure 3.7 – Seasonal AR-related fractional contribution to SWE in the sub-basins of the NRB according to the daily association of ERA5-Land (1950-2021) and AR Catalogue (1950-2021) data. The fractional values are associated with 4% of AR-days during spring, 9% in summer, 17% in fall and 6% in winter.

Table 3.3 – Seasonal average of the AR-related variables of the ERA5-Land (1950-2021) for the sub-basins of the NRB. Fractional results are for total seasonal values.

Season	Sub-basin	Total	Rainfall	Snowfall	SWE
		Precipitation mm (%)	mm (%)	mm (%)	mm (%)
Spring	Chilako	7.8 (7%)	6.0 (8%)	1.9 (5%)	1.1 (5%)
Spring	Endako	10.0 (9%)	7.2 (11%)	2.8 (5%)	2.1 (6%)
Spring	Lower Nechako	8.2 (7%)	6.3 (9%)	1.9 (5%)	1.2 (5%)
Spring	Lower Stuart	11.3 (9%)	7.2 (11%)	4.0 (7%)	2.8 (7%)
Spring	Stellako	16.1 (12%)	9.3 (15%)	6.8 (9%)	4.5 (8%)
Spring	Upper Nechako	24.4 (13%)	9.2 (16%)	15.3 (12%)	9.7 (10%)
Spring	Upper Stuart	19.8 (12%)	8.4 (14%)	11.4 (11%)	8.3 (9%)
Spring	NRB	14.0 (10%)	7.7 (12%)	6.3 (8%)	4.2 (7%)
Summer	Chilako	20.7 (13%)	20.7 (13%)	<0.1 (0%)	0.0 (0%)
Summer	Endako	24.5 (16%)	24.5 (16%)	<0.1 (0%)	0.0 (0%)
Summer	Lower Nechako	21.4 (14%)	21.4 (14%)	<0.1 (1%)	0.0 (0%)
Summer	Lower Stuart	24.4 (15%)	24.4 (15%)	<0.1 (1%)	0.0 (0%)
Summer	Stellako	26.2 (17%)	26.0 (17%)	0.1 (9%)	<0.1 (2%)
Summer	Upper Nechako	30.7 (17%)	30.1 (17%)	0.6 (11%)	0.4 (33%)
Summer	Upper Stuart	36.5 (17%)	36.3 (17%)	0.2 (5%)	<0.1 (2%)
Summer	NRB	26.3 (16%)	26.2 (16%)	0.2 (4%)	<0.1 (5%)
Fall	Chilako	47.7 (30%)	39.8 (34%)	7.9 (18%)	5.5 (13%)
Fall	Endako	68.1 (37%)	54.2 (45%)	13.9 (22%)	10.1 (17%)
Fall	Lower Nechako	54.6 (33%)	45.3 (39%)	9.2 (19%)	6.3 (14%)
Fall	Lower Stuart	69.0 (36%)	50.6 (44%)	18.3 (25%)	12.2 (18%)
Fall	Stellako	101.7 (41%)	75.4 (51%)	26.3 (27%)	18.2 (20%)
Fall	Upper Nechako	131.1 (39%)	83.0 (52%)	48.1 (27%)	33.8 (21%)
Fall	Upper Stuart	104.1 (40%)	60.1 (49%)	44.0 (31%)	33.1 (26%)
Fall	NRB	82.3 (37%)	58.3 (45%)	24.0 (24%)	17.0 (18%)
Winter	Chilako	16.5 (13%)	5.1 (30%)	11.4 (10%)	9.9 (9%)
Winter	Endako	23.5 (17%)	7.0 (49%)	16.5 (13%)	15.7 (12%)
Winter	Lower Nechako	18.8 (14%)	6.7 (39%)	12.1 (11%)	10.9 (10%)
Winter	Lower Stuart	23.7 (16%)	4.3 (46%)	19.4 (14%)	17.4 (12%)
Winter	Stellako	42.6 (20%)	10.9 (58%)	31.6 (17%)	28.6 (15%)
Winter	Upper Nechako	62.4 (21%)	9.7 (57%)	52.8 (18%)	44.8 (15%)
Winter	Upper Stuart	39.2 (20%)	2.3 (55%)	36.9 (19%)	32.8 (16%)
Winter	NRB	32.4 (17%)	6.6 (48%)	25.8 (15%)	22.9 (13%)

In spring, when ARs are less recurrent and intense, the Upper Nechako (24 mm – 13%), Upper Stuart (20 mm – 12%) and Stellako (16 mm – 12%) experience the most significant AR-related total precipitation (Figure 3.4). While AR-related rainfall is more common in spring across the

NRB, the Upper Nechako (15 mm) and Upper Stuart (11 mm) receive higher AR-related snowfall. Across all sub-basins, AR-related SWE remains relatively low ($\leq 10\%$) during spring (Figure 3.7 a). However, mountainous regions of the NRB, mainly the headwaters of the Upper Nechako, Upper Stuart, and Stellako, experience considerably greater accumulation of AR-related snowfall in the form of snowpack compared to the lower elevation regions (Lower Nechako, Lower Stuart, Endako, and Chilako). Significant ($p\text{-value} \leq 0.05$) trends are identified by the MK test on the seasonal scale. The MK test revealed significant trends of increasing AR-related rainfall ($p\text{-value} = 0.05$) in the Upper Stuart sub-basin during spring when AR activity over the region is reduced (Table 3.4).

During summer, AR-related total precipitation across the NRB increases, with the Upper Nechako (31 mm – 17%) receiving the most substantial contribution. AR-related rainfall is the only form of precipitation during summer, with the sub-basins receiving negligible (<1.0 mm) amounts of snowfall and SWE. AR-related SWE decreases substantially with rising temperatures from June to August, with the Upper Nechako recording the highest total at only 0.4 mm (33%). Regarding summer trends, the MK test revealed a significant reduction in AR-related snowfall for the Upper Nechako, Lower Nechako, and Stellako sub-basins of the NRB. The test also indicated a significant decrease in average AR-related snowfall across the entire NRB in the summer (Table 3.4). This reduction is unlikely to affect AR-related snowpack formation in the Nechako Reservoir due to the negligible amounts of landfalling AR-related snowfall in the summer months compared to the total AR-related snowpack formed chiefly in late fall and winter.

In autumn, the NRB receives a significant fraction of total precipitation from ARs, which are linked to 45% and 24% of the average seasonal rainfall (Figure 3.5c) and snowfall (Figure 3.6c),

respectively. The Upper Nechako (131 mm - 39%), Upper Stuart (104 mm - 40%) and Stellako (101 mm – 41%) are the most affected by AR-related precipitation totals in autumn. In winter, however, total precipitation from ARs in the NRB decreases by 60% compared to autumn. Fall exhibits the highest frequency and intensity of ARs compared to other seasons, although winter is also prone to low- to mid-intensity AR precipitation in the NRB. The increased contribution of ARs to winter rainfall (Figure 3.5 d) is an important factor to consider when assessing the impacts of ARs in the NRB. The percentage contribution of ARs to rainfall in winter (48%) is greater than in fall (45%), but the overall volume precipitated as rainfall during AR events in the winter is ~9 times smaller. Nevertheless, AR-related rain-on-snow events in winter can severely impact the snowpack and enhance flooding potential in the NRB.

AR-related snowfall totals prevail during the winter in all sub-basins compared to rainfall, with the Upper Nechako (53 mm – 18%) and Upper Stuart (37 mm – 19%) receiving the highest totals for the season. However, AR-related SWE is relatively higher in autumn (Figure 3.7 c) due to the increased frequency and intensity of ARs despite the often-warm temperatures that increase snowmelt. This results in a greater fractional contribution of ARs to snowpacks of the NRB in the fall (18%) compared to winter (13%), particularly in higher-elevation sub-basins such as the Upper Nechako (21%), Upper Stuart (26%), and Stellako (20%). Mountainous regions in these sub-basins can experience significant impacts from AR-related snowfall and subsequent SWE during the fall, as freezing temperatures often occur earlier than in other areas of the NRB.

During fall and winter, the Upper Stuart is relatively the most affected by AR-related snowfall and SWE due to its mountainous terrain and colder temperatures in the northern part of the NRB. ARs contribute more to total precipitation (83 mm) and rainfall (59 mm) in the fall than

in all other seasons combined, whereas the bulk of the AR-related snowfall and SWE is more evenly distributed in fall and winter. The MK test identified no significant trends for any of the assessed water budget input variables in fall and winter (Table 3.4) when the bulk of AR-related precipitation makes landfall in the NRB.

Table 3.4 –Results of the Mann-Kendall test applied to the time series of AR-related water budget input variables in the seasonal scale. Bold p values denote statistically-significant ($p \leq 0.05$) trends.

AR-related Water Budget Input Variable	Sub-basin	Spring		Summer		Fall		Winter	
		Kendall's tau	p-value	Kendall's tau	p-value	Kendall's tau	p-value	Kendall's tau	p-value
Rainfall	Upper Nechako	0.120	0.182	0.052	0.524	-0.074	0.363	-0.108	0.183
Rainfall	Lower Nechako	0.106	0.239	0.063	0.434	-0.027	0.745	-0.059	0.469
Rainfall	Upper Stuart	0.176	0.050	0.119	0.141	-0.088	0.274	-0.107	0.187
Rainfall	Lower Stuart	0.149	0.097	0.082	0.310	-0.099	0.222	-0.078	0.336
Rainfall	Endako	0.128	0.154	0.066	0.417	-0.091	0.261	-0.083	0.307
Rainfall	Chilako	0.050	0.583	0.037	0.651	0.012	0.888	-0.051	0.532
Rainfall	Stellako	0.108	0.229	0.057	0.481	-0.102	0.208	-0.099	0.222
Rainfall	NRB	0.126	0.162	0.077	0.343	-0.074	0.358	-0.106	0.193
Snowfall	Upper Nechako	0.008	0.932	-0.217	0.008	0.033	0.687	-0.058	0.475
Snowfall	Lower Nechako	0.023	0.799	-0.203	0.031	0.129	0.110	-0.014	0.866
Snowfall	Upper Stuart	0.060	0.505	-0.107	0.201	0.041	0.617	-0.015	0.858
Snowfall	Lower Stuart	0.073	0.417	-0.073	0.445	0.132	0.101	0.016	0.843
Snowfall	Endako	0.041	0.651	-0.098	0.310	0.123	0.128	0.022	0.789
Snowfall	Chilako	0.025	0.792	-0.143	0.149	0.144	0.074	-0.021	0.804
Snowfall	Stellako	0.049	0.592	-0.213	0.016	0.056	0.493	-0.027	0.743
Snowfall	NRB	0.033	0.714	-0.184	0.025	0.073	0.368	-0.015	0.858
Total Precip.	Upper Nechako	0.070	0.440	0.045	0.576	-0.006	0.942	-0.078	0.341
Total Precip.	Lower Nechako	0.084	0.353	0.063	0.434	0.038	0.644	-0.058	0.475
Total Precip.	Upper Stuart	0.140	0.120	0.117	0.146	-0.060	0.457	-0.037	0.648
Total Precip.	Lower Stuart	0.154	0.087	0.082	0.310	-0.001	0.996	-0.034	0.677
Total Precip.	Endako	0.122	0.174	0.066	0.417	0.007	0.934	-0.059	0.469
Total Precip.	Chilako	0.039	0.666	0.036	0.658	0.065	0.422	-0.049	0.551
Total Precip.	Stellako	0.082	0.360	0.055	0.499	-0.030	0.715	-0.088	0.279
Total Precip.	NRB	0.107	0.234	0.077	0.338	-0.014	0.865	-0.066	0.416
SWE	Upper Nechako	0.051	0.581	0.152	0.105	0.057	0.481	-0.068	0.404
SWE	Lower Nechako	0.036	0.728	-0.078	0.431	0.095	0.239	-0.049	0.551
SWE	Upper Stuart	0.120	0.186	0.005	0.958	-0.020	0.812	-0.016	0.843
SWE	Lower Stuart	0.092	0.339	0.008	0.944	0.120	0.138	-0.021	0.804
SWE	Endako	0.056	0.568	-0.007	0.962	0.103	0.205	-0.033	0.684
SWE	Chilako	-0.023	0.824	*	*	0.085	0.296	-0.048	0.558
SWE	Stellako	0.095	0.310	-0.088	0.355	0.074	0.363	-0.035	0.669
SWE	NRB	0.093	0.307	0.067	0.445	0.067	0.411	-0.040	0.627

* Insufficient data

3.4.3 Daily Analysis

This section examines AR and non-AR daily accumulated totals of the water budget input variables. The Upper Nechako is the westernmost sub-basin of the NRB, making it the most affected by ARs approaching BC from the Pacific Ocean. Thus, while this section contains discussions on daily contributions for many sub-basins, emphasis is given to the Upper Nechako. Daily results for the other sub-basins are presented in Appendix C (Figures C.1 to C.6).

Average daily precipitation in the NRB during AR events increases nearly threefold during AR days, with 1.7 mm and 4.8 mm for non-AR-related and AR-related precipitation, respectively. For the Upper Nechako, results show that daily precipitation events in the 0-20 mm range are, on average, 64% less frequent during AR days, while the 20-75 mm range is 72% more frequent (Figure 3.8 and Table 3.5). Further analysis shows a gradual increase of AR influence on precipitation in the binned daily totals ≤ 45 mm. Daily precipitation totals of 35-45 mm are over two times more likely to occur during AR days and reveal the strong influence of ARs on precipitation events within this range. Daily precipitation accumulations between 45-55 mm in the Upper Nechako are 50% more frequent during AR days. The influence of ARs on precipitation events in the Upper Nechako is pronounced, particularly for daily totals ≥ 20 mm (Figure 3.8). Daily precipitation > 60 mm occurs exclusively on AR days or is influenced by ARs impacting the Upper Nechako.

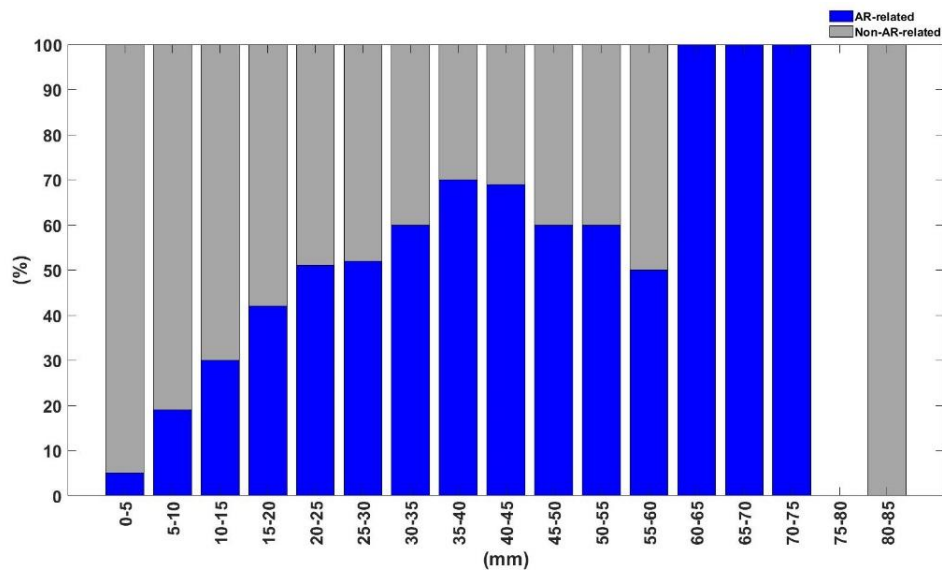


Figure 3.8 – Fractional representation of daily AR-related (blue) total precipitation compared to non-AR-related (gray) in the Upper Nechako divided into 5 mm bins.

Table 3.5 – The frequency of AR and non-AR-related daily precipitation in the Upper Nechako from 1950 to 2021 divided into 5 mm bins. * The single event causing the maximum daily total represented by the 80-85 mm bin is influenced or caused by an AR despite not being classified as an AR-day by the applied methodology.

Bin (mm)	AR-days (%)	non-AR-days (%)
0-5	1144 (5%)	20646 (95%)
5-10	553 (19%)	2358 (81%)
10-15	279 (30%)	647 (70%)
15-20	143 (42%)	196 (58%)
20-25	84 (51%)	82 (49%)
25-30	36 (52%)	33 (48%)
30-35	24 (60%)	16 (40%)
35-40	14 (70%)	6 (30%)
40-45	9 (69%)	4 (31%)
45-50	6 (60%)	4 (40%)
50-55	3 (60%)	2 (40%)
55-60	1 (50%)	1 (50%)
60-65	3 (100%)	0 (0%)
65-70	1 (100%)	0 (0%)
70-75	1 (100%)	0 (0%)
75-80	0 (0%)	0 (0%)
80-85	0 (0%)	1* (100%)
Total	2301 (9%)	23996 (91%)

The daily maximum total precipitation (84 mm) in the Upper Nechako occurred on 25 September 2010, a non-AR day by the applied methodology, but just after the passage of an AR in the region (52.5°N, 127.5°W) on 24 September 2010. This AR was registered at latitudes 52.5°N and 50°N from 23-26 September 2010, ranging from AR1-AR3 categories on the Ralph *et al.* (2019) scale, and is known to have caused catastrophic floods in Bella Coola (BC), located ~100 km south of the NRB (Sharma and Déry 2020b; Richards-Thomas *et al.*, 2024). The AR catalogue captured another AR starting on 27 September 2010 in the region, which may be the continuation of the previous AR partitioned into two events by the tracking algorithm or a secondary AR developed on the water vapour footprint of the previous AR. Therefore, this AR event influenced the daily precipitation maximum in the NRB and suggests that ARs may contribute to precipitation in the region after their river-shaped form has dissipated and are no longer classified as ARs by tracking algorithms. Before this sequence of events, an AR was only registered on 12 September, likely not influencing precipitation patterns starting 11 days later.

During a neutral transition period from La Niña to El Niño, the summer of 2006 was a very dry period in BC, followed by only two AR events of low intensities in September when AR activity usually amplifies in the province. Alongside rising anomalies on the SST of the Pacific Ocean, October 2006 registered the passage of three ARs at latitude 52.5°N from 14 to 28 October, with the last AR yielding the second-highest daily precipitation total in the Upper Nechako on record. On 28 October 2006, the sub-basin experienced precipitation of up to 72 mm caused by a drought-busting AR ranging from AR1-AR3, accounting for almost half of that year's AR-related total precipitation. During this event, the AR oscillated between latitudes 52.5°N and 50°N from 26-28 October and sustained AR2-AR3 conditions in the last 24 hours. The Lower Nechako (51 mm), Endako (52 mm), Chilako (33 mm), and Stellako (59 mm) also experienced

the highest daily total precipitation values related to ARs on that date. The difference in precipitation totals on different sub-basins suggests that factors such as topography, latitude, altitude, prevailing wind direction, and proximity to water bodies likely impact AR-related daily precipitation totals. The Lower Nechako, Lower Stuart, Endako, and Stellako share 28 October 2006 as the day with the highest values for AR-related snowfall and SWE accumulated totals. On average, these sub-basins received 42 mm of snowfall, increasing the SWE by 38 mm in 24 hours. The Upper Nechako saw its maximum daily AR-related snowfall (60 mm) on 12 November 1975 (during La Niña conditions), which led to the SWE daily maxima (64 mm) the following day. This isolated AR event occurred from 12-13 November, starting at latitude 52.5°N and rapidly shifting to latitude 50°N. Interestingly, both AR events leading to the highest daily precipitation totals in the Upper Nechako were influenced by sustained elevated AR categories during the ~24 hours before daily precipitation maxima. This reveals that higher AR intensity during longer periods is a main driver for maximum daily precipitation in the Upper Nechako, following the reasoning of Ralph *et al.* (2019) in creating a scale that considers AR durations and intensities.

AR-related rainfall in the Upper Nechako is often associated with maximum daily totals. On 15 October 1974, during La Niña conditions, an AR4 (mostly hazardous but also beneficial) event impacted the Upper Stuart with 31 mm of AR-related rainfall, making it the highest AR-related daily total for the sub-basin. However, this total was surpassed by six non-AR days during 1950-2021. In the Endako and Stellako, higher daily AR-related rainfall is more linked to AR2 than other AR classifications, although ARs are not the primary drivers of the highest daily totals. Nevertheless, non-AR days of high precipitation totals in the NRB may still be influenced by previous ARs that lose their river-shaped form or minimum integrated water vapour transport (IVT) thresholds on a specific day during an AR event. The Chilako registered more

equally distributed frequencies for elevated daily rainfall totals due to non-AR-related systems and the AR1-AR3 classifications of Ralph *et al.* (2019). ARs of higher classifications can carry increased moisture concentration further inland to the eastern portions of the NRB, such as the Chilako. Nevertheless, higher moisture concentration does not always yield more precipitation, as precipitation from ARs is better represented by the convergence of moisture flux towards a region and the initial state of air saturation (Mo *et al.*, 2021).

In spring, AR-related daily total precipitation reached maximum values in the Upper Nechako during AR1 (primarily beneficial) events on 29 March 1966 (34 mm) and 25 March 1997 (29 mm) during the El Niño phases of the ENSO. Although the AR1 event of 29 March 1966 mainly brought rainfall to the NRB, some snowfall was registered in the Upper Nechako (10 mm), whereas less snowfall was reported in the Upper Stuart (1 mm) and Stellako (2 mm). ARs are less frequent in the NRB region during summer, but AR3s occurred on 6 August 1978 and 24 August 1999 during La Niña conditions, bringing, on average, 12 mm and 15 mm of precipitation to the NRB, respectively. Except for the 45 mm received by the Upper Nechako on 3 January 2020, due to non-AR-related systems, all other top 10 maximum contributions for daily total precipitation during winter are AR-related, ranging from 42 to 67 mm. Hence, ARs contribute disproportionately more to mid- and high-intensity daily precipitation totals in the NRB, being more frequently attributed to such events than other meteorological phenomena.

In the Upper Nechako region, ARs have varying impacts on total precipitation throughout the year. October (44%) and September (42%) experience higher AR-related precipitation, while March, May, and June are the least affected, averaging 10%. August (28%) and November (29%) show similar AR-related precipitation averages, but intense ARs have a greater impact in November compared to all other months (Sobral and Déry, 2023). This observed pattern in

November may be attributed to an intensification of storm activity with stronger moisture advection. Subsequently, ARs of medium intensities contribute to substantial precipitation in the BC region in November, as recently seen in the 2021 BC floods (Gillett *et al.*, 2022).

The daily contribution of ARs to average precipitation shows a clear seasonal pattern (Figure 3.9). From mid-February to August, there is a decline in AR contributions, with daily values averaging below 40% from 1950 to 2021. In late summer and early fall, AR contributions to daily precipitation increase considerably, approaching 70% on certain days in September and October. The Upper Nechako region averages 46%, while the NRB sees an average of 42% during this active AR period, declining below 40% by early January. Figure 3.9 highlights a more pronounced impact of ARs on precipitation in the Upper Nechako compared to the entire NRB. However, from mid-September to early November, all days consistently show at least ~30% of precipitation being AR-related for the Upper Nechako and the NRB. Despite an overall seasonal pattern, the stochastic nature of ARs and precipitation events results in considerable day-to-day variations in their fractional contributions.

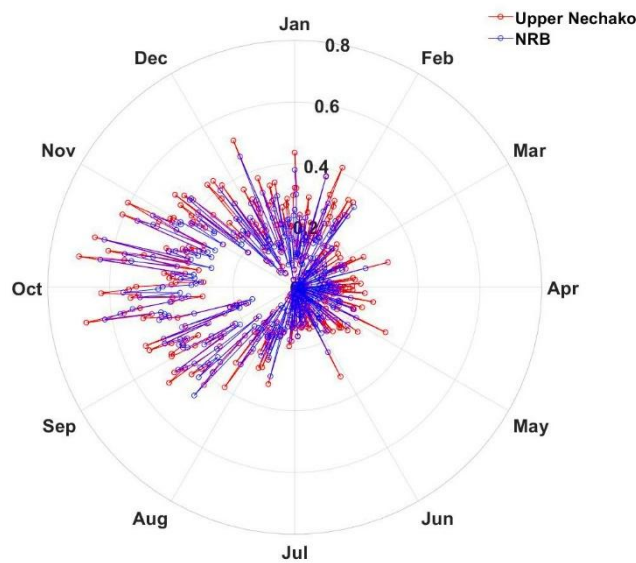


Figure 3.9 – Polar plot with average daily fractions for AR-related precipitation in the Upper Nechako (in red) and the NRB (in blue).

3.5 DISCUSSION

Understanding the spatial and seasonal variability of AR-related precipitation is crucial for effective water resource management, flood risk assessment, and climate adaptation strategies in central BC. The Upper Nechako and other western and northern sub-basins show a pronounced AR influence, underscoring the importance of topography and orographic forcing in AR precipitation. Interestingly, the consistent influence of ARs on the NRB from 1950 to 2021, shown by the lack of significant annual trends in AR-related water budget input variables, suggests that ARs play a stable role in the region's hydrology. In fall and winter, ARs contribute significantly to both rainfall and snowfall, playing a dual role in snowpack accumulation and posing flood and landslide risks during rain-on-snow events. In spring, an increasing trend in AR-related rainfall in the northern NRB, likely driven by warmer regional temperatures, may affect the rain-to-snow ratio during ARs in this season. This shift could impact snowmelt timing, advancing peak flows and directly impacting water supply to local stakeholders. Late summer ARs pose a potential threat for flash flooding at higher elevations of the NRB.

Similar effects have been observed in California's Sierra Nevada, where earlier snowmelt due to warmer temperatures has altered water management practices (Guan *et al.*, 2016). These findings have broader implications for watersheds with similar water budget input conditions, such as those in western and eastern North America, the UK, and parts of Asia, where ARs contribute to monsoonal rainfall patterns (Lavers *et al.*, 2011; Zhang *et al.*, 2021; Dong *et al.*, 2021; Knight *et al.*, 2024; Huan *et al.*, 2024). The western United States and Canada face similar challenges, with ARs contributing to winter flooding and impacting water management and supply (Neiman *et al.*, 2011). Although the connection between the ONI and ARs impacting the NRB seems weak based on Fig. B.1 (Appendix B), other teleconnections, like the Pacific Decadal Oscillation (PDO) and Pacific/North American (PNA) pattern, should be further explored to aid in predicting seasonal AR incidence and informing water management decisions in the NRB. According to Sharma and Déry (2020a), the British Columbia and southeastern Alaska (BCSAK) region, where the NRB lies, is impacted more so by ARs during neutral phases of the ENSO, and positive phases of the PDO and PNA. Moreover, Sharma and Déry (2020b) show that mountainous regions in BCSAK are more prone to the impacts of ARs and that higher AR-related precipitation occurs in September and October, matching the present findings. The Upper Nechako sub-basin's location on the leeward side of the Coast Mountains diminishes the contribution of ARs to water budget inputs as the topographic barrier impedes moisture transport to the Interior Plateau (Mo *et al.*, 2019). Therefore, the estimated contributions of ARs to the water budget input of the NRB are relatively smaller compared to the BCSAK coastal region, where a few expansive valleys along the Coast Mountains allow ARs to penetrate inland across the continent.

Low-intensity, short-duration ARs, despite their river shape, sometimes do not classify as ARs on the Ralph *et al.* (2019) scale but are considered as AR0s in Sobral and Déry (2023). These

low-intensity and short-duration ARs, which are mainly beneficial to the NRB, could be one of the drivers behind the more recent increasing trend in AR frequency found earlier by Sharma and Déry (2020a). Balancing the beneficial and detrimental impacts of ARs is challenging due to their spatiotemporal variability and precipitation intensities over confined regions. The results highlight the need for effective flood attenuation measures due to AR activity in the NRB, particularly in the Upper Nechako, Upper Stuart, and Stellako sub-basins. While ARs can alleviate droughts and wildfires by bringing beneficial water from oceans to inland areas, their high-intensity nature can sometimes overwhelm soils, rivers, and streams, leading to adverse impacts.

Several watersheds in all continents worldwide have their hydrological cycle influenced by ARs, necessitating advanced water management strategies to mitigate both their beneficial and adverse effects. In the western United States, similarly to BC, ARs contribute to a large portion of the region's annual precipitation and are critical for replenishing reservoirs, yet pose substantial flood and landslide risks (Dettinger *et al.*, 2011). Many European countries, including Ireland, the UK, Netherlands, Germany, Portugal, Spain, and Poland, experience AR-driven precipitation events that require coordinated flood management efforts in internationally managed watersheds to mitigate risks (Lavers *et al.*, 2013). In the Southern Hemisphere, eastern Australia's Murray-Darling Basin, a region supporting thousands of agricultural-related businesses, depends on AR activity that brings intense rainfall, critically shaping the watershed's hydrological cycle (Overton *et al.*, 2014). In South America, the Paraná River Basin, one of the continent's most significant watersheds, also experiences AR activity, impacting clean energy (hydroelectric) generation, rain-fed and irrigated agricultural practices, and public and industrial water supply (Abou Rafee *et al.*, 2020). These examples highlight the global relevance of ARs and the need for integrated watershed management strategies to

balance their benefits and mitigate their risks effectively in various mid-latitude regions worldwide.

Oscillations in precipitation due to AR variability significantly impact agricultural practices worldwide (Ionita *et al.*, 2020; Siirila-Woodburn *et al.*, 2023), affecting planting and harvesting schedules and yield productivity. Excessive AR-related precipitation can delay planting to avoid drenched soils, while during drought periods, crops can benefit from the intense and persistent precipitation patterns caused by ARs. Flooding from intense AR events poses additional threats to agricultural infrastructure, damaging roads and flooding farmland, potentially leading to crop damage and reduced offer of agricultural goods. ARs also affect local ecosystems, particularly waterways that serve as habitats for local fauna and flora. Changes in snowmelt timing and precipitation patterns linked to ARs may influence water levels in rivers and streams, impacting aquatic species and vegetation. These ecological shifts underscore the need for integrated water management strategies that balance societal, agricultural, and environmental needs during AR-related natural hazards.

Interdisciplinary research is key to addressing the complex challenges posed by ARs to watersheds globally. A collaborative approach enables the development of effective solutions for managing AR risks and benefits, considering multiple viewpoints and prioritizing needs. Since many regions worldwide also experience extreme surges in flows and water levels due to AR incidence, investigating their impacts can also enhance flood preparation strategies globally. Cities such as Vancouver, Canada; Lisbon, Portugal; Seville, Spain; and Tokyo, Japan, can use these insights to improve AR-related water resilience and natural hazard adaptation (Leung and Qian, 2009; Ramos *et al.*, 2015; Eiras-Barca *et al.*, 2021). The substantial increase in daily precipitation during mid- to high-intensity AR events in the NRB highlights

their potential to cause hazardous events. Knowledge of how ARs impact the NRB can be further integrated into atmospheric models to improve projections of AR impacts under different climate scenarios in western Canada, aiding the development of robust adaptation and mitigation strategies. This study uses the NRB to demonstrate the critical role ARs play in mid-latitude watersheds in western North America and offers valuable perspectives for other AR-affected regions worldwide.

While providing valuable insights into water resources management in central BC, this study has nonetheless some limitations. A primary limitation remains the availability and resolution of the utilized climate data. The reliance on historical datasets such as the SIO-R1-AR Catalogue and ERA5-Land reanalysis data might not adequately capture the finer details of ARs and their impacts, particularly in complex terrain like the Coast Mountains. Moreover, the study's temporal coverage of 1950 to 2021 may introduce inconsistencies due to changes in data collection methods over time, potentially impacting the reanalysis used in this effort. Additionally, the findings are specific to the unique geographic and climatic conditions of the NRB, which might limit their applicability to other regions. Lastly, while the study offers valuable insights into historical trends, it does not address the potential future AR behaviour under projected climate scenarios, which could influence long-term planning of water management and security in the NRB. Finally, the process of converting datasets of different timescales into a daily timescale may not provide the most precise representation of AR contributions when compared to datasets of improved spatiotemporal resolution.

3.6 CONCLUSIONS

This study enhances our understanding of regional hydrological processes by highlighting the critical role of ARs in sustaining the water resources of the NRB. ARs generally provide beneficial precipitation to the region, though they can occasionally pose natural hazards. The impact of ARs is more significant on rainfall compared to snowfall and SWE, with impacts being amplified in the watershed's mountainous areas during autumn and winter. On average, the NRB experiences AR influence on 33 days (9%) each year, contributing to one-fifth of the annual total precipitation. This contribution exhibits a decreasing pattern from west to east across all variables within the sub-basins. Notably, results show an increasing fractional contribution of rainfall in AR-related precipitation on a decadal scale beginning in the 2000s, which may reflect rising average air temperatures in the NRB.

In the Upper Nechako, AR-days account for at least 50% of daily precipitation events of mid-to-high intensity (20-75 mm) and 60% of daily precipitation within the 30-55 mm range. ARs that sustain higher intensities of water vapour transport during the final 24 hours of the event are associated with elevated daily precipitation totals in this region. The Upper Nechako, due to its larger catchment area in the southwestern part of the NRB, exhibits a pronounced influence of ARs on precipitation and regional water resource storage, accumulating higher AR-related water volumes across all water budget input variables compared to other sub-basins. This study finds no clear association between the contributions of AR-related water budget input variables to the NRB and oscillations in the ENSO phases.

Statistically significant reductions in AR-related snowfall during the summer associated with trends of increasing rainfall in the northern parts of the NRB during spring are likely due to regional warming. Nevertheless, these trends are not expected to substantially affect the

replenishment of key water resources, such as the Nechako Reservoir, due to very low overall annual contributions in summer. Sustainable water management that considers the impact of ARs on the Nechako Reservoir is crucial for ensuring water resiliency and security in the NRB. This is particularly important for the Lower Nechako region, where competing interests in water allocations could increase the demand for regional water resources, especially during prolonged droughts.

The findings demonstrate significant spatial variations in the contribution of ARs to the water budget input of the NRB. New sources of AR data, such as the high-resolution ($0.25^\circ \times 0.25^\circ$) global AR database based on ERA5 (Guan and Waliser, 2024), can significantly enhance AR assessment in future studies. This recently released database allows for more precise identification of the start and end of AR events and can be used to refine estimates and trends of AR contributions to water budget variables affecting the NRB and other regions worldwide. Further research on AR-related precipitation intensities is recommended to better comprehend the dynamics of ARs in the region, underscoring the need for continued efforts to advance understanding of AR impacts on the climate of western Canadian watersheds.

CHAPTER 4: METEOROLOGICAL DRIVERS OF AND HYDROLOGICAL RESPONSES TO EXCEPTIONAL ATMOSPHERIC RIVERS IN BRITISH COLUMBIA'S NECHAKO RIVER BASIN

ABSTRACT: Atmospheric Rivers (ARs) are increasingly recognized for their significant impact on global precipitation patterns, posing both hazards and benefits to various regions. This study focuses on three exceptional ARs affecting British Columbia's Nechako River Basin (NRB), a critical area for water resource management in western Canada. By analyzing comprehensive datasets, including the SIO-R1-AR Catalogue, ERA5/ERA5-Land climate datasets, and discharge and water level data, this research explores and depicts the atmospheric conditions, spatial distribution, and hydrological response of three exceptional AR events impacting the NRB between 1950-2021. The selected exceptional AR events occurred in 1952, 1978 and 2009. A latitudinal transect reveals a distinct west-to-east reduction in integrated water vapour transport (IVT), influencing precipitation patterns and the magnitude of the impact caused by ARs in the region. The convergence peak for all events occurs during or close to the lowest values of mean sea-level pressure and usually results in a precipitation peak. Exceptional ARs impact more the Upper Nechako than other sub-basins and received total precipitation volumes from the ARs of 1.22 km³ (87 mm), 1.18 km³ (84 mm), and 1.01 km³ (72 mm) in 1952, 1978, and 2009, respectively. Temperatures in the NRB are the primary driver influencing snowfall and runoff during the events. ARs contribute to critical water replenishment in the Nechako Reservoir, but rain-on-snow events from ARs significantly heighten flood risks by accelerating snowmelt and increasing runoff. A historically slight increase in the water level of the Nechako Reservoir in early November is observed as a hydrological response to the peak of the "AR season". The reliance of communities and

industries on the Nechako Reservoir for water, energy, and agriculture underscores the relevance of ARs to regional water resources and the need to study further exceptional river-shaped storms impacting BC. Future research should focus on enhancing AR forecasting models to allow for better flood management and water storage optimization in the Nechako Reservoir and other sub-basins of the NRB.

4.1 INTRODUCTION

In recent years, there has been a growing interest in atmospheric rivers (ARs) due to their potential to trigger intense and extended periods of precipitation, resulting in worldwide floods and landslides (Dezfuli *et al.*, 2021; Piecuch *et al.*, 2022; Vallejo-Bernal *et al.*, 2023; Wang *et al.*, 2023). ARs are characterized by atmospheric corridors that transport water vapour, resembling a terrestrial river in shape. They are responsible for a considerable fraction of the water resources in temperate climates (Slinskey *et al.*, 2020; van der Breggen and Hudson, 2024). Despite their well-known hazards worldwide, ARs also play a major beneficial role in replenishing water resources in western Canada (Sharma and Déry, 2020a; Sobral and Déry, 2023).

Given the rising average temperatures in the tropical Pacific region (Jiang *et al.*, 2024; Zhang *et al.*, 2024), where moisture builds up before travelling northeast to make landfall in British Columbia (BC), there is a concern that the province may experience more frequent and intense AR events. Recent findings show that a shift in AR incidence may be ongoing in the region, where lower-intensity ARs are becoming more frequent, and mid-intensity ARs are becoming scarcer and less intense (Sobral and Déry, 2023). In the northern regions of BC, ARs may occur coupled with sub-freezing temperatures, enhancing the potential for heavy snowfall, ice jams, and floods in lower areas. According to Gillett *et al.* (2022), in 2021, BC experienced one of the worst floods in its history after a series of ARs induced heavy precipitation over wet soils in November. Southwestern BC was the most affected region, but the impacts were spread across the province as railroads and highways were disrupted, impacting transportation, energy distribution, and supply chains.

One of the areas in BC recurrently affected by ARs is the Nechako River Basin (NRB), whose western headwaters include the Nechako Reservoir (Hartman, 1996; Albers *et al.*, 2016). The NRB is a crucial catchment in central BC, and chiefly through the Nechako Reservoir, it controls and supplies water to various stakeholders. ARs are estimated to contribute 21% of the total precipitation in the NRB (Sobral and Déry, 2024). Nonetheless, their contribution is uneven throughout the year, which enhances their impacts, particularly in the fall, when ARs are more frequent and intense in BC (Sharma and Déry, 2020b; Sobral and Déry, 2023).

To date, there have not been efforts to characterize the climatology of ARs causing disruptive impacts on the NRB. Therefore, the main objective of this study is to characterize and investigate similarities and differences in the synoptic setting of three exceptional AR events impacting the NRB and assess their hydrological response. Studies such as the present effort are necessary to better understand the general climate characteristics and spatial distribution of exceptional AR-related precipitation events in the NRB. Additionally, they provide useful insights for enhanced water management practices in the watershed and the Nechako Reservoir.

4.2 STUDY AREA

The NRB covers 47,200 km² (Parkes, 2021) in central BC from the Coast Mountains onto the Interior Plateau, spanning from latitudes 52.93° N to 56.17° N and longitudes 122.72° W to 127.78° W (Helm *et al.*, 1980; Picketts *et al.*, 2017; Sobral and Déry, 2023). Its catchment encompasses a variety of features, including mountains, plateaus, streams, rivers, temperate forests, and agricultural lands (Albers *et al.*, 2016; Goswami *et al.*, 2024). Within the NRB are smaller natural and regulated catchments, making water management a complex task, especially concerning the Nechako Reservoir's operation. This reservoir, constructed in the 1950s as part

of the Kemano Project (Desreumaux *et al.*, 2014; Tannant and Morgenroth, 2020), plays a crucial role in ensuring the reliability of regional water resources.

The Kemano Project was designed to support water supply by impounding the Nechako River at the Nechako Canyon through Kenney Dam (Figure 4.1). The impoundment created the Nechako Reservoir, and downstream west-to-east flows are regulated by the Skins Lake spillway (SLS) (Figure 4.1). Alongside the Kenney Dam and the Nechako Reservoir, infrastructure, such as water tunnels, transmission lines, a hydropower plant, and an aluminum smelter in Kitimat (BC), are among the components of the project. Rio Tinto manages the Nechako Reservoir's outflows, affecting natural flows (Larabi *et al.*, 2022; Khorsandi *et al.*, 2023), water temperatures (Macdonald *et al.*, 2012; Gilbert *et al.*, 2022; Charles *et al.*, 2023), and sediment transport (Gateuille *et al.*, 2019) downstream. Effective reservoir management is critical year-round but particularly during drought periods to sustain industrial activities, residential water consumption, and ecological needs. Currently, nearly 60% of the inflows to the Nechako Reservoir are diverted to the Kemano River system to generate electricity for the operation of the aluminum smelter (Desreumaux *et al.*, 2014).

The Nechako River is a vital waterway in central BC, flowing generally eastward before joining the Fraser River in Prince George, BC (Macdonald *et al.*, 2012; Picketts *et al.*, 2020). The western headwaters formed by the Upper Nechako sub-basin supply water to the Nechako Reservoir, which experiences the most significant impact from ARs in terms of all water budget input variables (Sobral and Déry, 2024). The Upper Nechako sub-basin lies on the leeward side of the Coast Mountains, where precipitation from ARs and other atmospheric systems is generally lower than on the windward side (Sharma and Déry, 2020c). However, its mountainous terrain and proximity to landfalling ARs along the BC coast make it stand out

compared to other sub-basins of the NRB. Thus, ARs can lead to a variety of impacts across the NRB and cause substantial precipitation in the Nechako Reservoir, enhancing its replenishment.

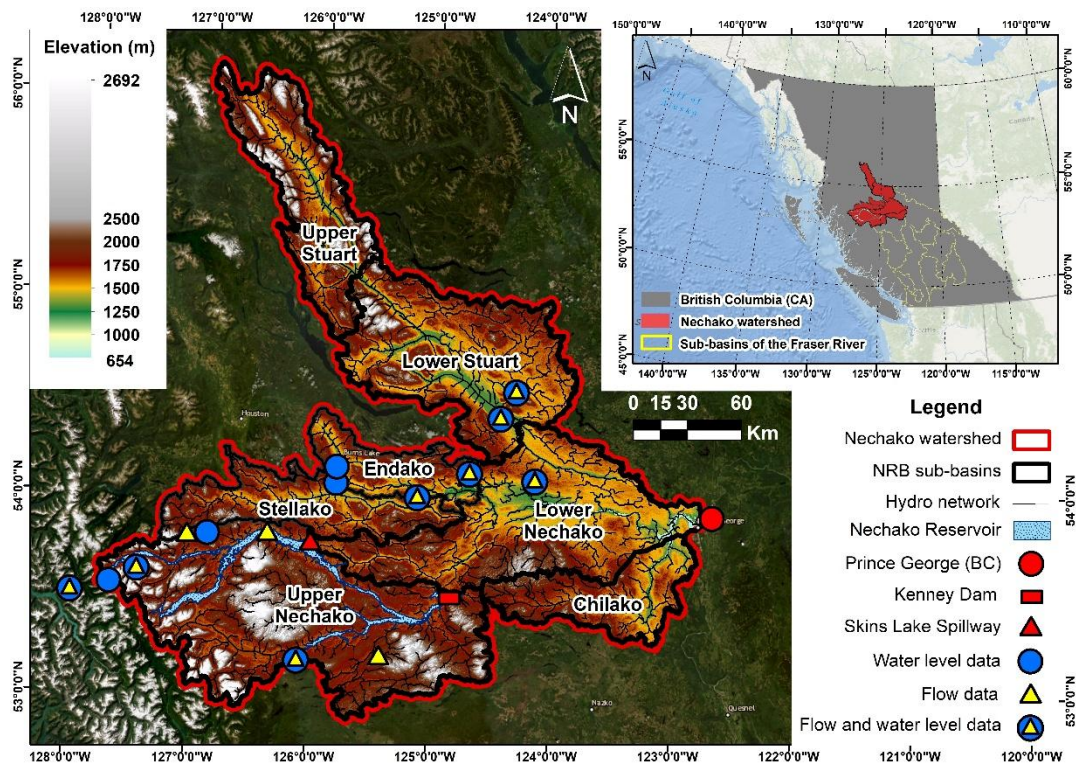


Figure 4.1 – Map of the NRB with sub-basins, elevation (m), hydrological network, the Nechako Reservoir, Kenney Dam, Skins Lake Spillway, Prince George (BC) and discharge or water level monitoring points within the NRB assessed by this study. Inset map with the location of the NRB in BC.

4.3 DATA AND METHODS

This study combines multiple datasets to assess ARs impacting the NRB. The SIO-R1-AR Catalogue identifies AR events based on integrated water vapour transport (IVT) and specific shape criteria, while ERA5 and ERA5-Land reanalysis datasets provide high-resolution data on AR and climate characteristics. Discharge and water level data from the NRB are also used to evaluate hydrological responses during the selected exceptional AR events. Key variables from the ERA5-Land dataset, including precipitation, snowfall, SWE, and runoff, along with data from ERA5 such as total column water vapour, IVT, moisture divergence, mean 2-meter air temperature, and mean sea-level pressure, are analyzed to characterize the impacts of each

exceptional AR. Temporal and spatial analyses, including time series plots and accumulation maps, track the evolution of synoptic and climate characteristics of ARs and highlight areas more prone to their detrimental impacts.

4.3.1 Datasets

4.3.1.1 AR Catalogue

The dataset used in this study to identify AR events impacting the west coast of North America is the SIO-R1-AR Catalogue (Gershunov *et al.*, 2017), provided by the Scripps Institution of Oceanography (SIO) of the University of California – San Diego, USA. It has been successfully used for the BC region in the works of Sharma and Déry (2020a, 2020b, 2020c) and Sobral and Déry (2023), and onward, it will be referred to as the AR Catalogue. The AR Catalogue has been widely used to study the impact of ARs on the west coast of North America (Corringham *et al.*, 2022; Hoffman *et al.*, 2022; DeFlorio *et al.*, 2024). It is presented on a six-hourly time step and is based on a combination of meteorological features, such as IVT above $250 \text{ kg m}^{-1} \text{ s}^{-1}$ and a minimum 2:1 ratio in the length and width of the AR.

It is important to highlight that while following these premises to characterize AR events, the tracking algorithm of the AR Catalogue may combine AR events into sequential independent events or split a long-lasting AR event into more than one, depending on how IVT and the shape of the AR vary. Each AR event tracked by the algorithm is assigned a sequential number alongside the position (latitude, longitude) with the respective IVT values, integrated water vapour column (IWV), and wind speed data at 850 hPa.

4.3.1.2 Hydroclimatic data

The European Centre for Medium-Range Weather Forecasts (ECMWF) fifth-generation reanalysis (ERA5) and its high-resolution land component (ERA5-Land) are gridded climate datasets that provide invaluable tools for climate research worldwide (Hersbach *et al.*, 2020; Muñoz-Sabater *et al.*, 2021). The datasets cover the 1940-present (ERA5) and 1950-present (ERA5-Land) periods, ensuring wide application within the scientific community (Hersbach *et al.*, 2020), particularly in regions where in situ data are unavailable or scarce (Perri *et al.*, 2024).

Previous studies have used ERA5 ($0.25^\circ \times 0.25^\circ$ resolution) to investigate many climatic phenomena, including extreme weather events (Li *et al.*, 2020; Lavers *et al.*, 2022; Xu *et al.*, 2022) and atmospheric circulation patterns (Tarek *et al.*, 2020; Sun *et al.*, 2021). As climate datasets constructed on reanalysis, their data assimilation from satellites, ground-based observations, and other sources enhances their accuracy and strengthens their applications for climate-related research. Similarly, ERA5-Land ($0.10^\circ \times 0.10^\circ$ resolution) has been widely applied in agricultural and hydrological studies (Zhang *et al.*, 2021; Kaori Matsunaga *et al.*, 2023; Dalla Torre *et al.*, 2024). It uses an improved resolution compared to ERA5, offering insights into land-related parameters such as soil moisture and temperature, snow depth, precipitation, and solar radiation, among others (Muñoz-Sabater *et al.*, 2021). To assess the impacts of each exceptional AR event, key variables from the ERA5-Land dataset are analyzed, including precipitation, snowfall, snow water equivalent (SWE), and runoff. Total precipitation, snowfall, and runoff values are directly extracted from the dataset, while rainfall is derived by subtracting snowfall from total precipitation. SWE is calculated based on positive variations in the SWE values provided within the dataset. The work of Goswami *et al.* (2024) is summarized

in Appendix H and serves as one of the main references validating the use of ERA5-Land data to characterize the NRB's climate.

In the scope of ARs, these datasets are vital for understanding the characteristics and impacts of these river-shaped storms. Recent notable studies include one by Thandlam *et al.* (2022), which evaluated the spatio-temporal variability of ARs over the Euro-Atlantic region and found a poleward shift in landfall from 1999-2018. Moreover, using ERA5 data from 1979-2020, Khouakhi *et al.* (2022) analyzed landfalling ARs and their association with rainfall on the annual and seasonal scales in Morocco to find that the frequency of these storms is ~36 events per year (similar to BC), with the highest occurrence during fall. In high-elevation areas of Asia (Nash *et al.*, 2022), New Zealand (Pohl *et al.*, 2023), and south-central Chile (Garreaud *et al.*, 2024), the ERA5 dataset has also been used to assess the influence of ARs on precipitation totals and extremes. Data from ERA5, including total column water vapour, integrated water vapour transport, moisture divergence, mean 2-meter air temperature and mean sea-level pressure, are used to characterize the exceptional AR events. The datasets' versatility and global applicability make them important assets in advancing our understanding of atmospheric processes and their climatic implications. With their global coverage and improved spatio-temporal resolution, they are at the forefront of advancing our knowledge of climate dynamics worldwide.

4.3.1.3 Discharge and Water Level Data

This study applies discharge ($\text{m}^3 \text{s}^{-1}$) and water level (m) data from the NRB sourced from the Water Survey of Canada and Rio Tinto to analyze the hydrological response during the assessed exceptional AR events. Table 4.1 lists the selected stations where hydrological impacts in

creeks, streams, lakes and reservoirs across the NRB are investigated. Station selection is based on data availability to assess varied hydrological responses within the region.

Table 4.1 – Water Survey of Canada hydrometric stations used to assess the hydrological response in the NRB and surrounding area. Stations are listed from west to east.

Station Name (ECCC)	Station Code (ECCC)	Latitude (°N)	Longitude (°W)	Data Type and Period	Data Period	Catchment Area (km ²)	Regulation Type
Kemano River above Powerhouse Tailrace	08FE003*	53° 33' 48"	127° 57' 08"	Flow and water level	1971-2022	556	Natural
Tahtsa Lake near Kemano	08JA030	53° 37' 02"	127° 41' 39"	Water level	1999-2013	NA	Regulated
Laventie Creek near the Mouth	08JA015	53° 39' 07"	127° 32' 15"	Flow and water level	1976-2022	87	Natural
Nadina Lake near Noralee	08JB007	53° 54' 14"	126° 58' 15"	Water level	1964-2023	NA	Regulated
Nadina River at the outlet of Nadina Lake	08JB008	53° 54' 09"	126° 57' 16"	Flow	1964-2022	369	Regulated
Macivor Creek near the Mouth	08JA016	53° 48' 02"	126° 21' 36"	Flow	1976-1995	53	Natural
Eutsuk River at the outlet of Eutsuk Lake	08JA028	53° 14' 03"	126° 06' 43"	Flow and water level	1993-2013	NA	Natural
Francois Lake at Southbank	08JB001	54° 01' 30"	125° 45' 55"	Water level	1935-1974	NA	Natural
Francois Lake at Francois Lake	08JB011	54° 03' 05"	125° 45' 16"	Water level	1974-1995	NA	Natural
Van Tine Creek near the Mouth	08JA014	53° 15' 48"	125° 24' 30"	Flow	1974-2006	150	Natural
Stellako River at Glenannan	08JB002	54° 00' 28"	125° 00' 32"	Flow and water level	1929-2023	3600	Natural
Nautley River near Fort Fraser	08JB003	54° 05' 06"	124° 36' 03"	Flow and water level	1950-2023	6030	Natural
Stuart River near Fort St. James	08JE001	54° 25' 00"	124° 16' 14"	Flow and water level	1929-2023	14200	Natural
Tsilcoh River near the Mouth	08JE004	54° 36' 38"	124° 14' 51"	Flow and water level	1975-2023	431	Natural
Nechako River at Vanderhoof	08JC001	54° 01' 36"	124° 00' 31"	Flow and water level	1915-2023	25200	Regulated

* Station located outside of the NRB, at an altitude near sea level and between Powell Peak and Mount Dubose.

4.3.2 Methods

4.3.2.1 Selection of exceptional AR events affecting the NRB

A systematic approach was employed to choose exceptional ARs impacting the NRB by refining data from two distinct datasets: the SIO-R1-AR and ERA5-Land. The study also uses the ERA5 dataset to assess atmospheric variables related to the exceptional AR events impacting the NRB. The SIO-R1-AR Catalogue is used for parameters such as date, time, duration, AR event number, and IVT values, aiding in the identification of AR events within three geographic positions (50°N, 125°W), (52.5°N, 127.5°W), and (55°N, 130°W). These positions represent the centre of 2.5° × 2.5° regions in the atmosphere where the AR Catalogue monitors AR activity. Among the 71 coastal geographic regions in Western North America monitored by SIO, the chosen three are the closest to the NRB. Due to their proximity to the NRB, AR activity in these regions is considered to potentially impact hydrological variables that integrate part of the NRB's water budget. With an improved grid resolution, the ERA5-Land dataset contributes essential data on precipitation, snowfall, 2-m air temperature, and runoff, while ERA5 provides water vapour columns, IVT, convergence, and mean sea-level pressure estimates during each AR event.

Initially, climate data are extracted from the AR Catalogue spanning 1950-2021, forming the main reference on the duration, intensity, wind speed and direction of exceptional AR events impacting the NRB. Similar methods were applied to extract data from the ERA5-Land dataset for the same period. By integrating both datasets on a daily scale, as presented in Sobral and Déry (2023), the overall contribution of each AR event (individually numbered by the AR Catalogue) to climate variables is estimated to further refine the selection of the exceptional AR events assessed in this study. AR events are then divided into deciles, emphasizing the 1st

decile of each criterion, capturing exceptional events marked by higher values of climate variables. Selection criteria are: (1) average IVT, and (2) maximum IVT based on the AR Catalogue; (3) average precipitation intensity (mm hr^{-1}) in the NRB using a combination of the AR Catalogue (duration) and ERA5-Land data (precipitation), (4) average total precipitation in the NRB, and (5) average total precipitation in the Upper Nechako sub-basin during each AR event of the series from 1950-2021. The intersection of the top 10% of these criteria significantly reduces the initial dataset of 2179 AR events of the AR Catalogue to a subset of 10 events (Table 4.2). A scoring mechanism is introduced to refine the selection process further. Criteria are organized in ascending order, and each criterion is assigned a score ranging from 1 to 10 based on its position. The final selection of the top three AR events is determined through cumulative scoring, pointing them as primary case studies for detailed examination.

The selected exceptional AR events occurred on 12-14 December 1952, 28 October to 1 November 1978 and 27-31 October 2009. Details of the pre-selected (top 10) and selected (top 3) AR events are presented in Table 4.2 and may also be a reference for future in-depth investigations regarding exceptional AR events impacting the NRB. This methodology ensures a data-driven and objective approach to selecting exceptional AR events for further exploration in this study.

Table 4.2 - Short list of AR events on the AR Catalogue impacting the NRB after applying the selection criteria based on the percentiles and the scoring mechanism

SIO-R1-AR Catalogue				Combination		ERA5-Land		Ranking		
AR Event # in the AR Catalogue	Days	Month	Year	Duration* (hours)	Average IVT ($\text{kg m}^{-1} \text{s}^{-1}$) on the (lat,lon) positions	Max. IVT ($\text{kg m}^{-1} \text{s}^{-1}$) on the (lat,lon) positions	Average Total Precipitation in NRB (mm)		Average Total Precipitation in Upper Nechako (mm)	
1808	30 Oct. to 1 Nov.		1978	54	630.2	1007.8	0.8	45.5	83.7	1
3723	29-31	Oct.	2009	36	706.1	833.3	1.3	47.9	72.1	2
296	12-14	Dec.	1952	54	668.0	885.0	0.8	40.9	86.9	3
2414	28 Sep. to 1 Oct.		1988	72	568.0	1122.6	0.6	43.0	71.8	4
611	7-9	Dec.	1957	42	557.0	938.6	0.8	33.9	67.2	5
164	3-4	Nov.	1950	42	609.7	868.1	0.6	25.5	55.0	6
3267	18-19	Sep.	2002	36	605.8	804.6	0.9	31.9	47.9	7
1941	10-11	Dec.	1980	36	586.7	842.1	0.7	24.9	45.8	8
608	22-24	Nov.	1957	66	585.6	851.3	0.6	39.5	43.0	9
1986	30 Oct. to 1 Nov.		1981	36	530.7	822.0	0.7	24.2	44.5	10

* The total duration of each AR event used as a selection criterion is based on data from the AR Catalogue and does not match the total duration of the AR events further presented to characterize the cumulative contributions of the selected events.

4.3.2.2 Data analysis

The data are organized into time series plots and accumulation maps for total precipitation, snowfall, rainfall, SWE and runoff, encompassing each AR event and a 24-hour window before and after the event. The time series plots illustrate the temporal evolution of the selected AR events on an hourly scale (in UTC) at the coordinates 53.6°N, 127.3°W. This position is situated leeward of the Coast Mountains and within the Upper Nechako, inside the Nechako Reservoir. Data characterizing the atmospheric conditions of exceptional AR events rely on the ERA5 dataset to provide several meteorological variables: (a) total column of water vapour, (b) IVT, (c) vertically integrated moisture divergence (convergence), (d) total precipitation, (e) snowfall, (f) 2-m air temperature, and (g) mean sea-level pressure at peak convergence. The start and end of the exceptional ARs estimated in this study are indicated by the light blue shaded area on the time series plots and are determined by the increasing (or oscillating) values for variables (a), (b), (d), (e), and (f) until the total precipitation returns to zero and IVT is under $250 \text{ kg m}^{-1} \text{ s}^{-1}$.

The time series plots present IVT data at five positions along a latitudinal transect from west of McCauley Island (53.6°N, 130.3°W) to east of the Nechako Reservoir (53.6°N, 125.8°W), near the SLS. In the spatial analyses for each event evidenced in the spatial plots, the transect is depicted in (b) with the same colour scheme used in the temporal analysis. The transect spans ~100 km between points, with an additional position at the peak of topography, equidistant (~50 km) from positions 2 (magenta) and 4 (black), situated in the foothills of the Coast Mountains and leeward of the Tahtsa Ranges, respectively. Data at these positions are analyzed individually as they can demonstrate how IVT intensities change from west to east during exceptional AR events and to characterize their synoptic setting.

The spatial representation of the event follows the same variable order as the temporal analysis, with runoff added to the spatial plots. Runoff is excluded from the temporal analysis due to its distinct calculation methodology, representing water column accumulation within a grid box from the AR event's start to end. This methodological difference could mislead comparisons with discharge – also assessed in the study – which employs different units and methodologies to calculate discharges at specific outlets. Nevertheless, the spatial representation of runoff is useful in visualizing areas with a higher potential for floods and landslides during exceptional AR events affecting the NRB and surrounding watersheds. Due to the wide range of discharges throughout the NRB caused by the diverse hydrological network, discharge data and water levels are depicted with standardized values to allow the comparison between catchments of diverse areas and between different hydrological variables (flows and water levels).

4.4 RESULTS

4.4.1 Climatology of exceptional AR events impacting the NRB

4.4.1.1 12-14 December 1952

This AR event impacted the Upper Nechako region from 12 to 14 December 1952. In the monitored position within the Nechako Reservoir, IVT (Fig. 4.2b) gradually increased from 12 to 13 December. Moisture convergence (Fig. 4.2c) and air temperature (Fig. 4.2f) also experienced a gradual rise in the initial 24 hours, influenced by escalating concentrations of warm moisture interacting with colder temperatures inland. The IVT (Fig. 4.2b) estimations along the transect reveal a distinct west-to-east reduction in the impact of ARs in the region. Positions located west of the Nechako Watershed observe higher concentrations of IVT, significantly diminishing after the storm crosses the Coast Mountains. Because orographic lifting enhances precipitation in high mountainous terrain, ARs become moisture-depleted on the leeward side of the Coast Mountains (Figures 4.3c, 4.5c and 4.7c).

Cumulative values of total precipitation and snowfall are calculated to depict the contribution of each AR event to these climate variables throughout the exceptional AR events and are represented in dark blue on the right axis of panels (d) and (e) in Figures 4.2, 4.4, and 4.6. Total precipitation (Fig. 4.2d) initially experiences a surge on 12 December, followed by a decrease in intensity before gradually increasing until mid-day on 13 December. The peak in total precipitation aligns with the peak of convergence, and similar patterns (with mirrored results) are observed in the behaviour of both variables throughout the AR event. Despite the increase in air temperatures throughout the event, due to near- or sub-freezing air temperatures, most precipitation was delivered as snow, evidenced by the similarities in the values depicted in Figures 4.2d and 4.2e.

A characteristic "AR signature" is evident on 12 December, marked by a temperature increase of approximately 6°C in the region influenced by the arrival of warm, moist air from the Pacific Ocean. The mean sea-level pressure (Fig. 4.2g) fluctuates during the event, reaching its lowest values close to the initial hours of 13 and 14 December. However, during the AR event, the mean sea-level pressure within the Nechako Reservoir remains lower than measurements before and after the passage of the AR, influenced by the proximity of the low of the mid-latitude cyclone that shapes the AR over the Pacific Ocean.

The spatial analysis depicted in Figure 4.3 indicates that the (a) water vapour column and (b) IVT are higher between the region formed by 125-130°W and 50-52.5°N. Maps for moisture convergence (Fig. 4.3c) and total precipitation (Fig. 4.3d) for the region closely mirror the spatial distribution of these variables, except for substantially higher moisture convergence. Both also align spatially with areas exhibiting increased runoff (Fig. 4.3h). The Upper Nechako recorded an average of 87 mm of total precipitation during the 1952 exceptional AR event, precipitating ~1.2 km³ of water to the Upper Nechako or 3.7% of the Nechako Reservoir's total volume (33 km³) (Déry *et al.*, 2012) during this event alone. Snowfall (Fig. 4.3e) peaks in the eastern part of the Upper Nechako, following average temperatures (Fig. 4.3f) during the event. Temperatures remain $\geq 0^{\circ}\text{C}$ and warm on the windward side and mainly $< 0^{\circ}\text{C}$ on the leeward side of the Coast Mountains of BC. This demonstrates how ARs may cause distinct temperature patterns in nearby regions separated by mountainous terrain and that the Nechako Reservoir also benefits from AR activity by accumulating snow. Warm moisture forced by the ARs toward mountainous terrain causes rapid temperature decreases due to adiabatic cooling, enhancing precipitation in the form of snow within the Nechako Reservoir region, where elevation makes temperatures lower than on the windward side of the Coast Mountains. During the peak of convergence, mean sea-level pressure isobars (Fig. 4.3g) exhibit a 40 hPa gradient

(984-1024 hPa) over the region, intensifying winds and contributing to orographic precipitation. The mean sea-level pressure and 500 hPa geopotential height maps at 00 and 12 UTC throughout the duration of this exceptional AR event are presented in Figures E.1 and E.2 (a to f) of Appendix E. In Appendix F, daily data for total precipitation (Figure F.1), rainfall (Figure F.2), snowfall (Figure F.3) and SWE (Figure F.4) are presented, distinguishing AR days (red crosses) from non-AR days during 1952.

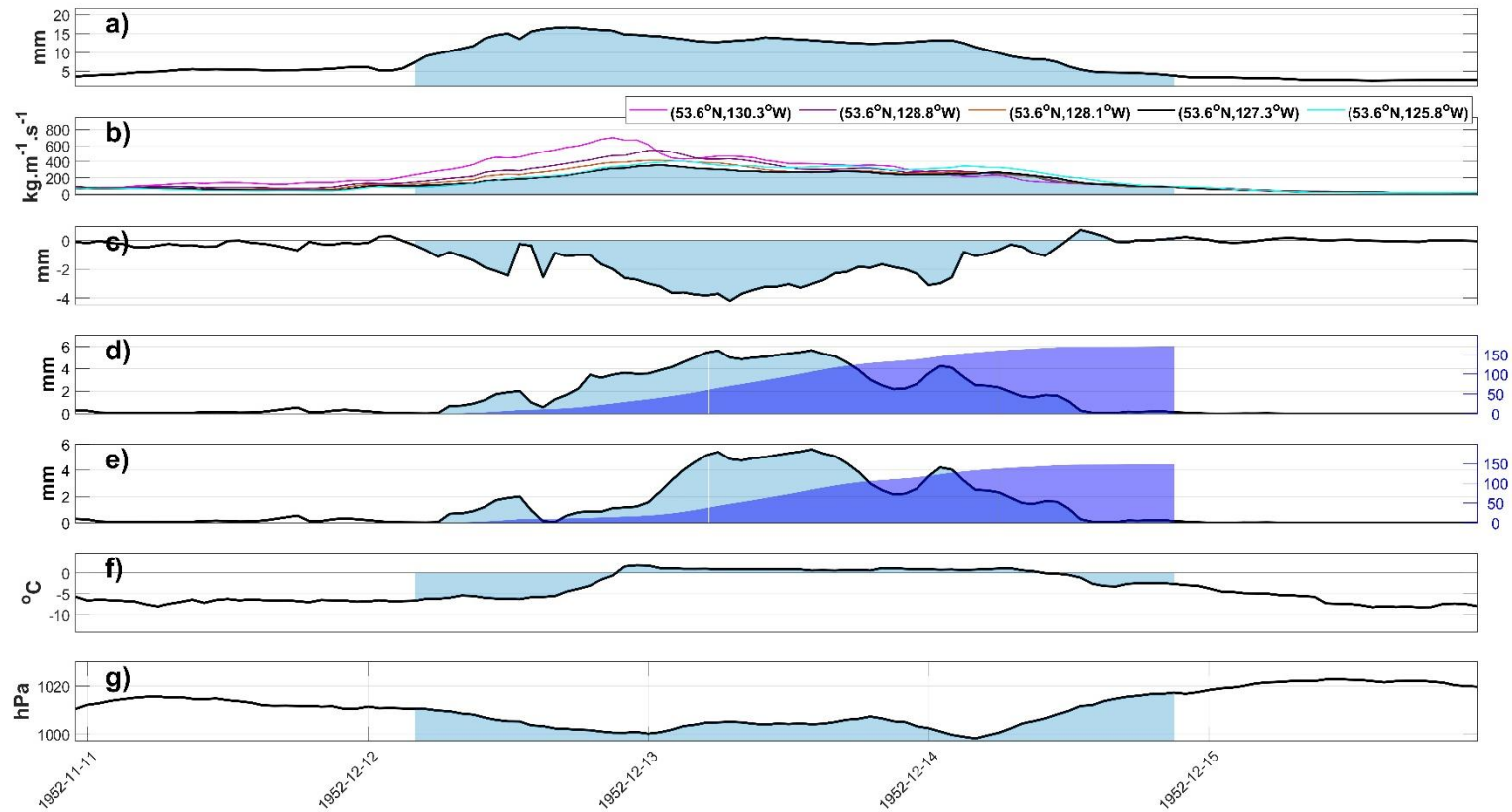


Figure 4.2 – Climogram of the AR event from 12-14 December 1952. The panels show (a) the total column of water vapour (mm), (b) integrated water vapour transport (IVT - $\text{kg m}^{-1} \text{s}^{-1}$) at five positions along a latitudinal transect, (c) moisture divergence (negative values mean convergence) (mm), (d) total precipitation in light blue (mm) and cumulative precipitation in dark blue (mm), (e) snowfall in light blue (mm of water equivalent) and cumulative snowfall in dark blue (mm), (f) 2-m air temperature ($^{\circ}\text{C}$), and (g) mean sea-level pressure (hPa) during the AR event (shaded in light blue) occurred on 12-14 October 1952.

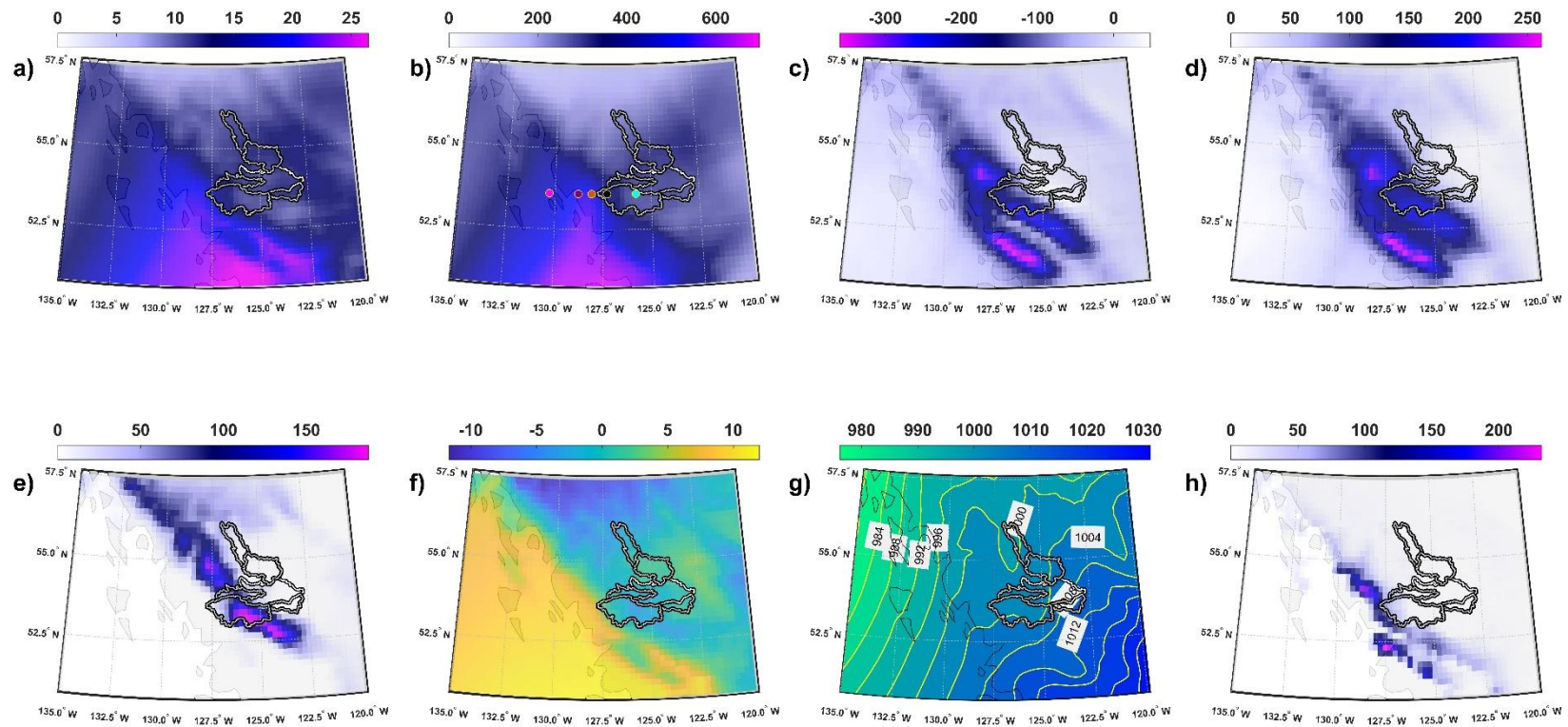


Figure 4.3 – Maps for (a) mean total column of water vapour (mm), (b) mean integrated water vapour transport (IVT - $\text{kg m}^{-1} \text{s}^{-1}$) and the location of the five positions along the latitudinal transect, (c) moisture divergence (negative values mean convergence) (mm), (d) total precipitation (mm), (e) snowfall (mm), (f) mean 2-m air temperature ($^{\circ}\text{C}$), (g) mean sea-level pressure (hPa) during the peak of moisture convergence with contour lines and (h) accumulated runoff (mm) during the AR event occurred on 12-14 October 1952.

4.4.1.2 28 October – 1 November 1978

For this AR event, the climogram (Figure 4.4) shows that water vapour concentration (Fig. 4.4a) inside the NRB starts to build up on 28 October and constantly rises until 31 October. Nevertheless, IVT (Fig. 4.4b) does not follow the same pattern, and from 29 to early 30 October, IVT diminishes substantially outside the NRB. At the same time, the monitored points inside the Nechako Reservoir (black and navy blue lines in Fig. 4.4b) present a stable increase until the peak of total precipitation (Fig. 4.4d) and convergence (Fig. 4.4c). Peaks in convergence, total precipitation and snowfall (Fig. 4.4e) occur a few hours after the lowest mean sea-level pressure (Fig. 4.4g) is registered near 1000 hPa. A well-known characteristic of ARs is the warmer temperature of the air mass coming from the sub-tropics compared to inland areas of northern BC, which can be observed by the positive variation inside the NRB (Fig 4.4f) during the event, passing from sub- to above-freezing air temperatures as the warm airmass moves inland and returning to near and below 0°C when the AR event ends. The temperature increase during AR events may enhance the rain-on-snow phenomenon, melting the snowpack and increasing the risk of floods. In this AR event, 82% (149 mm) of the precipitation west of the Nechako Reservoir was snow and likely contributed to increasing the snowpack rather than enhancing floods in the Upper Nechako.

During the event, the water vapour column (Fig. 4.5a) is concentrated in the 127.5-135.0°W and 50.0-53.5°N region, and the AR intersects the NRB in a southwest-to-northeast orientation. IWV and IVT maps at the peak of landfalling IVT for the 1978 AR event are presented in Figure G.1 – a and c (Appendix G). Convergence (Fig. 4.5c) and total precipitation (Fig. 4.5d) are spatially similar, but convergence is substantially higher and peaks at ~600 mm on the windward slopes compared to ~400 mm total precipitation west of the NRB. The NRB received an average of 46 mm of total precipitation, while the Upper Nechako had almost twice that

amount. During this AR, the accumulated total precipitation in the Upper Nechako averages 84 mm, for an estimated 1.18 km³ of water volume impacting the Upper Nechako. Within the NRB, snowfall (Fig. 4.5e) is greater west of the Upper Nechako and in the north of the Upper Stuart sub-basins, where temperatures (Fig. 4.5f) are lower than in the interior of the watershed throughout the exceptional 1978 AR event. Figures A.18 and A.19 (a to j) show the synoptic conditions at 12-hour intervals during the 1978 AR event, illustrating mean sea-level pressure isobars and 500 hPa geopotentials.

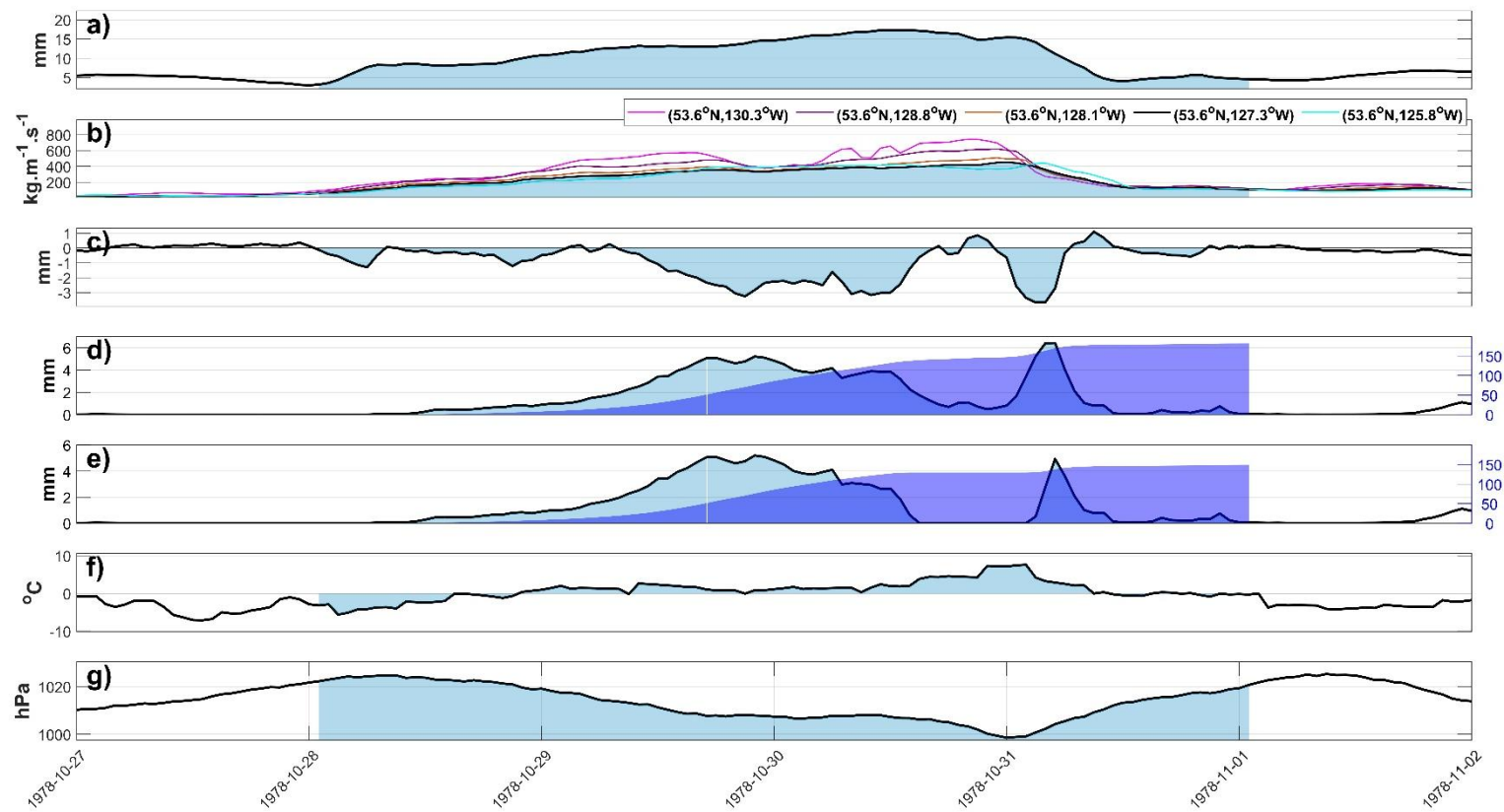


Figure 4.4 – Climogram of the AR event from 28 October to 1 November 1978. The panels show (a) the total column of water vapour (mm), (b) integrated water vapour transport (IVT - $\text{kg m}^{-1} \text{s}^{-1}$) at five positions along a latitudinal transect, (c) moisture divergence (negative values mean convergence) (mm), (d) total precipitation in light blue (mm) and cumulative precipitation in dark blue (mm), (e) snowfall in light blue (mm of water equivalent) and cumulative snowfall in dark blue (mm), (f) 2-m air temperature ($^{\circ}\text{C}$), and (g) mean sea-level pressure (hPa) during the AR event (shaded in light blue) occurred on 28 October to 1 November 1978.

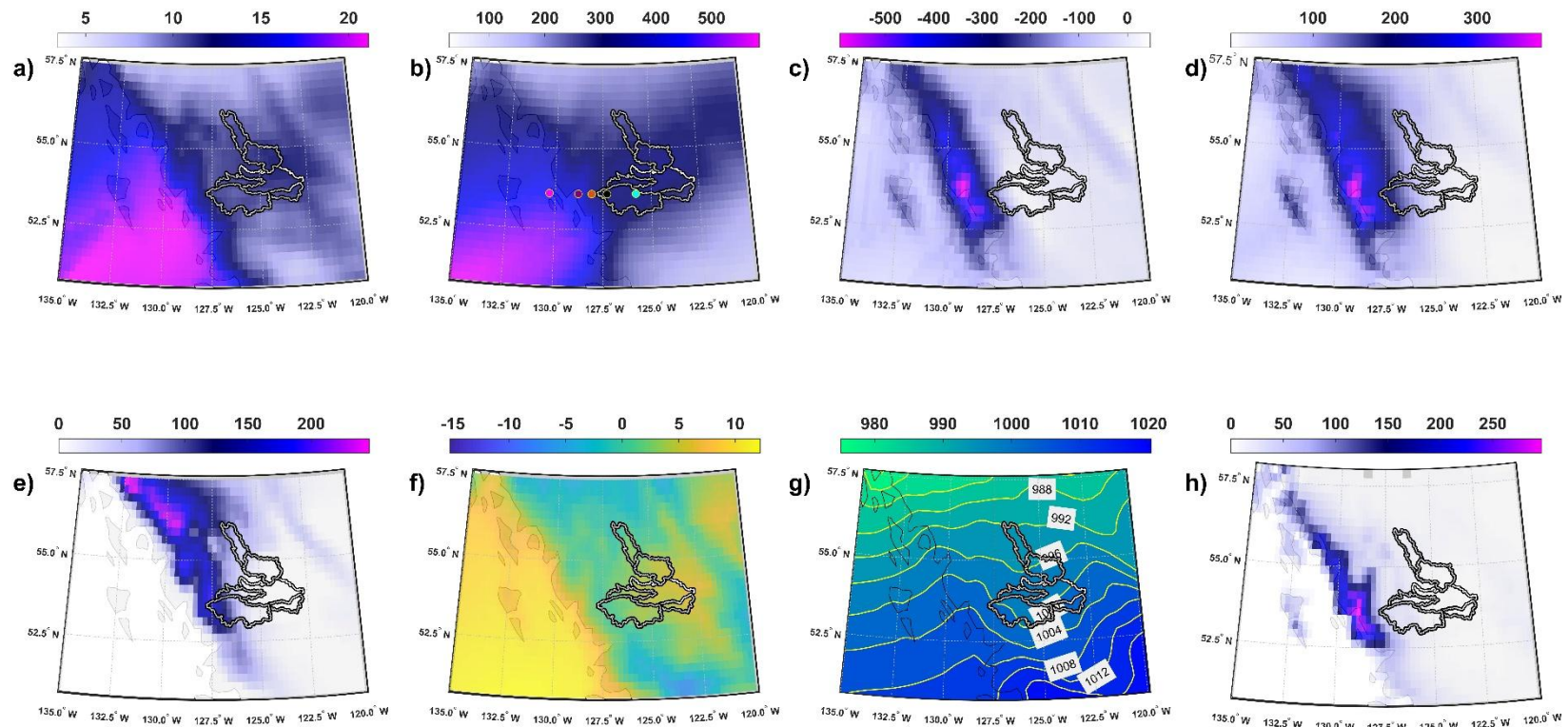


Figure 4.5 – Maps for (a) mean total column of water vapour (mm), (b) mean integrated water vapour transport (IVT - $\text{kg m}^{-1} \text{s}^{-1}$) and the location of the five positions along the latitudinal transect, (c) moisture divergence (negative values mean convergence) (mm), (d) total precipitation (mm), (e) snowfall (mm), (f) mean 2-m air temperature ($^{\circ}\text{C}$), (g) mean sea-level pressure (hPa) during the peak of moisture convergence with contour lines and (h) accumulated runoff (mm) during the AR event occurred on 28 October to 1 November 1978.

4.4.1.3 27-31 October 2009

This AR event began late on 27 October 2009 with an increase in the region's water vapour content (Fig. 4.6a), which stayed elevated, above 15 mm, for most of the event. The accumulation of water vapour southwest of the NRB began on 27 October and was carried by westerly winds, peaking in the watershed at midday on 29 October (Fig. 4.6b). Unlike the previous two events, this one exhibits two clear surges of IVT (Fig. 4.6b), suggesting that it may have been caused by two sequential ARs instead of just one. IVT (Fig. 4.6b) in the region started increasing as the column water vapour (Fig. 4.6a) built up, lasting initially for ~24 hours, then decreasing for ~12 hours before rising again on 29 October (Fig. 4.6c). Convergence (Fig. 4.6c), rainfall (Fig. 4.6d), and snowfall (Fig. 4.6e) also display two distinct periods that mirror the behaviour of IVT, supporting the idea of two ARs affecting the NRB during this significant event. As presented for the 1978 AR event, IWV and IVT maps at the peak of landfalling IVT for the 2009 AR event are presented in Figure G.1 – b and d (Appendix G). Convergence and total precipitation peak around midday on 29 October, while snowfall peaks during the initial AR before the warm air reaches the NRB, causing temperatures (Fig. 4.6f) to rise to positive values for ~48 hours. The mean sea-level pressure in the NRB also shows two distinct meteorological lows on 28 and 30 October, further suggesting the impact of two AR events on the watershed.

When examining the event on a spatial scale, similar to the 1978 event, the water vapour content (Fig. 4.7c) and IVT are concentrated southwest of the watershed. Convergence (Fig. 4.7c) and total precipitation (Fig. 4.7d) peak outside of the NRB, specifically southwest of the Upper Nechako, with convergence once again surpassing total precipitation (~350 mm compared to ~300 mm). Snowfall (Fig. 4.7e) also reaches its highest point outside the NRB, southwest of

the Upper Nechako and northwest of the Upper Stuart. Within the watershed, the highest values are recorded west of the Upper Nechako, as indicated by the black line in Fig.6e. The average total precipitation in the Upper Nechako during this AR event is 72 mm, contributing an estimated 1.01 km³ of precipitation to the Upper Nechako. As in the other exceptional AR events, air temperature (Fig.7f) in the NRB is the primary driver influencing snowfall (Fig.7e) and runoff (Fig.7h). Figures A.20 and A.21 (a to j) depict the synoptic conditions at 12-hour intervals during the 2009 AR event, showcasing mean sea-level pressure isobars and 500 hPa geopotentials.

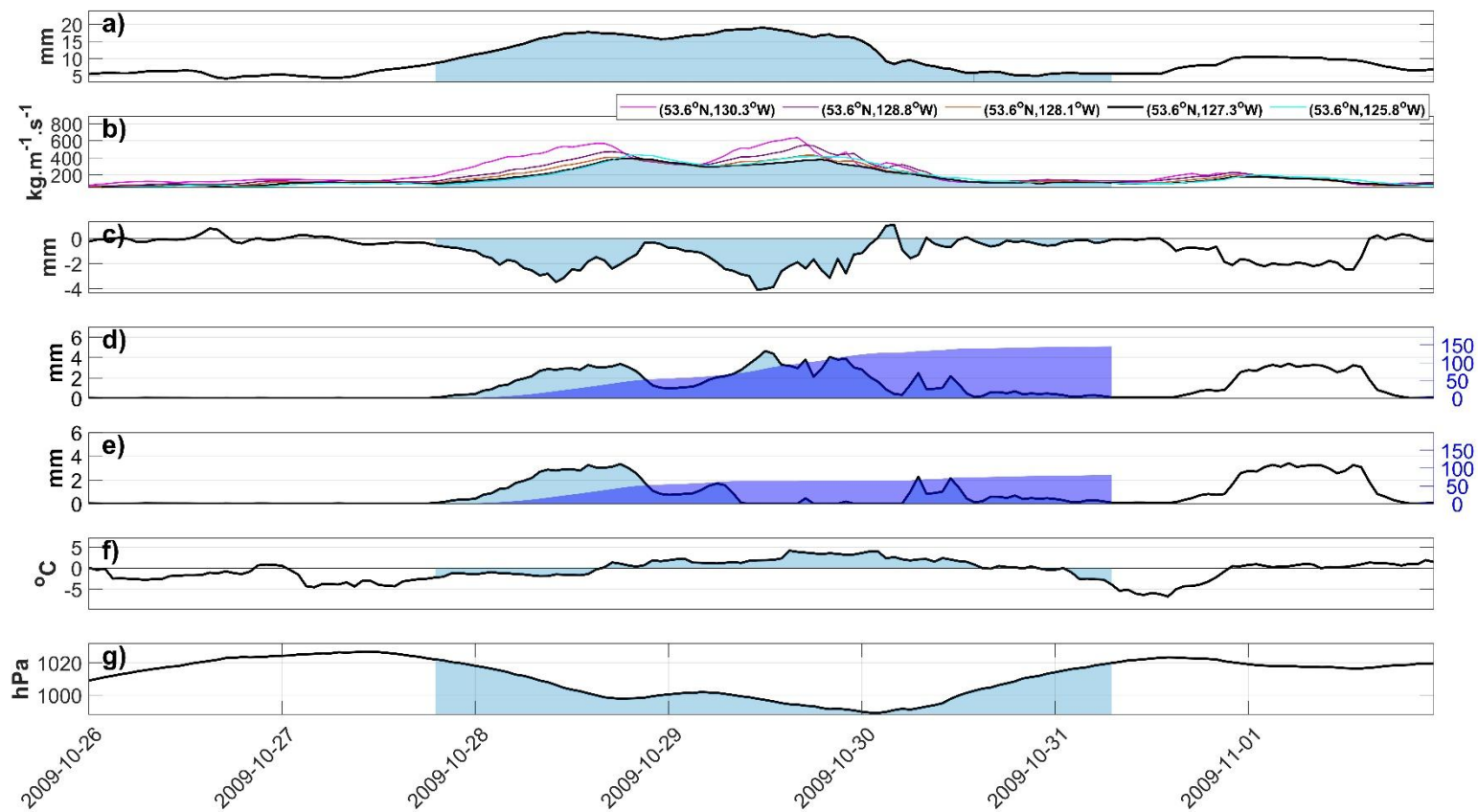


Figure 4.6 – Climogram of the AR event from 27-31 October 2009. The panels show (a) the total column of water vapour (mm), (b) integrated water vapour transport (IVT - $\text{kg m}^{-1} \text{s}^{-1}$) at five positions along a latitudinal transect, (c) moisture divergence (negative values mean convergence) (mm), (d) total precipitation in light blue (mm) and cumulative precipitation in dark blue (mm), (e) snowfall in light blue (mm of water equivalent) and cumulative snowfall in dark blue (mm), (f) mean 2-m air temperature ($^{\circ}\text{C}$), and (g) mean sea-level pressure (hPa) during the AR event (shaded in light blue) occurred on 27-31 October 2009.

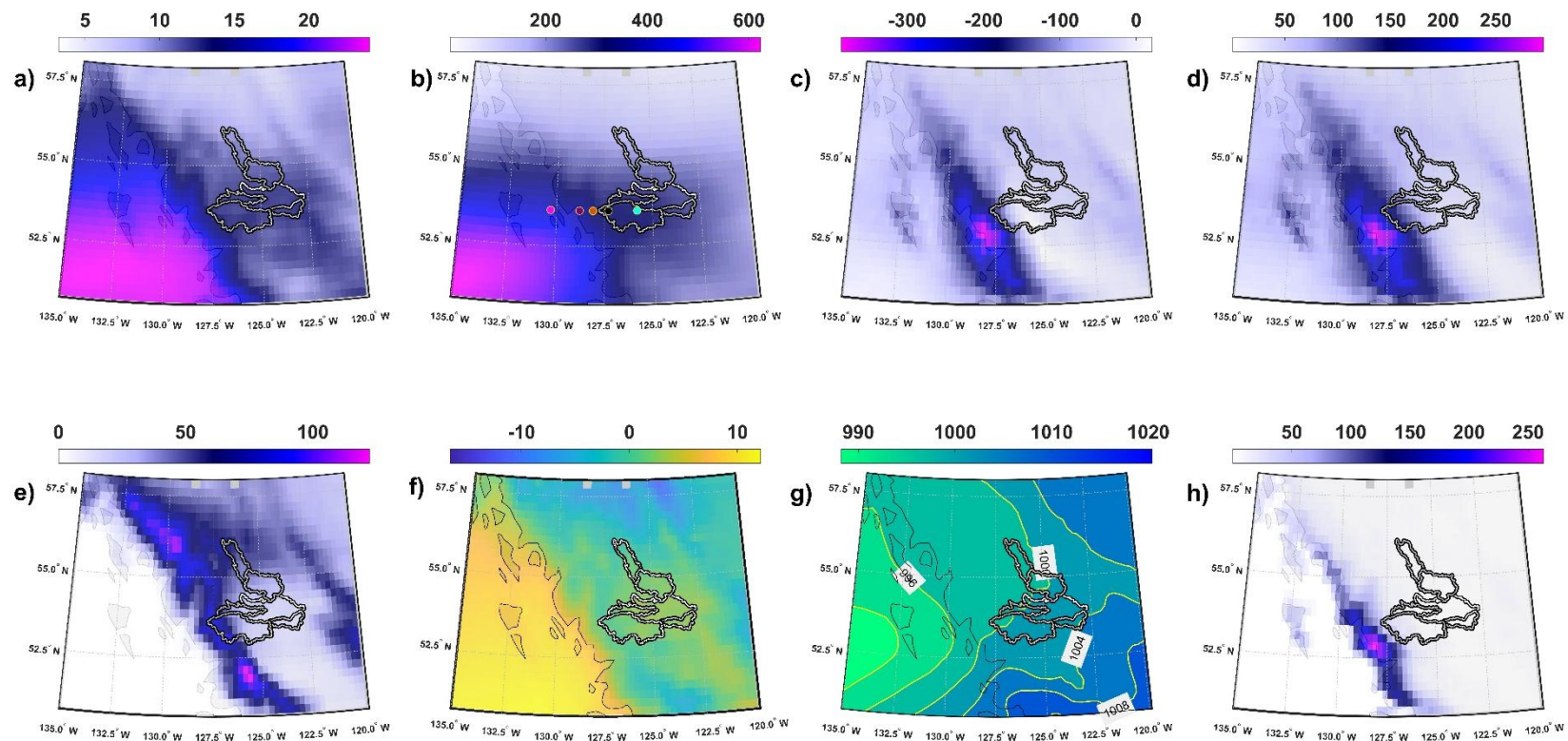


Figure 4.7 – Maps for (a) mean total column of water vapour (mm), (b) mean integrated water vapour transport (IVT - $\text{kg m}^{-1} \text{s}^{-1}$) and the location of the five positions along the latitudinal transect, (c) moisture divergence (negative values mean convergence) (mm), (d) total precipitation (mm), (e) snowfall (mm), (f) mean 2-m air temperature ($^{\circ}\text{C}$), (g) mean sea-level pressure (hPa) during the peak of moisture convergence with contour lines and (h) accumulated runoff (mm) during the AR event occurred on 27-31 October 2009.

The results highlight different synoptic patterns and hydrological responses in the NRB during the exceptional AR events. Each event demonstrates how ARs influence IVT, moisture convergence, air temperature, precipitation, and snowfall, with the Coast Mountains' orographic barriers playing a key role in shaping the impacts. For instance, the December 1952 event featured a sustained buildup of IVT, leading primarily to snowfall despite rising temperatures, while the October 1978 event saw a sharp peak in both IVT and moisture convergence. The 2009 event exhibited two distinct IVT peaks, indicating the passage of two consecutive ARs. These variations emphasize how the timing, temperature, and intensity of ARs create diverse downstream impacts, particularly regarding snowpack retention, discharge, and the timing of freshets in the spring of the following year.

In summary, each AR event plays a unique role in regional hydrological processes, adding a distinct "flavour" to the overall terrestrial response of the NRB. The spatial variation in AR impacts is also heavily influenced by orography and highlights the need for localized water management strategies in the Nechako region. Comparing these events provides valuable insights into AR-driven hydrology and emphasizes the necessity for future studies to account for this variability to improve water resource planning and flood risk assessments in the watershed.

4.4.2 Impacts of ARs on the NRB

A historically slight increase in the water level of the Nechako Reservoir (Figure 4.8 – black dashed line) in early November marks a hydrological response to the “AR season,” supporting Sobral and Déry’s (2023) findings on AR intensity peaking recurrently over the NRB during

mid to late fall. Different hydrological responses across the NRB throughout the exceptional AR events are depicted in the standardized discharges presented in Figure 4.9.

During the 1952 AR event, various impacts were observed on regional water bodies. As the Nechako Reservoir was being filled at the time, no reservoir level data are available, so the analysis for the 1952 AR event focuses on other water bodies. For instance, Francois Lake at Southbank (08JB001) observed a 3 cm water level rise between 14 and 18 December, indicating the AR's effect on local hydrology. Even small water level increases can significantly impact water storage when considering the lake's area. Discharge in the Nautley River near Fort Fraser (08JB003) increased by 23%, from 0.10 to 0.12 mm day⁻¹ (6.91 to 8.50 m³ s⁻¹) between 12 and 16 December 1952 (Appendix D – Figure D.5), while the Stuart River near Fort St. James (08JE001) saw a more modest hydrological impact with a ~7% rise in discharge during the same period (Appendix D – Figure D.7).

In the 1978 AR event, significant discharge increases were recorded at hydrometric stations around the NRB. For instance, the Kemano River above Powerhouse Tailrace station (08FE003) experienced a rapid runoff surge from 2.83 mm day⁻¹ (18.20 m³ s⁻¹) to 77.85 mm day⁻¹ (501.00 m³ s⁻¹) between 30 October and 1 November, followed by a sharp decline to 8.08 mm day⁻¹ (52.00 m³ s⁻¹) by 4 November. Laventie Creek (08JA015), within the Nechako Reservoir, registered a sharp rise in runoff, increasing 56-fold from 2.84 mm day⁻¹ (2.86 m³ s⁻¹) to 159.89 mm day⁻¹ (161.00 m³ s⁻¹) over the same period (Appendix D – Figure D.2). This is the highest discharge recorded at this station, exceeding the second-highest by nearly 50%. These findings emphasize the AR's potential to cause flash floods in the region, highlighting the need for further study of these atmospheric phenomena. In contrast, discharge at Van Tine Creek near the Mouth (08JA014) remained relatively stable throughout the event.

At Nadina Lake near Noralee (08JB007), water levels rose by 1 m ($\sim 0.01 \text{ km}^3$) in 72 hours, from 31 October to 3 November 1978, with sustained high levels until mid-December. Likewise, at the Nadina River at the outlet of Nadina Lake (08JB008), runoff surged from 0.48 mm day^{-1} ($2.05 \text{ m}^3 \text{ s}^{-1}$) on 31 October to 8.87 mm day^{-1} ($37.90 \text{ m}^3 \text{ s}^{-1}$) on 2 November, an 18-fold increase in ~ 48 hours. The Stellako River at Glenannan (08JB002) also showed a 42% increase in flow, from 0.19 mm day^{-1} ($8.01 \text{ m}^3 \text{ s}^{-1}$) on 31 October to 0.27 mm day^{-1} ($11.40 \text{ m}^3 \text{ s}^{-1}$) by 8 November (Appendix D – Figure D.5). Francois Lake (08JB011) experienced an 11 cm rise in water levels in early November, attributed at least partly to the AR event. The Stuart River (08JE001) showed almost no change in discharge during this time, and Stuart Lake (08JE003) experienced a delayed and gradual rise in water levels, continuing through December. The Nechako Reservoir saw a 32 cm water level increase ($\sim 0.30 \text{ km}^3$) from 1 to 9 November, which slowly rose further until mid-November (Figure 4.8). The water level stayed above the historical average by ~ 50 cm in the days after the event (Figure 4.8). Although discharges at other sub-basins were less affected, the impacts of this AR on the Upper Nechako were much greater. Despite this, the Nechako Reservoir's outflow remained stable during both the 1978 and 2009 AR events, allowing for water volume estimates to rely solely on water level changes.

In 2009, the Upper Nechako was again the most affected sub-basin, with the Nechako Reservoir rising from below to above the historical average following the AR event (Figure 4.8 – magenta line). Water levels remained above average for the rest of the year, during which 35 ARs were recorded, with an average IVT intensity of $453 \text{ kg m}^{-1} \text{ s}^{-1}$ over the region. At Tahtsa Lake near Kemano (08JA030), part of the Nechako Reservoir, water levels rose by 24 cm during the event, staying elevated until late December (Appendix D – Figure D.1). Nadina Lake (08JB007) similarly saw a water level increase from 0.48 m to 0.95 m between 28 October and 2

November, while the Nadina River (08JB008) showed a nearly nine-fold increase in runoff, from 0.23 mm day^{-1} ($0.97 \text{ m}^3 \text{ s}^{-1}$) to 2.13 mm day^{-1} ($9.10 \text{ m}^3 \text{ s}^{-1}$) in four days (Appendix D – Figure D.3). Meanwhile, the Eutsuk River at the outlet of Eutsuk Lake (08JA028) saw discharge more than double from $30.80 \text{ m}^3 \text{ s}^{-1}$ on 28 October to $80.20 \text{ m}^3 \text{ s}^{-1}$ by 9 November, maintaining high discharge rates until the end of the year. This pattern continued in the Eutsuk River, which experienced a "mini-freshet" after the AR, significantly replenishing local water resources.

The Nechako River near Vanderhoof (08JC001) saw no significant discharge increase during the 2009 AR event, despite a notable water volume increase ($\sim 0.17 \text{ km}^3$) in the Nechako Reservoir, as the SLS did not release water downstream. The Tsilcoh River (08JE004), though experiencing a 42% increase in discharge during the event, still recorded discharge levels far below those seen during the freshet period (Appendix D – Figure D.8). These AR events, while causing immediate increases in discharge, had little lasting impact on the freshet periods that followed, suggesting their short-term influence on the hydrological cycle of the NRB.

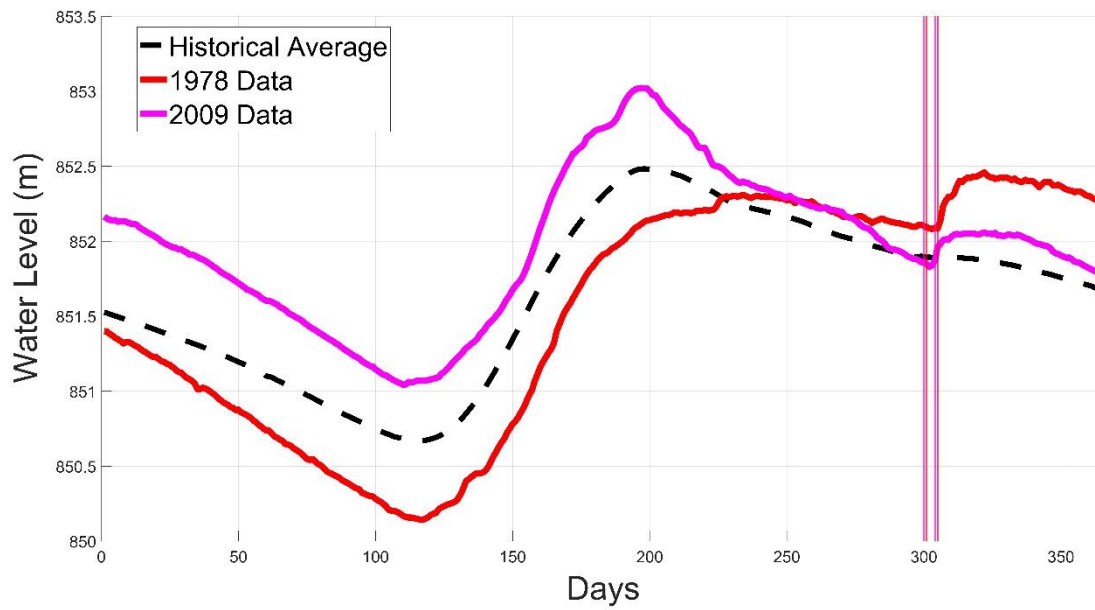


Figure 4.8 – Daily water level (m) in the Nechako Reservoir averaged for the historical period (1955-2021) (black dashed line), for the 1978 AR event (red line) and the 2009 AR event (magenta line). The vertical lines represent the occurrence period of the exceptional AR events in 1978 and 2009. No data are available for the Nechako Reservoir during the exceptional AR event in 1952.

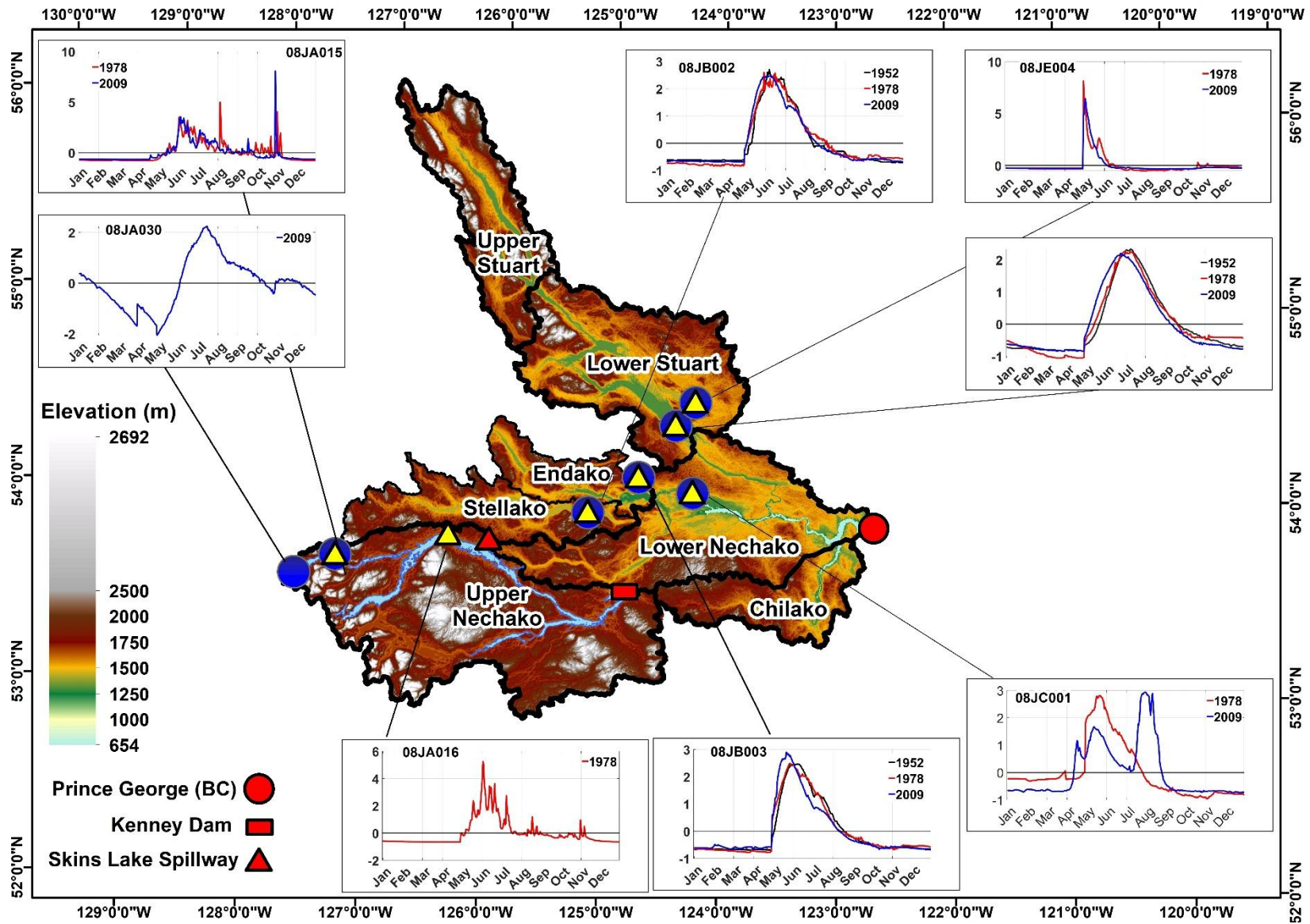


Figure 4.9 – Standardized discharge data across the NRB for the exceptional AR events of 1952 (black line), 1978 (red line), and 2009 (blue line)

4.5 DISCUSSION

The individualized analysis of exceptional AR events provides critical insights into how ARs affect the water budget input and hydrological dynamics in the NRB. The findings show that exceptional ARs may cause intense and sustained precipitation, impacting river discharge throughout the watershed and snowpack accumulation in mountainous regions. By understanding how AR events influence hydrological cycles in specific regions of the NRB, stakeholders can better anticipate changes in water levels, flooding risks, and overall seasonal water availability. In the case of the Nechako Reservoir, the impacts of ARs on snowpack retention in the Upper Nechako and the significant contributions to the reservoir's volume shows that these exceptional AR events play a key role in water replenishment, despite their downside impacts. High-intensity and duration ARs, as well as coupled mid-intensity AR events, bring to the NRB much-needed water for different stakeholders.

ARs are known to deliver large amounts of moisture to coastal and inland regions worldwide, and their influence on snow accumulation and rain-on-snow events is well documented in places like the West Coast of the United States (Curry *et al.*, 2019; Cao *et al.*, 2020). When comparing this study to Cordeira *et al.* (2013), Waliser and Guan (2017), Barth *et al.* (2017), Ralph *et al.* (2020), and Corringham *et al.* (2022), the findings align with the suggested patterns of frequency and intensity of ARs being greater in fall and winter. However, the current results for the NRB emphasize the critical role of orography, where the Coast Mountains act as a physical barrier, enhancing precipitation on the windward side (outside of the NRB). On the other hand, moisture transport to the leeward side, where the Upper Nechako and Stellako sub-basins lie, is much reduced, receiving AR contributions mainly through the “spillover effect” (Mo *et al.*, 2019). Differently, the Upper Stuart benefits from a through in the Coast Mountains

that allow ARs to reach further inland with a reduced influence of orography. Nevertheless, northern AR events such as the ones directly impacting the Upper Stuart occur earlier in the AR season and, thus, usually do not cause the detrimental impacts of exceptional AR events that occur in fall and winter.

Globally, AR events are increasingly studied due to their importance in both flooding and drought relief. In areas like Europe (Lavers and Villarini, 2013, 2015; Eiras-Barca *et al.*, 2021; van der Breggen and Hudson, 2024) and South America (Campos and Rondanelli, 2023), ARs present a marked seasonal contribution, as shown in this study for the NRB. However, the frequency, intensity and duration of ARs vary widely depending on latitudinal position, climate patterns, distance from the shoreline and topography. This study highlights the importance of not only the intensity and duration of ARs in causing copious precipitation but also their cumulative or sequential impacts. For example, the 2009 event, which was likely formed by two consecutive ARs instead of one longer AR event, may result in distinct and more extreme hydrological responses compared to isolated AR events. The cumulative impact of AR sequences can be more impactful than individual events of greater magnitude, a factor that may also be relevant in other mountainous and mid-latitudinal regions worldwide.

Furthermore, individualized studies of exceptional ARs highlight the potential for these river-shaped storms to cause flash floods, notably in mountainous regions prone to rain-on-snow events. In many parts of the world, including western Canada, rain-on-snow events caused by warm ARs can rapidly melt snowpacks, enhancing flooding. This research underscores the need for water managers to incorporate AR forecasts into flood risk assessments, ensuring that reservoirs and flood control systems are prepared for the impacts. The implications of this study extend beyond the NRB region, offering valuable insights for understanding AR impacts in

similar mountainous regions worldwide. The findings here can inform water resources management, flood preparedness, and climate adaptation strategies in the NRB and other regions that experience AR-driven hydrological impacts.

Similarities and differences between the AR events show that the total column of water vapour increases and remains relatively stable in the Upper Nechako until the end of all three AR events. In the AR events of 1978 and 2009, column water vapour overlying the Upper Nechako sharply decreased after the events, while in the 1952 winter event, the reduction was gradual. Likewise, convergence presents a more similar pattern of two distinct pulses during the AR events that occurred in the fall compared to the single, more sustained pulse of convergence in the 1952 winter event. Although all AR events exhibit IVT maxima that lead to peak precipitation inside the Nechako Reservoir, their spatial and temporal impacts over the NRB vary, with reduced impacts to the east and north of the watershed.

The 2-m air temperature in the Upper Nechako associated with each AR event shaped their hydrological responses differently. In 1952 and 1978, colder temperatures led to extensive snowfall in the Upper Nechako, while the 2009 AR event, influenced by a warmer atmospheric profile during its second IVT surge, resulted in a more balanced ratio of rain and snow. These contrasting temperature responses play a crucial role in determining whether AR-related precipitation reaches the land surface as snow or rain, which directly influences flooding and water resources management, particularly in mountainous catchments. For all events, air temperature consistently increases as the AR moves inland. However, in 1952, during winter, there was a sharper increase, likely due to the lower initial temperatures encountered by the warm airmass of the AR in mountainous terrain. Additionally, mean sea-level pressure steadily decreases and remains lower than in the preceding days during all AR events. This is attributed

to the proximity of the low-pressure system associated with the mid-latitude cyclone that shapes the AR.

A spatial analysis comparing the exceptional AR events shows that higher values of water vapour columns and IVT are observed southwest of the NRB during the 1978 and 2009 AR events, while in the 1952 event values are higher south of the watershed. Total precipitation, and thus rainfall and snowfall, have a northwest-to-southeast orientation in all events, which highlights once again the importance of the orography as one of the main drivers in causing AR-related precipitation in western Canada. Despite the colder temperatures across the upper Nechako during the 1952 AR event, the spatial patterns of 2-m air temperature are also similar during all events and are much controlled by the Coast Mountains orography as well.

The significant impacts of the first two ARs examined in this study have been documented by Septer *et al.* (2007) as notable natural hazards that include flooding and landslides in northern BC. During the AR event of December 1952, landslides and washouts were recorded in the adjacent Skeena River Basin (SRB), from Terrace to Prince Rupert, northwest and outside of the Upper Nechako sub-basin. As depicted in Figures 4.3c and 4.3d, regions located northwest and south of the Upper Nechako exhibit the highest accumulated totals for convergence and total precipitation, respectively. Washouts measuring up to 90 cm in depth were observed on the Yellowhead Highway at Kwinitza, situated on the leeward side of the Coast Mountains. A combination of rainfall and snowfall was documented during this event in the SRB area closer to the NRB. The dual nature of ARs, providing essential water replenishment while increasing flood risks, underscores the need for adaptive water management strategies. By incorporating real-time AR forecasting into reservoir management systems, decision-makers can maximize the benefits of AR events while mitigating their risks.

Given that the majority of precipitation within the NRB fell as snow (Fig. 4.3e) during the 1952 AR event, the immediate impacts of the event were largely experienced by regions within the SRB. The Upper Nechako received significant snow due to the lower temperatures in the Nechako Plateau during the 1952 AR event. Consequently, for the Nechako Reservoir, the event can be primarily beneficial for water (snow) storage purposes, potentially aiding in initially replenishing the reservoir through substantial snowpack buildup. However, elevated precipitation totals, particularly during high-intensity events, can result in considerable damage and likely contributed to the adverse effects in the area encompassing (and near) Entiako, Finger-Tatuk, and Kluskoil Lake Provincial Parks (Septer *et al.*, 2007). The socio-economic impacts of ARs, particularly in regions that rely on the Nechako Reservoir as their main water supply, emphasize the importance of early-warning systems and adaptive infrastructure that can cope with the immediate impacts of high-intensity ARs.

ARs are well-known in BC to be linked to regional natural disasters. From 29 October to 7 November 1978, northwestern BC experienced two floods, the first caused by the 1978 exceptional AR assessed by this study. Likewise the AR event of 1952, the greater impacts were registered outside (northwest) of the NRB. The remoteness of the Upper Nechako may explain the limited information available on its impacts during the 1978 AR event. However, the effects in this region were likely comparable to those observed in sub-basins situated northwest of the NRB. According to the Canadian Disaster Database records, the Kitimat Village, Thornhill, Lakelse Lake, and Old Reno areas were greatly affected by floods. Northwest of the NRB, the Terrace-Kitimat area was designated as a disaster zone, and the railway line between Smithers and Terrace was shut down. Kitimat witnessed an impressive accumulation of ~400 mm of precipitation in just four days (29 October to 1 November), while Prince Rupert recorded ~226 mm in the same period. Nearby waterways, such as the Hatchery

River, experienced a substantial increase in discharge, approximating the estimates of a rare 100-year event (Septer *et al.*, 2007).

ARs play a vital role in delivering much-needed precipitation to the Nechako Reservoir. However, when these ARs trigger rain-on-snow events, they can quickly accelerate snowmelt, increasing the risk of floods by sending more runoff into the reservoir. When that occurs, the balance between the long-term benefits of AR-driven precipitation for water storage and the immediate risks of flooding must be managed. Managing this balance has become even more critical when facing exceptional AR events, making it essential to integrate advanced AR forecasting into water management systems that control the Nechako Reservoir. With better forecasting, the reservoir's operator can be better prepared to respond to these events while still benefiting from the water ARs bring to the NRB.

Stakeholders that rely on the Nechako Reservoir face the challenge of ensuring a steady and sufficient water supply while also protecting against the dangers of floods and landslides caused by ARs. This highlights the need for greater investment in research and infrastructure to make these sectors more resilient to the downside impacts of exceptional AR events while maximizing their benefits. Close collaboration among various professionals (e.g., meteorologists, engineers, and hydrologists) as well as policymakers will be key in developing sustainable solutions that can meet water resource needs and cope with the adverse challenges posed by exceptional ARs.

4.6 CONCLUSIONS

This study provides a detailed characterization of the synoptic setting of three exceptional AR events that occurred in 1952, 1978, and 2009. All AR events are marked by increases in water vapour and IVT southwest of the watershed, with moisture convergence peaks leading to enhanced precipitation in the region. Decreases in the average sea-level pressure and increases in air temperature were also associated with these AR events due to the proximity of the mid-latitude cyclone to BC's shoreline and the increased temperatures with the water vapour coming from the southwest, respectively. In the NRB, AR landfalls can be associated with rainfall, snowfall, or a mix of both precipitation types depending mainly on air temperatures, which are related to elevation, proximity to the Pacific Ocean and seasonality. The interaction of these water budget input variables, along with local topography, the frequency, wind speed, and duration of AR events in the region, highlights the different "flavours" of ARs that can impact the NRB.

The exceptional AR events of 1952 and 1978 primarily contributed to snowpack formation in the Upper Nechako rather than immediate flooding. However, the 1978 event's rain-on-snow conditions may have enhanced flooding in mountainous streams and creeks at higher elevations. These events clearly demonstrate the significant benefits ARs bring to the NRB in terms of water replenishment, particularly to the Nechako Reservoir. The Upper Nechako received, on average, 1.14 km³ of total precipitation during the assessed exceptional AR events, which is approximately 3.5% of the Nechako Reservoir's total volume. The observed abrupt increases in water levels and discharge, particularly across streams and creeks in the mountainous catchments of the Upper Nechako, underscore the need for ongoing and expanded research to better understand and prepare for AR-induced hydrological impacts.

The 2009 AR event presented a distinct synoptic setting compared to the others. It likely comprised two sequential ARs, leading to more than one substantial increase in IVT and convergence and highlighting the dual nature of ARs in providing both immediate and sustained hydrological impacts. Notably, the AR events of 1978 and 2009 contributed substantially to elevating the water level of the Nechako Reservoir and show the potential of these river-shaped storms to serve as a main source of water replenishment for central BC.

Future studies should focus on understanding the associations of ARs with climate indices (teleconnections) and improving resilience against the impacts of extreme weather events linked to ARs in BC. Moreover, future studies should also employ advanced hydrological models and new AR datasets to simulate the effects of ARs on river discharge, air and water temperature, and reservoir levels using high-resolution climate data and machine learning technologies. With better predictions of AR behaviour, we can optimize flood management and water storage, particularly if AR events become more frequent and severe in the next decades as a consequence of sea-surface warming in the Pacific Ocean.

CHAPTER 5: KEY FINDINGS, IMPLICATIONS, CONCLUSIONS AND FUTURE STUDIES

5.1 SUMMARY

ARs are long and narrow bands of concentrated water vapour transport in the lower troposphere. Despite being mostly known for their detrimental impacts in BC, ARs play an important part in the hydrological cycle in western Canadian watersheds. This dissertation provides a thorough examination of ARs impacting Canada's west coast and their impacts on the Nechako River Basin. It addresses key aspects such as AR types, frequency, intensity, duration, trends, and hydrological responses of waterways within the NRB. By doing so, it contributes to the understanding of AR impacts on the regional hydrological cycle and the broader implications for the study area.

The study underscores the critical role of ARs in replenishing water resources within the NRB, particularly in mountainous terrain during the fall and winter seasons. The beneficial and detrimental impacts of ARs fade progressively from west to east across the basin. ARs are predominantly beneficial for the NRB; however, they can become hazardous under specific conditions such as landfall on saturated soils, steep rocky terrain, and during rain-on-snow events. The seasonal analysis indicates increased AR activity in September and October, with November experiencing the highest average AR intensity within the NRB.

Trend analyses reveal a notable shift in AR-related precipitation, with a move from mid- to low-intensity AR types in several sub-basins. This shift suggests a potentially positive impact on the regional water budget, as lower-intensity ARs are mostly beneficial and are less prone to cause hazardous impacts. Nonetheless, the reduced classification of common AR types could point to long-term changes in water availability. Increasing trends in total precipitation linked

to low-intensity ARs in the northern and western sectors of the NRB, along with rising AR-related rainfall contributions, may demand adjustments in water management practices of regulated water bodies of the NRB. These trends are also likely to affect the seasonal snowpack in the NRB's headwaters, emphasizing the need for coping strategies in water resource management.

ARs contribute to about one-fifth of the total precipitation in the NRB, bringing predominantly rainfall in autumn and a mix of rainfall and snowfall in winter. The study highlights that AR-days account for a significant portion of daily precipitation events of mid-to-high intensity in the Upper Nechako, illustrating ARs' substantial influence on total precipitation, rainfall, snowpack formation, runoff, and, consequently, regional water budgets. Since the 2000s, there has been an observed increase in the fraction of rainfall in AR-related precipitation within certain NRB sub-basins, alongside rising average air temperatures in Western Canada. This change is particularly evident in the reduction of AR-related snow during summer and the increasing trends of rainfall in the northern parts of the NRB during spring. Despite these statistically significant changes in spring and summer, their overall impact on the Nechako Reservoir's replenishment should be minimal due to the low fractional annual contributions. The study emphasizes significant spatial variations in AR contributions to the NRB's hydrological cycle and highlights the importance of utilizing new high-resolution AR datasets, such as the recently published ERA5-based global AR databases by Mo (2024) and Guan and Waliser (2024), in future studies.

Exceptional AR events are characterized by increased column water vapour and transport southwest of the watershed, leading to increased precipitation in the NRB. These events are linked to decreased sea-level pressure and increased temperatures in the NRB region due to the

proximity of mid-latitude cyclones that shape the ARs to BC's shoreline. Historical exceptional AR events, such as those in 1952 and 1978, significantly contributed to snowpack formation in the Upper Nechako, highlighting the dual role of ARs in both water replenishment and potential natural hazards like landslides, floods, and reservoir overflow.

5.1.1 AR Impacts on the NRB's Ecosystem

ARs significantly influence the ecohydrological dynamics within the NRB. The variations in intensity, frequency, duration, and seasonality of ARs directly affect the basin's water resources, impacting aquatic and terrestrial ecosystems. During the fall and winter, ARs sustain river flows after the snowmelt-induced freshet and contribute to snowpack formation in mountainous regions. This snowpack acts as a critical water reserve, gradually melting to support river flows in spring and early summer. However, the large volumes of precipitation in short periods brought by ARs can cause rapid changes in streamflow, water levels, and temperatures, adversely affecting the NRB, including the habitat of aquatic species. For instance, salmon migrating ~1,500 km through the Fraser River to spawn in the NRB are particularly sensitive to changes in water temperature and flow regimes caused by ARs. The timing of the "salmon run" overlaps with the "AR season" and can support or hinder their migration, depending on whether the precipitation leads to increased flows or sudden shifts in water conditions (e.g., turbidity, oxygen concentration, water temperature, etc.).

Beyond their impact on water volume and flow, ARs also affect water quality in the NRB. The heavy rains associated with ARs, particularly in the fall, can increase sediment transport from surrounding landscapes into waterways, increasing turbidity and reducing water quality. This influx of sediments during or after AR events can lower oxygen levels and introduce nutrients or pollutants that alter the chemical composition of aquatic habitats, stressing species adapted

to cold-water environments, such as salmonids. These cumulative impacts highlight the need for a deeper understanding of ARs' role in the NRB ecosystem, balancing their benefits in replenishing water resources with the potential risks they pose to aquatic and terrestrial environments.

5.1.2 Implications for Rio Tinto's Operations of the Nechako Reservoir

The changing patterns of ARs impacting the Nechako Reservoir may require Rio Tinto to adapt its management strategies to address shifts in the region's hydrological cycle. The observed decrease in mid-magnitude ARs and the rise in lower-magnitude ARs suggest a potential reduction in long-term natural hazards like severe flooding and landslides. However, this shift could also mean a decrease in AR contributions to the reservoir's water resources, particularly during the crucial fall and early winter periods. Continuous monitoring of ARs is essential to verify these trends and adjust water management practices accordingly.

Despite the absence of significant trends for higher-magnitude AR events, the potential for high-intensity, long-duration ARs to cause significant fluctuations in water levels and discharge remains, mainly during fall. While the lack of an increasing trend in high-magnitude ARs might reduce hazardous impacts in the long term, it does not remove the risk of occasional extreme AR events. Thus, Rio Tinto should stay vigilant and maintain adaptive management protocols to handle these outlier events caused by ARs.

To manage the reservoir effectively, Rio Tinto might consider lowering reservoir levels if near full-capacity in late summer and early fall to create additional capacity for AR inflows. This approach would reduce the need for emergency releases, minimize downstream flooding risks, and maintain more natural flow conditions in rivers year-round. However, the unpredictability

of AR activity also requires keeping a safe water storage volume to avoid shortages if AR activity declines, as observed in past periods like from 1968 to 1986. Still, AR activity impacting the Nechako Reservoir with positive variations to the average became more common starting in the 1990s.

Additionally, developing advanced hydrological modelling and real-time monitoring systems could enhance Rio Tinto's ability to predict and respond to AR events. These tools would provide critical data on ARs, allowing for more precise adjustments to the Nechako Reservoir's inflows and managed outflows. By integrating state-of-the-art models into daily operations, Rio Tinto can optimize water management strategies and practices, ensuring the long-term sustainability of the Nechako Reservoir's water resources while minimizing adverse environmental impacts downstream of the Upper Nechako sub-basin.

5.1.3 Recommendations for Future-Related Research

While this dissertation explores the impacts of ARs on the NRB, further research is necessary to fully understand these river-shaped phenomena and their long-term implications for the NRB's water budget. Future studies should focus on how projected climate scenarios might affect AR activity in the NRB. With global temperatures rising, potential changes in the frequency, intensity, and duration of ARs could alter the region's hydrological dynamics. Modelling these changes under different climate scenarios will be crucial for assessing their impact on future water availability, flood risks, and ecosystem health. Research should also investigate the "hydrometeor drift" effect, where moisture is transported across the Coast Mountains into the NRB, interacting with the orography. Understanding how this might change under future climate conditions is vital for enhancing water resources management in the NRB and Nechako Reservoir.

Ongoing monitoring of ARs, through initiatives like the MECHE (Monitoring Extreme Climate and Hydrometeorological Events) observatory and TRARE (Tahtsa Ranges Atmospheric River Experiment), is essential for collecting detailed data on AR characteristics and understanding their impacts in western BC. These efforts should be complemented by studies on water vapour transport from the Pacific Ocean to BC, AR-related precipitation, sediment transport, water temperature changes, and overall impacts on water quality. Integrating advanced hydrological models with monitoring data may provide more realistic models and improve our ability to foresee and mitigate AR-related risks in the NRB. Collaborative research that combines Indigenous traditional ecological knowledge with the western scientific method could lead to more effective and inclusive water management strategies. Addressing these research areas will deepen our understanding of ARs and their role in the NRB, ultimately supporting the development of more resilient and adaptive water management practices in central BC.

REFERENCES

- Abou Rafee, S. A., Freitas, E. D., Matins, J. A., Martins, L. D., Domingues, L. M., Nascimento, J. M. P., Machado, C. B., Santos, E. B., Rudke, A. P. Fujita, T., Souza, R. A. F., Hallak, R., and Uvo, C. B. (2020). Spatial Trends of Extreme Precipitation Events in the Paraná River Basin. *Journal of Applied Meteorology and Climatology*, 59(3), 443-454. <https://doi.org/10.1175/JAMC-D-19-0181.1>.
- Addinsoft (2022) XLSTAT Statistical and Data Analysis Solution. Available at <https://www.xlstat.com>.
- Aditya, F., Gusmayanti, E., and Sudrajat, J. (2021). Rainfall trend analysis using Mann-Kendall and Sen's slope estimator test in West Kalimantan. *Earth and Environmental Science*. 893(1):012006. <https://doi.org/10.1088/1755-1315/893/1/012006>.
- Ahrens, D. C., Jackson, P. L., and Jackson, C. E. J. (2016). *Meteorology Today: An Introduction to Weather, Climate, and the Environment* (2nd Canadian edition).
- Albers, S. J., Déry, S. J., and Petticrew, E. L. (2016). Flooding in the Nechako River Basin of Canada: A random forest modelling approach to flood analysis in a regulated reservoir system. *Canadian Water Resources Journal*, 41(1–2), 250–260. <https://doi.org/10.1080/07011784.2015.1109480>.
- Alexander, M. A., Scott, J. D., Friedland, K. D., Mills, K. E., Nye, J. A., Pershing, A. J., and Thomas, A. C. (2018). Projected sea surface temperatures over the 21st century: Changes in the mean, variability and extremes for large marine ecosystem regions of Northern Oceans. *Elementa: Science of the Anthropocene*, 6(9), 9. <https://doi.org/10.1525/elementa.191>.
- Arias, P. A., Rivera, J. A., Sörensson, A. A., Zachariah, M., Barnes, C., Philip, S., Kew, S., Vautard, R., Koren, G., Pinto, I., Vahlberg, M., Singh, R., Raju, E., Li, S., Yang, W., Vecchi, G. A., and Otto, F. E. L. (2024). Interplay between climate change and climate variability:

- the 2022 drought in Central South America. *Climatic Change*, 177(1), 1-22. <https://doi.org/10.1007/s10584-023-03664-4>.
- Baek, S. H., Battalio, J. M., and Lora, J. M. (2023). Atmospheric river variability over the last millennium driven by annular modes. *American Geophysical Union Advances*, 4(1), 3. <https://doi.org/10.1029/2022AV000834>.
- Barth, N. A., Villarini, G., Nayak, M. A., and White, K. (2017). Mixed populations and annual flood frequency estimates in the western United States: The role of atmospheric rivers. *Water Resources Research*, 53(1), 257-269. <https://doi.org/10.1002/2016WR019064>.
- Benassi, M., Conti, G., Gualdi, S., Ruggieri, P., Materia, S., García-Serrano, J., Palmeiro, F.M., Batté, L., and Ardilouze, C. (2022). El Niño teleconnection to the Euro-Mediterranean late-winter: the role of extratropical Pacific modulation. *Climate Dynamics*, 58(7–8), 2009–2029. <https://doi.org/10.1007/s00382-021-05768-y>.
- Bush, E., and Lemmen, D. S. (2019). Canada's changing climate report. Accessed on 7 July, 2024. <https://changingclimate.ca/CCCR2019>.
- Campos, D., and Rondanelli, R. (2023). ENSO-Related Precipitation Variability in Central Chile: The Role of Large Scale Moisture Transport. *Journal of Geophysical Research: Atmospheres*, 128(17), 1-13. <https://doi.org/10.1029/2023JD038671>.
- Cao, Q., Gershunov, A., Shulgina, T., Ralph, F. M., Sun, N., and Lettenmaier, D. P. (2020). Floods due to atmospheric rivers along the U.S. West Coast: The role of antecedent soil moisture in a warming climate. *Journal of Hydrometeorology*, 21(8), 1827–1845. <https://doi.org/10.1175/JHM-D-19-0242.1>.
- Chagas, V. B. P., Chaffe, P. L. B., and Blöschl, G. (2022). Climate and land management accelerate the Brazilian water cycle. *Nature Communications*, 13(1), 5136. <https://doi.org/10.1038/s41467-022-32580-x>.

- Charles, P., Arsenault, R., Martel, J. L., Gatién, P., and St-Hilaire, A. (2023). Quantifying the evolution of ensemble water temperature forecasts as a function of weather forecast lead-time: case study on the Nechako River watershed. *Canadian Water Resources Journal*. <https://doi.org/10.1080/07011784.2022.2163189>.
- Cordeira, J. M., Ralph, F. M., and Moore, B. J. (2013). The development and evolution of two atmospheric rivers in proximity to western North Pacific tropical cyclones in October 2010. *Monthly Weather Review*, 141(12), 4234–4255. <https://doi.org/10.1175/MWR-D-13-00019.1>.
- Corringham, T. W., McCarthy, J., Shulgina, T., Gershunov, A., Cayan, D. R., and Ralph, F. M. (2022). Climate change contributions to future atmospheric river flood damages in the western United States. *Scientific Reports*, 12(1), 13747. <https://doi.org/10.1038/s41598-022-15474-2>.
- Costa, R. L., Macedo de Mello Baptista, G., Gomes, H. B., Daniel dos Santos Silva, F., Lins da Rocha Júnior, R., de Araújo Salvador, M., and Herdies, D. L. (2020). Analysis of climate extremes indices over northeast Brazil from 1961 to 2014. *Weather and Climate Extremes*, 28(March), 100254. <https://doi.org/10.1016/j.wace.2020.100254>.
- Curry, C. L., Islam, S. U., Zwiers, F. W., and Déry, S. J. (2019). Atmospheric rivers increase future flood risk in Western Canada's largest Pacific river. *Geophysical Research Letters*, 46(3), 1651–1661. <https://doi.org/10.1029/2018GL080720>.
- Dalla Torre, D., Di Marco, N., Menapace, A., Avesani, D., Righetti, M., and Majone, B. (2024). Suitability of ERA5-Land reanalysis dataset for hydrological modelling in the Alpine region. *Journal of Hydrology: Regional Studies*, 52, 101718. <https://doi.org/10.1016/j.ejrh.2024.101718>.
- de Carvalho, A. A., Abelardo, A. A., da Silva, H. P., Lopes, I., de Moraes, J. E. F., and da Silva, T. G. F. (2020). Trends of rainfall and temperature in Northeast Brazil. *Revista Brasileira*

de Engenharia Agrícola e Ambiental, 24(1), 15–23. <https://doi.org/10.1590/1807-1929/agriambi.v24n1p15-23>.

DeFlorio, M. J., Sengupta, A., Castellano, C. M., Wang, J., Zhang, Z., Gershunov, A., Guirguis, K., Nino, R. L., Clemesha, R. E. S., Pan, M., Xiao, M., Kawzenuk, B., Gibson, P. B., Sheftic, W., Broxton, P. D., Switanek, M. B., Yuan, J., Dettinger, M. D., Hecht, C. W., Cayan, D. R., Cornuelle, B. D., Miller, A. J., Kalansky, J., Monache, L. D., Ralph, F. M., Waliser, D. E., Robertson A. W., Zeng, X., DeWitt, D. J., Jones, J. and Anderson, M. L. (2024). From California's Extreme Drought to Major Flooding, Evaluating and Synthesizing Experimental Seasonal and Subseasonal Forecasts of Landfalling Atmospheric Rivers and Extreme Precipitation during Winter 2022/23. *Bulletin of the American Meteorological Society*, 105(1), E84–E104. <https://doi.org/10.1175/BAMS-D-22-0208.1>.

Déry, S. J., Hernández-Henríquez, M. A., Owens, P. N., Parkes, M. W., and Petticrew, E. L. (2012). A century of hydrological variability and trends in the Fraser River Basin. *Environmental Research Letters*, 7(2), 024019. <https://doi.org/10.1088/1748-9326/7/2/024019>.

Déry, S. J., Hernández-Henríquez, M. A., Stadnyk, T. A., and Troy, T. J. (2021): Vanishing weekly hydropeaking cycles in American and Canadian rivers, *Nature Communications*, 12, 7154, doi: 10.1038/s41467-021-27465-4.

Déry, S. J., Martins, E. G., Owens, P. N., and Petticrew, E. L. (2024). Extreme hydrometeorological events induce abrupt and widespread freshwater temperature changes across the Pacific Northwest of North America. *Communications Earth and Environment*, 5, 228. <https://doi.org/10.1038/s43247-024-01407-6>.

Desreumaux, Q., Leconte, R., and Côté, P. (2014). Role of hydrologic information in stochastic dynamic programming: a case study of the Kemano hydropower system in British Columbia.

- Canadian Journal of Civil Engineering*, 41(9), 839–844. <https://doi.org/10.1139/cjce-2013-0370>.
- Dettinger, M. D., Ralph, F. M., Das, T., Neiman, P. J., and Cayan, D. R. (2011). Atmospheric rivers, floods and the water resources of California. *Water (Switzerland)*, 3(2), 445–478. <https://doi.org/10.3390/w3020445>.
- Dezfuli, A., Bosilovich, M. G., and Barahona, D. (2021). A Dusty Atmospheric River Brings Floods to the Middle East. *Geophysical Research Letters*, 48(23), e2021GL095441. <https://doi.org/10.1029/2021GL095441>.
- Dong, W., Zhao, M., Tan, Z., Ramaswamy, V. (2024). Atmospheric rivers over eastern US affected by Pacific/North America pattern. *Science Advances*, 10(4), eadj3325. <https://doi.org/10.1126/sciadv.adj3325>.
- Eiras-Barca, J., Ramos, A. M., Algarra, I., Vázquez, M., Dominguez, F., Miguez-Macho, G., Nieto, R., Gimeno, L., Taboada, T., and Ralph, F. M. (2021). European West Coast atmospheric rivers: A scale to characterize strength and impacts. *Weather and Climate Extremes*, 31(100305). <https://doi.org/10.1016/j.wace.2021.100305>.
- Espinoza, J. C., Jimenez, J. C., Marengo, J. A., Schongart, J., Ronchail, J., Lavado-Casimiro, W., and Ribeiro, J. V. M. (2024). The new record of drought and warmth in the Amazon in 2023 related to regional and global climatic features. *Scientific Reports*, 14(1), 1-13. <https://doi.org/10.1038/s41598-024-58782-5>.
- Fatolahzadeh Gheysari, A., Maghoul, P., Ojo, E. R., Shalaby, A. (2024). Reliability of ERA5 and ERA5-Land reanalysis data in the Canadian Prairies. *Theoretical and Applied Climatology*, 155, 3087–3098. <https://doi.org/10.1007/s00704-023-04771-z>.
- Fish, M. A., Wilson, A. M., and Ralph, F. M. (2019). Atmospheric river families: Definition and associated synoptic conditions. *Journal of Hydrometeorology*, 20(10), 2091–2108. <https://doi.org/10.1175/JHM-D-18-0217.1>.

- Garcia-Soto, C., Cheng, L., Caesar, L., Schmidtko, S., Jewett, E. B., and Cheripka, A. (2021). An overview of ocean climate change indicators: Sea surface temperature, ocean heat content, ocean pH, dissolved oxygen concentration, Arctic sea ice extent, thickness and volume, sea level and strength of the Atlantic Meridional Overturning Circulation (AMOC). *Frontiers in Marine Science*, 8(13), 642372. <https://doi.org/10.3389/fmarA.2021.642372>.
- Garreaud, R. D., Jacques-Coper, M., Marín, J. C., and Narváez, D. A. (2024). Atmospheric Rivers in South-Central Chile: Zonal and Tilted Events. *Atmosphere*, 15(4), 406. <https://doi.org/10.3390/atmos15040406>.
- Gateuille, D., Owens, P. N., Petticrew, E. L., Booth, B. P., French, T. D., and Déry, S. J. (2019). Determining contemporary and historical sediment sources in a large drainage basin impacted by cumulative effects: the regulated Nechako River, British Columbia, Canada. *Journal of Soils and Sediments*, 19(9), 3357–3373. <https://doi.org/10.1007/s11368-019-02299-2>.
- Geertsema, M., Schwab, J. W., Blais-Stevens, A., and Sakals, M. E. (2009). Landslides impacting linear infrastructure in west central British Columbia. *Natural Hazards*, 48(1), 59–72. <https://doi.org/10.1007/s11069-008-9248-0>.
- Gershunov, A., Shulgina, T., Clemesha, R. E. S., Guirguis, K., Pierce, D. W., and Dettinger, M. D. (2019). Precipitation regime change in Western North America: The role of atmospheric rivers. *Scientific Reports*, 9(1), 9944. <https://doi.org/10.1038/s41598-019-46169-w>.
- Gershunov, A., Shulgina, T., Ralph, F. M., Lavers, D. A., and Rutz, J. J. (2017). Assessing the climate-scale variability of atmospheric rivers affecting western North America. *Geophysical Research Letters*, 44(15), 7900–7908. <https://doi.org/10.1002/2017GL074175>.

- Gilbert, D. E., Morris, J. E., Kaveney, A. R., and Déry, S. J. (2022). Sub-hourly water temperature data collected across the Nechako Watershed, 2019-2021. *Data in Brief*, 43, 108425. <https://doi.org/10.1016/j.dib.2022.108425>.
- Gillett, N. P., Cannon, A. J., Malinina, E., Schnorbus, M., Anslow, F., Sun, Q., and Kirchmeier-Young, M., Zwiers, F., Seiler, C., Zhang, X., Flato, G., Wan, H., Li, G., and Castellan, A. (2022). Human influence on the 2021 British Columbia floods. *Weather and Climate Extremes*, 36, 100441. <https://doi.org/10.1016/j.wace.2022.100441>.
- Glantz, M. H., and Ramirez, I. J. (2020). Reviewing the Oceanic Niño Index (ONI) to Enhance Societal Readiness for El Niño's Impacts. *International Journal of Disaster Risk Science*, 11(3), 394–403. <https://doi.org/10.1007/s13753-020-00275-w>.
- Goswami, U. P., Déry, S. J., and Fortin, V. (2024). Performance Evaluation of High-resolution Reanalysis Datasets Over North-central British Columbia. *Atmosphere – Ocean*, 62(3), 222–242. <https://doi.org/10.1080/07055900.2024.2308878>.
- Goudard, G., Limberger, L., Carpenedo, C.B. (2024). Influence of Eastern, Central and Mix El Niño on the variability of rainfall in southeastern South America. *Frontiers in Earth Science*, 12(1), 1-17. <https://doi.org/10.3389/feart.2024.1134782>.
- Guan, B., and Waliser, D. E. (2019). Tracking Atmospheric Rivers Globally: Spatial Distributions and Temporal Evolution of Life Cycle Characteristics. *Journal of Geophysical Research: Atmospheres*, 124(3), 12523-12552. <https://doi.org/10.1029/2019JD031205>.
- Guan, B., and Waliser, D. E. (2024). A regionally refined quarter-degree global atmospheric rivers database based on ERA5. *Scientific Data*. 11(1), 440. <https://doi.org/10.1038/s41597-024-03258-4>.
- Guan, B., Waliser, D. E., and Ralph, M. R. (2023). Global Application of the Atmospheric River Scale. *Journal of Geophysical Research: Atmospheres*, 128(3), 1-28. <https://doi.org/10.1029/2022JD037180>.

- Guan, B., Waliser, D. E., Ralph, M. R., Fetzer, E. J., and Neiman, P. J. (2016). Hydrometeorological characteristics of rain-on-snow events associated with atmospheric rivers. *Geophysical Research Letters*, 43(6), 2964-2973. <https://doi.org/10.1002/2016GL067978>.
- Guirguis, K., Gershunov, A., Hatchett, B., Shulgina, T., Delforio, M., Subramanian, A., Guzman-Morales, J., Aguilera, R., Clemesha, R., Corringham, T., Delle Monache, L., Reynolds, D., Tardy, A., and Small, I., and Ralph, F. (2021). Weather Patterns Driving Atmospheric Rivers, Santa Ana Winds, Floods, and Wildfires During California Winters Provide Evidence for Increasing Fire Risk. American Geophysical Union Fall Meeting 2021, 13-17. <https://ui.adsabs.harvard.edu/abs/2021AGUFMGC52A..02G>.
- Guirguis, K., Gershunov, A., Shulgina, T., Clemesha, R. E. S., and Ralph, F. M. (2019). Atmospheric rivers impacting Northern California and their modulation by a variable climate. *Climate Dynamics*, 52(11), 6569–6583. <https://doi.org/10.1007/s00382-018-4532-5>.
- Gurbuz, G. and Jin, S. (2017). Long-time variations of precipitable water vapour estimated from GPS, MODIS and radiosonde observations in Turkey. *International Journal of Climatology*, 37, 5170–5180. <https://doi.org/10.1002/joc.5153>.
- Hartman, G. F. (1996). Impacts of growth in resource use and human population on the Nechako River: A major tributary of the Fraser River, British Columbia, Canada. *GeoJournal*, 40(1–2), 147–164. <https://doi.org/10.1007/BF00222540>.
- Hartmann, B., and Wendler, G. (2005). The significance of the 1976 Pacific climate shift in the climatology of Alaska. *Journal of Climate*, 18(22), 4824–4839. <https://doi.org/10.1175/JCLI3532.1>.

- Helm, R., Macdonald, D., Sinclair, B., Chan, D., Herrington, T., Chalmers, A., and Shepherd, B. G. (1980). A Review of the Nechako River Watershed. Internal Report (Fisheries and Environment Canada), 128.
- Hersbach, H., Bell, B., Berrisford, P., Hirahara, S., Horányi, A., Muñoz-Sabater, J., Nicolas, J., Peubey, C., Radu, R., Schepers, D., Simmons, A., Soci, C., Abdalla, S., Abellan, X., Balsamo, G., Bechtold, P., Biavati, G., Bidlot, J., Bonavita, M., ... Thépaut, J. N. (2020). The ERA5 global reanalysis. *Quarterly Journal of the Royal Meteorological Society*, 146(730), 1999–2049. <https://doi.org/10.1002/qj.3803>.
- Heyn, I., Quaas, J., Salzmann, M., and Mülmenstädt, J. (2017). Effects of diabatic and adiabatic processes on relative humidity in a GCM, and relationship between mid-tropospheric vertical wind and cloud-forming and cloud-dissipating processes. *Tellus A: Dynamic Meteorology and Oceanography*, 69(1), 1-14. <https://doi.org/10.1080/16000870.2016.1272753>.
- Hoffman, L., Mazloff, M. R., Gille, S. T., Giglio, D., and Varadarajan, A. (2022). Ocean Surface Salinity Response to Atmospheric River Precipitation in the California Current System. *Journal of Physical Oceanography*, 52(8), 1865–1885. <https://doi.org/10.1175/JPO-D-21>.
- Hou, Y., Wei, X., Vore, M., Déry, S. J., Pypker, T., and Giles-Hansen, K. (2022). Cumulative forest disturbances decrease runoff in two boreal forested watersheds of the northern interior of British Columbia, Canada. *Journal of Hydrology*, 605, 127362. <https://doi.org/10.1016/j.jhydrol.2021.127362>.
- Hu, Z., Liu, S., Zhong, G., Lin, H., and Zhou Z. (2020). Modified Mann-Kendall trend test for hydrological time series under the scaling hypothesis and its application. *Hydrological Sciences Journal*. 65(14), 2419–2438. <https://doi.org/10.1080/02626667.2020.1810253>.

- Huang, W., Hua, L., Zhong, L., Yang, Y., and Gong, Z. (2024). Recent Opposite Trends of Atmospheric Rivers Over East Asia and Western North Pacific Driven by the Pacific Decadal Oscillation. *Journal of Geophysical Research: Atmospheres*, 129(1), e2023JD039147. <https://doi.org/10.1029/2023JD039147>.
- Huang, S., Zhang, X., Chen, N., Li, B., Ma, H., Xu, L., Li, R., and Niyogi, D. (2021). Drought propagation modification after the construction of the Three Gorges Dam in the Yangtze River Basin. *Journal of Hydrology*, 603, Part C, 127138. <https://doi.org/10.1016/j.jhydrol.2021.127138>.
- Jiang, N., Zhu, C., Hu, Z. Z., McPhaden, M. J., Chen, D., Liu, B., Ma, S., Yan, Y., Zhou, T., Qian, W., Luo, J., Yang, X., Liu, F., and Zhu, Y. (2024). Enhanced risk of record-breaking regional temperatures during the 2023–24 El Niño. *Scientific Reports*, 14(1), 2521. <https://doi.org/10.1038/s41598-024-52846-2>.
- Jiqin, H., Gelata, F. T., and Gameda, S. C. (2023). Application of MK trend and test of Sen's slope estimator to measure impact of climate change on the adoption of conservation agriculture in Ethiopia. *Journal of Water and Climate Change*, 14(3), 977–988. <https://doi.org/10.2166/wcc.2023.508>.
- Kendall, M. G. (1975). Rank correlation methods. London: Charles Griffin.
- Khorsandi, M., St-Hilaire, A., Arsenault, R., Martel, J. L., Larabi, S., Schnorbus, M., and Zwiers, F. (2023). Future flow and water temperature scenarios in an impounded drainage basin: implications for summer flow and temperature management downstream of the dam. *Climatic Change*, 176(12), 164. <https://doi.org/10.1007/s10584-023-03634-w>.
- Khouakhi, A., Driouech, F., Slater, L., Waine, T., Chafki, O., Chehbouni, A., and Raji, O. (2022). Atmospheric rivers and associated extreme rainfall over Morocco. *International Journal of Climatology*, 42(15), 7766–7778. <https://doi.org/10.1002/joc.7676>.

- Knight, C. A., Anderson, L., and Presnetsova, L. (2024). Atmospheric river activity during the late Holocene exceeds modern range of variability in California. *Communications Earth and Environment*, 5(216), 1-8. <https://doi.org/10.1038/s43247-024-01357-z>.
- Larabi, S., Schnorbus, M. A., and Zwiers, F. (2022). A coupled streamflow and water temperature (VIC-RBM-CE-QUAL-W2) model for the Nechako Reservoir. *Journal of Hydrology: Regional Studies*, 44 (101237). <https://doi.org/10.1016/j.ejrh.2022.101237>.
- Lavers, D. A., Allan, R. P., Wood, E. F., Villarini, G., Brayshaw, D. J., and Wade, A. J. (2011). Winter floods in Britain are connected to atmospheric rivers. *Geophysical Research Letters*, 38(23), 1–8. <http://dx.doi.org/10.1029/2011GL049783>.
- Lavers, D. A., and Villarini, G. (2013). The nexus between atmospheric rivers and extreme precipitation across Europe. *Geophysical Research Letters*, 40(12), 3259-3264. <https://doi.org/10.1002/grl.50636>.
- Lavers, D. A., and Villarini, G. (2015). The contribution of atmospheric rivers to precipitation in Europe and the United States. *Journal of Hydrology*, 522, 382–390. <https://doi.org/10.1016/j.jhydrol.2014.12.010>.
- Lavers, D. A., Simmons, A., Vamborg, F., and Rodwell, M. J. (2022). An evaluation of ERA5 precipitation for climate monitoring. *Quarterly Journal of the Royal Meteorological Society*, 148(748), 3152–3165. <https://doi.org/10.1002/qj.4351>.
- Leung, L. R., and Qian, Y. (2009). Atmospheric rivers induced heavy precipitation and flooding in the western U.S. simulated by the WRF regional climate model. *Geophysical Research Letters*, 36(3), L03820. <https://doi.org/10.1029/2008GL036445>.
- Li, F., Chavas, D. R., Reed, K. A., and Dawson, D. T. (2020). Climatology of severe local storm environments and synoptic-scale features over North America in ERA5 reanalysis and CAM6 simulation. *Journal of Climate*, 33(19), 8339–8365. <https://doi.org/10.1175/JCLI-D-19-0986.1>.

- Liang, J., and Yong, Y. (2020). Climatology of atmospheric rivers in the Asian monsoon region. *International Journal of Climatology*, 41(S1), E801-E818. <https://doi.org/10.1002/joc.6729>.
- Macdonald, J. S., Morrison, J., and Patterson, D. A. (2012). The efficacy of reservoir flow regulation for cooling migration temperature for sockeye Salmon in the Nechako River watershed of British Columbia. *North American Journal of Fisheries Management*, 32(3), 415–427. <https://doi.org/10.1080/02755947.2012.675946>.
- Mann, H. B. (1945). Non-parametric test against trend. *Econometrika*, 13, 245–259.
- Matsunaga, W. K., Sales, E. S. G., and Júnior, G. C. A. (2024). Application of ERA5-Land reanalysis data in zoning of climate risk for corn in the state of Bahia - Brazil. *Theoretical and Applied Climatology*, 155, 945–963. <https://doi.org/10.1007/s00704-023-04670-3>.
- McClenny, E. E., Ullrich, P. A., and Grotjahn, R. (2020). Sensitivity of atmospheric river vapour transport and precipitation to uniform sea surface temperature increases. *Journal of Geophysical Research: Atmospheres*, 125(21), e2020JD033421. <https://doi.org/10.1029/2020JD033421>.
- Mihalevich, B. A., Neilson, B. T., and Buahin, C. A. (2022). Evaluation of the ERA5-Land reanalysis data set for process-based river temperature modeling over data sparse and topographically complex regions. *Water Resources Research*, 58(7), e2021WR031294. <https://doi.org/10.1029/2021WR031294>.
- Mo, R., Brugman, M. M., Milbrandt, J. A., Goosen, J., Geng, Q., Emond, C., Bau, J., and Erfani, A. (2019). Impacts of hydrometeor drift on orographic precipitation: Two case studies of landfalling atmospheric rivers in British Columbia, Canada. *Weather and Forecasting*, 34(5), 1211–1237. <https://doi.org/10.1175/WAF-D-18-0176.1>.
- Mo, R., So, R., Brugman, M. M., Mooney, C., Liu, A. Q., Jakob, M., Castellan, A., and Vingarzan, R. (2021). Column relative humidity and primary condensation rate as two useful

- supplements to atmospheric river analysis. *Water Resources Research*, 57(11), e2021WR029678. <https://doi.org/10.1029/2021WR029678>.
- Moore, R. D. (1991). Hydrology and water supply in the Fraser River basin. In: Water in sustainable development: exploring our common future in the Fraser River basin. A. H. J. Dorsey and J. R. Griggs (editors). University of British Columbia, Westwater Res. Cent., Vancouver, B.C., pp. 21–40.
- Muñoz-Sabater, J., Dutra, E., Agustí-Panareda, A., Albergel, C., Arduini, G., Balsamo, G., Boussetta, S., Choulga, M., Harrigan, S., Hersbach, H., Martens, B., Miralles, D. G., Piles, M., Rodríguez-Fernández, N. J., Zsoter, E., Buontempo, C., and Thépaut, J. (2021). ERA5-Land: a state-of-the-art global reanalysis dataset for land applications. *Earth System Science Data*, 13(9), 4349–4383. <https://doi.org/10.5194/essd-13-4349-2021>.
- Nash, D., Carvalho, L. M. V., Jones, C., and Ding, Q. (2022). Winter and spring atmospheric rivers in High Mountain Asia: climatology, dynamics, and variability. *Climate Dynamics*, 58(9–10), 2309–2331. <https://doi.org/10.1007/s00382-021-06008-z>.
- Nash, D., Waliser, D., Guan, B., Ye, H., and Ralph, F. M. (2018). The role of atmospheric rivers in extratropical and polar hydroclimate. *Journal of Geophysical Research: Atmospheres*, 123(13), 6804–6821. <https://doi.org/10.1029/2017JD028130>.
- Neiman, P. J., Schick, L. J., Ralph, F. M., Hughes, M., and Wick, G. A. (2011). Flooding in Western Washington: The Connection to Atmospheric Rivers. *Journal of Hydrometeorology*, 12(6), 1337-1358. <https://doi.org/10.1175/2011JHM1358.1>.
- Oceanic Niño Index. (2023). Cold and Warm Episodes by Season. National Weather Service. Climate Prediction Center. https://origin.cpc.ncep.noaa.gov/products/analysis_monitoring/ensostuff/ONI_v5.php.
- Overton, I. C., Smith, D. M., Dalton, J., Barchiesi, S., Acreman, M. C., Stromberg, J. C., and Kirby, J. M. (2014). Implementing environmental flows in integrated water resources

- management and the ecosystem approach. *Hydrological Sciences Journal*, 59(3–4), 860–877. <https://doi.org/10.1080/02626667.2014.897408>.
- Pan, M., Lu, M. and Lall, U. (2024). Diversity of cross-Pacific atmospheric river main routes. *Communications Earth and Environment*, 5(378), 1-14. <https://doi.org/10.1038/s43247-024-01552-y>.
- Parkes, M. W. (2021). River conversations: A confluence of lessons and emergence from the Taieri River and the Nechako River. *River Research and Applications*, 38(3), 443–452. <https://doi.org/10.1002/rra.3907>.
- Parkes, M. W., Déry, S. J., Owens, P. N., Peticrew, E. L., and Booth, B. (2024). Towards an integrative understanding of British Columbia's Nechako Watershed: Connecting knowledge systems to strengthen understanding of climate change, watershed security, health and well-being. *PLOS Water*, 3(7), e0000263. <https://doi.org/10.1371/journal.pwat.0000263>.
- Payne, A. E., and Magnusdottir, G. (2014). Dynamics of landfalling atmospheric rivers over the North Pacific in 30 years of MERRA reanalysis. *Journal of Climate*, 27(18), 7133–7150. <https://doi.org/10.1175/JCLI-D-14-00034.1>.
- Payne, A. E., Demory, M. E., Leung, L. R., Ramos, A. M., Shields, C. A., Rutz, J. J., Siler, N., Villarini, G., Hall, A., Ralph, F. M. (2020). Responses and impacts of atmospheric rivers to climate change. *Nature Reviews Earth and Environment*, 1(3), 143–157. <https://doi.org/10.1038/s43017-020-0030-5>.
- Perri, D. V., Hurtado, S. I., Bruzzone, O., and Easdale, M. H. (2024). Optimal automatic enhanced ERA5 daily precipitation data for environmental and agricultural monitoring tools in scarce data regions. *Theoretical and Applied Climatology*, 155(3), 1847–1856. <https://doi.org/10.1007/s00704-023-04730-8>.

- Picketts, I. M., Parkes, M. W., and Déry, S. J. (2017). Climate change and resource development impacts in watersheds: Insights from the Nechako River Basin, Canada. *The Canadian Geographer / Le Géographe Canadien*, 61(2), 196–211. <https://doi.org/10.1111/cag.12327>
- Picketts, I., Déry, S. J., Parkes, M. W., Sharma, A. R., and Matthews, C. A. (2020). Scenarios of climate change and natural resource development: Complexity and uncertainty in the Nechako Watershed. *The Canadian Geographer / Le Géographe Canadien*, 64(3), 475–488. <https://doi.org/10.1111/cag.12609>.
- Piecuch, C. G., Coats, S., Dangendorf, S., Landerer, F. W., Reager, J. T., Thompson, P. R., and Wahl, T. (2022). High-Tide Floods and Storm Surges During Atmospheric Rivers on the US West Coast. *Geophysical Research Letters*, 49(2), e2021GL096820. <https://doi.org/10.1029/2021GL096820>.
- Pohl, B., Prince, H. D., Wille, J., Kingston, D. G., Cullen, N. J., and Fauchereau, N. (2023). Atmospheric Rivers and Weather Types in Aotearoa New Zealand: A two-way story. *Journal of Geophysical Research: Atmospheres*, 2023(15), e2022JD037209. <https://doi.org/10.1029/2022jd037209>.
- Prince, H. D., Cullen, N. J., Gibson, P. B., Conway, J., and Kingston, D. G. (2021). A climatology of atmospheric rivers in New Zealand. *Journal of Climate*, 34(11), 4383–4402. <https://doi.org/10.1175/JCLI-D-20-0664.1>.
- Ralph, F. M., Dettinger, M. D., and Lavers, D. A. (2013). Atmospheric rivers as drought busters on the US West Coast. *Journal of Hydrometeorology*, 20(1), 42–61. <https://doi.org/10.1175/JHM-D-13-02.1>.
- Ralph, F. M., Dettinger, M., Lavers, D., Gorodetskaya, I. V., Martin, A., and Viale, M. (2017). Atmospheric rivers emerge as a global science and applications focus. *Bulletin of the American Meteorological Society*, 98(9), 1969–1973. <https://doi.org/10.1175/BAMS-D-16-0262.1>.

- Ralph, F. M., Dettinger, M. D., Cairns, M. M., Galarneau, T. J., and Eylander, J. (2018). Defining “Atmospheric River”: How the Glossary of Meteorology Helped Resolve a Debate. *Bulletin of the American Meteorological Society*, 99(4), 837–839. <https://doi.org/10.1175/bams-d-17-0157.1>.
- Ralph, F. M., Neiman, P. J., and Wick, G. A. (2004). Satellite and CALJET aircraft observations of atmospheric rivers over the eastern North Pacific Ocean during the winter of 1997/98. *Monthly Weather Review*, 132(7), 1721–1745, [https://doi.org/10.1175/1520-0493\(2004\)132<1721:SACAOO>2.0.CO;2](https://doi.org/10.1175/1520-0493(2004)132<1721:SACAOO>2.0.CO;2).
- Ralph, F. M., Rutz, J. J., Cordeira, J. M., Dettinger, M., Anderson, M., Reynolds, D., Schick, L. J., and Smallcomb, C. (2019). A scale to characterize the strength and impacts of atmospheric rivers. *Bulletin of the American Meteorological Society*, 100(2), 269–289. <https://doi.org/10.1175/BAMS-D-18-0023.1>.
- Ralph, M. F., Dettinger, M. D., Rutz, J. J., and Waliser, D. E. (2020). Atmospheric Rivers. 252p. Springer Cham, Switzerland. ISBN 978-3-030-28905-8. <https://doi.org/doi.org/10.1007/978-3-030-28906-5>.
- Ramos, A. M., Trigo, R. M., Liberato, M. L. R., and Tomé, R. (2015). Daily Precipitation Extreme Events in the Iberian Peninsula and its Association with Atmospheric Rivers. *Journal of Hydrometeorology*, (16), 579–597. <https://doi.org/10.1175/JHM-D-14-0103.1>.
- Richards-Thomas, T. S., Déry, S. J., Stewart, R. E., and Thériault, J. M., (2024): Climatological Context of the Mid-November 2021 Floods in the Province of British Columbia, Canada. *Weather and Climate Extremes*, 45, 100705. <https://dx.doi.org/10.2139/ssrn.4626551>.
- Rostami, A., Akhoondzadeh, M., and Amani, M. (2022). A fuzzy-based flood warning system using 19-year remote sensing time series data in the Google Earth Engine cloud platform. *Advances in Space Research*, 70(5), 1406–1428. <https://doi.org/10.1016/j.asr.2022.06.008>.

- Septer, D. (2007). Flooding and landslide events northern British Columbia 1820-2006. BC Ministry of Environment, 141p. Accessed on 14 June 2023.
- Shabbar, A., Bonsal, B., and Khandekar, M. (1997). Canadian precipitation patterns associated with the Southern Oscillation. *Journal of Climate*, 10(1), 3016–3027. [https://doi.org/10.1175/1520-0442\(1997\)010<3016:CPPAWT>2.0.CO;2](https://doi.org/10.1175/1520-0442(1997)010<3016:CPPAWT>2.0.CO;2).
- Sharma, A. R., and Déry, S. J. (2020a). Variability and trends of landfalling atmospheric rivers along the Pacific Coast of northwestern North America. *International Journal of Climatology*, 40(1), 544-558. <https://doi.org/10.1002/joc.6227>.
- Sharma, A. R., and Déry, S. J. (2020b). Contribution of Atmospheric Rivers to Annual, Seasonal, and Extreme Precipitation Across British Columbia and Southeastern Alaska. *Journal of Geophysical Research: Atmospheres*, 125(9). e2019JD031823, <https://doi.org/10.1029/2019JD031823>.
- Sharma, A. R. ., and Déry, S. J. (2020c). Linking atmospheric rivers to annual and extreme river runoff in British Columbia and southeastern Alaska. *Journal of Hydrometeorology*, 21(11), 2457–2472. <https://doi.org/10.1175/JHM-D-19-0281.1>.
- Shields, C. A., Rutz, J. J., Leung, L.-Y., Ralph, F. M., Wehner, M., Kawzenuk, B., Lora, J. M., McClenny, E., Osborne, T., Payne, A. E., Ullrich, P., Gershunov, A., Goldenson, N., Guan, B., Qian, Y., Ramos, A. M., Sarangi, C., Sellars, S., Gorodetskaya, I., Kashinath, K., Kurlin, V., Mahoney, K., Muszynski, G., Pierce, R., Subramanian, A. C., Tome, R., Waliser, D., Walton, D., Wick, G., Wilson, A., Lavers, D., Prabhat, Collow, A., Krishnan, H., Magnusdottir, G., and Nguyen, P. Atmospheric River Tracking Method Intercomparison Project (ARTMIP): project goals and experimental design. *Geoscientific Model Development*, 11(6), 2455–2474. <https://doi.org/10.5194/gmd-11-2455-2018>, 2018.
- Shrestha, R. R., Schnorbus, M. A., Werner, A. T., and Berland, A. J. (2012). Modelling spatial and temporal variability of hydrologic impacts of climate change in the Fraser River basin,

- British Columbia, Canada. *Hydrological Processes*, 26(12), 1840–1860.
<https://doi.org/10.1002/hyp.9283>.
- Siirila-Woodburn, E. R., Dennedy-Frank, P. J., Rhoades, A., Vahmani, P., Maina, F., Hatchett, B., Zhou, Y., and Jones, A. (2023). The role of atmospheric rivers on groundwater: Lessons learned from an extreme wet year. *Water Resources Research*, 59, e2022WR033061.
<https://doi.org/10.1029/2022WR033061>.
- Silva, K. A., Rolim, G. S., Valeriano, T. T. B, and de Moraes, J. R. S. C. (2020). Influence of El Niño and La Niña on coffee yield in the main coffee-producing regions of Brazil. *Theoretical and Applied Climatology*, 139(3–4), 1019–1029.
<https://doi.org/10.1007/s00704-019-03039-9>.
- Sliniskey, E. A., Loikith, P. C., Waliser, D. E., Guan, B., and Martin, A. (2020). A Climatology of Atmospheric Rivers and Associated Precipitation for the Seven U.S. National Climate Assessment Regions. *Journal of Hydrometeorology*, 21, 2439–2456.
<https://doi.org/10.1175/JHM-D-20>.
- Sobral, B. S., and Déry, S. J. (2023). Spatiotemporal distribution and trend analyses of atmospheric rivers affecting British Columbia’s Nechako Watershed. *International Journal of Climatology*, 43(14), 6720–6732. <https://doi.org/10.1002/joc.8230>.
- Sobral, B. S., and Déry, S. J. (2024). Water budget input Linked to Atmospheric Rivers in British Columbia’s Nechako River Basin. *Hydrological Processes*, 38(10), e15301.
<https://doi.org/10.1002/hyp.15301>.
- Stahl, K., Moore, R. D., and McKendry, I. G. (2006). The role of synoptic-scale circulation in the linkage between large-scale ocean-atmosphere indices and winter surface climate in British Columbia, Canada. *International Journal of Climatology*, 26(4), 541–560.
<https://doi.org/10.1002/joc.1268>.

- Sun, H., Su, F., Yao, T., He, Z., Tang, G., Huang, J., Zheng, B., Meng, F., Ou, T., and Chen, D. (2021). General overestimation of ERA5 precipitation in flow simulations for High Mountain Asia basins. *Environmental Research Communications*, 3, 121003. <https://doi.org/10.1088/2515-7620/ac40f0>.
- Tannant, D. D., and Morgenroth, J. (2020). Kemano Project – 70 Years of Development. 2020 GeoVirtual Conference: Resilience and Innovation (14-16 September 2020).
- Tarek, M., Brissette, F. P., and Arsenault, R. (2020). Evaluation of the ERA5 reanalysis as a potential reference dataset for hydrological modelling over North America. *Hydrology and Earth System Sciences*, 24(5), 2527–2544. <https://doi.org/10.5194/hess-24-2527-2020>.
- Thandlam, V., Rutgersson, A., and Sahlee, E. (2022). Spatio-temporal variability of atmospheric rivers and associated atmospheric parameters in the Euro-Atlantic region. *Theoretical and Applied Climatology*, 147(1–2), 13–33. <https://doi.org/10.1007/s00704-021-03776-w>.
- Towner, J., Cloke, H. L., Zsoter, E., Flamig, Z., Hoch, J. M., Bazo, J., Coughlan, E., and Stephens, E. M. (2019). Assessing the performance of global hydrological models for capturing peak river flows in the Amazon Basin. *Hydrology and Earth System Sciences*, 23(7), 3057-3080. <https://doi.org/10.5194/hess-2019-44>.
- Vallejo-Bernal, S. M., Wolf, F., Boers, N., Traxl, D., Marwan, N., and Kurths, J. (2023). The role of atmospheric rivers in the distribution of heavy precipitation events over North America. *Hydrology and Earth System Sciences*, 27(14), 2645–2660. <https://doi.org/10.5194/hess-27-2645-2023>.
- van der Breggen, N. N., and Hudson, P. F. (2024). Influence of atmospheric rivers on extreme rainfall and high streamflow events in northwestern Europe: Rur (Roer) River basin. *Journal of Hydrology: Regional Studies*, 51 (101644). <https://doi.org/10.1016/j.ejrh.2023.101644>.

- Vincent, L. A., Zhang, X., Brown, R., Feng, Y., Mekis, É., Milewska, E. J., Wan, H., and Wang, X. L. (2015). Observed trends in Canada's climate and influence of low-frequency variability modes. *Journal of Climate*, 28(11), 4545-4560. <https://doi.org/10.1175/JCLI-D-14-00697.1>.
- Vore, M. E., Déry, S. J., Hou, Y., and Wei, X. (2020). Climatic influences on forest fire and mountain pine beetle outbreaks and resulting runoff effects in large watersheds in British Columbia, Canada. *Hydrological Processes*, 34(24), 4560–4575. <https://doi.org/10.1002/hyp.13908>.
- Waliser, D., and Guan, B. (2017). Extreme winds and precipitation during landfall of atmospheric rivers. *Nature Geosciences*, 10, 179–183. <https://doi.org/10.1038/ngeo2894>.
- Wang, S., Ma, X., Zhou, S., Wu, L., Wang, H., Tang, Z., Xu, G., Jing, Z., Chen, Z., and Gan, B. (2023). Extreme atmospheric rivers in a warming climate. *Nature Communications*, 14(1). <https://doi.org/10.1038/s41467-023-38980-x>.
- Warner, M. D., Mass, C. F. and Salathé, E. P. (2015). Changes in winter atmospheric rivers along the North American west coast in CMIP5 climate models. *Journal of Hydrometeorology*, 16, 118–128. <https://doi.org/10.1175/JHM-D-14-0080.1>.
- Williams, A. P., Anchukaitis, K. J., and Varuolo-Clarke, A. M. (2024). Atmospheric Rivers are Responsible for Cyclicity in Sierra Nevada Precipitation. *Journal of Climate*, 37(1), 1613–1627. <https://doi.org/10.1175/JCLI-D-23>.
- Xu, W., Lei, X., Chen, S., Yu, T., Hu, Z., Zhang, M., Jiang, L., Bao, R., Guan, X., Ma, M., Wei, J., Gao, L., and Feng, A. (2022). How Well Does the ERA5 Reanalysis Capture the Extreme Climate Events Over China? Part II: Extreme Temperature. *Frontiers in Environmental Science*, 10, 921659. <https://doi.org/10.3389/fenvA.2022.921659>.
- Xu, Y., Zhu, X., Cheng, X., Gun Z., Lin, J., Zhao, J., Yao, L., and Zhou, C. (2022). Drought assessment of China in 2002–2017 based on a comprehensive drought index. *Agricultural*

and *Forest Meteorology*, 319, 108922.
<https://doi.org/10.1016/J.AGRFORMET.2022.108922>.

Zhang, Y., Cabilio, P., and Nadeem, K. (2016). Improved Seasonal Mann–Kendall Tests for Trend Analysis in Water Resources Time Series. In: Li, W., Stanford, D., Yu, H. (eds) *Advances in Time Series Methods and Applications. Fields Institute Communications*, 78. https://doi.org/10.1007/978-1-4939-6568-7_10

Zhang, R., Li, L., Zhang, Y., Huang, F., Li, J., Liu, W., Mao, T., Xiong, Z., and Shangguan, W. (2021). Assessment of agricultural drought using soil water deficit index based on era5-land soil moisture data in four southern provinces of China. *Agriculture (Switzerland)*, 11(5), 11050411. <https://doi.org/10.3390/agriculture11050411>.

Zhang, X., Vincent, L. A., Hogg, W. D., and Niitsoo, A. (2019). Temperature and precipitation trends in Canada during the 20th century. *Atmosphere-Ocean*, 38(3), 395-429. <https://doi.org/10.1080/07055900.2000.9649654>.

Zhang, L., Zhao, Y., Cheng, T. F., and Lu, M. (2024). Future Changes in Global Atmospheric Rivers Projected by CMIP6 Models. *Journal of Geophysical Research: Atmospheres*, 129(3), e2023JD039359. <https://doi.org/10.1029/2023JD039359>.

Zhu, Y., and Newell, R. E. (1994). Atmospheric rivers and bombs. *Geophysical Research Letters*, 21(18), 1999–2002. <https://agupubs.onlinelibrary.wiley.com/doi/abs/10.1029/94GL01710>.

Zhu, Y., and Newell, R. E. (1998). A proposed algorithm for moisture fluxes from atmospheric rivers. *Monthly Weather Review*, 126(3), 725–735. [https://doi.org/10.1175/1520-0493\(1998\)126<0725:APAFMF>2.0.CO;2](https://doi.org/10.1175/1520-0493(1998)126<0725:APAFMF>2.0.CO;2).

APPENDIX A

Table A.1: Summarized results for the 364 climate datasets showing basic descriptive statistics and Mann-Kendall's tau and p-values ($\alpha=5\%$, 95% confidence).

#	AR-monitored Region	AR-Days (ARDs) Classification	Scale	Season	Sub-basin	Variable	Min.	Max.	Mean	Std. deviation	Kendall's tau	MK p-value
1	South (52.5° N, 127.5° W)	ARD	Annual	NA	NA	AR-days Frequency	18.00	54.00	32.00	7.70	0.07	0.42
2	South (52.5° N, 127.5° W)	ARD0	Annual	NA	NA	AR-days Frequency	8.00	32.00	18.30	5.20	0.18	0.03
3	South (52.5° N, 127.5° W)	ARD1	Annual	NA	NA	AR-days Frequency	3.00	17.00	8.40	3.20	0.04	0.60
4	South (52.5° N, 127.5° W)	ARD2	Annual	NA	NA	AR-days Frequency	0.00	14.00	3.90	3.10	-0.14	0.10
5	South (52.5° N, 127.5° W)	ARD3	Annual	NA	NA	AR-days Frequency	0.00	6.00	1.10	1.50	-0.23	0.01
6	South (52.5° N, 127.5° W)	ARD4	Annual	NA	NA	AR-days Frequency	0.00	2.00	0.20	0.50	-0.04	0.65
7	South (52.5° N, 127.5° W)	ARD5	Annual	NA	NA	AR-days Frequency	0.00	1.00	0.00	0.10	0.01	0.92
8	North (55° N, 130° W)	ARD	Annual	NA	NA	AR-days Frequency	11.00	40.00	26.75	5.94	-0.07	0.42
9	North (55° N, 130° W)	ARD0	Annual	NA	NA	AR-days Frequency	4.00	33.00	15.30	4.80	0.05	0.57
10	North (55° N, 130° W)	ARD1	Annual	NA	NA	AR-days Frequency	0.00	16.00	6.70	3.20	-0.13	0.12
11	North (55° N, 130° W)	ARD2	Annual	NA	NA	AR-days Frequency	0.00	13.00	3.40	2.60	-0.11	0.20
12	North (55° N, 130° W)	ARD3	Annual	NA	NA	AR-days Frequency	0.00	6.00	1.10	1.60	0.00	0.98
13	North (55° N, 130° W)	ARD4	Annual	NA	NA	AR-days Frequency	0.00	2.00	0.20	0.50	-0.02	0.82
14	North (55° N, 130° W)	ARD5	Annual	NA	NA	AR-days Frequency	0.00	0.00	0.00	0.00	NA	NA
15	South (52.5° N, 127.5° W)	ARD	Annual	NA	NA	AR-days Intensity	382.63	666.96	495.56	58.70	-0.02	0.77

#	AR-monitored Region	AR-Days (ARDs) Classification	Scale	Season	Sub-basin	Variable	Min.	Max.	Mean	Std. deviation	Kendall's tau	MK p-value
16	South (52.5° N, 127.5° W)	ARD0	Annual	NA	NA	AR-days Intensity	329.10	399.40	362.30	16.30	-0.01	0.91
17	South (52.5° N, 127.5° W)	ARD1	Annual	NA	NA	AR-days Intensity	367.80	598.30	473.80	52.80	-0.08	0.30
18	South (52.5° N, 127.5° W)	ARD2	Annual	NA	NA	AR-days Intensity	0.00	790.50	486.90	187.10	0.01	0.95
19	South (52.5° N, 127.5° W)	ARD3	Annual	NA	NA	AR-days Intensity	0.00	915.60	327.60	338.20	-0.08	0.34
20	South (52.5° N, 127.5° W)	ARD4	Annual	NA	NA	AR-days Intensity	0.00	1027.30	132.90	317.00	-0.03	0.73
21	South (52.5° N, 127.5° W)	ARD5	Annual	NA	NA	AR-days Intensity	0.00	1122.50	15.60	132.30	0.01	0.92
22	North (55° N, 130° W)	ARD	Annual	NA	NA	AR-days Intensity	371.08	638.18	489.31	55.17	-0.04	0.62
23	North (55° N, 130° W)	ARD0	Annual	NA	NA	AR-days Intensity	316.20	423.60	366.60	20.50	0.05	0.54
24	North (55° N, 130° W)	ARD1	Annual	NA	NA	AR-days Intensity	0.00	699.60	476.30	91.80	-0.01	0.90
25	North (55° N, 130° W)	ARD2	Annual	NA	NA	AR-days Intensity	0.00	820.60	490.50	196.20	0.04	0.59
26	North (55° N, 130° W)	ARD3	Annual	NA	NA	AR-days Intensity	0.00	880.30	288.30	330.10	-0.06	0.52
27	North (55° N, 130° W)	ARD4	Annual	NA	NA	AR-days Intensity	0.00	1101.40	70.20	237.00	-0.03	0.78
28	North (55° N, 130° W)	ARD5	Annual	NA	NA	AR-days Intensity	0.00	0.00	0.00	0.00	NA	NA
29	South (52.5° N, 127.5° W)	ARD	Seasonal	Fall	NA	AR-days Frequency	7.00	31.00	14.96	4.60	-0.04	0.67
30	South (52.5° N, 127.5° W)	ARD0	Seasonal	Fall	NA	AR-days Frequency	2.00	15.00	6.99	2.72	0.09	0.29
31	South (52.5° N, 127.5° W)	ARD1	Seasonal	Fall	NA	AR-days Frequency	0.00	11.00	4.35	2.51	0.05	0.53
32	South (52.5° N, 127.5° W)	ARD2	Seasonal	Fall	NA	AR-days Frequency	0.00	10.00	2.63	2.21	-0.19	0.02
33	South (52.5° N, 127.5° W)	ARD3	Seasonal	Fall	NA	AR-days Frequency	0.00	6.00	0.82	1.36	-0.16	0.07
34	South (52.5° N, 127.5° W)	ARD4	Seasonal	Fall	NA	AR-days	0.00	2.00	0.17	0.44	-0.09	0.33

#	AR-monitored Region	AR-Days (ARDs) Classification	Scale	Season	Sub-basin	Variable	Min.	Max.	Mean	Std. deviation	Kendall's tau	MK p-value
						Frequency						
35	South (52.5° N, 127.5° W)	ARD5	Seasonal	Fall	NA	AR-days Frequency	0.00	1.00	0.01	0.12	0.01	0.92
36	South (52.5° N, 127.5° W)	ARD	Seasonal	Spring	NA	AR-days Frequency	0.00	10.00	3.28	2.56	0.05	0.59
37	South (52.5° N, 127.5° W)	ARD0	Seasonal	Spring	NA	AR-days Frequency	0.00	7.00	2.46	1.95	0.02	0.78
38	South (52.5° N, 127.5° W)	ARD1	Seasonal	Spring	NA	AR-days Frequency	0.00	5.00	0.71	1.22	0.09	0.33
39	South (52.5° N, 127.5° W)	ARD2	Seasonal	Spring	NA	AR-days Frequency	0.00	3.00	0.10	0.42	-0.01	0.91
40	South (52.5° N, 127.5° W)	ARD3	Seasonal	Spring	NA	AR-days Frequency	0.00	1.00	0.01	0.12	-0.15	0.12
41	South (52.5° N, 127.5° W)	ARD4	Seasonal	Spring	NA	AR-days Frequency	0.00	0.00	0.00	0.00	NA	NA
42	South (52.5° N, 127.5° W)	ARD5	Seasonal	Spring	NA	AR-days Frequency	0.00	0.00	0.00	0.00	NA	NA
43	South (52.5° N, 127.5° W)	ARD	Seasonal	Summer	NA	AR-days Frequency	2.00	22.00	8.49	4.05	0.10	0.25
44	South (52.5° N, 127.5° W)	ARD0	Seasonal	Summer	NA	AR-days Frequency	0.00	13.00	5.56	2.80	0.08	0.36
45	South (52.5° N, 127.5° W)	ARD1	Seasonal	Summer	NA	AR-days Frequency	0.00	9.00	1.92	2.19	0.07	0.42
46	South (52.5° N, 127.5° W)	ARD2	Seasonal	Summer	NA	AR-days Frequency	0.00	5.00	0.81	1.32	0.08	0.38
47	South (52.5° N, 127.5° W)	ARD3	Seasonal	Summer	NA	AR-days Frequency	0.00	3.00	0.18	0.54	0.00	0.99
48	South (52.5° N, 127.5° W)	ARD4	Seasonal	Summer	NA	AR-days Frequency	0.00	1.00	0.03	0.17	0.00	0.99
49	South (52.5° N, 127.5° W)	ARD5	Seasonal	Summer	NA	AR-days Frequency	0.00	0.00	0.00	0.00	NA	NA
50	South (52.5° N, 127.5° W)	ARD	Seasonal	Winter	NA	AR-days Frequency	0.00	12.00	5.25	2.91	0.03	0.69
51	South (52.5° N, 127.5° W)	ARD0	Seasonal	Winter	NA	AR-days Frequency	0.00	9.00	3.32	2.05	0.12	0.17
52	South (52.5° N, 127.5° W)	ARD1	Seasonal	Winter	NA	AR-days Frequency	0.00	5.00	1.44	1.30	-0.06	0.49

#	AR-monitored Region	AR-Days (ARDs) Classification	Scale	Season	Sub-basin	Variable	Min.	Max.	Mean	Std. deviation	Kendall's tau	MK p-value
53	South (52.5° N, 127.5° W)	ARD2	Seasonal	Winter	NA	AR-days Frequency	0.00	3.00	0.40	0.80	-0.07	0.46
54	South (52.5° N, 127.5° W)	ARD3	Seasonal	Winter	NA	AR-days Frequency	0.00	3.00	0.08	0.50	-0.12	0.24
55	South (52.5° N, 127.5° W)	ARD4	Seasonal	Winter	NA	AR-days Frequency	0.00	0.00	0.00	0.00	NA	NA
56	South (52.5° N, 127.5° W)	ARD5	Seasonal	Winter	NA	AR-days Frequency	0.00	0.00	0.00	0.00	NA	NA
57	South (52.5° N, 127.5° W)	ARD	Seasonal	Fall	NA	AR-days Intensity	348.96	561.52	447.83	42.71	-0.13	0.10
58	South (52.5° N, 127.5° W)	ARD0	Seasonal	Fall	NA	AR-days Intensity	294.45	415.19	366.09	27.81	-0.06	0.47
59	South (52.5° N, 127.5° W)	ARD1	Seasonal	Fall	NA	AR-days Intensity	0.00	724.19	469.66	124.80	0.00	0.99
60	South (52.5° N, 127.5° W)	ARD2	Seasonal	Fall	NA	AR-days Intensity	0.00	790.45	459.55	231.43	0.03	0.73
61	South (52.5° N, 127.5° W)	ARD3	Seasonal	Fall	NA	AR-days Intensity	0.00	915.57	249.82	331.42	-0.08	0.37
62	South (52.5° N, 127.5° W)	ARD4	Seasonal	Fall	NA	AR-days Intensity	0.00	1027.30	121.56	306.74	-0.09	0.36
63	South (52.5° N, 127.5° W)	ARD5	Seasonal	Fall	NA	AR-days Intensity	0.00	1122.50	15.59	132.29	0.01	0.92
64	South (52.5° N, 127.5° W)	ARD	Seasonal	Spring	NA	AR-days Intensity	0.00	503.99	316.70	154.88	0.04	0.63
65	South (52.5° N, 127.5° W)	ARD0	Seasonal	Spring	NA	AR-days Intensity	0.00	475.73	298.61	152.59	0.12	0.13
66	South (52.5° N, 127.5° W)	ARD1	Seasonal	Spring	NA	AR-days Intensity	0.00	665.90	162.81	232.58	0.06	0.50
67	South (52.5° N, 127.5° W)	ARD2	Seasonal	Spring	NA	AR-days Intensity	0.00	665.20	36.98	138.15	0.00	0.98
68	South (52.5° N, 127.5° W)	ARD3	Seasonal	Spring	NA	AR-days Intensity	0.00	509.47	7.08	60.04	-0.15	0.12
69	South (52.5° N, 127.5° W)	ARD4	Seasonal	Spring	NA	AR-days Intensity	0.00	0.00	0.00	0.00	NA	NA
70	South (52.5° N, 127.5° W)	ARD5	Seasonal	Spring	NA	AR-days Intensity	0.00	0.00	0.00	0.00	NA	NA
71	South (52.5° N, 127.5° W)	ARD	Seasonal	Summer	NA	AR-days	269.17	527.34	373.19	45.85	0.00	1.00

#	AR-monitored Region	AR-Days (ARDs) Classification	Scale	Season	Sub-basin	Variable	Min.	Max.	Mean	Std. deviation	Kendall's tau	MK p-value
						Intensity						
72	South (52.5° N, 127.5° W)	ARD0	Seasonal	Summer	NA	AR-days Intensity	0.00	406.85	336.25	64.40	0.01	0.89
73	South (52.5° N, 127.5° W)	ARD1	Seasonal	Summer	NA	AR-days Intensity	0.00	623.11	242.54	223.75	0.06	0.47
74	South (52.5° N, 127.5° W)	ARD2	Seasonal	Summer	NA	AR-days Intensity	0.00	644.41	186.31	241.46	0.12	0.19
75	South (52.5° N, 127.5° W)	ARD3	Seasonal	Summer	NA	AR-days Intensity	0.00	848.52	78.59	211.83	0.01	0.93
76	South (52.5° N, 127.5° W)	ARD4	Seasonal	Summer	NA	AR-days Intensity	0.00	845.68	22.88	136.37	0.00	0.97
77	South (52.5° N, 127.5° W)	ARD5	Seasonal	Summer	NA	AR-days Intensity	0.00	0.00	0.00	0.00	NA	NA
78	South (52.5° N, 127.5° W)	ARD	Seasonal	Winter	NA	AR-days Intensity	0.00	608.78	433.04	81.27	-0.13	0.11
79	South (52.5° N, 127.5° W)	ARD0	Seasonal	Winter	NA	AR-days Intensity	0.00	480.85	356.44	96.69	-0.04	0.64
80	South (52.5° N, 127.5° W)	ARD1	Seasonal	Winter	NA	AR-days Intensity	0.00	740.11	391.69	252.48	0.01	0.86
81	South (52.5° N, 127.5° W)	ARD2	Seasonal	Winter	NA	AR-days Intensity	0.00	938.63	160.53	287.98	-0.09	0.35
82	South (52.5° N, 127.5° W)	ARD3	Seasonal	Winter	NA	AR-days Intensity	0.00	646.56	16.43	98.30	-0.11	0.24
83	South (52.5° N, 127.5° W)	ARD4	Seasonal	Winter	NA	AR-days Intensity	0.00	0.00	0.00	0.00	NA	NA
84	South (52.5° N, 127.5° W)	ARD5	Seasonal	Winter	NA	AR-days Intensity	0.00	0.00	0.00	0.00	NA	NA
85	South (52.5° N, 127.5° W)	ARD	Seasonal	Fall	NA	AR-days Frequency	1.00	12.00	5.60	2.62	-0.09	0.30
86	North (55° N, 130° W)	ARD0	Seasonal	Fall	NA	AR-days Frequency	1.00	10.00	5.75	2.65	-0.01	0.87
87	North (55° N, 130° W)	ARD1	Seasonal	Fall	NA	AR-days Frequency	0.00	9.00	3.32	1.90	-0.19	0.03
88	North (55° N, 130° W)	ARD2	Seasonal	Fall	NA	AR-days Frequency	0.00	10.00	2.32	2.06	-0.01	0.95
89	North (55° N, 130° W)	ARD3	Seasonal	Fall	NA	AR-days Frequency	0.00	6.00	0.88	1.51	-0.03	0.74

#	AR-monitored Region	AR-Days (ARDs) Classification	Scale	Season	Sub-basin	Variable	Min.	Max.	Mean	Std. deviation	Kendall's tau	MK p-value
90	North (55° N, 130° W)	ARD4	Seasonal	Fall	NA	AR-days Frequency	0.00	2.00	0.13	0.47	-0.04	0.69
91	North (55° N, 130° W)	ARD5	Seasonal	Fall	NA	AR-days Frequency	0.00	0.00	0.00	0.00	NA	NA
92	North (55° N, 130° W)	ARD	Seasonal	Spring	NA	AR-days Frequency	0.00	5.00	1.15	1.19	0.02	0.80
93	North (55° N, 130° W)	ARD0	Seasonal	Spring	NA	AR-days Frequency	0.00	7.00	2.10	1.63	0.01	0.89
94	North (55° N, 130° W)	ARD1	Seasonal	Spring	NA	AR-days Frequency	0.00	4.00	0.38	0.83	-0.02	0.82
95	North (55° N, 130° W)	ARD2	Seasonal	Spring	NA	AR-days Frequency	0.00	5.00	0.19	0.72	-0.05	0.59
96	North (55° N, 130° W)	ARD3	Seasonal	Spring	NA	AR-days Frequency	0.00	0.00	0.00	0.00	NA	NA
97	North (55° N, 130° W)	ARD4	Seasonal	Spring	NA	AR-days Frequency	0.00	0.00	0.00	0.00	NA	NA
98	North (55° N, 130° W)	ARD5	Seasonal	Spring	NA	AR-days Frequency	0.00	0.00	0.00	0.00	NA	NA
99	North (55° N, 130° W)	ARD	Seasonal	Summer	NA	AR-days Frequency	0.00	10.00	3.13	2.15	0.07	0.40
100	North (55° N, 130° W)	ARD0	Seasonal	Summer	NA	AR-days Frequency	0.00	17.00	5.04	3.05	-0.02	0.80
101	North (55° N, 130° W)	ARD1	Seasonal	Summer	NA	AR-days Frequency	0.00	8.00	2.11	1.93	0.11	0.20
102	North (55° N, 130° W)	ARD2	Seasonal	Summer	NA	AR-days Frequency	0.00	5.00	0.63	1.16	-0.04	0.66
103	North (55° N, 130° W)	ARD3	Seasonal	Summer	NA	AR-days Frequency	0.00	5.00	0.17	0.69	0.12	0.23
104	North (55° N, 130° W)	ARD4	Seasonal	Summer	NA	AR-days Frequency	0.00	0.00	0.00	0.00	NA	NA
105	North (55° N, 130° W)	ARD5	Seasonal	Summer	NA	AR-days Frequency	0.00	0.00	0.00	0.00	NA	NA
106	North (55° N, 130° W)	ARD	Seasonal	Winter	NA	AR-days Frequency	0.00	6.00	1.58	1.42	0.00	1.00
107	North (55° N, 130° W)	ARD0	Seasonal	Winter	NA	AR-days Frequency	0.00	6.00	2.43	1.72	0.19	0.03
108	North (55° N, 130° W)	ARD1	Seasonal	Winter	NA	AR-days	0.00	8.00	0.93	1.36	0.08	0.40

#	AR-monitored Region	AR-Days (ARDs) Classification	Scale	Season	Sub-basin	Variable	Min.	Max.	Mean	Std. deviation	Kendall's tau	MK p-value
						Frequency						
109	North (55° N, 130° W)	ARD2	Seasonal	Winter	NA	AR-days Frequency	0.00	4.00	0.29	0.78	-0.20	0.04
110	North (55° N, 130° W)	ARD3	Seasonal	Winter	NA	AR-days Frequency	0.00	3.00	0.07	0.39	-0.12	0.22
111	North (55° N, 130° W)	ARD4	Seasonal	Winter	NA	AR-days Frequency	0.00	2.00	0.03	0.24	0.04	0.74
112	North (55° N, 130° W)	ARD5	Seasonal	Winter	NA	AR-days Frequency	0.00	0.00	0.00	0.00	NA	NA
113	North (55° N, 130° W)	ARD	Seasonal	Fall	NA	AR-days Intensity	350.85	661.85	468.29	62.96	-0.08	0.31
114	North (55° N, 130° W)	ARD0	Seasonal	Fall	NA	AR-days Intensity	280.14	473.23	377.70	35.24	-0.06	0.44
115	North (55° N, 130° W)	ARD1	Seasonal	Fall	NA	AR-days Intensity	0.00	699.57	479.86	130.66	0.05	0.52
116	North (55° N, 130° W)	ARD2	Seasonal	Fall	NA	AR-days Intensity	0.00	820.58	429.29	258.63	-0.01	0.93
117	North (55° N, 130° W)	ARD3	Seasonal	Fall	NA	AR-days Intensity	0.00	899.00	227.98	320.57	-0.05	0.60
118	North (55° N, 130° W)	ARD4	Seasonal	Fall	NA	AR-days Intensity	0.00	1101.40	59.20	220.83	-0.04	0.66
119	North (55° N, 130° W)	ARD5	Seasonal	Fall	NA	AR-days Intensity	0.00	0.00	0.00	0.00	NA	NA
120	North (55° N, 130° W)	ARD	Seasonal	Spring	NA	AR-days Intensity	0.00	568.64	247.55	190.06	0.07	0.43
121	North (55° N, 130° W)	ARD0	Seasonal	Spring	NA	AR-days Intensity	0.00	476.81	291.68	144.42	0.06	0.44
122	North (55° N, 130° W)	ARD1	Seasonal	Spring	NA	AR-days Intensity	0.00	595.89	96.16	193.93	0.00	0.98
123	North (55° N, 130° W)	ARD2	Seasonal	Spring	NA	AR-days Intensity	0.00	644.90	49.69	155.22	-0.04	0.66
124	North (55° N, 130° W)	ARD3	Seasonal	Spring	NA	AR-days Intensity	0.00	0.00	0.00	0.00	NA	NA
125	North (55° N, 130° W)	ARD4	Seasonal	Spring	NA	AR-days Intensity	0.00	0.00	0.00	0.00	NA	NA
126	North (55° N, 130° W)	ARD5	Seasonal	Spring	NA	AR-days Intensity	0.00	0.00	0.00	0.00	NA	NA

#	AR-monitored Region	AR-Days (ARDs) Classification	Scale	Season	Sub-basin	Variable	Min.	Max.	Mean	Std. deviation	Kendall's tau	MK p-value
127	North (55° N, 130° W)	ARD	Seasonal	Summer	NA	AR-days Intensity	0.00	731.16	372.78	127.97	0.06	0.45
128	North (55° N, 130° W)	ARD0	Seasonal	Summer	NA	AR-days Intensity	0.00	464.93	327.61	98.42	0.04	0.62
129	North (55° N, 130° W)	ARD1	Seasonal	Summer	NA	AR-days Intensity	0.00	731.16	335.29	221.57	0.08	0.36
130	North (55° N, 130° W)	ARD2	Seasonal	Summer	NA	AR-days Intensity	0.00	904.42	169.40	257.83	0.00	0.97
131	North (55° N, 130° W)	ARD3	Seasonal	Summer	NA	AR-days Intensity	0.00	778.37	52.16	176.25	0.11	0.27
132	North (55° N, 130° W)	ARD4	Seasonal	Summer	NA	AR-days Intensity	0.00	0.00	0.00	0.00	NA	NA
133	North (55° N, 130° W)	ARD5	Seasonal	Summer	NA	AR-days Intensity	0.00	0.00	0.00	0.00	NA	NA
134	North (55° N, 130° W)	ARD	Seasonal	Winter	NA	AR-days Intensity	0.00	612.89	338.46	207.98	-0.01	0.89
135	North (55° N, 130° W)	ARD0	Seasonal	Winter	NA	AR-days Intensity	0.00	498.19	331.50	143.22	0.21	0.01
136	North (55° N, 130° W)	ARD1	Seasonal	Winter	NA	AR-days Intensity	0.00	699.25	272.35	278.50	0.12	0.16
137	North (55° N, 130° W)	ARD2	Seasonal	Winter	NA	AR-days Intensity	0.00	793.36	90.70	220.05	-0.21	0.03
138	North (55° N, 130° W)	ARD3	Seasonal	Winter	NA	AR-days Intensity	0.00	771.70	27.58	134.21	-0.12	0.21
139	North (55° N, 130° W)	ARD4	Seasonal	Winter	NA	AR-days Intensity	0.00	793.34	11.02	93.50	0.04	0.74
140	North (55° N, 130° W)	ARD5	Seasonal	Winter	NA	AR-days Intensity	0.00	0.00	0.00	0.00	NA	NA
141	South (52.5° N, 127.5° W)	Unstratified series (AR + Non-AR-related)	Annual	NA	Upper Nechako	Rain (mm)	267.85	571.32	406.13	71.98	0.19	0.02
142	South (52.5° N, 127.5° W)	ARD0	Annual	NA	Upper Nechako	Rain (mm)	8.55	104.90	48.30	21.84	0.12	0.15
143	South (52.5° N, 127.5° W)	ARD1	Annual	NA	Upper Nechako	Rain (mm)	3.22	93.48	38.47	21.15	0.02	0.77
144	South (52.5° N, 127.5° W)	ARD2	Annual	NA	Upper Nechako	Rain (mm)	0.00	108.72	29.58	24.81	-0.19	0.02
145	South (52.5° N, 127.5° W)	ARD3	Annual	NA	Upper Nechako	Rain (mm)	0.00	69.88	10.19	15.70	-0.18	0.04
146	South (52.5° N, 127.5° W)	ARD4	Annual	NA	Upper Nechako	Rain (mm)	0.00	44.99	3.15	9.17	-0.03	0.76

#	AR-monitored Region	AR-Days (ARDs) Classification	Scale	Season	Sub-basin	Variable	Min.	Max.	Mean	Std. deviation	Kendall's tau	MK p-value
147	South (52.5° N, 127.5° W)	ARD5	Annual	NA	Upper Nechako	Rain (mm)	0.00	33.15	0.46	3.91	0.01	0.92
148	South (52.5° N, 127.5° W)	Non-AR-related	Annual	NA	Upper Nechako	Rain (mm)	144.69	449.63	275.98	61.55	0.25	0.00
149	South (52.5° N, 127.5° W)	Unstratified series (AR + Non-AR-related)	Annual	NA	Lower Nechako	Rain (mm)	237.90	458.68	351.85	57.53	0.07	0.39
150	South (52.5° N, 127.5° W)	ARD0	Annual	NA	Lower Nechako	Rain (mm)	6.87	89.60	36.33	17.76	0.15	0.07
151	South (52.5° N, 127.5° W)	ARD1	Annual	NA	Lower Nechako	Rain (mm)	0.20	52.13	21.83	11.91	0.05	0.54
152	South (52.5° N, 127.5° W)	ARD2	Annual	NA	Lower Nechako	Rain (mm)	0.00	60.68	14.20	12.77	-0.20	0.01
153	South (52.5° N, 127.5° W)	ARD3	Annual	NA	Lower Nechako	Rain (mm)	0.00	45.11	4.91	8.40	-0.15	0.08
154	South (52.5° N, 127.5° W)	ARD4	Annual	NA	Lower Nechako	Rain (mm)	0.00	19.69	1.02	3.13	-0.02	0.83
155	South (52.5° N, 127.5° W)	ARD5	Annual	NA	Lower Nechako	Rain (mm)	0.00	14.20	0.20	1.67	0.01	0.92
156	South (52.5° N, 127.5° W)	Non-AR-related	Annual	NA	Lower Nechako	Rain (mm)	153.75	392.36	273.36	52.31	0.05	0.54
157	South (52.5° N, 127.5° W)	Unstratified series (AR + Non-AR-related)	Annual	NA	Upper Stuart	Rain (mm)	238.19	552.97	396.95	68.68	0.22	0.01
158	South (52.5° N, 127.5° W)	ARD0	Annual	NA	Upper Stuart	Rain (mm)	7.58	97.82	45.49	19.78	0.16	0.05
159	South (52.5° N, 127.5° W)	ARD1	Annual	NA	Upper Stuart	Rain (mm)	2.81	83.56	29.68	18.55	0.03	0.76
160	South (52.5° N, 127.5° W)	ARD2	Annual	NA	Upper Stuart	Rain (mm)	0.00	90.09	20.68	18.17	-0.12	0.16
161	South (52.5° N, 127.5° W)	ARD3	Annual	NA	Upper Stuart	Rain (mm)	0.00	61.99	6.92	10.78	-0.15	0.08
162	South (52.5° N, 127.5° W)	ARD4	Annual	NA	Upper Stuart	Rain (mm)	0.00	31.49	2.49	6.31	-0.04	0.69
163	South (52.5° N, 127.5° W)	ARD5	Annual	NA	Upper Stuart	Rain (mm)	0.00	23.20	0.32	2.73	0.01	0.92
164	South (52.5° N, 127.5° W)	Non-AR-related	Annual	NA	Upper Stuart	Rain (mm)	134.46	415.64	291.37	63.83	0.19	0.02
165	South (52.5° N, 127.5° W)	Unstratified series (AR + Non-AR-related)	Annual	NA	Lower Stuart	Rain (mm)	208.26	492.37	353.20	61.31	0.05	0.51
166	South (52.5° N, 127.5° W)	ARD0	Annual	NA	Lower Stuart	Rain (mm)	6.10	85.83	36.53	17.60	0.15	0.06
167	South (52.5° N, 127.5° W)	ARD1	Annual	NA	Lower Stuart	Rain (mm)	0.71	63.67	24.13	14.11	0.02	0.83
168	South (52.5° N, 127.5° W)	ARD2	Annual	NA	Lower Stuart	Rain (mm)	0.00	64.25	17.01	14.84	-0.17	0.03
169	South (52.5° N, 127.5° W)	ARD3	Annual	NA	Lower Stuart	Rain (mm)	0.00	34.03	5.51	7.76	-0.16	0.07
170	South (52.5° N, 127.5° W)	ARD4	Annual	NA	Lower Stuart	Rain (mm)	0.00	32.54	1.90	5.38	-0.03	0.79

#	AR-monitored Region	AR-Days (ARDs) Classification	Scale	Season	Sub-basin	Variable	Min.	Max.	Mean	Std. deviation	Kendall's tau	MK p-value
171	South (52.5° N, 127.5° W)	ARD5	Annual	NA	Lower Stuart	Rain (mm)	0.00	13.77	0.19	1.62	0.01	0.92
172	South (52.5° N, 127.5° W)	Non-AR-related	Annual	NA	Lower Stuart	Rain (mm)	135.12	399.70	267.93	59.07	0.04	0.58
173	South (52.5° N, 127.5° W)	Unstratified series (AR + Non-AR-related)	Annual	NA	Endako	Rain (mm)	230.36	469.83	351.19	59.38	0.04	0.62
174	South (52.5° N, 127.5° W)	ARD0	Annual	NA	Endako	Rain (mm)	5.53	96.30	38.83	19.11	0.13	0.12
175	South (52.5° N, 127.5° W)	ARD1	Annual	NA	Endako	Rain (mm)	0.26	61.22	26.18	14.19	0.03	0.75
176	South (52.5° N, 127.5° W)	ARD2	Annual	NA	Endako	Rain (mm)	0.00	68.79	18.46	16.13	-0.20	0.01
177	South (52.5° N, 127.5° W)	ARD3	Annual	NA	Endako	Rain (mm)	0.00	39.24	5.96	8.98	-0.16	0.07
178	South (52.5° N, 127.5° W)	ARD4	Annual	NA	Endako	Rain (mm)	0.00	37.46	1.91	5.86	-0.02	0.82
179	South (52.5° N, 127.5° W)	ARD5	Annual	NA	Endako	Rain (mm)	0.00	19.72	0.27	2.32	0.01	0.92
180	South (52.5° N, 127.5° W)	Non-AR-related	Annual	NA	Endako	Rain (mm)	147.86	381.32	259.58	52.15	0.03	0.74
181	South (52.5° N, 127.5° W)	Unstratified series (AR + Non-AR-related)	Annual	NA	Chilako	Rain (mm)	248.01	496.78	365.93	56.76	0.06	0.42
182	South (52.5° N, 127.5° W)	ARD0	Annual	NA	Chilako	Rain (mm)	7.09	76.85	34.61	16.50	0.14	0.08
183	South (52.5° N, 127.5° W)	ARD1	Annual	NA	Chilako	Rain (mm)	0.11	52.67	18.77	11.10	0.03	0.70
184	South (52.5° N, 127.5° W)	ARD2	Annual	NA	Chilako	Rain (mm)	0.00	60.83	11.99	11.15	-0.19	0.02
185	South (52.5° N, 127.5° W)	ARD3	Annual	NA	Chilako	Rain (mm)	0.00	49.33	4.31	8.13	-0.14	0.11
186	South (52.5° N, 127.5° W)	ARD4	Annual	NA	Chilako	Rain (mm)	0.00	11.74	0.56	1.79	-0.02	0.85
187	South (52.5° N, 127.5° W)	ARD5	Annual	NA	Chilako	Rain (mm)	0.00	10.07	0.14	1.19	0.01	0.92
188	South (52.5° N, 127.5° W)	Non-AR-related	Annual	NA	Chilako	Rain (mm)	161.05	432.01	295.55	53.53	0.05	0.51
189	South (52.5° N, 127.5° W)	Unstratified series (AR + Non-AR-related)	Annual	NA	Stellako	Rain (mm)	253.02	529.29	377.95	66.75	0.07	0.36
190	South (52.5° N, 127.5° W)	ARD0	Annual	NA	Stellako	Rain (mm)	6.72	100.84	44.21	20.59	0.11	0.17
191	South (52.5° N, 127.5° W)	ARD1	Annual	NA	Stellako	Rain (mm)	1.93	89.85	35.55	19.16	0.03	0.69
192	South (52.5° N, 127.5° W)	ARD2	Annual	NA	Stellako	Rain (mm)	0.00	102.19	27.55	23.60	-0.21	0.01
193	South (52.5° N, 127.5° W)	ARD3	Annual	NA	Stellako	Rain (mm)	0.00	57.49	8.81	13.58	-0.18	0.04
194	South (52.5° N, 127.5° W)	ARD4	Annual	NA	Stellako	Rain (mm)	0.00	53.38	3.29	9.77	-0.03	0.79

#	AR-monitored Region	AR-Days (ARDs) Classification	Scale	Season	Sub-basin	Variable	Min.	Max.	Mean	Std. deviation	Kendall's tau	MK p-value
195	South (52.5° N, 127.5° W)	ARD5	Annual	NA	Stellako	Rain (mm)	0.00	32.52	0.45	3.83	0.01	0.92
196	South (52.5° N, 127.5° W)	Non-AR-related	Annual	NA	Stellako	Rain (mm)	133.69	404.76	258.09	54.86	0.13	0.12
197	South (52.5° N, 127.5° W)	Unstratified series (AR + Non-AR-related)	Annual	NA	Upper Nechako	Snow (mm)	363.99	842.60	596.64	107.36	-0.10	0.23
198	South (52.5° N, 127.5° W)	ARD0	Annual	NA	Upper Nechako	Snow (mm)	10.82	144.02	61.32	29.45	0.05	0.50
199	South (52.5° N, 127.5° W)	ARD1	Annual	NA	Upper Nechako	Snow (mm)	0.00	119.51	35.97	25.67	0.04	0.62
200	South (52.5° N, 127.5° W)	ARD2	Annual	NA	Upper Nechako	Snow (mm)	0.00	126.90	12.69	20.16	-0.15	0.07
201	South (52.5° N, 127.5° W)	ARD3	Annual	NA	Upper Nechako	Snow (mm)	0.00	48.57	2.88	8.61	-0.18	0.05
202	South (52.5° N, 127.5° W)	ARD4	Annual	NA	Upper Nechako	Snow (mm)	0.00	11.38	0.37	1.62	-0.09	0.34
203	South (52.5° N, 127.5° W)	ARD5	Annual	NA	Upper Nechako	Snow (mm)	0.00	0.00	0.00	0.00	NA	NA
204	South (52.5° N, 127.5° W)	Non-AR-related	Annual	NA	Upper Nechako	Snow (mm)	305.30	699.29	483.41	90.20	-0.10	0.23
205	South (52.5° N, 127.5° W)	Unstratified series (AR + Non-AR-related)	Annual	NA	Lower Nechako	Snow (mm)	80.98	320.23	207.81	46.39	-0.06	0.45
206	South (52.5° N, 127.5° W)	ARD0	Annual	NA	Lower Nechako	Snow (mm)	0.01	35.52	14.75	8.93	0.06	0.44
207	South (52.5° N, 127.5° W)	ARD1	Annual	NA	Lower Nechako	Snow (mm)	0.00	33.70	5.66	6.73	0.02	0.77
208	South (52.5° N, 127.5° W)	ARD2	Annual	NA	Lower Nechako	Snow (mm)	0.00	43.11	1.79	6.53	-0.08	0.35
209	South (52.5° N, 127.5° W)	ARD3	Annual	NA	Lower Nechako	Snow (mm)	0.00	16.98	0.48	2.44	-0.11	0.23
210	South (52.5° N, 127.5° W)	ARD4	Annual	NA	Lower Nechako	Snow (mm)	0.00	1.26	0.02	0.15	-0.16	0.09
211	South (52.5° N, 127.5° W)	ARD5	Annual	NA	Lower Nechako	Snow (mm)	0.00	0.00	0.00	0.00	NA	NA
212	South (52.5° N, 127.5° W)	Non-AR-related	Annual	NA	Lower Nechako	Snow (mm)	73.30	314.38	185.12	42.05	-0.09	0.25
213	South (52.5° N, 127.5° W)	Unstratified series (AR + Non-AR-related)	Annual	NA	Upper Stuart	Snow (mm)	295.96	548.83	439.02	59.52	-0.07	0.38
214	South (52.5° N, 127.5° W)	ARD0	Annual	NA	Upper Stuart	Snow (mm)	8.91	89.07	43.90	19.81	0.15	0.06
215	South (52.5° N, 127.5° W)	ARD1	Annual	NA	Upper Stuart	Snow (mm)	0.02	64.87	28.48	17.19	0.03	0.72
216	South (52.5° N, 127.5° W)	ARD2	Annual	NA	Upper Stuart	Snow (mm)	0.00	85.98	12.97	15.07	-0.15	0.07
217	South (52.5° N, 127.5° W)	ARD3	Annual	NA	Upper Stuart	Snow (mm)	0.00	48.56	3.13	8.25	-0.11	0.21
218	South (52.5° N, 127.5° W)	ARD4	Annual	NA	Upper Stuart	Snow (mm)	0.00	30.88	1.42	5.20	-0.18	0.06

#	AR-monitored Region	AR-Days (ARDs) Classification	Scale	Season	Sub-basin	Variable	Min.	Max.	Mean	Std. deviation	Kendall's tau	MK p-value
219	South (52.5° N, 127.5° W)	ARD5	Annual	NA	Upper Stuart	Snow (mm)	0.00	0.46	0.01	0.05	0.01	0.92
220	South (52.5° N, 127.5° W)	Non-AR-related	Annual	NA	Upper Stuart	Snow (mm)	235.59	469.71	349.11	52.61	-0.09	0.28
221	South (52.5° N, 127.5° W)	Unstratified series (AR + Non-AR-related)	Annual	NA	Lower Stuart	Snow (mm)	145.46	384.99	275.90	48.33	0.01	0.94
222	South (52.5° N, 127.5° W)	ARD0	Annual	NA	Lower Stuart	Snow (mm)	0.95	57.62	24.33	13.51	0.10	0.20
223	South (52.5° N, 127.5° W)	ARD1	Annual	NA	Lower Stuart	Snow (mm)	0.00	44.00	11.52	9.92	0.14	0.08
224	South (52.5° N, 127.5° W)	ARD2	Annual	NA	Lower Stuart	Snow (mm)	0.00	48.21	3.46	7.21	-0.10	0.24
225	South (52.5° N, 127.5° W)	ARD3	Annual	NA	Lower Stuart	Snow (mm)	0.00	34.22	1.21	4.81	-0.14	0.12
226	South (52.5° N, 127.5° W)	ARD4	Annual	NA	Lower Stuart	Snow (mm)	0.00	6.45	0.22	0.94	-0.09	0.37
227	South (52.5° N, 127.5° W)	ARD5	Annual	NA	Lower Stuart	Snow (mm)	0.00	0.00	0.00	0.00	NA	NA
228	South (52.5° N, 127.5° W)	Non-AR-related	Annual	NA	Lower Stuart	Snow (mm)	125.01	361.15	235.15	45.15	-0.07	0.38
229	South (52.5° N, 127.5° W)	Unstratified series (AR + Non-AR-related)	Annual	NA	Endako	Snow (mm)	112.55	358.80	246.68	50.21	0.00	1.00
230	South (52.5° N, 127.5° W)	ARD0	Annual	NA	Endako	Snow (mm)	0.04	46.35	20.08	11.78	0.08	0.35
231	South (52.5° N, 127.5° W)	ARD1	Annual	NA	Endako	Snow (mm)	0.00	40.94	8.51	9.05	0.09	0.25
232	South (52.5° N, 127.5° W)	ARD2	Annual	NA	Endako	Snow (mm)	0.00	64.92	2.94	9.80	-0.11	0.20
233	South (52.5° N, 127.5° W)	ARD3	Annual	NA	Endako	Snow (mm)	0.00	24.29	0.85	3.73	-0.12	0.20
234	South (52.5° N, 127.5° W)	ARD4	Annual	NA	Endako	Snow (mm)	0.00	3.25	0.06	0.40	-0.09	0.37
235	South (52.5° N, 127.5° W)	ARD5	Annual	NA	Endako	Snow (mm)	0.00	0.00	0.00	0.00	NA	NA
236	South (52.5° N, 127.5° W)	Non-AR-related	Annual	NA	Endako	Snow (mm)	100.34	347.81	214.23	44.19	-0.05	0.52
237	South (52.5° N, 127.5° W)	Unstratified series (AR + Non-AR-related)	Annual	NA	Chilako	Snow (mm)	77.61	308.51	197.57	47.47	-0.06	0.46
238	South (52.5° N, 127.5° W)	ARD0	Annual	NA	Chilako	Snow (mm)	0.00	38.73	13.96	9.17	0.11	0.18
239	South (52.5° N, 127.5° W)	ARD1	Annual	NA	Chilako	Snow (mm)	0.00	35.91	5.04	6.39	-0.04	0.60
240	South (52.5° N, 127.5° W)	ARD2	Annual	NA	Chilako	Snow (mm)	0.00	34.58	1.29	4.40	-0.03	0.72
241	South (52.5° N, 127.5° W)	ARD3	Annual	NA	Chilako	Snow (mm)	0.00	15.44	0.41	2.18	-0.10	0.29
242	South (52.5° N, 127.5° W)	ARD4	Annual	NA	Chilako	Snow (mm)	0.00	0.39	0.01	0.05	-0.09	0.35

#	AR-monitored Region	AR-Days (ARDs) Classification	Scale	Season	Sub-basin	Variable	Min.	Max.	Mean	Std. deviation	Kendall's tau	MK p-value
243	South (52.5° N, 127.5° W)	ARD5	Annual	NA	Chilako	Snow (mm)	0.00	0.00	0.00	0.00	NA	NA
244	South (52.5° N, 127.5° W)	Non-AR-related	Annual	NA	Chilako	Snow (mm)	69.91	303.72	176.87	43.40	-0.11	0.18
245	South (52.5° N, 127.5° W)	Unstratified series (AR + Non-AR-related)	Annual	NA	Stellako	Snow (mm)	214.77	539.39	367.35	69.32	-0.04	0.62
246	South (52.5° N, 127.5° W)	ARD0	Annual	NA	Stellako	Snow (mm)	1.96	81.97	34.99	18.71	0.06	0.46
247	South (52.5° N, 127.5° W)	ARD1	Annual	NA	Stellako	Snow (mm)	0.00	56.96	19.24	15.21	0.09	0.26
248	South (52.5° N, 127.5° W)	ARD2	Annual	NA	Stellako	Snow (mm)	0.00	103.34	7.13	15.02	-0.13	0.12
249	South (52.5° N, 127.5° W)	ARD3	Annual	NA	Stellako	Snow (mm)	0.00	27.70	1.60	4.93	-0.17	0.06
250	South (52.5° N, 127.5° W)	ARD4	Annual	NA	Stellako	Snow (mm)	0.00	6.78	0.22	0.99	-0.09	0.34
251	South (52.5° N, 127.5° W)	ARD5	Annual	NA	Stellako	Snow (mm)	0.00	0.00	0.00	0.00	NA	NA
252	South (52.5° N, 127.5° W)	Non-AR-related	Annual	NA	Stellako	Snow (mm)	172.40	452.47	304.17	59.01	-0.07	0.41
253	South (52.5° N, 127.5° W)	Unstratified series (AR + Non-AR-related)	Annual	NA	Upper Nechako	Total Precip. (mm)	743.85	1360.93	1002.77	129.73	0.01	0.88
254	South (52.5° N, 127.5° W)	ARD0	Annual	NA	Upper Nechako	Total Precip. (mm)	31.19	203.25	109.62	41.28	0.07	0.39
255	South (52.5° N, 127.5° W)	ARD1	Annual	NA	Upper Nechako	Total Precip. (mm)	16.30	188.55	74.44	37.30	0.06	0.43
256	South (52.5° N, 127.5° W)	ARD2	Annual	NA	Upper Nechako	Total Precip. (mm)	0.00	148.51	42.27	35.71	-0.18	0.03
257	South (52.5° N, 127.5° W)	ARD3	Annual	NA	Upper Nechako	Total Precip. (mm)	0.00	94.96	13.07	21.75	-0.19	0.03
258	South (52.5° N, 127.5° W)	ARD4	Annual	NA	Upper Nechako	Total Precip. (mm)	0.00	45.03	3.51	10.11	-0.03	0.76
259	South (52.5° N, 127.5° W)	ARD5	Annual	NA	Upper Nechako	Total Precip. (mm)	0.00	33.15	0.46	3.91	0.01	0.92
260	South (52.5° N, 127.5° W)	Non-AR-related	Annual	NA	Upper Nechako	Total Precip. (mm)	558.34	1047.11	759.40	98.53	0.03	0.67
261	South (52.5° N, 127.5° W)	Unstratified series (AR + Non-AR-related)	Annual	NA	Lower Nechako	Total Precip. (mm)	425.26	717.23	559.66	65.70	0.03	0.72
262	South (52.5° N, 127.5° W)	ARD0	Annual	NA	Lower Nechako	Total Precip. (mm)	17.05	111.41	51.08	20.27	0.18	0.03
263	South (52.5° N, 127.5° W)	ARD1	Annual	NA	Lower Nechako	Total Precip. (mm)	2.01	72.74	27.48	14.69	0.07	0.40

#	AR-monitored Region	AR-Days (ARDs) Classification	Scale	Season	Sub-basin	Variable	Min.	Max.	Mean	Std. deviation	Kendall's tau	MK p-value
264	South (52.5° N, 127.5° W)	ARD2	Annual	NA	Lower Nechako	Total Precip. (mm)	0.00	61.08	15.99	14.79	-0.18	0.03
265	South (52.5° N, 127.5° W)	ARD3	Annual	NA	Lower Nechako	Total Precip. (mm)	0.00	45.11	5.39	9.43	-0.15	0.08
266	South (52.5° N, 127.5° W)	ARD4	Annual	NA	Lower Nechako	Total Precip. (mm)	0.00	19.69	1.04	3.16	-0.02	0.81
267	South (52.5° N, 127.5° W)	ARD5	Annual	NA	Lower Nechako	Total Precip. (mm)	0.00	14.20	0.20	1.67	0.01	0.92
268	South (52.5° N, 127.5° W)	Non-AR-related	Annual	NA	Lower Nechako	Total Precip. (mm)	312.74	583.56	458.47	59.35	-0.03	0.70
269	South (52.5° N, 127.5° W)	Unstratified series (AR + Non-AR-related)	Annual	NA	Upper Stuart	Total Precip. (mm)	640.34	1046.00	835.97	88.58	0.10	0.22
270	South (52.5° N, 127.5° W)	ARD0	Annual	NA	Upper Stuart	Total Precip. (mm)	29.18	179.98	89.39	30.52	0.23	0.00
271	South (52.5° N, 127.5° W)	ARD1	Annual	NA	Upper Stuart	Total Precip. (mm)	12.51	147.17	58.16	26.51	0.04	0.63
272	South (52.5° N, 127.5° W)	ARD2	Annual	NA	Upper Stuart	Total Precip. (mm)	0.00	115.03	33.65	25.85	-0.14	0.09
273	South (52.5° N, 127.5° W)	ARD3	Annual	NA	Upper Stuart	Total Precip. (mm)	0.00	70.37	10.05	14.46	-0.15	0.08
274	South (52.5° N, 127.5° W)	ARD4	Annual	NA	Upper Stuart	Total Precip. (mm)	0.00	52.93	3.91	10.37	-0.04	0.68
275	South (52.5° N, 127.5° W)	ARD5	Annual	NA	Upper Stuart	Total Precip. (mm)	0.00	23.66	0.33	2.79	0.01	0.92
276	South (52.5° N, 127.5° W)	Non-AR-related	Annual	NA	Upper Stuart	Total Precip. (mm)	468.25	804.60	640.48	74.66	0.04	0.60
277	South (52.5° N, 127.5° W)	Unstratified series (AR + Non-AR-related)	Annual	NA	Lower Stuart	Total Precip. (mm)	500.79	765.46	629.10	65.39	0.05	0.56
278	South (52.5° N, 127.5° W)	ARD0	Annual	NA	Lower Stuart	Total Precip. (mm)	17.18	143.45	60.86	23.78	0.20	0.02
279	South (52.5° N, 127.5° W)	ARD1	Annual	NA	Lower Stuart	Total Precip. (mm)	4.90	92.49	35.65	18.13	0.08	0.32
280	South (52.5° N, 127.5° W)	ARD2	Annual	NA	Lower Stuart	Total Precip. (mm)	0.00	65.03	20.47	16.30	-0.14	0.08
281	South (52.5° N, 127.5° W)	ARD3	Annual	NA	Lower Stuart	Total Precip. (mm)	0.00	43.06	6.72	9.85	-0.14	0.11
282	South (52.5° N, 127.5° W)	ARD4	Annual	NA	Lower Stuart	Total Precip.	0.00	35.09	2.12	5.94	-0.03	0.77

#	AR-monitored Region	AR-Days (ARDs) Classification	Scale	Season	Sub-basin	Variable	Min.	Max.	Mean	Std. deviation	Kendall's tau	MK p-value
						(mm)						
283	South (52.5° N, 127.5° W)	ARD5	Annual	NA	Lower Stuart	Total Precip. (mm)	0.00	13.77	0.19	1.62	0.01	0.92
284	South (52.5° N, 127.5° W)	Non-AR-related	Annual	NA	Lower Stuart	Total Precip. (mm)	372.48	686.67	503.09	62.23	-0.02	0.82
285	South (52.5° N, 127.5° W)	Unstratified series (AR + Non-AR-related)	Annual	NA	Endako	Total Precip. (mm)	468.04	748.58	597.88	66.77	0.01	0.89
286	South (52.5° N, 127.5° W)	ARD0	Annual	NA	Endako	Total Precip. (mm)	15.66	133.86	58.92	23.46	0.16	0.05
287	South (52.5° N, 127.5° W)	ARD1	Annual	NA	Endako	Total Precip. (mm)	2.40	97.62	34.69	18.34	0.08	0.32
288	South (52.5° N, 127.5° W)	ARD2	Annual	NA	Endako	Total Precip. (mm)	0.00	83.22	21.41	18.93	-0.16	0.05
289	South (52.5° N, 127.5° W)	ARD3	Annual	NA	Endako	Total Precip. (mm)	0.00	42.70	6.81	10.72	-0.15	0.08
290	South (52.5° N, 127.5° W)	ARD4	Annual	NA	Endako	Total Precip. (mm)	0.00	37.51	1.97	5.97	-0.02	0.80
291	South (52.5° N, 127.5° W)	ARD5	Annual	NA	Endako	Total Precip. (mm)	0.00	19.72	0.27	2.32	0.01	0.92
292	South (52.5° N, 127.5° W)	Non-AR-related	Annual	NA	Endako	Total Precip. (mm)	333.61	615.85	473.81	59.03	-0.01	0.87
293	South (52.5° N, 127.5° W)	Unstratified series (AR + Non-AR-related)	Annual	NA	Chilako	Total Precip. (mm)	425.28	749.57	563.50	68.94	0.01	0.89
294	South (52.5° N, 127.5° W)	ARD0	Annual	NA	Chilako	Total Precip. (mm)	18.67	96.83	48.57	19.35	0.18	0.02
295	South (52.5° N, 127.5° W)	ARD1	Annual	NA	Chilako	Total Precip. (mm)	2.01	63.79	23.81	13.45	0.04	0.61
296	South (52.5° N, 127.5° W)	ARD2	Annual	NA	Chilako	Total Precip. (mm)	0.00	60.85	13.28	12.16	-0.16	0.05
297	South (52.5° N, 127.5° W)	ARD3	Annual	NA	Chilako	Total Precip. (mm)	0.00	49.33	4.71	8.92	-0.13	0.12
298	South (52.5° N, 127.5° W)	ARD4	Annual	NA	Chilako	Total Precip. (mm)	0.00	11.74	0.57	1.81	-0.02	0.85
299	South (52.5° N, 127.5° W)	ARD5	Annual	NA	Chilako	Total Precip. (mm)	0.00	10.07	0.14	1.19	0.01	0.92
300	South (52.5° N, 127.5° W)	Non-AR-related	Annual	NA	Chilako	Total Precip. (mm)	316.27	619.91	472.42	62.65	-0.02	0.83

#	AR-monitored Region	AR-Days (ARDs) Classification	Scale	Season	Sub-basin	Variable	Min.	Max.	Mean	Std. deviation	Kendall's tau	MK p-value
301	South (52.5° N, 127.5° W)	Unstratified series (AR + Non-AR-related)	Annual	NA	Stellako	Total Precip. (mm)	557.04	1000.20	745.29	92.46	0.01	0.88
302	South (52.5° N, 127.5° W)	ARD0	Annual	NA	Stellako	Total Precip. (mm)	22.94	154.93	79.20	30.49	0.09	0.26
303	South (52.5° N, 127.5° W)	ARD1	Annual	NA	Stellako	Total Precip. (mm)	8.65	133.48	54.79	27.65	0.08	0.34
304	South (52.5° N, 127.5° W)	ARD2	Annual	NA	Stellako	Total Precip. (mm)	0.00	128.77	34.69	30.30	-0.18	0.03
305	South (52.5° N, 127.5° W)	ARD3	Annual	NA	Stellako	Total Precip. (mm)	0.00	73.07	10.41	16.76	-0.18	0.04
306	South (52.5° N, 127.5° W)	ARD4	Annual	NA	Stellako	Total Precip. (mm)	0.00	53.39	3.50	10.31	-0.03	0.77
307	South (52.5° N, 127.5° W)	ARD5	Annual	NA	Stellako	Total Precip. (mm)	0.00	32.52	0.45	3.83	0.01	0.92
308	South (52.5° N, 127.5° W)	Non-AR-related	Annual	NA	Stellako	Total Precip. (mm)	393.72	771.48	562.25	73.47	0.02	0.79
309	South (52.5° N, 127.5° W)	Unstratified series (AR + Non-AR-related)	Annual	NA	Upper Nechako	SWE (mm)	0.34	0.82	0.56	0.11	-0.09	0.26
310	South (52.5° N, 127.5° W)	ARD0	Annual	NA	Upper Nechako	SWE (mm)	5.63	102.43	43.52	21.40	0.07	0.42
311	South (52.5° N, 127.5° W)	ARD1	Annual	NA	Upper Nechako	SWE (mm)	0.00	111.92	29.47	23.10	0.03	0.67
312	South (52.5° N, 127.5° W)	ARD2	Annual	NA	Upper Nechako	SWE (mm)	0.00	143.68	10.24	19.73	-0.11	0.18
313	South (52.5° N, 127.5° W)	ARD3	Annual	NA	Upper Nechako	SWE (mm)	0.00	55.53	2.60	8.50	-0.14	0.15
314	South (52.5° N, 127.5° W)	ARD4	Annual	NA	Upper Nechako	SWE (mm)	0.00	24.95	0.48	3.03	-0.13	0.19
315	South (52.5° N, 127.5° W)	ARD5	Annual	NA	Upper Nechako	SWE (mm)	0.00	0.00	0.00	0.00	NA	NA
316	South (52.5° N, 127.5° W)	Non-AR-related	Annual	NA	Upper Nechako	SWE (mm)	290.10	752.60	476.50	96.40	-0.10	0.23
317	South (52.5° N, 127.5° W)	Unstratified series (AR + Non-AR-related)	Annual	NA	Lower Nechako	SWE (mm)	0.06	0.31	0.18	0.05	-0.06	0.47
318	South (52.5° N, 127.5° W)	ARD0	Annual	NA	Lower Nechako	SWE (mm)	0.00	29.74	10.44	6.51	0.04	0.64
319	South (52.5° N, 127.5° W)	ARD1	Annual	NA	Lower Nechako	SWE (mm)	0.00	28.69	5.32	6.00	0.03	0.70
320	South (52.5° N, 127.5° W)	ARD2	Annual	NA	Lower Nechako	SWE (mm)	0.00	46.50	1.84	6.54	-0.04	0.68
321	South (52.5° N, 127.5° W)	ARD3	Annual	NA	Lower Nechako	SWE (mm)	0.00	10.97	0.35	1.62	-0.11	0.24

#	AR-monitored Region	AR-Days (ARDs) Classification	Scale	Season	Sub-basin	Variable	Min.	Max.	Mean	Std. deviation	Kendall's tau	MK p-value
322	South (52.5° N, 127.5° W)	ARD4	Annual	NA	Lower Nechako	SWE (mm)	0.00	1.17	0.02	0.14	-0.11	0.28
323	South (52.5° N, 127.5° W)	ARD5	Annual	NA	Lower Nechako	SWE (mm)	0.00	0.00	0.00	0.00	NA	NA
324	South (52.5° N, 127.5° W)	Non-AR-related	Annual	NA	Lower Nechako	SWE (mm)	52.29	303.26	164.19	43.98	-0.10	0.23
325	South (52.5° N, 127.5° W)	Unstratified series (AR + Non-AR-related)	Annual	NA	Upper Stuart	SWE (mm)	0.27	0.53	0.42	0.06	-0.05	0.56
326	South (52.5° N, 127.5° W)	ARD0	Annual	NA	Upper Stuart	SWE (mm)	5.95	65.86	32.79	14.90	0.17	0.04
327	South (52.5° N, 127.5° W)	ARD1	Annual	NA	Upper Stuart	SWE (mm)	0.00	66.47	24.08	16.28	-0.01	0.93
328	South (52.5° N, 127.5° W)	ARD2	Annual	NA	Upper Stuart	SWE (mm)	0.00	88.72	11.19	14.58	-0.14	0.08
329	South (52.5° N, 127.5° W)	ARD3	Annual	NA	Upper Stuart	SWE (mm)	0.00	35.12	2.85	7.67	-0.15	0.09
330	South (52.5° N, 127.5° W)	ARD4	Annual	NA	Upper Stuart	SWE (mm)	0.00	39.82	1.32	5.71	-0.14	0.16
331	South (52.5° N, 127.5° W)	ARD5	Annual	NA	Upper Stuart	SWE (mm)	0.00	3.57	0.05	0.42	0.01	0.92
332	South (52.5° N, 127.5° W)	Non-AR-related	Annual	NA	Upper Stuart	SWE (mm)	244.13	467.06	347.52	53.36	-0.05	0.53
333	South (52.5° N, 127.5° W)	Unstratified series (AR + Non-AR-related)	Annual	NA	Lower Stuart	SWE (mm)	0.12	0.35	0.25	0.05	0.02	0.79
334	South (52.5° N, 127.5° W)	ARD0	Annual	NA	Lower Stuart	SWE (mm)	0.09	42.22	16.79	8.98	0.13	0.11
335	South (52.5° N, 127.5° W)	ARD1	Annual	NA	Lower Stuart	SWE (mm)	0.00	41.22	10.41	9.23	0.05	0.53
336	South (52.5° N, 127.5° W)	ARD2	Annual	NA	Lower Stuart	SWE (mm)	0.00	48.20	3.44	7.11	0.00	0.97
337	South (52.5° N, 127.5° W)	ARD3	Annual	NA	Lower Stuart	SWE (mm)	0.00	23.55	0.86	3.47	-0.05	0.61
338	South (52.5° N, 127.5° W)	ARD4	Annual	NA	Lower Stuart	SWE (mm)	0.00	5.81	0.13	0.75	-0.11	0.25
339	South (52.5° N, 127.5° W)	ARD5	Annual	NA	Lower Stuart	SWE (mm)	0.00	0.00	0.00	0.00	NA	NA
340	South (52.5° N, 127.5° W)	Non-AR-related	Annual	NA	Lower Stuart	SWE (mm)	91.43	337.57	218.56	45.97	-0.03	0.70
341	South (52.5° N, 127.5° W)	Unstratified series (AR + Non-AR-related)	Annual	NA	Endako	SWE (mm)	0.09	0.35	0.23	0.05	0.01	0.91
342	South (52.5° N, 127.5° W)	ARD0	Annual	NA	Endako	SWE (mm)	0.02	36.17	14.92	8.58	0.06	0.47
343	South (52.5° N, 127.5° W)	ARD1	Annual	NA	Endako	SWE (mm)	0.00	36.84	8.22	8.47	0.06	0.46
344	South (52.5° N, 127.5° W)	ARD2	Annual	NA	Endako	SWE (mm)	0.00	68.55	3.34	10.05	0.01	0.89
345	South (52.5° N, 127.5° W)	ARD3	Annual	NA	Endako	SWE (mm)	0.00	17.28	0.77	3.10	-0.06	0.55

#	AR-monitored Region	AR-Days (ARDs) Classification	Scale	Season	Sub-basin	Variable	Min.	Max.	Mean	Std. deviation	Kendall's tau	MK p-value
346	South (52.5° N, 127.5° W)	ARD4	Annual	NA	Endako	SWE (mm)	0.00	3.76	0.07	0.46	-0.10	0.32
347	South (52.5° N, 127.5° W)	ARD5	Annual	NA	Endako	SWE (mm)	0.00	0.00	0.00	0.00	NA	NA
348	South (52.5° N, 127.5° W)	Non-AR-related	Annual	NA	Endako	SWE (mm)	73.88	338.21	201.54	47.53	-0.03	0.69
349	South (52.5° N, 127.5° W)	Unstratified series (AR + Non-AR-related)	Annual	NA	Chilako	SWE (mm)	0.06	0.29	0.17	0.05	-0.06	0.44
350	South (52.5° N, 127.5° W)	ARD0	Annual	NA	Chilako	SWE (mm)	0.00	31.61	9.68	6.97	0.08	0.34
351	South (52.5° N, 127.5° W)	ARD1	Annual	NA	Chilako	SWE (mm)	0.00	23.58	4.74	5.31	-0.01	0.91
352	South (52.5° N, 127.5° W)	ARD2	Annual	NA	Chilako	SWE (mm)	0.00	39.34	1.45	4.99	-0.04	0.66
353	South (52.5° N, 127.5° W)	ARD3	Annual	NA	Chilako	SWE (mm)	0.00	11.05	0.29	1.48	-0.07	0.47
354	South (52.5° N, 127.5° W)	ARD4	Annual	NA	Chilako	SWE (mm)	0.00	0.42	0.01	0.05	-0.09	0.35
355	South (52.5° N, 127.5° W)	ARD5	Annual	NA	Chilako	SWE (mm)	0.00	0.00	0.00	0.00	NA	NA
356	South (52.5° N, 127.5° W)	Non-AR-related	Annual	NA	Chilako	SWE (mm)	49.62	285.06	154.94	43.77	-0.09	0.29
357	South (52.5° N, 127.5° W)	Unstratified series (AR + Non-AR-related)	Annual	NA	Stellako	SWE (mm)	0.19	0.51	0.34	0.07	-0.03	0.75
358	South (52.5° N, 127.5° W)	ARD0	Annual	NA	Stellako	SWE (mm)	0.39	62.65	25.60	13.79	0.05	0.55
359	South (52.5° N, 127.5° W)	ARD1	Annual	NA	Stellako	SWE (mm)	0.00	58.25	16.57	13.86	0.07	0.37
360	South (52.5° N, 127.5° W)	ARD2	Annual	NA	Stellako	SWE (mm)	0.00	109.94	6.15	15.01	-0.05	0.51
361	South (52.5° N, 127.5° W)	ARD3	Annual	NA	Stellako	SWE (mm)	0.00	24.35	1.43	4.80	-0.10	0.30
362	South (52.5° N, 127.5° W)	ARD4	Annual	NA	Stellako	SWE (mm)	0.00	15.15	0.30	1.87	-0.16	0.09
363	South (52.5° N, 127.5° W)	ARD5	Annual	NA	Stellako	SWE (mm)	0.00	0.00	0.00	0.00	NA	NA
364	South (52.5° N, 127.5° W)	Non-AR-related	Annual	NA	Stellako	SWE (mm)	145.58	472.55	288.37	62.45	-0.05	0.53

APPENDIX B

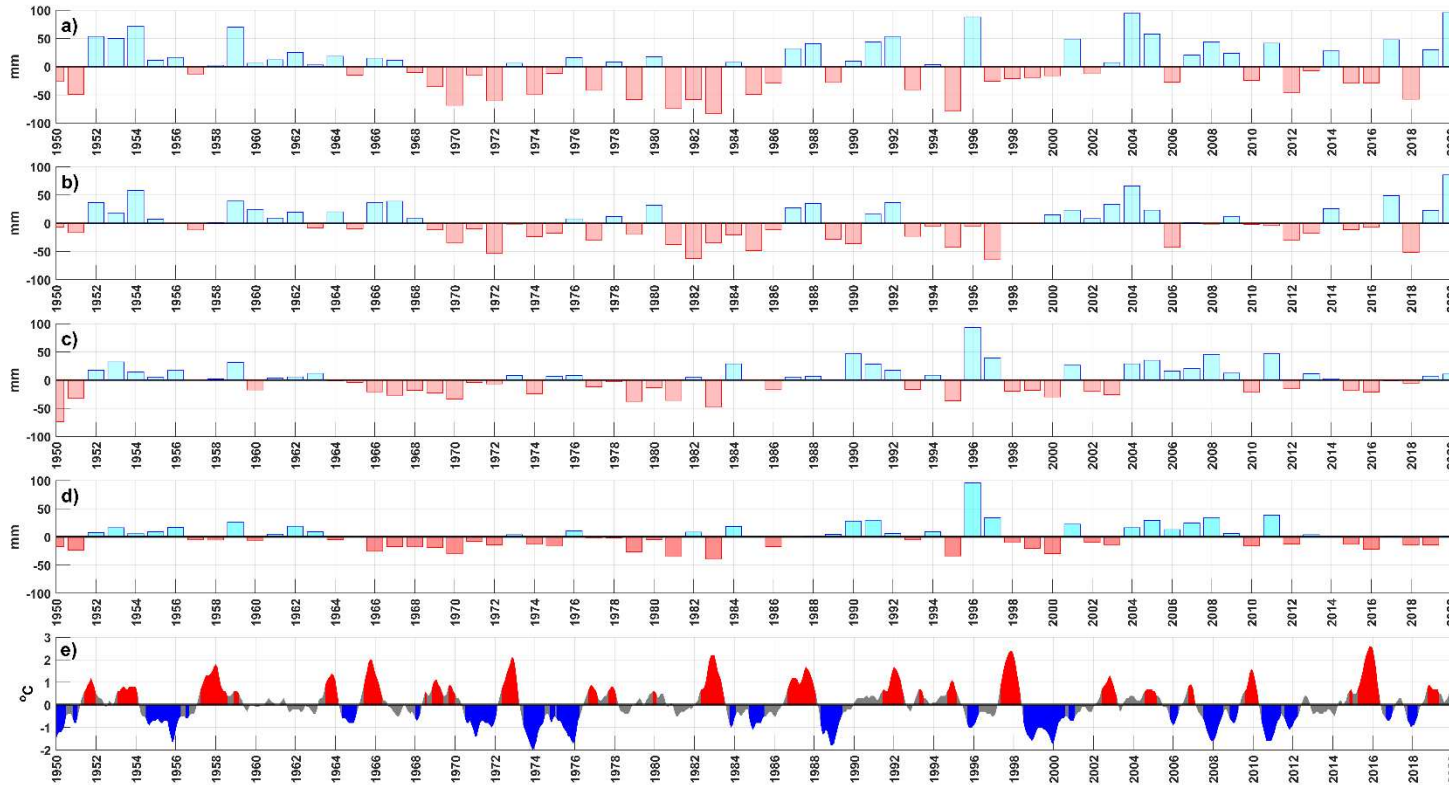


Figure B.1 – Annual anomalies related to Atmospheric Rivers (AR) for (a) total precipitation, (b) rainfall, (c) snowfall, and (d) SWE in the NRB, based on daily data from the ERA5-Land (1950-2021) and the AR Catalogue (1950-2021). Panel (e) shows the maximum and minimum values of the ONI. In panels (a), (b), (c), and (d), light blue and light red bars indicate positive and negative anomalies, respectively, from the mean. In panel (e), red areas represent El Niño phases, blue areas represent La Niña phases, and gray areas represent neutral phases of the ENSO climate pattern.

APPENDIX C

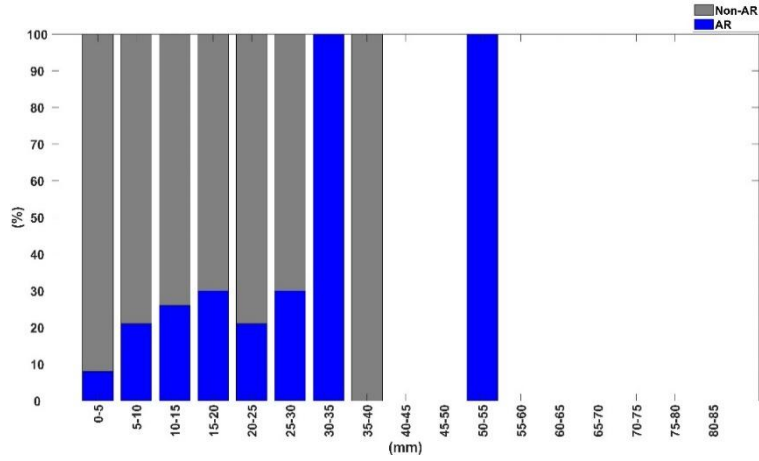


Figure C.1 – Fraction (%) of daily AR-related (blue) total precipitation compared to non-AR-related (gray) in the Lower Nechako divided into 5 mm bins.

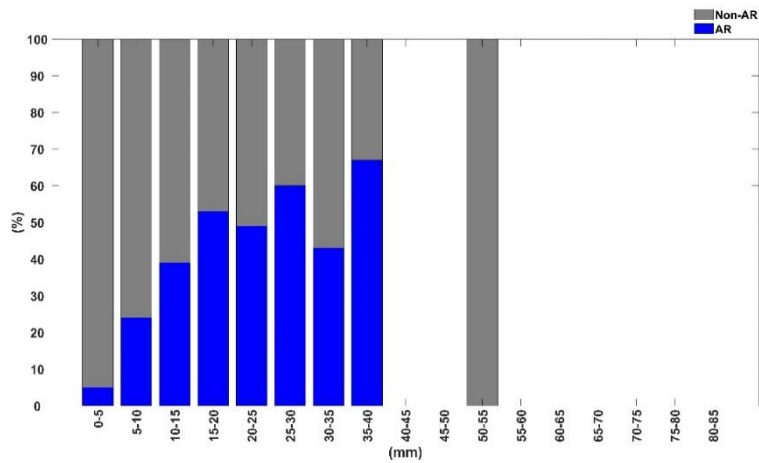


Figure C.2 – Fraction (%) of daily AR-related (blue) total precipitation compared to non-AR-related (gray) in the Upper Stuart divided into 5 mm bins.

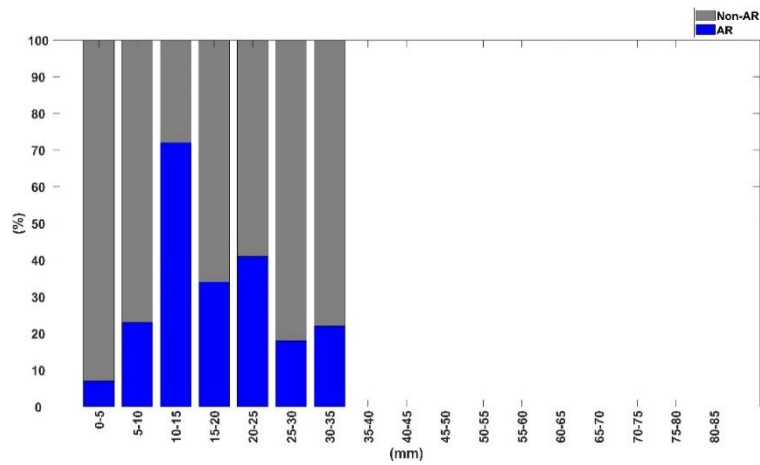


Figure C.3 – Fraction (%) of daily AR-related (blue) total precipitation compared to non-AR-related (gray) in the Lower Stuart divided into 5 mm bins.

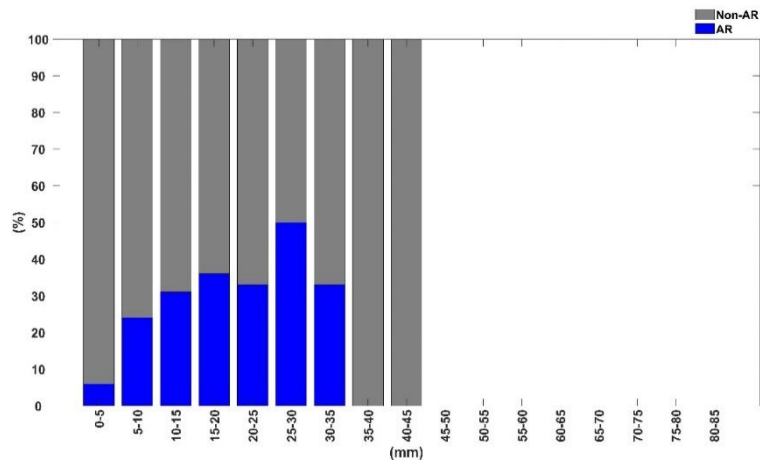


Figure C.4 – Fraction (%) of daily AR-related (blue) total precipitation compared to non-AR-related (gray) in the Endako divided into 5 mm bins.

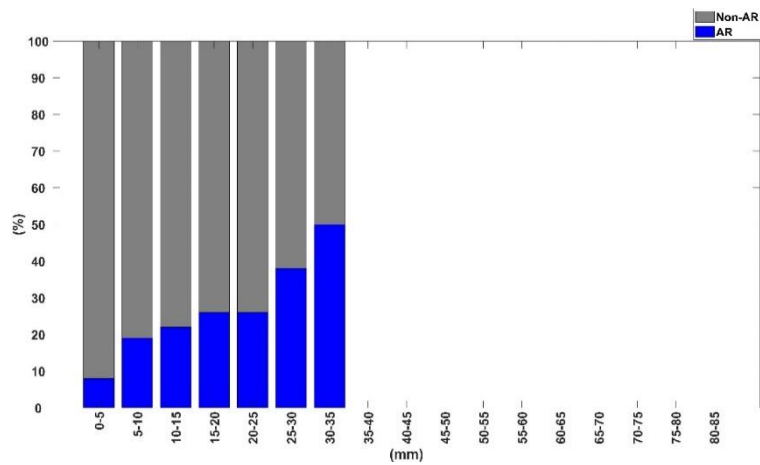


Figure C.5 – Fraction (%) of daily AR-related (blue) total precipitation compared to non-AR-related (gray) in the Chilako divided into 5 mm bins.

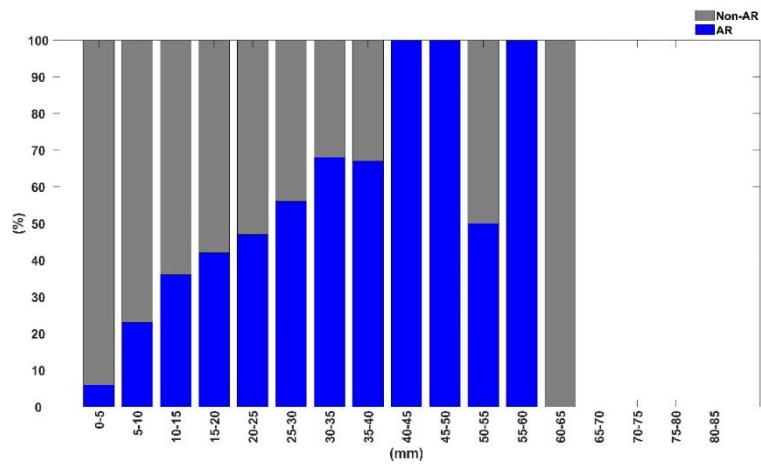


Figure C.6 – Fraction (%) of daily AR-related (blue) total precipitation compared to non-AR-related (gray) in the Stellako divided into 5 mm bins.

APPENDIX D

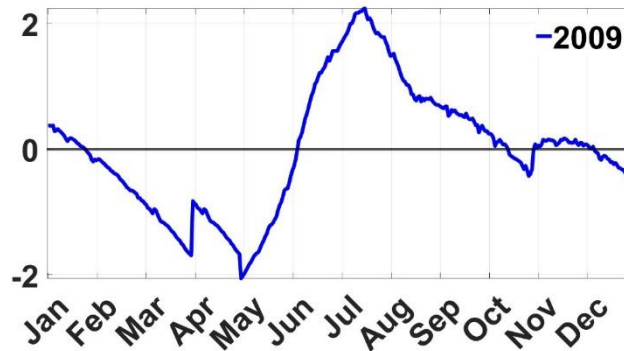


Figure D.1: Daily standardized water level graph at the Tahtsa Lake near Kemano station (08JA030) during the exceptional AR event of 2009. No data are available at this station for the 1952 and 1978 AR events.

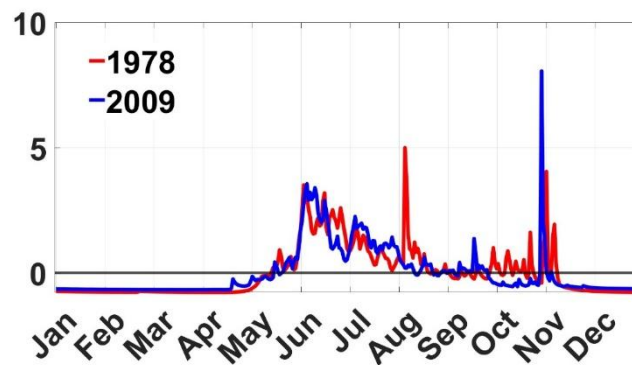


Figure D.2: Daily standardized discharge graph at the Laventie Creek near the Mouth station (08JA015) during the exceptional AR events of 1978 (red) and 2009 (blue). No data are available at this station for the 1952 AR event.

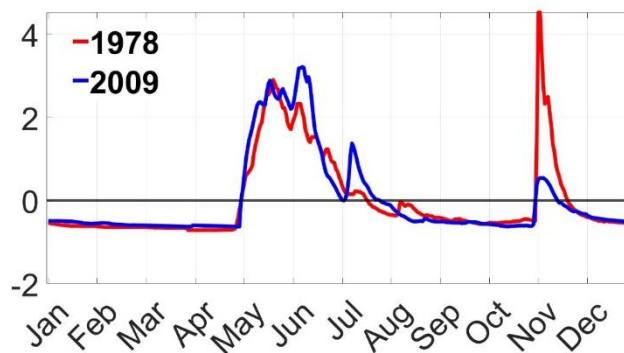


Figure D.3: Daily standardized discharge graph at the Nadina River at the outlet of Nadina Lake station (08JB008) during the exceptional AR events of 1978 (red) and 2009 (blue). No data are available at this station for the 1952 AR event.

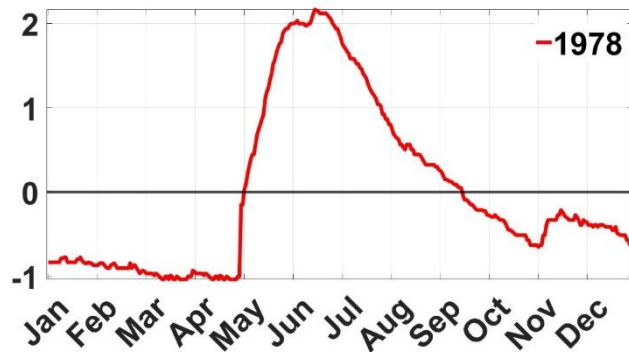


Figure D.4: Daily standardized water level graph at Francois Lake station (08JB011) during the exceptional AR event of 1978. No data are available at this station for the 1952 and 2009 AR events.

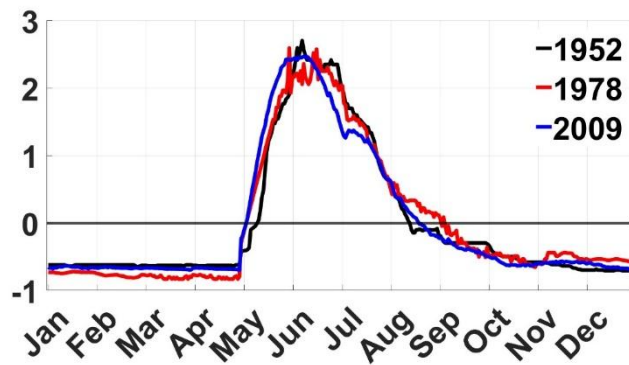


Figure D.5: Daily standardized discharge graph at the Stellako River at Glenannan station (08JB002) during the exceptional AR events of 1952 (black), 1978 (red), and 2009 (blue).

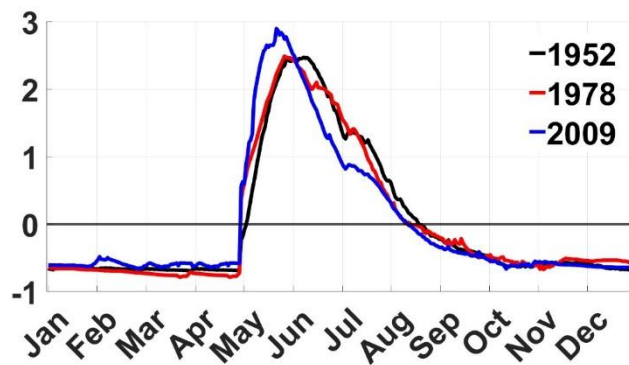


Figure D.6: Daily standardized discharge graph at the Nautley River near Fort Fraser station (08JB003) during the exceptional AR events of 1952 (black), 1978 (red), and 2009 (blue).

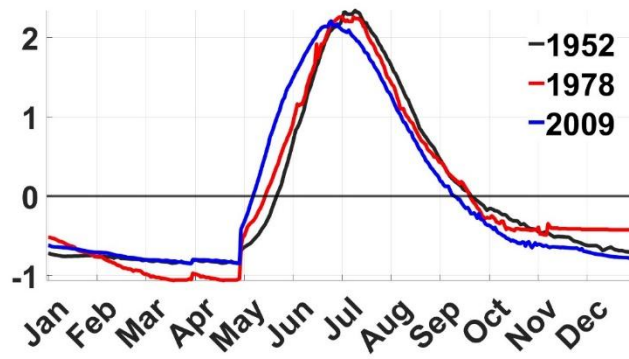


Figure D.7: Daily standardized discharge graph at the Stuart River near Fort St. James station (08JE001) during the exceptional AR events of 1952 (black), 1978 (red), and 2009 (blue).

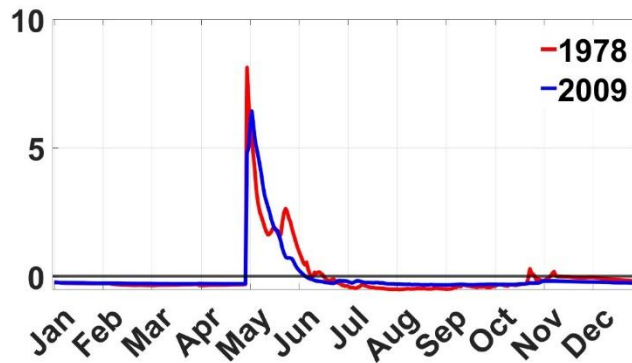


Figure D.8: Daily standardized discharge graph at the Tsilcoh River near the Mouth station (08JE004) during the exceptional AR events of 1978 (red) and 2009 (blue).

APPENDIX E

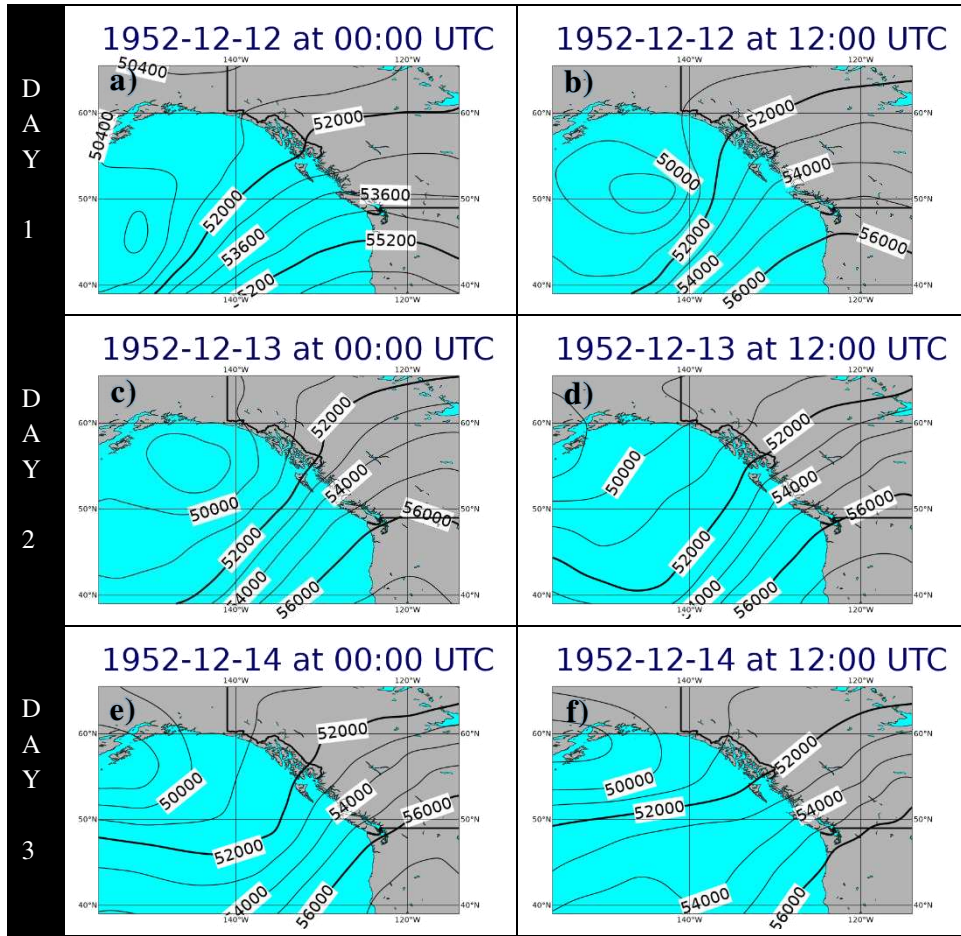


Figure E.1: Sequence of the geopotential at 500 hPa (a to f - in $m^2 s^{-2}$) in the 12-hourly (UTC) scale during the 1952 exceptional AR event.

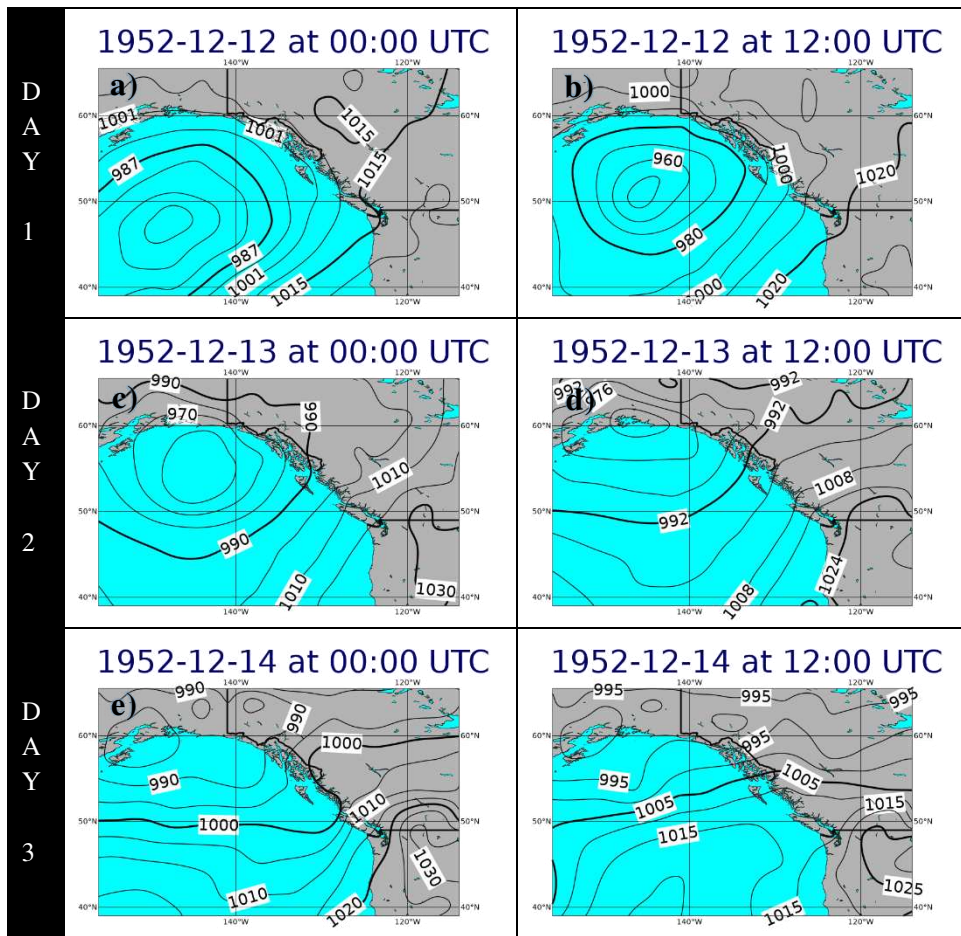


Figure E.2: Sequence of the mean sea-level pressure (a to f - in hPa) in the 12-hourly (UTC) scale during the 1952 exceptional AR event.

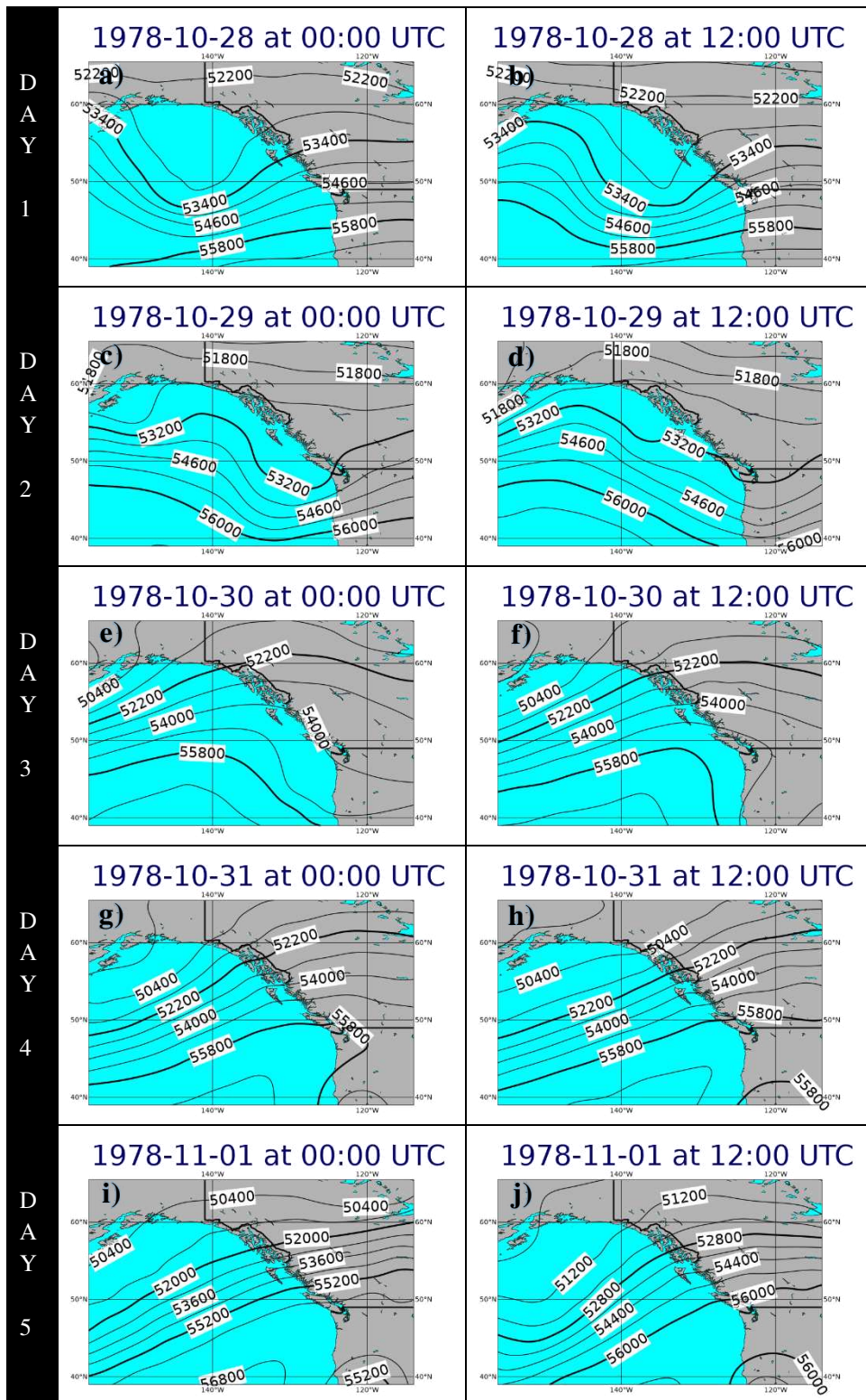


Figure E.3: Sequence of the geopotential at 500 hPa (a to j - in $\text{m}^2 \text{s}^{-2}$) in the 12-hourly (UTC) scale during the 1978 exceptional AR event.

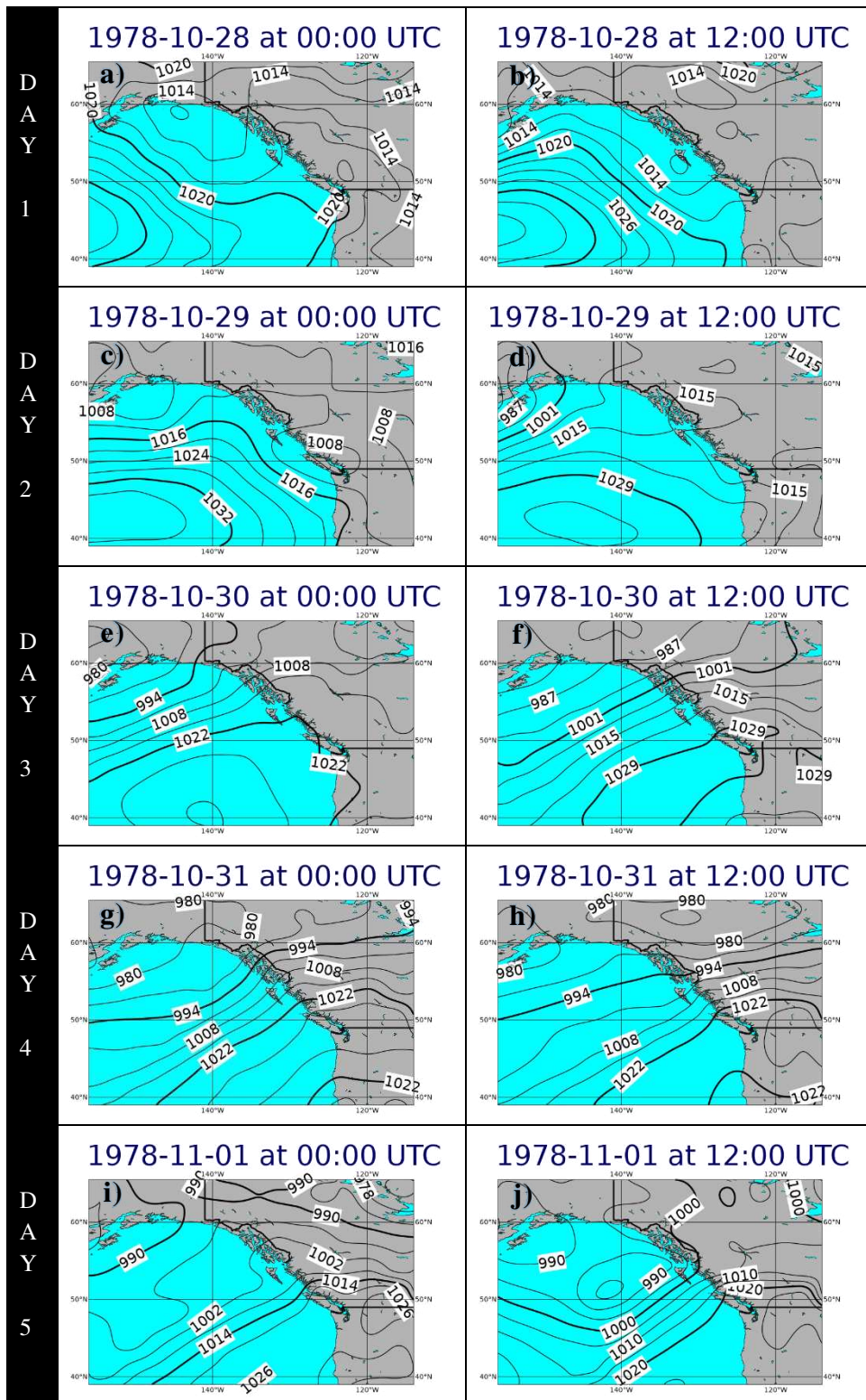


Figure E.4: Sequence of the mean sea-level pressure (a to j - in hPa) in the 12-hourly (UTC) scale during the 1978 exceptional AR event.

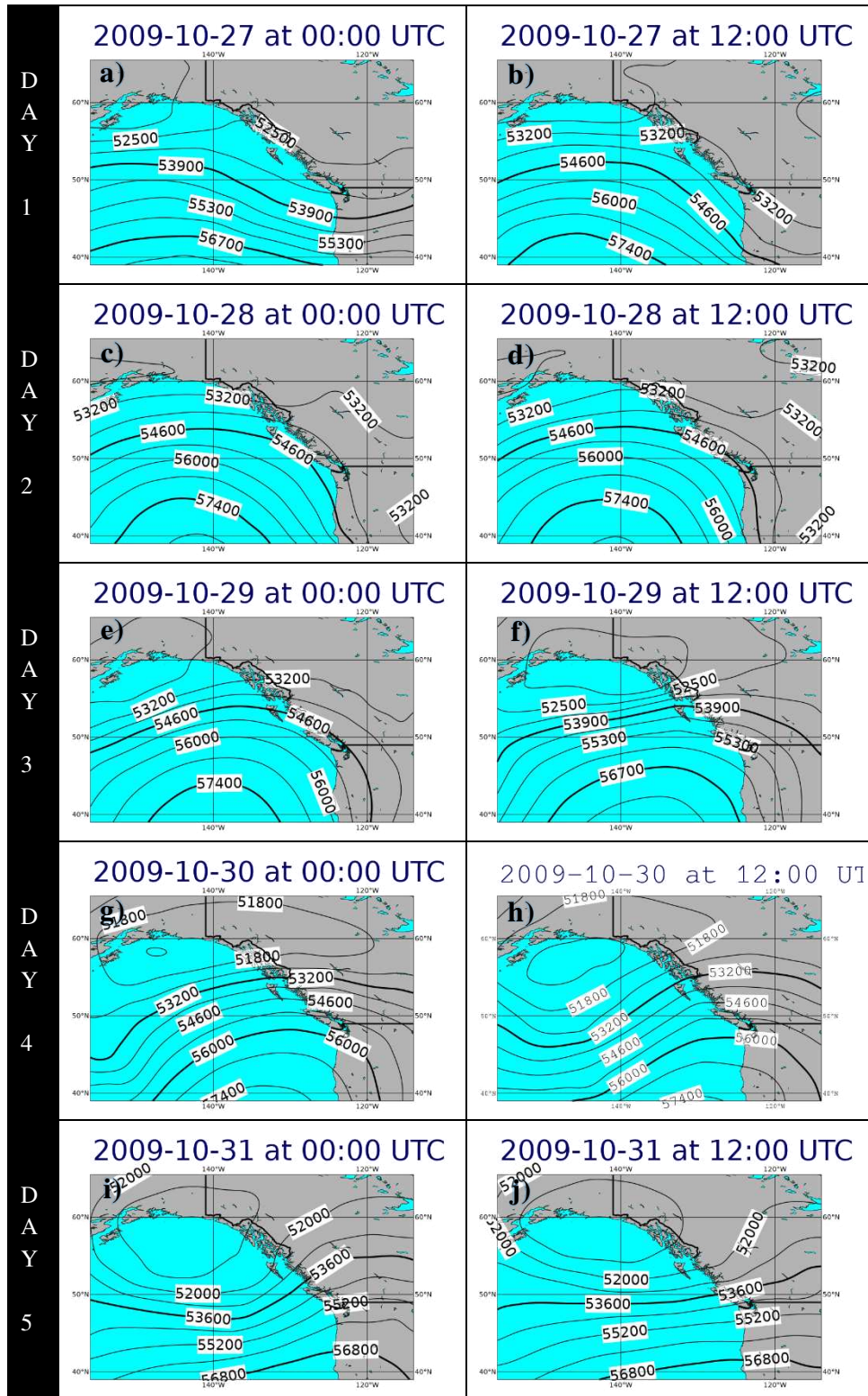


Figure E.5: Sequence of the geopotential at 500 hPa (a to j - in $m^2 s^{-2}$) in the 12-hourly (UTC) scale during the 2009 exceptional AR event.

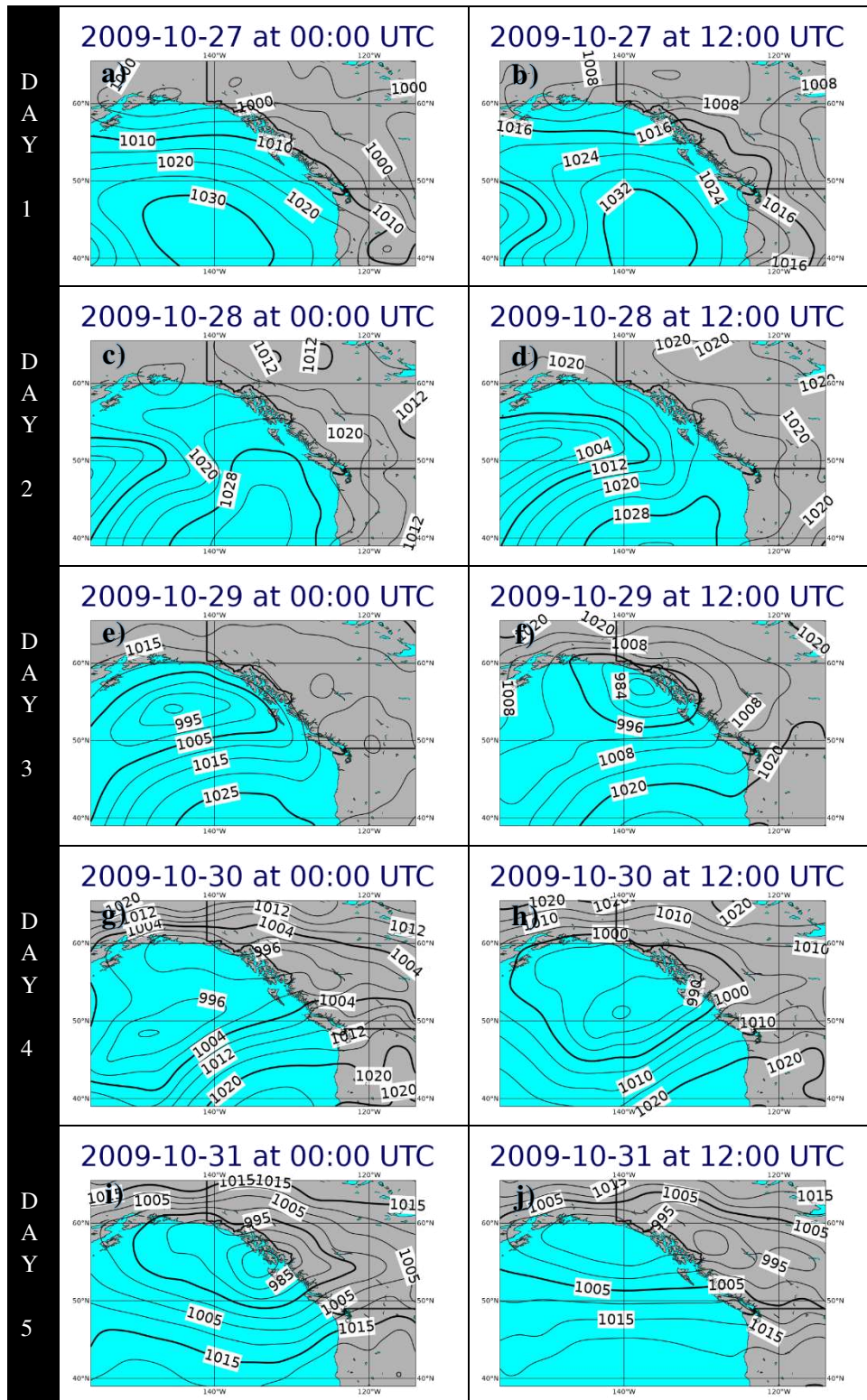


Figure E.6: Sequence of the mean sea-level pressure (a to j - in hPa) in the 12-hourly (UTC) scale during the 2009 exceptional AR event.

APPENDIX F

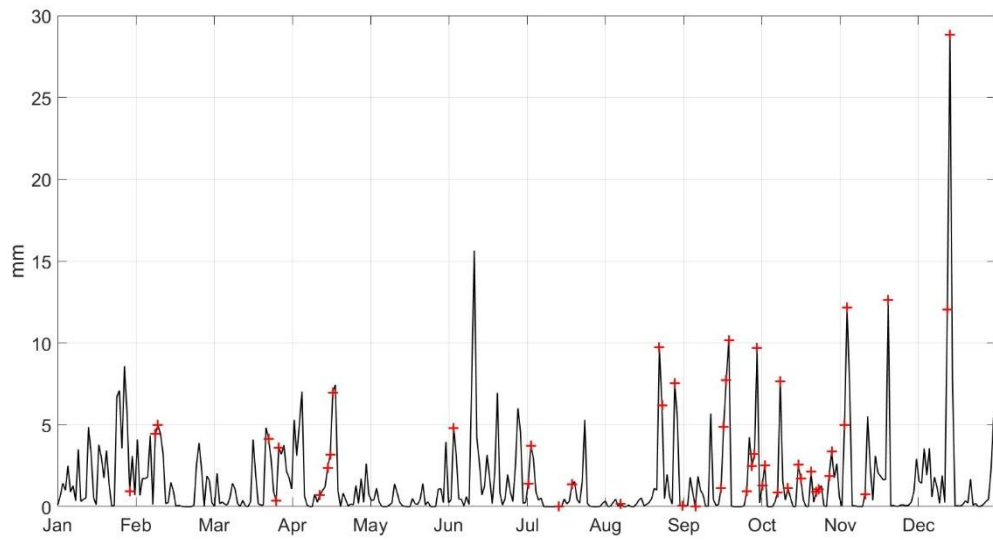


Figure F.1: Daily total precipitation (mm) in the NRB in 1952. Red crosses indicate AR Days or days when total precipitation is associated with ARs.

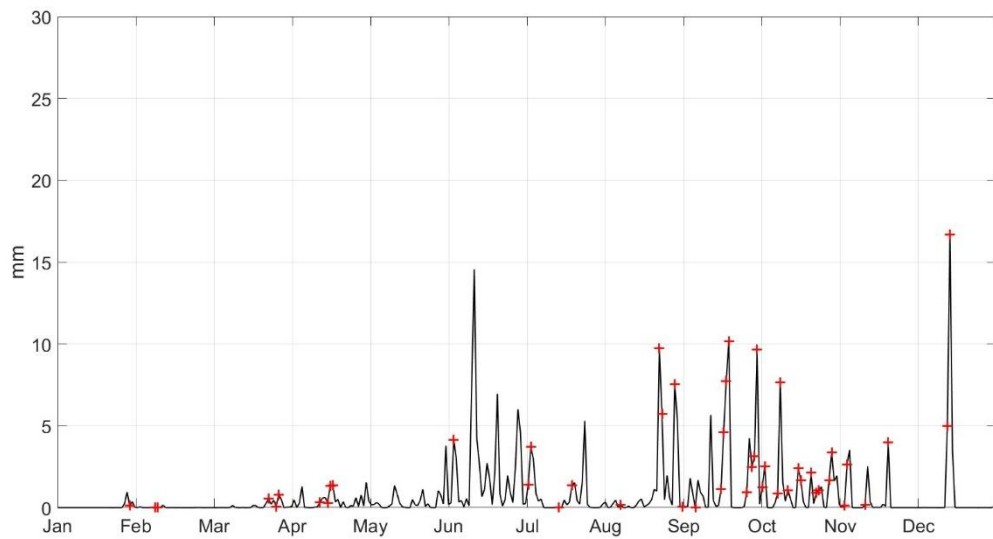


Figure F.2: Daily rainfall (mm) in the NRB in 1952. Red crosses indicate AR Days or days when rainfall is associated with ARs.

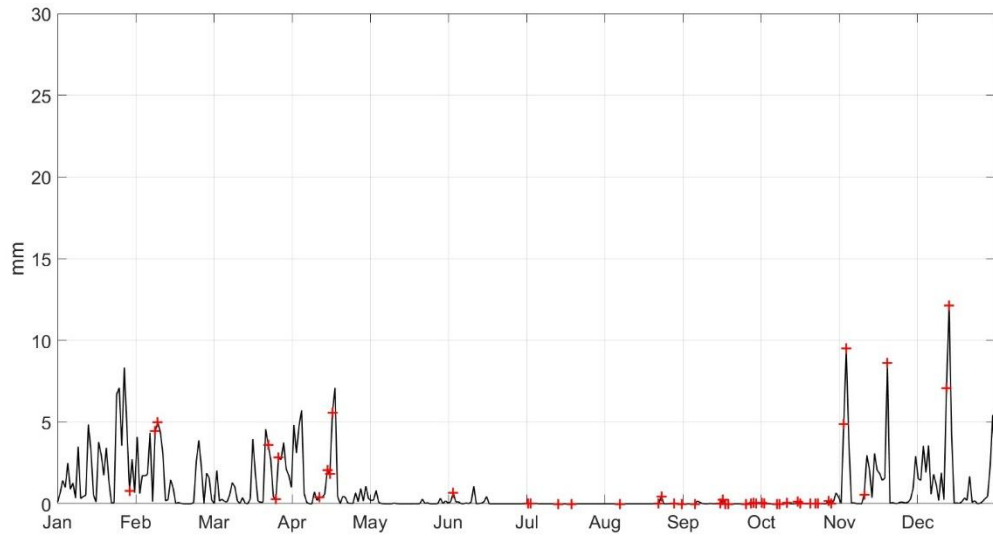


Figure F.3: Daily snowfall (mm) in the NRB in 1952. Red crosses indicate AR Days or days when snowfall is associated with ARs.

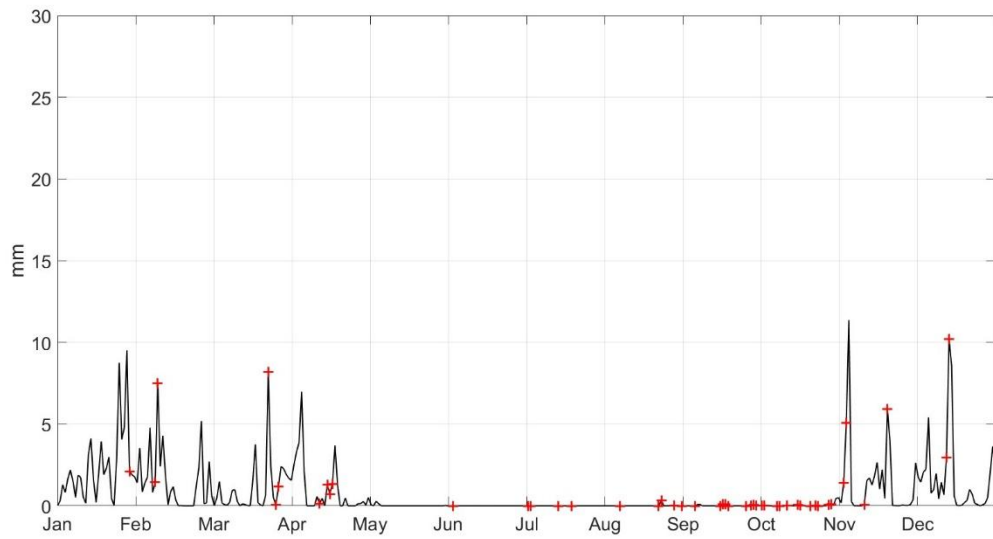


Figure F.4: Daily SWE (mm) in the NRB in 1952. Red crosses indicate AR Days or days when SWE is associated with ARs.

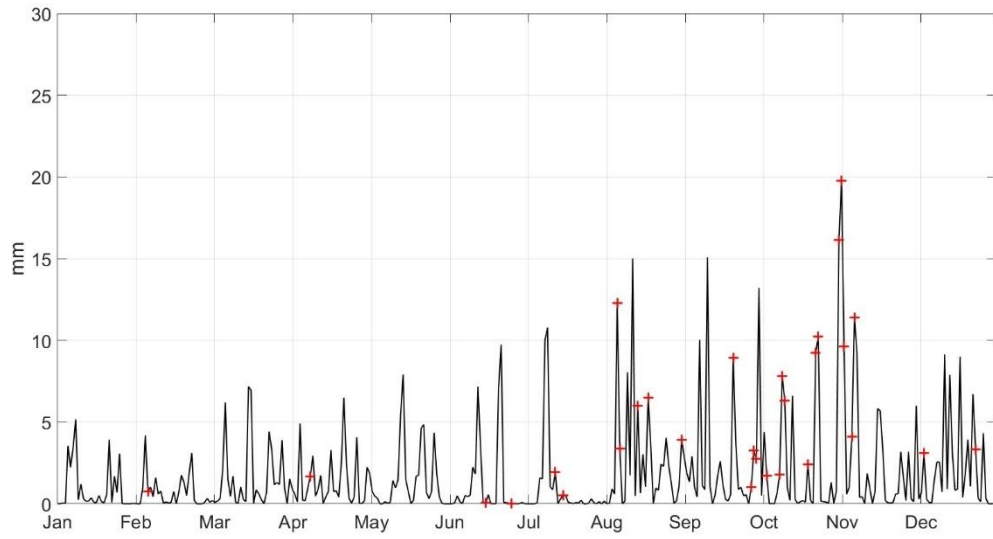


Figure F.5: Daily total precipitation (mm) in the NRB in 1978. Red crosses indicate AR Days or days when total precipitation is associated with ARs.

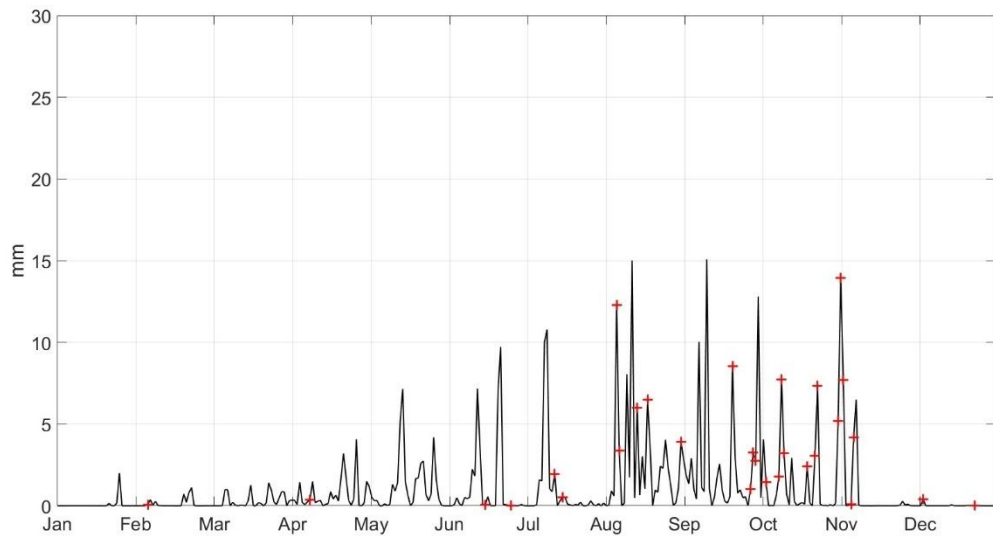


Figure F.6: Daily rainfall (mm) in the NRB in 1978. Red crosses indicate AR Days or days when rainfall is associated with ARs.

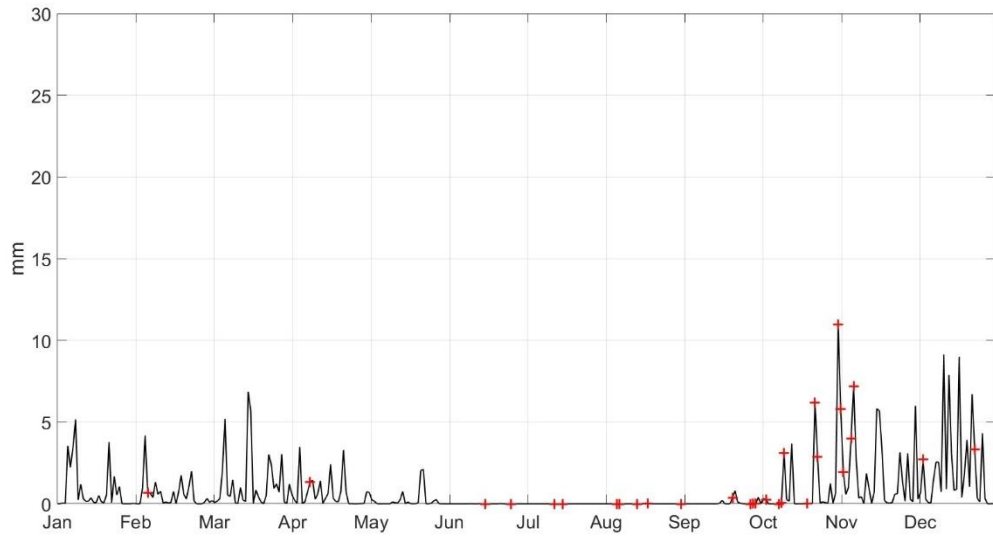


Figure F.7: Daily snowfall (mm) in the NRB in 1978. Red crosses indicate AR Days or days when snowfall is associated with ARs.

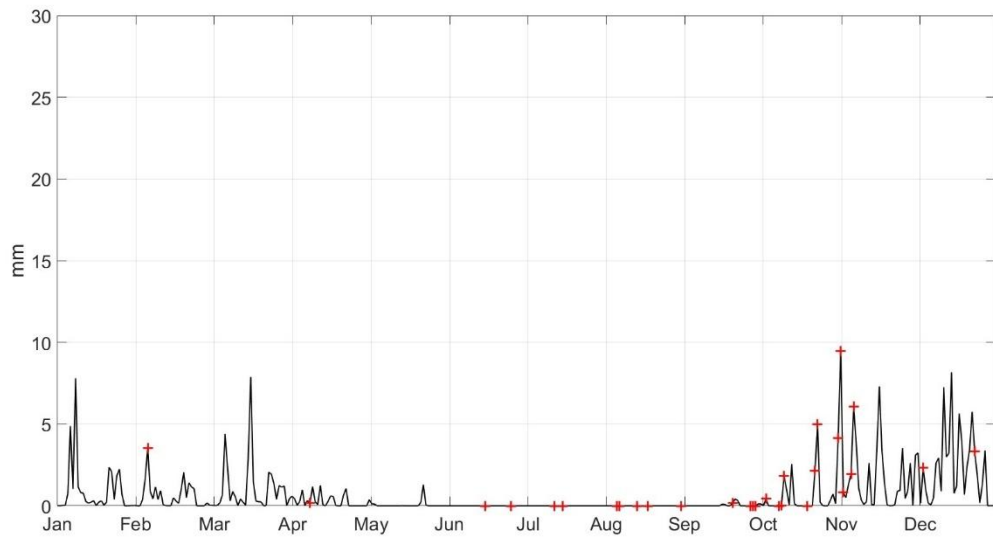


Figure F.8: Daily SWE (mm) in the NRB in 1978. Red crosses indicate AR Days or days when SWE is associated with ARs.

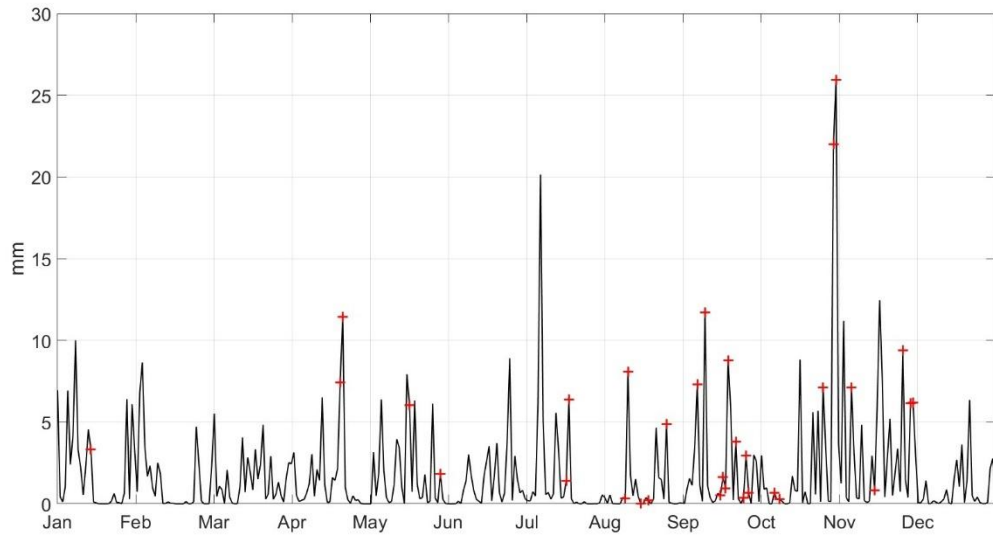


Figure F.9: Daily total precipitation (mm) in the NRB in 2009. Red crosses indicate AR Days or days when total precipitation is associated with ARs.

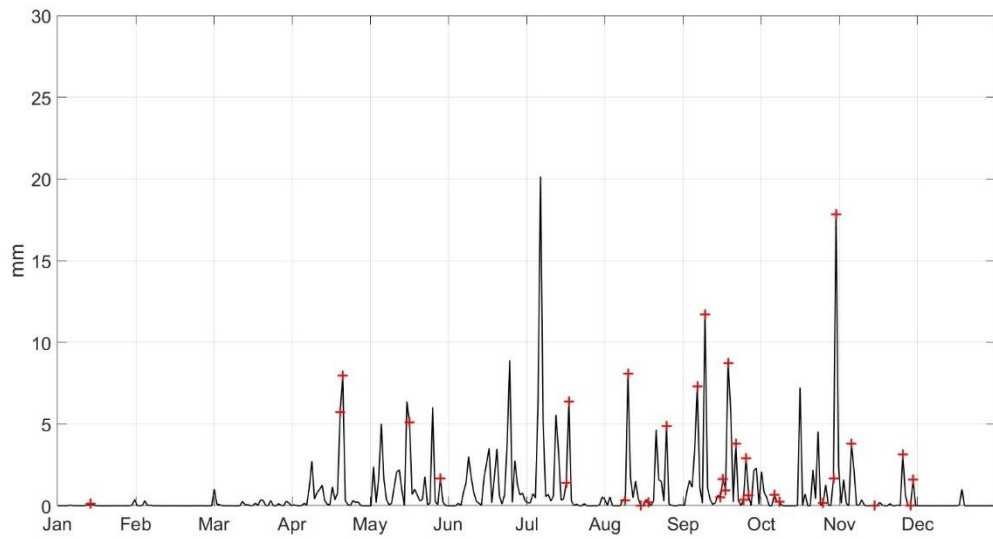


Figure F.10: Daily rainfall (mm) in the NRB in 2009. Red crosses indicate AR Days or days when rainfall is associated with ARs.

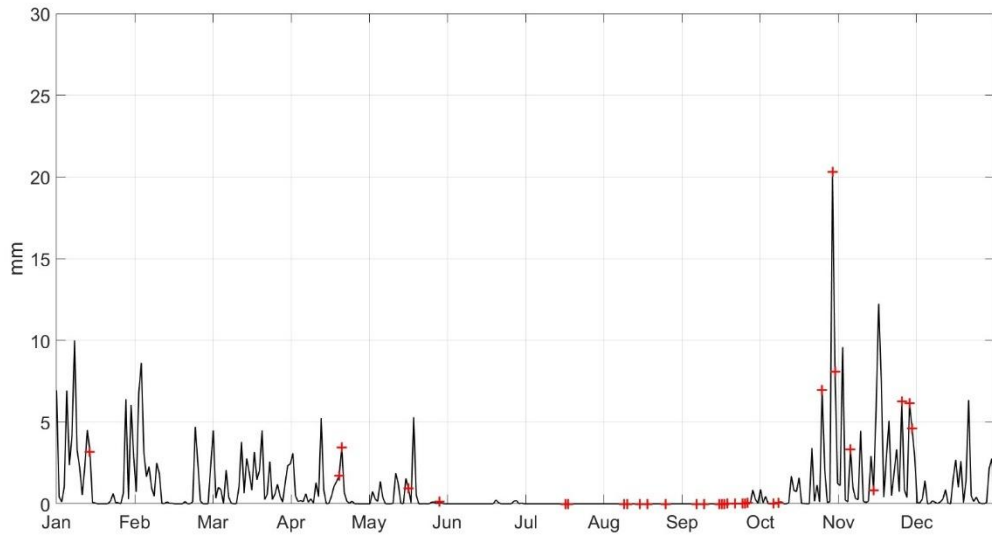


Figure F.11: Daily snowfall (mm) in the NRB in 2009. Red crosses indicate AR Days or days when snowfall is associated with ARs.

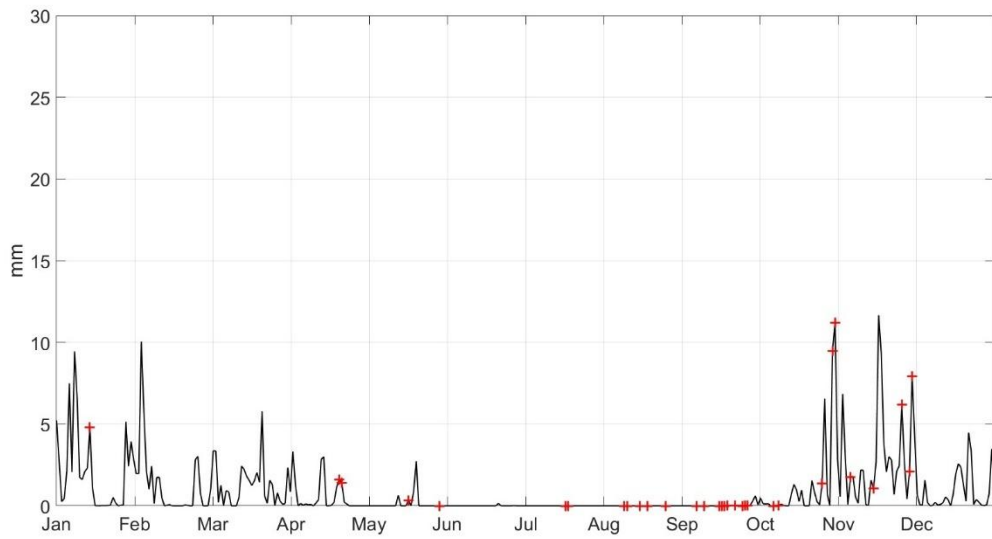


Figure F.12: Daily SWE (mm) in the NRB in 2009. Red crosses indicate AR Days or days when SWE is associated with ARs.

APPENDIX G

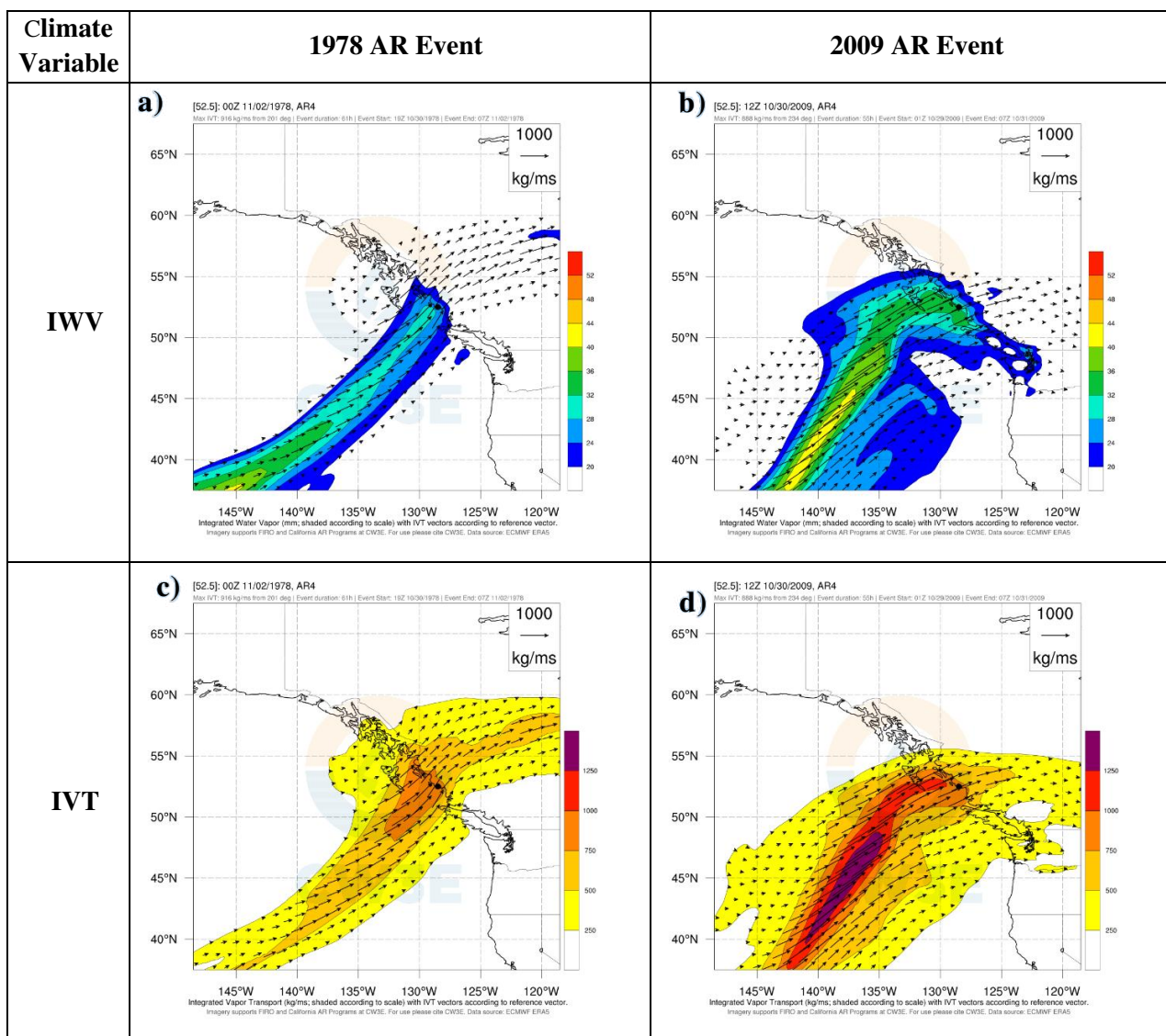


Figure G.1: IWV and IVT maps at the time of maximum landfalling IVT for the 1978 (a and c) and 2009 (b and d) exceptional AR events.

APPENDIX H

Goswami *et al.* (2024) presents a comparison between the ERA5-Land and Climate Change Canada's Canadian Surface Reanalysis (CaSR) reanalysis datasets, with a focus on their performance in the Nechako and Skeena River basins of BC. The study concludes that the ERA5-Land dataset performs particularly well in the NRB. This is largely attributed to the watershed's simpler topography and a more extensive network of meteorological stations compared to the Skeena.

Key factors supporting the reliability of ERA5-Land in the NRB include its handling of air temperature and precipitation data. While ERA5-Land consistently shows a cold bias in annual temperatures, this bias is systematic and can be corrected, making the dataset useful for specific climate applications involving temperature simulations. Additionally, the ERA5-Land dataset tends to overestimate precipitation in the NRB. Despite this, the precipitation trends align well with observed wetting patterns in the NRB. Furthermore, the authors state that the ERA5-Land dataset effectively captures long-term trends in both air temperature and precipitation, confirming its reliability as a resource for long-term climate analysis.

In summary, despite some biases in temperature (not assessed in this PhD dissertation) and precipitation, ERA5-Land proves to be a valuable tool for studying regional climate variability in the NRB. Findings suggest that ERA5-Land can be used effectively in climate research and policymaking related to trends in the NRB, though careful interpretation of certain variables, such as temperature and precipitation, is recommended.